STUDIES ON SI ENGINE SIMULATION AND AIR/FUEL RATIO CONTROL SYSTEMS DESIGN

A thesis submitted for the degree of Doctor of Philosophy

By

Yang Bai

School of Engineering and Design

Brunel University

London, United Kingdom

September 2013

Brunel University
School of Engineering and Design
London, United Kingdom

Yang Bai

Studies on SI Engine Simulation and Air/Fuel Ratio Control Systems Design

September 2013, PhD

Abstract

More stringent Euro 6 and LEV III emission standards will immediately begin execution on 2014 and 2015 respectively. Accurate air/fuel ratio control can effectively reduce vehicle emission. The simulation of engine dynamic system is a very powerful method for developing and analysing engine and engine controller. Currently, most engine air/fuel ratio control used look-up table combined with proportional and integral (PI) control and this is not robust to system uncertainty and time varying effects.

This thesis first develops a simulation package for a port injection spark-ignition engine and this package include engine dynamics, vehicle dynamics as well as driving cycle selection module. The simulations results are very close to the data obtained from laboratory experiments. New controllers have been proposed to control air/fuel ratio in spark ignition engines to maximize the fuel economy while minimizing exhaust emissions. The PID control and fuzzy control methods have been combined into a fuzzy PID control and the effectiveness of this new controller has been demonstrated by simulation tests. A new neural network based predictive control is then designed for further performance improvements. It is based on the combination of inverse control and predictive control methods. The network is trained offline in which the control output is modified to compensate control errors. The simulation evaluations have shown that the new neural controller can greatly improve control air/fuel ratio performance. The test also revealed that the improved AFR control performance can effectively restrict engine harmful emissions into atmosphere, these reduce emissions are important to satisfy more stringent emission standards.

Acknowledgments

Many people have helped me in the completion of this thesis and it is with appreciation that these individuals are acknowledged here.

First and foremost, I would like to express my greatest respect, admiration and gratitude to Dr Jie Chen for his interest, guidance and support throughout the course of my four-year PhD research life. I personally feel so proud and fortunate to have him as my research and academic supervisor.

I am also grateful to Professor Hua Zhao, who has given academic advice and provided guidance throughout my time at Brunel.

I would like to thank my good friends and colleagues, Dr Yan Zhang, Mr Jun Ma, Dr ChoYu Lee for their continuous help, support and friendship to keep me motivated and give me a wonderful life experience.

I would also like to thank my parents, YongChun Bai and Ling Jin, for their help and support that has allowed me to progress to this point.

Finally, I am indebted to my fiancée Yang Cao, for listening, supporting and encouraging me through this period of my life.

Thank you all. Without your help it would have been never possible for me to pursue a Philosophy Doctorate Degree. I will be forever grateful.

Table of Contents

List of Table

List of Figure

Nomenclature

Symbol	Definition
A	Frontal area of the vehicle
AFR_s	Air/fuel ratio
$A(\theta)$	Cross-sectional area of throttle opening
$A(\theta_{max})$	Maximum cross-sectional area of throttle opening
A_f	The area of the surface on which the evaporation takes place
a	Vehicle acceleration
a_T	Throttle angle
$a_T\|_{\Delta t}$	Throttle angle (n-1)
a_x	Acceleration about the x-axis
B	Spalding number
C_D	Aerodynamic drag coefficient
C_d	Discharge coefficient
C_{d1}	Function of the throttle angle
C_{d2}	Function of the pressure ratio across the throttle.
c_p	Heat capacity at constant pressure
D	Throttle bore diameter
d	Throttle shaft diameter
e	Controlled error
f_r	Rolling resistance coefficient
h_m	Mass transfer coefficient
$I_{a/f}$	Air/fuel ratio influenc
I_e	Engine rotational inertia
I_{eff}	Effective inertia
I_{engine}	Engine rotational inertia
I_t	Transmission rotational inertia
I_x	Moment of inertia about the x-axis
$I_{\Delta SA}$	Sparking timing influence
is_*	Assumed sparking timing influence function parameters
K_p	Proportional gain, a tuning parameter

K_i	Integral gain, a tuning parameter
K_d	Derivative gain, a tuning parameter:
M	Air mass
MA	Maximum possible air flow through the throttle body
MBT	Optimal spark timing
MBT_{AFR}	MBT consider AFR change
m	Vehicle mass
$\dot{m}_{ai}$	Air mass flow in intake manifold
$\dot{m}_{ap}$	Air mass flow into intake port
$\dot{m}_{at}$	Air mass flow rate through throttle valve
ma_*	Assumed MBT influence consider on AFR change parameters
m_{cal}	Idle air mass flow rate through the throttle
m_{IAC}	Idle air mass flow rate into the cylinder
m_{ic}	Fuel mass flow into the cylinder
m_{ii}	Fuel mass flow from injector
$\dot{m}_{in}$	Intake manifold air mass rate
m_{ov}	Air mass lost during overlap
m_{wf}	Fuel film mass flow
N	Engine speed
N_t	Numerical ratio of the transmission
O_k	Output vector for the node k of the output layer
P	Cylinder pressure
P_e	Exhaust manifold pressure
P_m	Intake manifold air pressure
PRI	Normalized flow of pressure ratio
Q	Mass of intake air
R	Ideal gas constant
r	Compression ratio
r_{engine}	Engine rotational speed
SA	Spark timing
s_m	Physical constant
T	Temperature
T_0	Up-stream stagnation temperature
$T_0\|_{cal}$	Idle air temperature

T_{brake}	Brake torque
TC	Normalized flow of the cross-sectional area
$T_{f\,\&\,p}$	Friction and pumping torque
T_i	Indicated torque
T_{ideal}	Indicated torque in ideal condition
T_{ov}	Mean temperature during valve overlap
T_L	Engine rotating torque
T_m	Intake manifold air temperature
t_{oxygen}	Oxygen sensor transport delay
T_{sum}	Actual torque delivered to vehicle
T_x	Torques about the x-axis
t_i	Event end time
t_{is}	Spark ignition timing
t_{IVC}	Inlet-valve closing timing
ti_*	Assumed Indicated torque in ideal condition function parameters
t_0	Event start time
V_f	Vehicle forward velocity
V_m	Engine volume
V_{ik}	Weight between hidden layer and output layer
W	Weight of the vehicle
W_{ij}	Weight between hidden layer and the input layer
X_j	Vector for the node j of the Input layer
X'_i	Input vector for the node i of the hidden layer
X''_i	Output vector for the node i of the hidden layer
X'''_k	Input vector for the node k of the output layer
y_m	Physical constant
η	Learning rate
η_{vol}	Volumetric efficiency
Θ	Throttle open angle
θ_0	Angle for minimum leakage area
k	Ratio of specific heat
κ	Ratio of the specific heats = 1.4
κ_c	Coefficients (percentage of fuel from injector and adsorbed fuel)

λ_D	Desired lambda,
λ_F	Feedback lambda,
$\lambda_F\|_{\Delta t}$	Feedback lambda (n-1),
$\lambda_F\|_{2\Delta t}$	Feedback lambda (n-2),
ρ	Throttle throat pressure
ρ_a	Air density
ρ_0	Up-stream stagnation pressure
$\rho_0\|_{cal}$	Idle air pressure
ρ_f	The density of the liquid fuel
τ	Coefficients (rate of fuel film mass change until next stroke)
τ_s	System response
ω_x	Engine speed about the x-axis
w_{e_0}	Event start engine speed
ΔMBT_{AFR}	MBT influence consider on AFR change
ΔSA	Difference of spark timing between the MBT
$\Delta\ T$	Mean temperature rise of the intake air during the intake stroke
Δt	Time delay for each intake stroke
Δt_{MBT}	Intake to torque delay
Δt_{SA}	Injection to torque delay
$\Delta t_{a/f}$	Spark to torque delay
$\Delta t_{f\ \&\ p}$	Intake to exhaust delay
$\Delta\varphi_{in}$	Intake delay
$\Delta\varphi_{com}$	Combination delay
$\Delta\varphi_{ex}$	Exhaust delay

Subscripts

ec	Exhaust valve close
eo	Exhaust valve open
io	Intake valve open
ic	Intake valve close
TDC	Top dead center
BDC	Bottom dead center
in	Intake operation

out	Output operation
ov	During the overlap period
is	Intake of fresh mixture starts
IN-OUT	From intake to output pressing

Chapter1: Introduction

1.1 Introduction

It was estimated by relevant data that in 2010 the world had 1,016,760,000 cars in use (Sousanis, 2011), which was equivalent to 165 vehicles per 1000 persons or one car every 6 persons, motorization rate in Europe are 559 vehicles per 1000 persons (OICA, 2011). Following the increase of population the number of cars globally will exceed 2,000,000,000 after 10 to 20 years (Sperling, Gordon & Schwarzenegger, 2009). The increasing car ownership can not only bring convenient transportation to people all over the world but also consumes a lot of resources, negatively affecting environment. Since the traditional car fuel consumed is mainly un-renewable fossil fuel, the increasing number of cars has also dramatically increased fuel consumption. This will in turn reduce petroleum resources and even increase the possibility of petroleum exhaustion. In addition, fossil fuel consumption by cars produces a lot of harmful emissions, such as carbon dioxide (CO_2), hydrocarbons (HC), hydrogen nitrogen compounds (NO_x) and particulate matter (PM). CO is toxic and can be lethal to people if inhaled a lot due to hypoxia and asphyxia. NO_x is easily converted into nitric acid in hot and humid environment and if inhaled into a human body with air it will affect the normal functioning of the respiratory system and internal organs, causing many diseases. CO_2, CH_4 and other greenhouse gases can both thin the ozone layer and reduce the amount of ozone, causing higher the earth's temperature, intensified ultraviolet. These effects will be a threat to the survival and the development of human beings.

Since the birth of the automobile, global carmakers have been continuously improving the performance of existing models by introducing new car technologies. In order to cope with both the energy crisis and the problem of deteriorated environment, many countries and regions have introduced various measures to limit the amount of vehicle emissions, aiming to reduce the impact on energy and the environment. Local cultural varies, national car technologies and performance are not exactly the same, hence the formulated car emissions laws and regulations are not the same for different countries and regions. So far, the most widely used emission regulations and standards of the world are the ones set by the United States, the Europe and Japan. In the United States, the California has the most stringent emission regulations. As an emerging economy,

China has witnessed rapid developments of its car industry in recent years with a combination of foreign auto manufacturer influx and growing domestic carmakers. Following the increasing car ownership people have begun to realise car emission pollution to the environment, therefore the Chinese government has also issued a series of auto emission standards and regulations.

In order to effectively reduce the harmful gas after engine combustion, there is a three-way catalytic converter install at exhaust system which can converts exhaust, such as CO, HC and NO_x and other harmful gases into harmless ones, i.e. carbon dioxide, water and nitrogen through oxidation and reduction. Its conversion efficiency mainly depends on the air/fuel ratio (AFR) during combustion and the optimum AFR is 14.7 (Heywood, 1998). The AFR will be deviate from its optimum value significantly when the engine is in unsteady state conditions. A small variation around this value may cause severe loss in its fuel efficiency, and 1% variation of AFR may cause up to a 50% reduction of the efficiency of the catalytic converter in reducing pollutants to reduce tail-pipe emissions (Falk & Mooney, 1980). Using a three-way catalytic converter, the AFR should be controlled very precisely in both the steady state and transient engine operations, i.e. the AFR variation should be within ± 0.2% (Benninger & Plapp, 1991). Because of intake charge/discharge effect, fuel film dynamic and signals delay, the air and the fuel mass into the cylinder may not be in a stable ratio. The air through the throttle into engine cylinder, the throttle is considered as the only controlling parameter of engine operation. In order to reduce instability the fuel injection quantity will be controlled.

Following the development of modern control theories many new control methods have been used for controlling AFR, such as: PID, PID-Fuzzy control, adaptive control, predictive control, sliding mode control, switching frequency control and so on. New AFR control methods have been continuously researched and developed. The testing of new controllers on real engine experiments is a costly and time-consuming process. Fortunately research on accurate and efficient ratio controllers can be carried out in the engine simulation platform. This research method was originated by Cassidy et al, who built the engine simulation models in 1970s (Dobner, 1980). There are also scientists who have successfully established simulation platforms for car engines. However, there is still a need to develop a simulation package which can deal with a wide range of control problem.

1.2 Project Objectives

The objectives of this research are

- To develop MATLAB/SIMULINK-based engine dynamics simulation package according to engine operation principles and engine test requirements. This package will include engine dynamics as well as vehicles dynamics. The modular structure and GUI will make it possible to modify and evaluate different controllers for different engines.
- To design, improve and optimise the PID controller for achieving good AFR control performance utilizing MATLAB's optimization tools.
- To develop a new a fuzzy-PID controller structure and to design fuzzy control rule table suitable for port injection engine.
- To propose a new AFR control strategy by combining predictive control and neural control principles.

1.3 Thesis Outline

Following the introduction, Chapter 2 reviews the relevant literature related to this research. In this Chapter wide varieties of engineering simulation software are reviewed. This is followed by the engine simulation method and structure. The engine simulation package components are then reviewed one by one. After that, the engine control system is discussed and meanwhile different engine emissions standards are presented. Finally, the AFR control problem and current methods are discussed.

Chapter 3 begins with the engine operation and simulation structure outlined in Chapter 2. Mathematical modelling of engine dynamics are divided into five parts: throttle body model, intake manifold dynamic model, fuel delivery model, torque production model and engine rotational dynamics. These five parts are then analysed in details, and different part use different types of equation to achieve best performance. When it is possible, nonlinear physical principles equations are used. If the equation accuracy is not high enough or the equation parameters are difficult to obtain, the mean value model equation will be used. To lay the foundation of achieving an accurate and realistic engine dynamic simulation, the transport delay between engine events and sensor

signals are introduced.

Chapter 4 presents the SIMULINK-based engine dynamic simulation package. The engine dynamic simulation model is based on engine standards and dynamic equation which is studied in Chapter 3. This package will be used for the development of AFR controllers in later stage. In this chapter, the driving cycle model, vehicle dynamics and the control model are all introduced. Finally, the engine model simulation results are produced and they are compared with experimental data.

Chapter 5 is used to present two types of AFR control method. The first one is PID control. After the introduction of PID controller basics, a real engine AFR controller is implemented on the engine simulation package. The SIMULINK Design Optimization Toolbox is used to tune PID controller parameters to achieve its best performance. To overcome the limitations of conventional PID controller performance, the second type of controller, the fuzzy PID controller is designed and this is a combination of fuzzy control and PID control principles. The simulation results are presented to demonstrate their efficiency, the advantages and disadvantages are analysed and summarized. Finally, further improvements on the AFR control system are discussed.

Chapter 6 begins with the brief introduction of neural networks and neural networks based control methods. The neural controller based off-line network tuning is then studied. After that, a neural network (NN) controller is designed in the MATLAB environment, and this is followed by the presentation of the controller testing. Finally, the results are discussed and conclusions are given.

Chapter 7 provides the summary and the main conclusions of this study, recommendations and suggestions being given for further research in engine simulation and AFR control.

Some additional materials, such as US emission standards, the volumetric efficiency thermodynamics equation of four-stroke engine, ten driving cycle details, catalytic converter model, are presented in Appendices A-D. The engine dynamic simulation package developed in this study is summarised in Appendix E and F.

Chapter 2: Literature Review

2.1 Introduction

Global environmental concerns such as greenhouse effect, ozone layer depletion and weather disaster have attractive considerable attentions in recent years. Vehicles with internal combustion engines are considered as one of the major sources of impairing the environment due to their dangerous exhaust emissions such as oxides of nitrogen (NO_x), hydrocarbons (HC), carbon monoxide (CO) and particulate matter (PM). For example, within the European Union the road transport is responsible for about 20% of all CO2 emissions with passenger cars contributing about 12% (European Union Report, 2007). Emissions from road traffic have been considered as the major source of air pollution in cities such as London (TFL, 2008). An effective method of reducing these emissions and improving air quality has been through the introduction of the emission standards legislation, which has been imposed for new vehicles sold in Europe since 1992 and a new more stringent Euro Regulations 6 by has been planned to introduced in 2014.

Research has shown that accurate AFR control can effectively reduce emission of dangerous exhaust, such as carbon dioxide, oxides of nitrogen and unburned hydrocarbon (Falk & Mooney, 1998; Franklin, Powell & Naeini, 2009; McCartney, 2003). Evaluating AFR control strategies on real engines is a time consuming and costly process. A computer-based simulation facility would greatly accelerate the development of new AFR control systems. The simulation of the engine dynamic system is not only a very helpful tool for engine manufacturing, but also a very powerful method of developing and analysing the engine for the engine control research and development. A wide range of AFR control methods such as advanced PI, fuzzy, neural network, adaptive and predictive controls can be effectively and easily evaluated on a engine dynamic system simulation facility.

This chapter will first review the current available engine simulation software, where advantages and disadvantages of different types of specialist simulation software packages are discussed. Follow this, the current development of various type of engine control researches (especially engine AFR control) are reviewed.

2.2 Engine Simulation Software

There is a wide variety of engineering simulation software on the market because engine simulation cannot work without software support. Simulation software is based on the process of modelling a real phenomenon with a complete set of mathematical expressions. The software allows operators to observe an operation through a simulated process without actually performing that operation. Therefore, simulation software is widely used in equipment design so that the final product will be as close to design specification as possible without extra expense introduced by experimental manipulation. In automotive field, the simulation can be grouped into two categories: engine commercial simulation software and custom developed simulation package based on programming software.

2.2.1 Commercial Engine Simulation Software

There are number of commercial simulation software available for engine simulation. For example, Ricardo wave, GT-SUITE, Avl Cruise and Lotus Engine Simulation (Chan et al., 2013). Those four products are developed by specialist software companies which solely focus on the engine and vehicle industry.

Ricardo Wave (Ricardo WAVE user's manual, 2009): is a specialized computational fluid dynamics software focused on 1D engine and gas dynamics simulation. It is used in motor sport, automotive, motorcycle, truck, agricultural, locomotive, marine and power generation. The program allows users to define any engine and this couples together customer designed intake and exhaust systems, the program is practically enable to simulate any type of engine system.

Gamma Technologies is a specialist software company which solely focuses on the engine and vehicle industry. GT-SUITE has a wide variety of vehicle and engine technical applications, which include engine performance modelling and vehicle dynamics (GT-SUITE Overview, 2009). In its foundation, GT-SUITE is a versatile multiphysics platform for constructing a wide range of engineering models through a combination of the flow, acoustics, thermal, mechanical, electric, chemistry and

controls.

AVL CRUISE is used to perform vehicle simulation and powertrain analysis (AVL Product Description Cruise, 2009). It is designed to develop and optimize low emission engines, reliable powertrains, and sophisticated control systems of engines, cooling, and transmission systems. It supports the engineer throughout the entire engine and vehicle development process in standard applications, such as fuel economy and full load acceleration tests, hill climbing performance and traction diagrams, as well as computational concept studies including the mechanical, electrical, thermal, and control systems.

Lotus engine simulation is an engine cycle simulation tool that lines up to high expectations of Lotus' own engine research and development department (Lotus Engineering Software user menu, 2011). The Lotus engine simulation software is developed by engineers with extensive expertise of applying performance simulation to engine design projects. Lotus Engine Simulation can be used to simulate the performance of two stroke, four stroke, gasoline, diesel, naturally aspirated, supercharged and turbocharged engines using advanced numerical algorithms to model the gas dynamics in the engine manifolds. The use of sensors and actuators enables the virtually complex operating modes used in modern engines to be simulated.

The main advantages of engine commercial simulation software: (1) They have ability to handle a wide variety of vehicle and engine technical applications. (2) Advanced graphical user interface and model construction methods enable users to build simulation using drag-and-drop element library. (3) They include accurate engine performance block and engine component blocks, dynamic control blocks for real-time simulation. Some of the software also include vehicle dynamics blocks. These blocks make it possible to analyse engine combustion and emissions; in addition, simulated are fast, and the results are accurate. (4) They have strong teams to update modules and solve problems customs may have. Essentially, the simulation software help car designers to make the right decisions which will lead to competitive vehicles in term of fuel efficiency, emissions, performance and drivability.

2.2.2 Custom Developed Simulation Package Based on Programming Software

Simulation software can be developed through writing source code in the program to implement functions needed using programming languages such as C++, VB, VF, Java, Python, etc. Among the plethora of programming software there are some specially designed for mathematical operations and data processing, such as Modelica, Dymola, VisSim and MATLAB. They have algorithmic components and toolbox similar to statements or blocks, and one only needs to enter the equation or logical relationship to make them operational. The process of writing source code requires expertise in many different subjects, including knowledge of the application domain, specialized algorithms and formal logic.

MATLAB is a high-level programming language, and a problem-solving environment for mathematical and scientific calculations. Developed by Mathworks that was founded in 1984, it was originated in the late 1970s with an attempt by Cleve Moler to provide interactive access to the FORTRAN linear algebra software packages EISPACK and LINPACK (Moler, 2004). MATLAB can be used as a tool to analyse data, develop algorithms and create models and applications. More importantly, Mathworks developed an additional package called SIMULINK in 2002 which is a graphical block diagramming environment for multidomain simulation and model-based design. It offers seamless integration with the rest of the MATLAB environment and can either drive MATLAB or be scripted from it. From the outset MATLAB/SIMULIINK provides great user experience. The MATLAB and SIMULINK are promoted quickly by much higher performance requirement of numerical analysis and signal processing according to the evolution in the fields of Engineering and Science. It is probably fair to say that one of the three or four most important developments in numerical computation in the past decade is the emergence of MATLAB as the preferred language by tens of thousands of leading scientists and engineers (Trefethen, 1996).

2.2.3 Advantages of using MATLAB and SIMULINK for the Development of Engine Simulation

There are a number of disadvantages to use commercial simulation software are: (1) All

four software packages mentioned in Section 2.2.1 are limited to automotive engineering only, but real automotive engine developments, require wide range of engineering knowledge such as manufacturing process, material science, mechanical engineering (fluid mechanics, thermodynamics and aerodynamics). The commericial software specially design for automotive engineering field will have compatibility problem when all those engineering knowledge work together. (2) All of the blocks in the commericial software have already been predefined and only block parameters can be changed by users. Moreover the same block in different software may need different parameters. These parameters are dependent on the experimental platform and measuring tools. If one parameter is unknown the simulation may not be proceeded. (3) Developing tools in these simulation software are not aimed for engine control systems design and analysis, and hence they do not have the engine control block which is essential for the development and testing of new control algorithms. In short, commercial engine simulation software have a lot of advantages for engine simulation, but they are not suitable for developing and optimizing engine control systems.

The development of simulation package from scratch with programming language is a difficult and time consuming task which requires good programming skills. However, the possibility of implementing some functions that commercial simulation software cannot provide and the flexibility of modified some simulation blocks especially control blocks outweigh the difficult involved. The available commercial engine simulation packages are easy to use and different one has different features. However, there is still a need to develop a simulation platform which has offers capability and flexibility which enables engine control algorithms evaluation and development.

There are six reasons to select MATLAB/SIMULINK for developing engine simulation platform and designing engine control systems.

1. The high level of the programming language, powerful and user-friendly graphics.
2. The large number of users and installed capacity.
3. The language, tools, and built-in math functions make it possible to explore multiple approaches and reach a solution faster than with spreadsheets or traditional programming languages, such as C/C++ or Java.

4. The SimDriveline toolbox, which provides component libraries for modelling and simulating one-dimensional mechanical systems. The toolbox includes models of rotational and translational components, such as worm gears, planetary gears, lead screws, and clutches. A developer can use these components to model the transmission of mechanical power in helicopter drivetrains, industrial machinery, vehicle powertrains, and other applications. Automotive components, such as engines, tires, transmissions, and torque converters, are also included. SimDriveline models can be converted into C code for real-time test of controller hardware.

5. The SIMULINK Control Design toolbox enables easy design and analysis of control systems. For example, users can automatically tune the gains of PID controllers to meet performance requirements. With this toolbox users can also nonintrusively find operating points and compute exact linearization of SIMULINK models at various operating conditions. SIMULINK Control Design provides tools for computing simulation-based frequency responses without modifying the simulation model. A graphical user interface (GUI) lets users design and analyse arbitrary control structures modelled in SIMULINK, such as cascaded, prefilter, regulation, and multiloop architectures.

6. The SIMULINK Design Optimization toolbox allows the controller design improvements by estimating and tuning model parameters using numerical optimization. Users can increase model accuracy by using test data to calibrate physical parameters. They can then automatically tuning design parameters in their SIMULINK models. For example, one can use design optimization techniques to optimize controller gains to meet rise-time and overshoot constraints, or jointly optimize both physical and algorithmic parameters to maximize overall system performance.

2.3 Review of Engine Simulation

2.3.1 Engine Simulation Models

All simulation system require mathematical models. Physical analysis models, empirical models and hybrid models are three kinds of common modelling methods. At the end of

the 70's, the Cassidy Model, developed by Cassidy et al (Dobner, 1980) has been widely accepted for describing engine systems. This model includes four system components: exhaust gas recirculation, ignition, intake and fuel systems. The model performs well for simulation, but its complexity makes it unsuitable for developing and evaluating engine control systems. The model is built on a number of experimental and simulation results and the universality of the model is limited. Some model equations and parameters are obtained by linearization, and hence they may not correctly reflect the dynamic characteristics of engine. Since 1980s both the static engine model and the quasi static engine model have been used in the electronic controlled engine (Hendricks, Vesterholm & Sorenson, 1992; Hendricks & Sorenson, 1990). The model data are sourced from steady state experiments of engine and so that they can well reflect the various engine performance parameters in stable conditions. Besides the fact that these models are not able to reflect the dynamic characteristics under transient working conditions of engine, they heavily rely on a large amount of experimental data, requiring a lot of manpower and material resources to be invested and therefore are not widely used.

In order to overcome the problem of the above engine models in simulating the dynamic characteristics, the mean value engine model was proposed and further developed by a number of researchers (Aquino, 1981; Cook & Powell, 1988; Moskwa, 1988). The mean model was finally summarized it systematically by Hendricks (Hendricks & Sorenson, 1990; Hendricks, 1991). In principle, the model uses the average value of variables for engine cycle system to describe the dynamic process of the engine, and hence can also reflect the dynamic characteristics of the engine during its transient conditions. Since the Hendricks version, scholars and researchers have further developed and the improved the mean value engine model, particularly in the areas of the oil film and the torque models.

With the further development of science and technology, many researchers have improved the mean value model, meanwhile, intelligent control and hybrid models have also been applied. Muller et al (1998) widened the scope of application of the mean model by applying it to a turbocharged gasoline engine; Yoon et al (2000) took into consideration the impact of air/fuel ratio and spark angle on the output torque so that the mean model can be applied to lean burn engine, with a reported model accuracy error below 5%. Balluchi et al (1999) established a hybrid model for modelling gasoline

engine.

2.3.2 Engine Simulation Structure

Alippi et al (2003) presented an engine simulation structure with some fundamental constituting blocks as shown in Fig 2.1. The engine model has six inputs which are: engine angular speed (N), throttle valve open angle ($alpha$), external temperature (T_e), external pressure (P_e), engine temperature (T_m), and fuel injection time (T_{i-com}). The output of the simulation block can be considered as the AFR. In fact, using a combination of manifold air intake block, manifold pressure dynamic block and cylinder air intake block, the calculations of the air mass into the cylinder can be carried out. Fuel injector and fuel film deposition dynamic together can be used to determine the fuel mass into the cylinder. Both the air to fuel ratio block and exhaust pipe block are described as engine air fuel ratio by a suitable physical driven model.

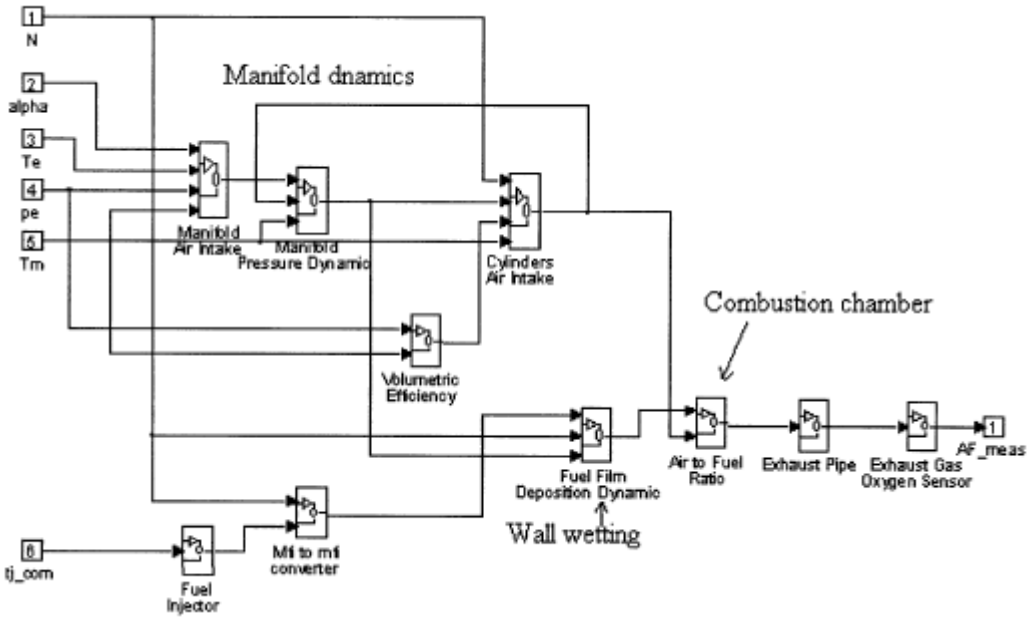

Figure 2.1: Engine Simulation Fundamental Block Constituting (Alippi, Russis & Piuri, 2003)

Wang and Yu (2008) published an engine simulation model as shown in Fig 2.2. The engine simulation model has two input variables (throttle position (u) and fuel injection rate (m_{fi})), and one output (AFR (afr)). In the simulation model P_i, n, m_f, T_i, m_{at} and m_{ap} represent intake manifold pressure, engine speed, fuel to the intake valve, intake air temperature, air mass flow past throttle plate and air mass flow into the intake port, respectively. The AFR block calculates the AFR by using air and fuel mass flow into the intake port which comes from the manifold pressure block and fuel injection block.

Meanwhile, the engine speed is computed using the engine speed block. The AFR time delay may be introduced during the engine simulation and this is simulated in the time delay block. Manifold temperature model refers to the air mass flow into the intake port, intake manifold pressure and air mass flow past throttle plate to calculate the intake manifold temperature. The fuel injection model simulates fuel film dynamics of the intake ports.

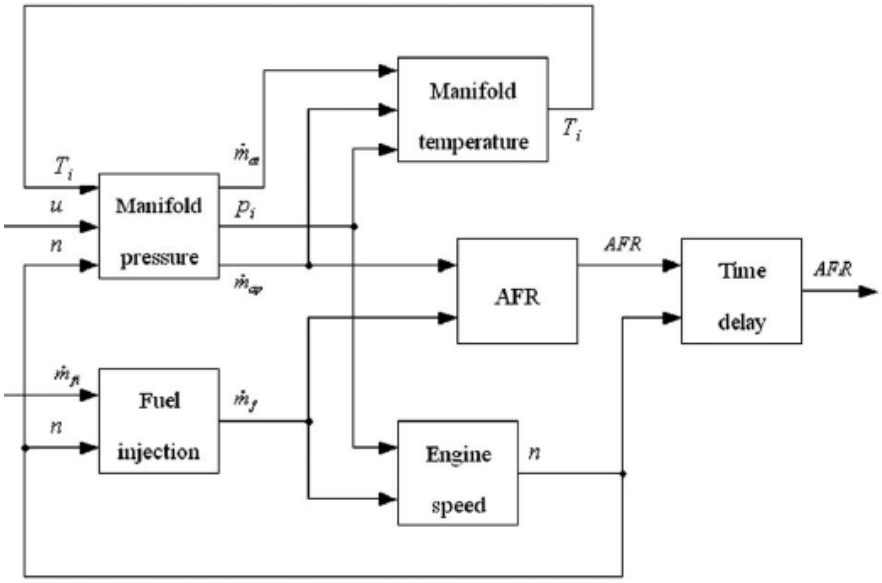

Figure 2.2: Engine Simulation Model (Wang & Yu, 2008)

Yoon et al (2000) introduced a nonlinear dynamic engine model in 2000, which is applicable to a wide operating range of SI engines. As shown in Fig 2.3, the engine simulation model consists of three input variables: throttle angle (α), fuel flow rate (m_{fi}), and spark timing (SA), one disturbance: load torque (T_L), four state variables: air mass in throttle (m_{at}), air mass into cylinder (m_{ap}), AFR (λ_c), engine brake torque (T_{br}) and fuel mass in the fuel film (m_{fc}) and three output variables: intake manifold pressure (P_{man}), engine speed (N) and time delay AFR (λ_e). Similar to two previous models, the model first calculates the air mass and fuel mass into the cylinder, and then the engine AFR followed by torque production model to calculate the engine brake torque. The model of Yoon et al includes intake manifold dynamics, fuel film dynamics and engine rotational dynamics with transport delays inherent in the four stroke engine cycles.

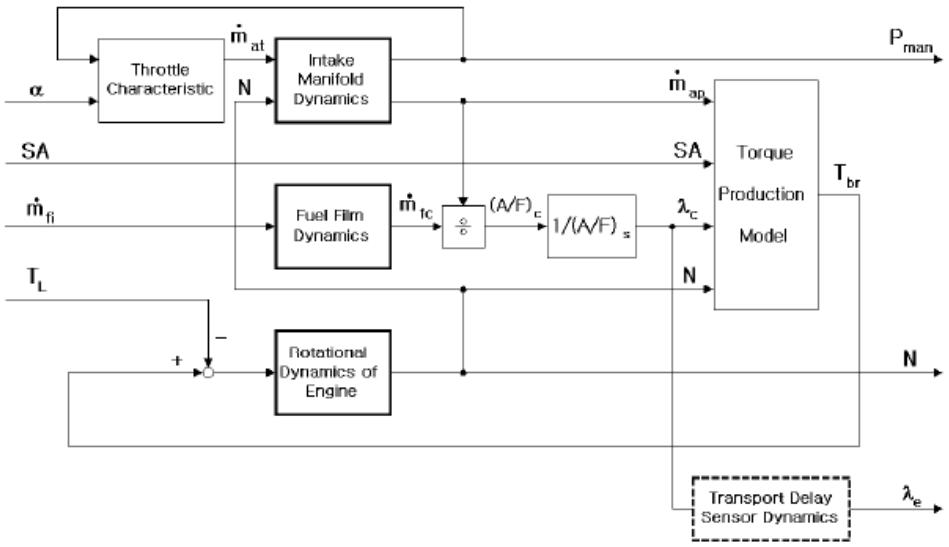

Figure 2.3: Nonlinear Dynamic Engine Model (Yoon et al., 2000)

Cook and Powell (1988) reported a nonlinear engine model as illustrated in Fig 2.4. This study has no thermodynamic model for automotive internal combustion engines and the simulation model contains representations of the throttle body, engine pumping phenomena, induction process dynamics, fuel system, engine torque generation, rotating inertia and exhaust gas recirculation system dynamics.

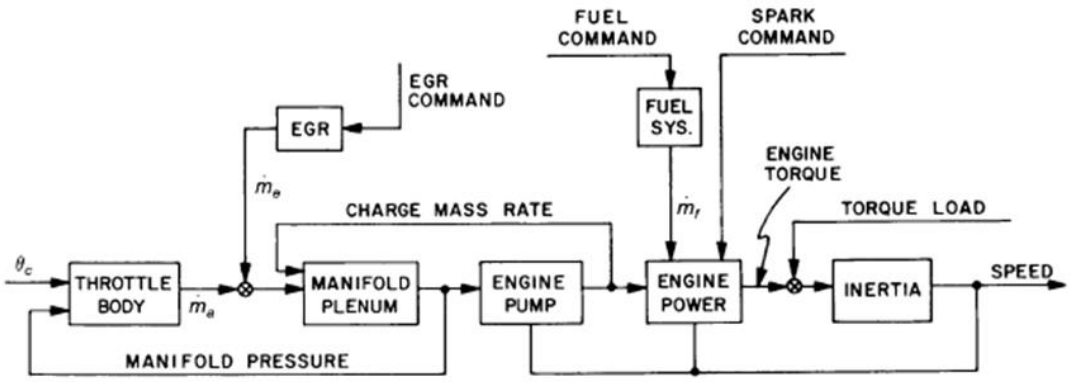

Figure 2.4: Nonlinear Engine Model (Cook & Powell, 1988)

Wagner et al (2003) published an internal combustion engine simulation scheme as shown Fig 2.5. In this scheme, air flows through the throttle body block via the throttle plate into the intake manifold block with auxiliary air flow regulated by the idle air block. The ECU sends signals to the fuel delivery block. The fuel injected into the air mixture using intake manifold block (i.e., port fuel). Once the combustion process is completed in the engine dynamics block, the system will output the engine speed. The oxygen sensor block generates a feedback signal based on the combustion process block in relation to the oxygen concentration.

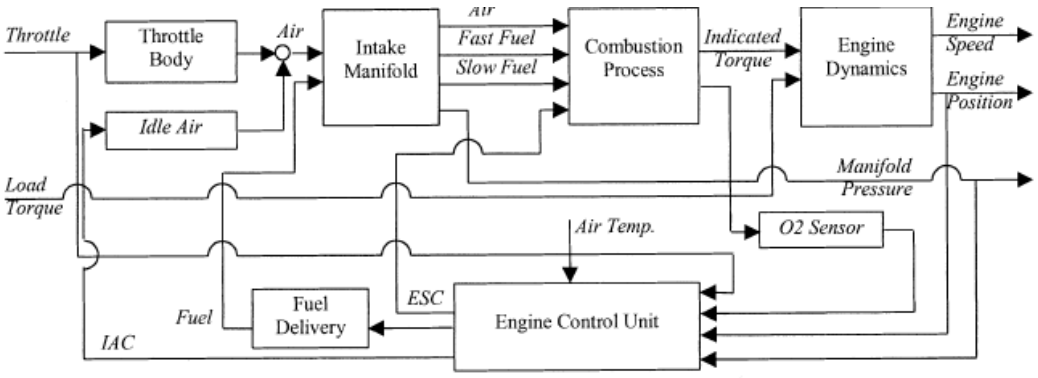

Figure 2.5: Internal Combustion Engine Schematic Simulation (Wagner, Dawson & Liu, 2003)

There are a lot of simulation model structures that are not referred to in this literature review because some of them similar to models discussed in here and some of them lack sufficient details.

Rational for Developing a New Engine Simulation Facility

Some common features can be found in five simulation models reviewed above. For example, the entire model can be divided into three parts: the first part is for calculation of air mass into cylinder; the second part calculates the fuel mass into cylinder, and the third part analyses engine speed or torque output or AFR model according to the first two parts calculations. However, there are some different characteristics in each of models. Alippi's simulation model considers exhaust pipe dynamics. Wang has simulated the intake air temperature. Yoon's model accounts for both the sparking time influence and throttle dynamics. The only model which has an exhaust gas recirculation system dynamic block is the Powell's simulation model, and lastly Wagner's model has an idle air module.

One of main objective for this research is to develop AFR controllers. This will require an engine simulation package which can effectively simulate the intake air and fuel dynamics. The simulation should also have a dynamic output module which generates the engine speed and torque response based on the test model which is used to emulate the emissions and driving cycle. The engine simulation models of Alippi and Wang have good dynamic simulation for intake air and fuel, but the torque dynamic simulation is not available. Yoon and Powell models provide a good structure for engine simulation, but they did not consider throttle dynamics and exhaust model. Yoon's torque

production model presents a very good representation of spark time influence and AFR influence. In view of limitation in existing simulation models available for engine control system evaluation and development, a new simulation package with controller module is needed. The first major task of this research is to develop such a simulation package which is able to produce simulation results close to laboratory experiment test results.

2.4 Engine Simulation Package Components

2.4.1 Engine Schematic

The engine structure is very complicated, being a typical spark ignition engine schematic shown in Fig 2.6. The basic engine working principle can be described as: By controlling acceleration pedal (14), the air flows through the throttle body via the throttle plate (2) into the intake manifold (3). Meanwhile the ECU (1) sends out pulse-width signals to the fuel-injection (5). Fuel injected into intake manifold port with air and is mixed into cylinder. The ECU delivers a control signal to the ignition spark and coil to ignite the air–fuel mixture at the appropriate timing (base on knocking sensor (10)). Once the combustion process is completed the exhaust valve opens and the gases are expelled into the exhaust manifold and the catalytic converter removes pollutants. The oxygen sensor (12) is located at the exhaust manifold that generates the feedback signal in relation to the oxygen concentration in the exhaust gases.

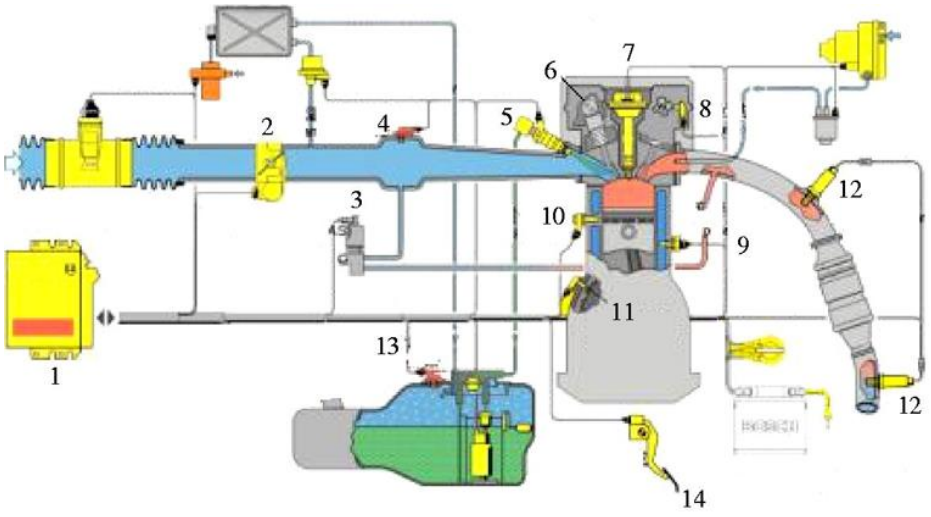

Figure 2.6: Typical Engine System Layout (Zhao, Lai & Harrington, 1999)
Notes: (1) ECU; (2) Throttle valve and bypass air valve; (3) Intake manifold; (4) Manifold absolute pressure sensor; (5) Fuel injection; (6) Intake Valve; (7) Ignition spark; (8) Camshaft position sensor;

(9) Engine temperature sensor; (10) Knocking sensor; (11) Crankshaft position sensor; (12) Oxygen sensor; (13) Fuel pressure sensor; (14) Acceleration pedal.

According to the above engine schematic diagram and the engine simulation models reviewed, an engine simulation system can be split into seven major parts: throttle body model, intake manifold dynamics model, lambda dynamic model, injection dynamic model, wall-wetting dynamics model, torque production model and crankshaft rotational dynamics model. The engine simulation system signal flow graph as shown in Fig 2.7. The system first calculates the air mass and fuel mass into the cylinder, and then the engine AFR followed by torque production model and crankshaft rotational dynamics model to calculate the engine torque output and speed. They each are discussed as follows.

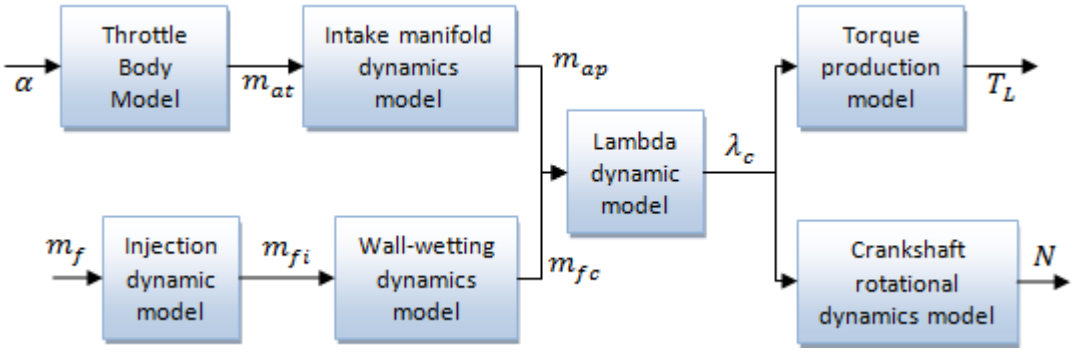

Figure 2.7: Engine Simulation System Signal Flow Graph
where: throttle open angle (α), air mass in throttle (m_{at}), air mass into cylinder (m_{ap}), AFR (λ_c), torque output (T_L), fuel flow rate (m_f), fuel mass injected (m_{fi}), fuel mass into cylinder (m_{fc}), engine speed (N).

2.4.2 Throttle Body Model

In a gasoline engine, air is an essential compound for the internal combustion process. The air flow system directly influences the engine performance, i.e., the power, torque, speed and low emission (Jansri & Sooraksa, 2012). The throttle body is the first component for air to pass through engine. Fig 2.8 left is throttle valve section view, and right is throttle valve and some of its fundamental parts. From this Figure, one can see the air passes from atmosphere through orifice into intake manifold. The assumption of isentropic flow through the throttle body is physically unrealistic in a number of ways, and thus the throttle body block can be assumed as a more realistic model as two physically separated parallel flow fields. The throttle body block calculates the total mass flow rate of air into the intake manifold. In the studies of Scattolini et al (1997),

Yoon et al (2000), Mercorelli (2009) and Harrison et al (2004) study, the throttle flow rate equation is considered as a function of throttle angle and intake manifold pressure.

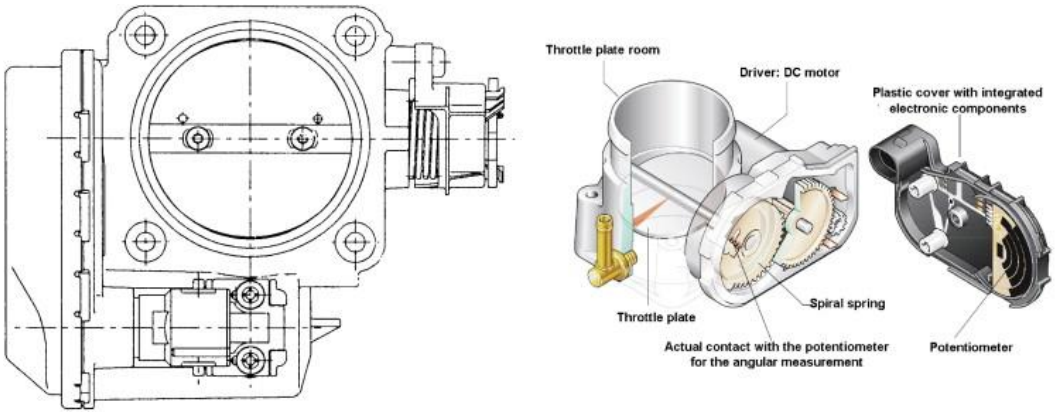

Figure 2.8: Throttle Body Structure (Mercorelli, 2009)

2.4.3 Intake Manifold Dynamics Model

The engine intake manifold dynamics structure is very difficult to simulate, as shown in Fig 2.9 where an intake manifold schematic is presented. Yoon et cl (2000), Ceviz (2007), Ceviz et al (2010), Hashimoto et al (2006), Wang et al (2007) and Hendricks et al (1996) show that the mass flow rate of the air that passes through the throttle and is sucked into the intake manifold which can be described to related to the throttle angle, atmospheric pressure and manifold pressure. The mass flow rate of the air from the intake manifold to the cylinder can be determined by the mean value model which is a function of engine speed and intake manifold pressure (Yoon, Park & Sunwoo, 2000; Hashimoto et al., 2006; Hendricks et al., 1996).

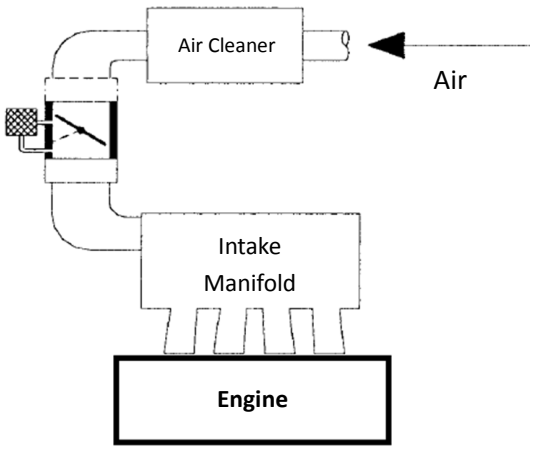

Figure 2.9: Intake Manifold Schematic

2.4.4 Lambda Dynamic Model

The lambda dynamic block is used for simulating a lambda sensor (or oxygen sensor) structure and operation theory. The lambda sensor is an electronic device that measures the proportion of oxygen (O_2) at exhaust gas from car to analyse the engine combustion state. The lambda dynamic model can be assumed to be a function of air mass flow and fuel mass flow into cylinder as shown by Yoon et al (2000), Hendricks and Sorenson(1991) and Wagner et al (2003).

2.4.5 Injection Dynamic Model

Fuel passes through the injection solenoid valve which is electrically controlled by injection signal into an internal combustion engine for which, a variety of fuel injection system and different inject positions may contribute to different results (Heywood, 1998). The injection dynamic model is primarily a fuel delivery system in the engine simulation, where the amount of fuel injected into the intake manifold is be determined by the air/fuel control system, this being expressed as a function of injected time and diameter of fuel spray nozzle (Suh, Park & Lee, 2009).

2.4.6 Wall-Wetting Dynamics Model

The injection model of the engine can be summarized into two types: one is direct injection in cylinder, as shown in Fig 2.10-2. This injection model does not necessarily consider the effect of oil film, and the injected fuel amount by the injector is equal to the air-fuel mixture at the bottom of the cylinder. Another type is port injection, in which the total injected fuel cannot directly reach the engine port, and therefore a fraction of it forms a fuel film on the wall of the intake whilst the rest reaches the cylinder, as can be seen from Fig 2.10-1. The fuel film then evaporates and reaches the engine port with a delay, producing on oil film effect. The oil film phenomenon will affect the quality of fuel in cylinder and hence it should be taken into consideration by this injection type.

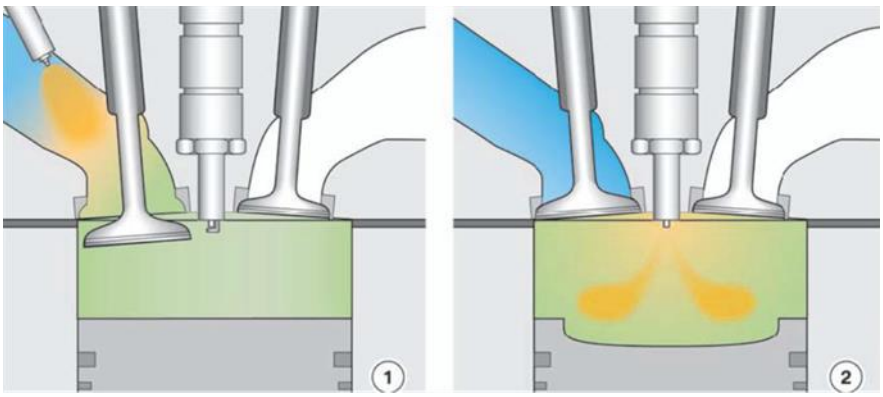

Figure 2.10: Engine Fuel Injection Mode (BMW, 2013)

In general, it is difficult to accurately model the fuel wall-wetting dynamics, because the changes strongly depend on the fuel characteristics, engine intake port structure, and the engine temperature during operation (Guzzella & Onder, 2010). The wall-film model is widely used to represent the amount of fuel injected into each cylinder during the induction stroke (Aquino, 1981). According to Hendrick's identification experiments with SI engine, the fuel flow dynamics can be described as a function of constant time, fuel deposited constant and injected fuel mass (Hendricks & Sorenson, 1991):

Aquino (1981) first proposed a double-parameter X-t model for oil film. The X-t model can better describe the dynamic characteristics of oil film, and by applying it on the transient AFR control effect can be achieved. Hendricks & Sorenson (1991) further modified the X-t model by adding another time constant in addition to fuel evaporation constant time t. The extra parameter can be physically interpreted as a fuel transfer constant time. Experimental results show that this double constant time model for oil film in a single point injection system is better than the X-t model in terms of compensation of the effect on oil film; however, its improvement is less obvious in the multi-port injection systems.

2.4.7 Torque Production Model

The internal combustion engine is a torque conversion system that can be powered by fuel oil. Ignite the air and fuel mixture in combustion chamber, and then push cylinder pistons motion generates useful mechanical energy and transfer CAM shaft rotation. The engine torque block is necessary to detail and correctly predict thermodynamic simulations. Guzzella (1996) said that *'For control purposes, however, such simulations are too time-consuming. Thus, alternative approaches have been investigated.'*

Many researchers suggest that the best method to determine the torque is to use mean-value model (Togun, Baysec & Kara, 2012; Baruah, 1990; Guzzella & Onder, 2010; Hendricks & Sorenson, 1990; Muller, Hendricks & Sorenson, 1998; Yoon, Park & Sunwoo, 2000, etc.,). Based on calculations of Yoon et al (2000) the torque generated by an engine depends on the ignition of the cylinder charge, the mixture formation, and engine specific physical parameters. In addition, Togun et al (2012) points out that torque is influenced by other factors. Using physical insight to research all possible relationship and impact of variables and the engine torque block is divided into several low-dimensional models. '*The mean-value engine torque is a nonlinear function of many variables, such as fuel mass in cylinder, AFR, engine speed, ignition or injection timing, EGR rate, etc.'* (Guzzella & Onder, 2010)

2.4.8 Crankshaft Rotational Dynamics Model

Crankshaft rotational dynamics model output is the engine speed which is related to the crankshaft velocity. The operation of the crankshaft system depends on the relationship between the pressure and torque (Rizzoni, 2002). The crankshaft velocity can be calculated by an integral of the resulting torque divided by the engine inertia (Yoon, Park & Sunwoo, 2000; Thomas & Sharma 2007), and resulting torque can be expressed as engine torque plus friction torque. Thus, crankshaft rotational dynamics block is obtained from Newton's laws follows: $J\dot{\omega} = \tau_e + \tau_f$ where J denotes the inertia moment of the crankshaft; ω denotes engine speed; τ_e engine torque and τ_f friction torque.

2.5 Overview of SI Engine Control

To ensure internal combustion engine operational in its optimal condition, the engine control unit is required. In order to guarantee internal combustion engine running in clean, fuel efficient and safe operation, the engine requires very precisely signal controlled by the engine control unit. The four most important control loops for port injection spark-ignited gasoline engines are the AFR control, the idle speed control, the exhaust gas recirculation control and the engine knock control (Guzzella & Onder, 2010).

2.5.1 Idle Speed Control

Idle speed control is a classical problem in automotive control and the celebrated Watt's governor (1796) was, in fact, a speed controller for a steam engine. Even though idle speed control is implemented in most vehicles on the road today, increasingly stringent requirements from both industry regulators and customers demand continuous and further improvement. For instance, a better performing idle speed control can improve fuel economy by both reducing spark reserve and lowering idle speed set-point; in addition, it can also accommodate changes in sensors and actuators (e.g., a replacement of an air-by pass valve by the electronic throttle or reduction in sensor or actuator cost). Designs of idle speed control that can lower calibration time and effort can help reduce time-to-market, which is a key priority for auto manufacturers (Yildiz et al., 2009).

The idle speed control system regulates engine idle speed by adjusting the volume of air through its throttle valve. In practice the status of the engine idle condition can account for about 30% of running time. If idle speed control is too high, then fuel consumption will increase, otherwise toxic exhaust produced by engine idling may increase at a low idle speed (Heywood, 1998). Typically, the adjustment for air volume through the throttle valve falls into two types shown in Fig 2.11: throttle valve directly operated type and air bypass valve type. Due to better quality of dynamic response characteristics the air bypass valve type is more common for idle speed control. Idle speed control is based on the input signals received from various sensors. The system is necessary to provide stabilization of curb idle when loading is applied to the engine to provide cold fast idle on some applications. Depending on application the idle speed control system regulates idle speed under at least one or more of the following conditions: stability idle, fast idle, engine warm up idle, air conditioner load, electrical load, transmission load.

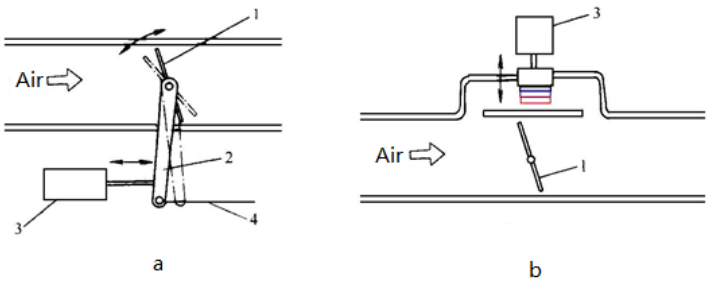

Figure 2.11: Idle Speed Air Valve Adjustment Type
where Fig 2.11-a is throttle valve directly operated type, Fig 2.11-b air bypass valve type, 1- Throttle Valve, 2- throttle control lever, 3-idle speed controller ,4- accelerator pedal.

In fact, engine idle speed control is feedback control. The idle state model will go through the different conditions to choose the optimum idle parameters (engine speed). Hence, an idle speed control system constantly monitors the engine speed and compares it with the optimum idle engine speed. When the engine idle speed fluctuates and deviates from the target speed, the control system will output pulse actuator signal to adjust the intake valve, so that the engine speed is controlled within a range of target speed.

There are many different feed-forward control methods proposed for engine idle speed. For example, idle speed control design using an H_∞ control approach was presented by Williams et al (1989). Filippi et al (2005) presented an H_2 idle speed control method of a F1 racing engine. Kjergaardet al (1994) and Li et al (2001) demonstrated sliding mode control with application to engine idle speed control. Model predictive control based idle speed control for IC engine was published by Cairano et al (2011). Kim et al (2007), Hsieh et al (2007) and Yildiz et al (2011) have shown that the use of adaptive idle speed control for spark-ignition engines. At present, most of the idle speed control methods use either PI or PID control (Kokotovic & Rhode, 1986; Yurkovich & Simpson, 1997; Gangopadhyay & Meckl, 1999; Wang, Stefanopoulou & Levin, 1999; Grizzle, Buckland & Sun, 2001).

2.5.2 Exhaust Gas Recirculation Control

In internal combustion engines, the exhaust gas recirculation is a nitrogen oxide emissions reduction technique used in both petrol and diesel engines (Heywood, 1998). Exhaust gas recirculation works by recirculating a portion of an engine's exhaust gas back to the engine cylinders. In a gasoline engine, this inert exhaust displaces the amount of combustible matter in the cylinder. Nitrogen oxide is primarily generated in a chamber that has both high temperature and a mixture of nitrogen and oxygen, and hence the lower combustion chamber temperature caused by exhaust gas recirculation reduces the amount of nitrogen oxide the combustion generates (Agrawal et al., 2004). Most modern engines now require exhaust gas recirculation to meet emissions standards (Chandra, Jha & Laxmi, 2013).

The exhaust gas recirculation is a process of introducing exhaust gas into the fresh air, diluting the air and fuel charge, and lowering the combustion temperature. Exhaust gas

can be introduced into the cylinder in various ways: some engines use variable valve actuation systems on the exhaust valves to “trap” exhaust gas from a previous combustion event (sometimes referred to as “trapped residual”) whist others use electronically controlled valves or throttles off the exhaust stream through low-pressure or high-pressure loops to regulate exhaust gas flow into the intake manifold (Fig 2.12).

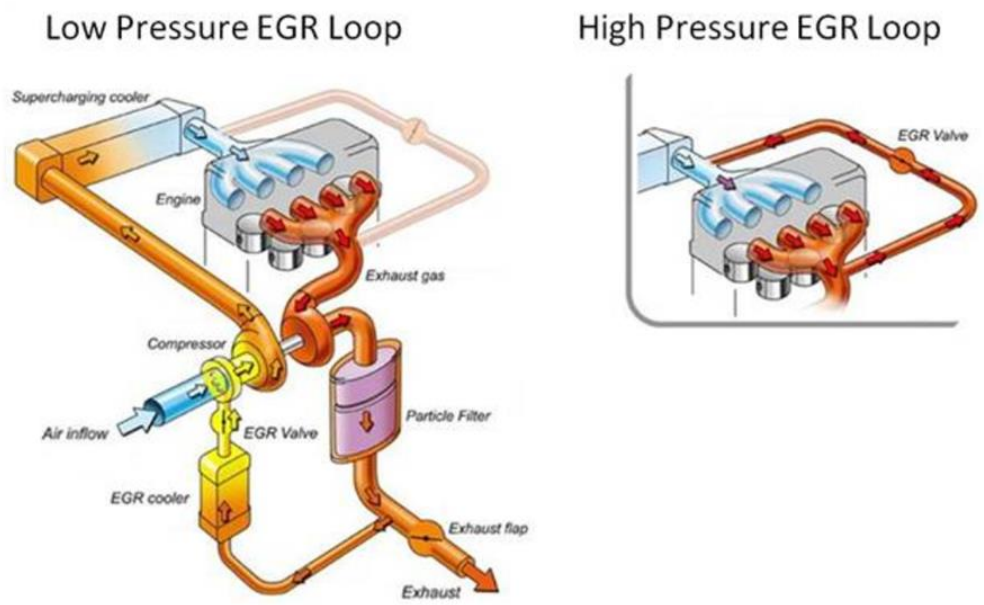

Figure 2.12: High-Pressure and Low-Pressure EGR Diagram (National Instruments, 2012)

In a typical automotive spark-ignited engine between 5% and 20% of the exhaust gas can be routed back to the intake as exhaust gas recirculation (Zheng, Reader & Hawley, 2004). The maximum quantity is limited by the requirement of the mixture to sustain a contiguous flame front during the combustion event, and excessive exhaust gas recirculation in poorly setup applications can cause misfires and partial burns. Although exhaust gas recirculation does measurably slow combustion, this can largely be compensated for by advancing spark timing. The impact of exhaust gas recirculation on engine’s efficiency largely depends on the specific engine design, and sometimes leads to compromise between efficiency and nitrogen oxide emissions. A properly operating exhaust gas recirculation can theoretically increase the efficiency of gasoline engines.

The percentage of exhaust gas recirculated into cylinder is controlled by the exhaust gas recirculation valve based upon readings from the manifold absolute pressure sensor and engine temperature and speed. As discussed previously, higher percentages of exhaust gas recirculation lowers nitrogen oxide content; however, other performance metrics

(e.g., brake specific fuel consumption, hydrocarbon) deteriorate with higher exhaust gas recirculation (Aken, Willems & Jong, 2007). In other word, the exhaust gas recirculation and AFR loops interact.

Exhaust gas recirculation is typically not employed at high loads because it would reduce peak power output owning to the reduction of the intake charge density. Exhaust gas recirculation is also omitted at the idle working condition, e.g. low-speed and zero load because it would cause unstable combustion, resulting in rough idle. The exhaust gas recirculation valve also cools the exhaust valves and makes them last far longer, which is a very important benefit under light cruise conditions.

2.5.3 Knock Control

Engine knock is closely related to engine ignition timing. From the review of Zhen *et al.* (2012) there are many causes of engine knock. The first one related to mechanical issues, such as fuel oil octane rating, carbon build-up in engine, defects in cylinder block and cooling system. The second one related to control problems, for example if the ignition timing is too earlier, the combustion pressure can be so high that engine knocking may occur. When ignition timing near the timing starts producing engine knock, the engine output will reach the maximum torque (Heywood, 1998), so the ignition timing should be set near the knocking limit area. But if ignition timing is far away from the knock limit of ignition lags, engine torque will be decreased and power output will be lowered, increasing fuel consumption. A modern engine knock control system sets ignition timing as earlier as possible in order to maximise both engine power and fuel economy. Tests have shown that a slight knock will improve engine power, economy and combustion; however, excessive knock can damage the engine quickly. Therefore, the idea of critical knocks is needed and should be discussed, because it can restrict spark ignition engines to improve the compression ratio and strengthen combustion technology in spark ignition engines. In fact, real-time knocking control has become the main concern of the control system.

Engine knock control system improves the engine performance by detecting, differentiating and regulating the knock sensor readings. The process of an engine knock control system is shown in Fig 2.13, where the knock control system detects the knock signal, and goes through control algorithm to differentiate the knock signal and

adjusts the ignition angle. According to the control cycle the ignition angle is changed in the next cycle to achieve the control engine knock.

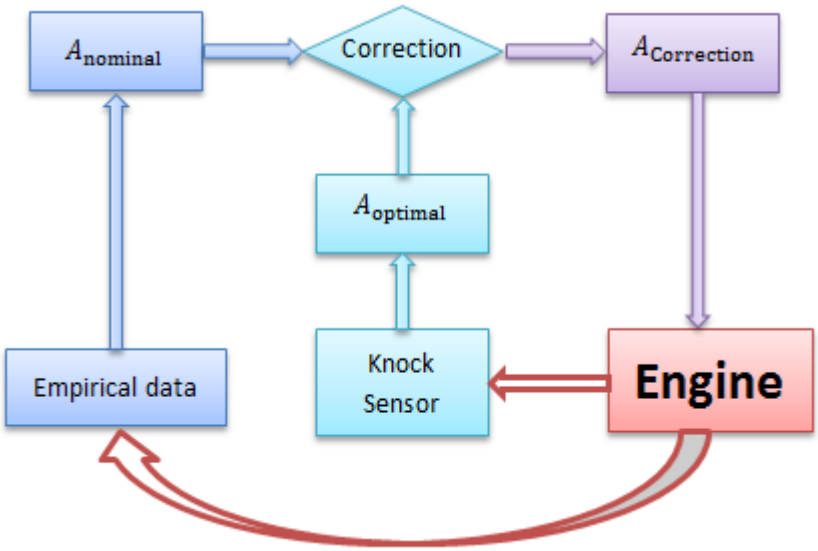

Figure 2.13: Engine Knock Control System

In order to achieve better stability and response speed, the control system combines open-loop control with closed-loop control. Open-loop control determines the nominal ignition angle according to the engine operation condition whereas closed-loop control determines the optimal ignition angle according to the feedback of knock signal. The ignition angle correction is finally determined by the below method: Correction ignition angle = Nominal ignition angle + Optimal ignition angle.

The Fig 2.14 shows the signal flow of a knock controller: the orange dotted box is closed-loop control whist the green dotted box indicates open-loop control. Open-loop control: When engine operation condition changes suddenly the ignition angle should be directly determined according to look-up table in order to achieve quick response. Nominal ignition angles are mainly determined by plenty of experimental data, e.g. *nominal ignition angle= function (engine speed, engine torque, intake temperature, knock sensor signal)*. Closed-loop control: There is no widely recognized definition of knock since there is no standard procedure to detect and quantify (Stotsky, 2008). Therefore it is necessary to adopt a statistical method to analyse knock signals detected by an engine knock sensor. Usually, during the analysis a computing algorithm should be used to define knocking intensity, and then optimise the ignition angle. As shown in the orange dotted box of Fig2.14 if engine knock occur the ignition time angle for the

considered cylinder is retarded by 3°. Afterwards, the ignition angle is advanced again at the rate of 1° per second as long as the engine occur knock again. Delay general ignition timing by 2°~5° can effectively eliminate the engine knocking (Brunt, Pond & Biundo, 1998).

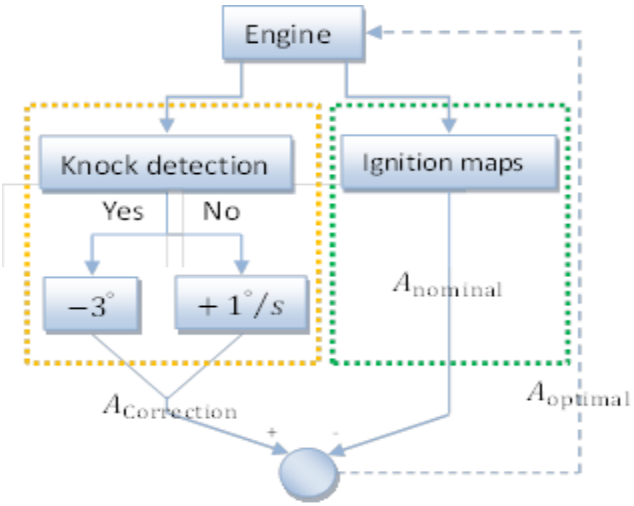

Figure 2.14: Signal Flow of Knock Controller

2.5.4 Air/Fuel Control

The fine control of the air-to-fuel ratio is a fundamental solution to minimise exhaust emissions in automotive fuel injection systems (Alippi, Russis & Piuri, 1998). The engine AFR is the mass ratio of air to fuel present during combustion. In traditional petrol engines maximal efficiency of the catalytic converter requires that AFR to be kept constant at the stoichiometric value AFR = 14.7 (Heywood, 1998), and engines can produce more exhaust emissions or air pollution at a different ratio. The TFL (Transport for London) report has shown that the major source of air pollution in cities such as London is emissions from road traffic. Today, there are at least 13 countries in the world, including the EU and the US, that have promulgated their own laws for restricting vehicle exhaust emissions.

2.6 Engine Emissions Standards (DieselNet, 2013)

An effective way to reduce emissions and improve air quality is to enforce legislation on car emission standards. As discussed previously the major pollutants released from burning fossil fuel in internal combustion gasoline engines are carbon monoxide, oxides

of nitrogen and unburnt hydrocarbons. They are indispensable gas wastes owning to the absence of practically alternative fuel resource produced by gasoline engine technology. In addition, they also have raised serious concerns with their connection to environmental pollution. Hence, stricter band of legislation related to emission of these pollutants has been laid out by heavily car-use countries, such as China, the United States, Japan and Europe countries, which leads to big large achievements in terms of engine technologies.

EU Emission Legislation

EU emission legislation was first introduced in the 1970s, which imposes emission restrictions on new vehicles sold in Europe since 1992. That is, it gives acceptable limits for exhaust emissions of all new vehicles that are sold in the EU, covering oxides of nitrogen (NO_x), hydrocarbons (HC), carbon monoxide (CO) and particulate matter (PM). These limits are set at six different levels for different vehicle types and compliance is determined by running a vehicle's engine over a standard test cycle for a set of time. Table 2.1 shows the trend of significant reduction in emissions limits that are required at every steps. Since the Euro 2 stage EU regulations have introduced different emission limits for diesel and petrol vehicles, and based on Figure it is clearly seen that they are stricter for each stage over time. For example, the Euro 6 stage, this is supposed to come into force in October 2014，is the strictest than ever. The EC Directives also specify a second date — one year later — which applies to the first registration (entry into service) of existing, previously type-approved vehicle models.

Table 2.1: EU Emission Standards for Passenger Cars (g/km)

Tire	Year	Type	CO	HC	$HC + NO_X$	NO_X	PM
Euro 1	1992	CI	2.72	-	0.97	-	0.14
		PI	2.72	-	0.97	-	-
Euro 2	1996.10.01	CI	1		0.7		0.08
		PI	2.2	-	0.5		
Euro 3	2000.10.01	CI	0.64		0.56	0.5	0.05
		PI	2.3	0.2	-	0.15	
Euro 4	2006.10.01	CI	0.5		0.3	0.25	0.025
		PI	1	0.1	-	0.08	
Euro 5	2009.10.01	CI	0.5	-	0.23	0.18	0.005
		PI	1	0.1	-	0.06	0.005
Euro 6	2014.10.01	CI	0.5	-	0.17	0.08	0.005
		PI	1	0.1		0.06	0.005

Key: PI = Positive Ignition, CI = Compression Ignition

The US Standards

1) Federal Standards

Emission standards for engines and vehicles in the US, including emission standards for greenhouse gas emissions, are established by the Environmental Protection Agency. The Environmental Protection Agency authority, which regulates both engine emissions and the air quality in general is based on the Clean Air Act, most recently amended in 1990. The development of engine emission standards occurs according to the procedures of the US rule making process. New regulations are first published as proposed rules. Following a period of public discussion, these new rules are finalized and signed to become law. New regulatory proposals and regulations are published in the Federal Register, and consolidated regulations become a part of the Code of Federal Regulations.

Presently there are three standards for cars: Tier 1 standards, which were published as a final ruling on June 5, 1991 and phased-in progressively between 1994 and 1997. Tier 2 standards, which were adopted on December 21, 1999, with a phase-in implementation schedule from 2004 to 2009. The Tier 2 regulation introduced more stringent numerical emission limits relative to the previous Tier 1 requirements, and a number of additional changes also made the standards more stringent for larger vehicles. On March 29, 2013 the US Environmental Protection Agency signed a proposed rule for Tier 3 emission standards. The structure of Tier 3 standards is similar to the Tier 2 standards and starting from 2017 they are phased-in completely in 2025.

2) California Standards

The State of California is the only state vested with the authority to develop its own emission regulations, which are often deemed to be more stringent than the federal rules. Engine and vehicle emission regulations are adopted by the California Air Resources Board, a regulatory body within the California Environmental Protection Agency. Other states have a choice to either implement the federal emission standards, or adopt California requirements. States that adopted California Clean Car Standards, including the California LEV II and greenhouse gas emission standards are listed in the Appendix A.

LEV Emission Standards are applied through model year 2003. In November 1998, the California Air Resources Board adopted LEV II emission standards which were phased-in from 2004 through 2010. Manufacturers can still certify vehicles to LEV II emission standards (categories) until model year 2019. The LEV III emission standards, adopted in January 2012, are phased-in over the 2015-2025 model years. Manufacturers can certify vehicles to the LEV III standards before model year 2015. Beginning with model year 2020 all vehicles must be certified to LEV III standards.

The LEV III standards modified the LEV II standards in several ways: (1) combine non-methane organic gases ($NMOG$) and NO_x standards into one $NMOG + NO_x$ standard. (2) introduce a more stringent combined $NMOG + NO_x$ fleet average requirement for 2015-2025 model years. (3) add several emission standard bins. (4) increase the durability requirements for emission control systems.

Chinese Emission Standards

Due to rapid expansion of wealth and prosperity the number of cars on China's roads is growing sharply, creating an on-going pollution problem. Hence, China enacted its first emissions controls on automobiles in 2000, which is equivalent to Euro I standards. Since then Chinese emission standards for new passenger cars are all based on European regulations with some changes. Emission implementation schedules are listed in Table 2.2 for gasoline and diesel vehicles. The nationwide dates generally refer to new type approvals, e.g. first registration of existing vehicle models is typically allowed for one more year. In some cases, conformity of production requirements is relaxed and/or delayed relative to the type approval requirements.

Japanese Emission Standards

Japan introduced first new engine emissions standards for on-road vehicles in the late 1980's. The Japanese standards, however, remained relaxed through the 1990's. In 2003 the MOE finalized very stringent 2005 emission standards for both light and heavy vehicles. At the time they came to force the 2005 heavy-duty emission standards (NO_x = 2 g/kWh, PM = 0.027 g/kWh) were the most stringent diesel emission regulation in the world. Effective in 2009 these limits are further tightened (NO_x = 0.7 g/kWh, PM =

0.01 g/kWh) to a level between the US 2010 and Euro 5 requirements.

Table 2.2: Chinese Emission Implementation Schedules

Tire	data	Region	Reference
China 1	2000.1	Nationwide	Euro 1
China 2	2002.08	Beijing	Euro 2
	2003.03	Shanghai	
	PI: 2004.07 CI: 2003.09	Nationwide	
China 3	2005.12	Beijing	Euro 3
	2006.10	Guangzhou	
	2007.01	Shanghai	
	2007.07	Nationwide	
China 4	2008.03	Beijing	Euro 4
	2009.11	Shanghai	
	PI: 2011.07 CI: 2015.07	Nationwide	
China 5	2013.02	Beijing	Euro 5
China 6	Proposed in 2016	Beijing	Euro 6

In-Use Vehicle Regulations：In 1992, to cope with NO_x pollution from existing vehicle fleets the MOE adopted the motor vehicle NO_x Law, which aimed at the elimination of the oldest, most polluting vehicles from in-use fleets in certain geographical areas. In 2001 the regulation was amended to also include PM emission requirements and renamed as Automotive NO_x and PM Law.

Tokyo Retrofit Program: The Tokyo municipal government and several neighbouring prefectures adopted diesel emission regulations, which require retrofitting of older in-use diesel vehicles with PM control devices (catalytic converters or particulate filters), or else replacing them with newer, cleaner models. The Tokyo retrofit requirements became effective in October 2003.

It can be summarised that the US legislation is significantly different from EU standards, because it is based on a “Fleet-averaged” emission strategy. In other word, the automotive manufacturers only need to meet the prescribed limits of the US standards with their average emission levels of the total sales for each products range. Therefore, it is not applicable to directly compare the EU standard to US Environmental Protection Agency standard due to the differences in the test drive cycle and measurement methods. Through the normalization of the EU and US standards the level of hydrocarbon by US and EU Emission standards are roughly similar whereas US Environmental Protection Agency permits are approximately half of the EU amount of

hydrocarbon emissions (Johnson, 2002).

In addition to the above emission standards, CO_2 emissions are also limited by government policy in the UK and many European countries in order to reduce the impact on global climate change (Foley & Fergusson, 2003). This limitation usually takes forms of heavy taxation of fuel or advantages on Road Fund Duty/road tax for small capacity vehicles. Recently "company car tax" has been introduced that imposes heavy penalties for operating vehicles with high CO_2 emissions. A number of European car manufacturers have also reached a voluntary agreement on their fleet average CO_2 emissions, which is aimed to be cut from the current 160 g/km to 120 g/km by the year 2012, equivalent 25 per cent reduction in the fuel consumption (Foley & Fergusson, 2003).

2.7 Overview of Air/Fuel Ratio (AFR) Control

2.7.1 The Importance of AFR Control

Exhaust of gas engine combustion is eventually released into air by a three-way catalyst. The three way catalytic converter is the most important cleansing device externally installed in the exhaust system of the car (Falk & Mooney, 1998). It converts exhaust, such as CO, HC and NO_x and other harmful gases into harmless ones, i.e. carbon dioxide, water and nitrogen through oxidation and reduction (Stefanopoulou, 1996; Alippi et al., 1998; Ebrahimi et al., 2012). Its conversion efficiency mainly depends on two factors: one is the three-way temperature and the other is the AFR during combustion. Hence, the combustion AFR directly affects the efficiency of catalyst and Fig 2.15 demonstrates its efficiency. If the engine AFR can be controlled at 14.7 that will be a very effective method to reduce the harmful exhaust.

2.7.2 Purpose of AFR Control

The issue of air fuel ratio control can be divided into two parts. The first part is the target AFR setting, as shown in Fig 2.16 that plots the curve of AFRs against power. It can be seen that the maximum output power can be obtained when the AFR is set to 12.6. However, the engine is the most fuel-efficient when the ratio is 15.4. Meanwhile, the efficiency of the three-way catalytic should also be taken into consideration. Now

there are some engines that can achieve better fuel lean combustion technology, but a three-way catalytic have to be specifically designed in order to fit their AFRs. In addition, the AFR will be temporarily lifted to achieve better power performance for prompt acceleration. Therefore, the controller needs first to select a target AFR. The proper AFR is chosen by a selector according to the analysis of the car engine running condition.

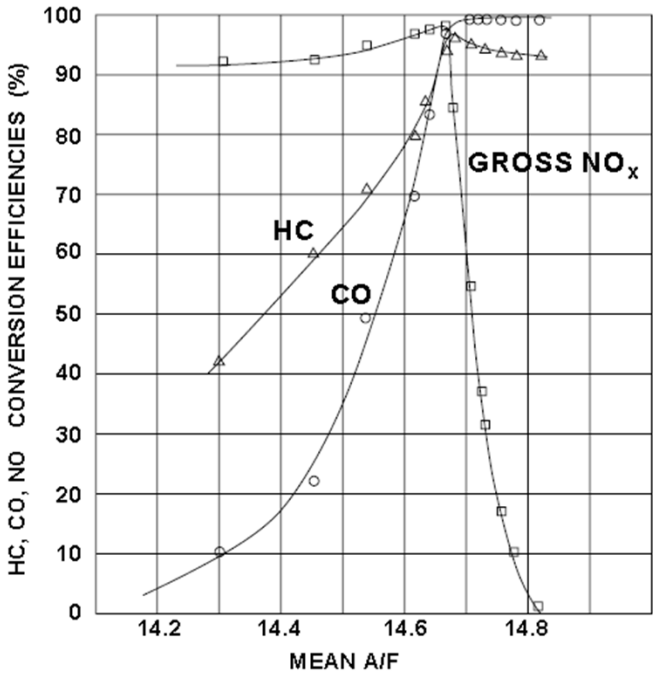

Figure 2.15: Typical Three-Way Catalytic Converter Efficiency Curves (Stefanopoulou, 1996)

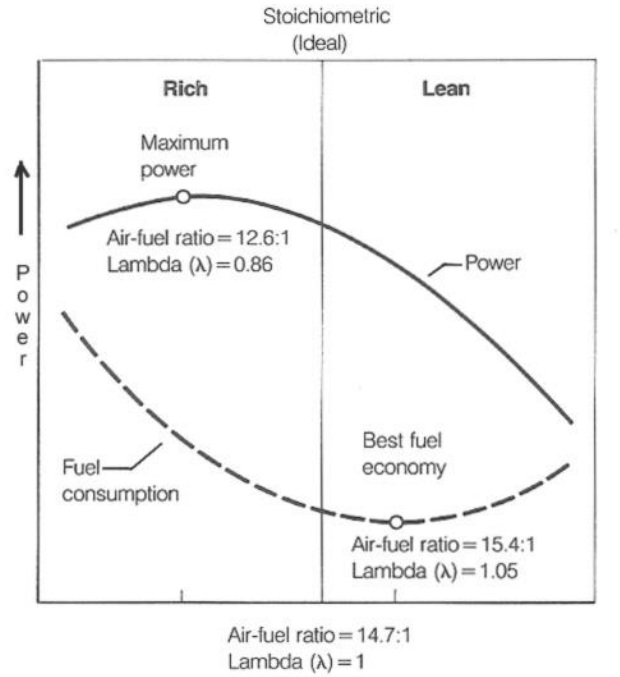

Figure 2.16: The Curve of AFRs against Power (Barry, 1998)

Once the AFR is determined fuel can be injected according to the amount of the engine's air intake. There are many ways to measure air intake volume, such as by an air flow meter directly or calculate the amount per cycle based on the engine speed and the pressure of the air intake pipe. In steady working conditions the air intake volume can determined from the look up table and information from combustion sensors and AFRs. However, when the engine is running in its transitory conditions such as speed and load are changing, the expected air amount can be measured by sensors. Meanwhile, PID feedback through switch type oxygen sensors control the fuel amount into the cylinder. Nevertheless, excessive conditions influence the AFR due to the following reasons.

(1) The intake charge/discharge effect: The engine intake manifold is a body with volume and gas filling or discharging process requires a certain amount of time. When the engine is in transition conditions its engine throttle open completely, so there will be a "charging and discharging effect". For example, when the engine throttle angle is small the internal gas manifold pressure decreases more slowly because the execution time of the throttle angle movement is much shorter than the time required for internal gas manifold stability. In this case, there is still high pressure for the gas cylinder filling and the air volume through the throttle must be less than the actual amount of air into the cylinder. The intake air quantity is measured near the throttle because it is difficult to obtain at the engine intake manifold, and hence the actual air flow and the measured one are different, causing the AFR control error. Conversely, the "charging and discharging effect" can happen at the moment when the throttle angle is changing bigger.

(2) Dynamic effects of oil film: In the process of fuel injection outside of the gasoline engine cylinder a layer of oil film can be found in the air intake pipe, airway and the back of the intake valve. The oil film likes a "capacitor", causing different amount of fuel into the oil film and oil film evaporation at the time of throttle angle changes. This leads to the difference between the quantity of the fuel injected by the fuel injector and the volume of the fuel into the cylinder, and the deviation for the purpose of AFR control.

(3) Delay of sensor signals and ECU calculations: Sensor signals collected from ECU are analysed and calculated to find out whether the injector injected fuel or not, and this process requires a certain amount of time. Injected fuel starts to combust in the cylinder

and until combustion waste is transmitted to the exhaust pipe the oxidation sensor cannot detect the AFR; meanwhile, the sensor itself has some time lag. Consequently, the signal produced by the oxidation sensor is not the best for current signal detection, e.g. there is a certain lag.

Owning to issues existing in the above processes for air fuel ratio control various strategies and methods can only improve the control precision no matter which theory they are based on, whether the classical control theory, modern control theory or intelligent control theory. Following better theoretical knowledge of engine these control strategies and methods need to be improved continuously to realize high precise control which will lead to engine emission control. Therefore, the development of better AFR control system is another main objective for this research.

2.7.3 Overview of AFR Control Methods

There are wide ranges of literatures which deal with AFR control systems. Because of the advances of modern control theory and intelligent control, the AFR control accuracy and system robustness is enhanced. There are many control methods being used for control AFR, such as: PID, PID-Fuzzy control, an adaptive control, predictive control, sliding mode control, switching frequency control and so on, some control methods are based on NN.

Observer-based air/fuel control method was proposed by Chang et al (1995), Powell et al (1998) and Choi et al (1998). In addition, sliding mode control method has present by Won et al (1998), Pieper et al (1999), Souder et al (2004). Choi et al (1994) have conducted observer-based sliding mode control and a Gaussian NN AFR controller, and it is shorter settling than the conventional sliding mode control. Also with the new controller the time consuming gain tuning process can be avoided.

Guzzella et al (1997) have developed a feedback linearization robust controller. The main drawbacks of their approach are a lack of robustness against noisy measurements and the time delay introduced by the lambda sensor. A nonlinear feedforward controller was explored by Guzzella (1995). Meyer et al (2012) uses air-to-fuel ratio switching frequency control for SI engine AFR, and it reduces the output errors from 1.6% to 0.9%.

Ebrahimi et al (2011) proposed a parameter-varying filtered PID control strategy for air–fuel ratio control in spark ignition engines. The control strategy exhibited excellent performance and can be used for the lean-burn engine as well, in the same year, Gao et al. (2011) reduced the AFR of coal-bed gas engine from 8.02% to 2.32% which based on fuzzy PID control. Jansri et al (2012) increased 10% AFR control performance by using Enhanced model and fuzzy strategy of air to fuel ratio control. Further, Ghaffari et al (2008) have proposed PID-fuzzy control scheme for AFR control, and it gives better results in comparison to PID controller.

Wang et al (2006) have investigated the effectiveness and feasibility of Adaptive neural network (NN) model based predictive control for AFR of Spark-Ignition engines. A new approach for engine control is proposed by Liu et al (2008), which is an implementation of adaptive critic designs for self-learning control of SI engines. The design is based on NN learning using approximate dynamic programming. The control results have demonstrated that controller is a powerful alternative approach for engine control. Successful adaptive control approaches are also presented in by Ault et al. (1994), Turin & Geering (1995), Jones et al. (1995), Rupp, Onder & Guzzella (2008), Rupp (2009), and Kovalenko, Liu & Javaherian, (2004). The adaptive posicast control is a recently developed control design approach that is especially suitable for plants with large time-delays and parametric uncertainties (Niculescu & Annaswamy, 2003, Yildiz et al., 2010).

Alippi et al (1998) studied the identification of an engine dynamic system with neural networks to estimate the AFR, and the identified neural model has a single hidden layer of 15 hidden neurons. The identified neural model is used as a reference model for predictive control the AFR. The model reference predictive controller reduces AFR error by 75%, but controller needs more time to stabilize AFR. Saraswati et al (2010) optimized the neural networks algorithm. Their results presented that by using multiple ARX model based AFR predictive control deviations of AFR comes approximately in the range of 0.96 to 1.1, whereas using the Optimization Algorithm lies in the range of 0.96 to 1.036. Zhai et al (2010) investigated engine modelling with the diagonal recurrent NN and proposed such a model-based predictive control for AFR. The diagonal recurrent NN model was made adaptive on-line to deal with engine time varying dynamics; therefore the control robustness performance was greatly enhanced.

Takahashi et al (1995) used state estimation and using dynamic models prediction to control the AFR control in gasoline engines. Compared with the conventional method the HC, CO and NO_x in the exhaust emissions is reduced by 15%, l0%, and 35%, respectively, and the AFR control error is reduced by about 50%. Muske (2006) have presented good performance over a wide range of SI engine operation AFR control using an analytical model-predictive controller for SI engine AFR. In 2011, Abdi et al (2011) published spark injection engines AFR control using model predictive control method, and the reference model based on NN. In fact, the robustness of this method against the error estimation of parameters is considerably high.

Tomforde et al (1995) presented a model-based control for the AFR, the controller is designed by using the linear quadratic regulators algorithm which use the oxygen storage states model to predict the desired values. The measurements revealed a good control quality and integral of the absolute value of AFR deviations has been reduced by almost 45% compared to a commonly used PI-controller. Ohata et al (1995) have used linear quadratic regulators algorithm AFR control to reduce more than 5% control error. Success of using adaptive linear quadratic regulators control approaches are presented also in references (Onder & Geering, 1993).

Wong et al (2012) used AFR model predictive control on real engine. Sequential Relevance Vector Machine Model Predictive control can effectively reduce the lambda deviation and overshoot from target lambda value up to 62% and 67%, respectively. Hou et al (2008) have controlled the AFR error at 2% by predictive controller which is based on adaptive expand particle swarm optimization. Model predictive controllers also are mentioned by Poloni et al (2007). The use of an electronic throttle as an additional control actuator (Chang et al., 1993) or secondary/port throttles (Stefanopoulou, Grizzle & Freudenberg, 1994) has been also explored, which can provide more variables for model predictive control in the future.

From the perspective of AFR control methods we can summarise that AFR control is changing from traditional error analysing control methods to modern and intelligent control methods. More and more predictive control methods have been used for engine AFR control, meanwhile, there are many controllers and model identifications based on the NN. However, these control methods still have the following problems: (1) Some of

the controller developers are the expert in control fields or mathematics, they concentrate on research on control error analysis and control logic to optimize control performance, but they do not focus on the physical and mechanical analysis of error causes. (2) The engine dynamics system is complex nonlinear system, traditional mathematical methods cannot obtain accurate identification model, and therefore the reference model of model predictive controller accuracy is not high. (3) There are many controllers employing the fuel film dynamic equation as compensation strategies or predictive model, but due to lots of integral and differential used in the fuel film dynamic equation, the inverse equation or inverse model is very difficult to correct performance of the fuel film dynamics, so these controllers cannot effectively reduce the control error. Based on the above shortcomings it is pertinent to design an AFR controller that can inherit advantages and avoid disadvantages, realising the AFR control more precisely.

2.8 Summary

This chapter firstly introduces engine related simulation software that includes methods and components of simulation and proves both the feasibility of engine simulations using MATLAB and the possibility of applying a simulation module to research on engine control. By analyzing the different kinds of MATLAB and SIMULINK based engine simulation model for the purpose of testing AFR control objective, it is concluded that existing engine simulation models cannot support capabilities required. A new engine simulation platform will be developed in this research and this platform ensures better simulation results and flexibilities by taking advantages of all reviewed models with some necessary modifications. Through the review of the AFR control methods, one can see that all the control methods are based on the target error analysis. They don’t explore in-depth understanding of the causes of deviation of the controlled system. Numerical based analysis can result in unpredictable instability no matter how good the controller is. The shortcomings of those methods suggest us to try to think differently. The new control method should look at the analysis of error causes. By a combination of target error analysis and error cause analysis, better control performances can be achieved.

Chapter 3: Mathematical Modelling of Engine Dynamics for Simulation

3.1 Introduction

In order to investigate the engine performance and to develop the engine control methods, a simulation package for engine dynamics and control systems needs to be developed. The package must be able to simulate a wide range of operation conditions, and guarantee its accuracy over wide operation testing conditions. The mathematical model of a specific plant can be obtained from physical laws or observations of input to output relations. Even though the model is derived from physical principles, the experimental tuning process of model parameters is always needed. Thus the modelling methodology should be selected carefully with respect to the objectives of the modelling. Fig 3.1 shows the engine simulation structure, each part will be studied for its working principle and mathematical formulas. Reasonable organization of mathematical formulas for the simulation model will then be discussed.

In Spark-Ignition engines the air and fuel are usually mixed together in the intake system prior to entering the engine cylinder (Heywood, 1998). Combustion of the air and fuel mixture in the cylinder generates high pressure gas to push the connecting rod to produce torque. The mix ambient air and heated air are used to control the air temperature which flow into the intake system. In order to ensure the reliable combustion in cylinder the ratio of air mass flow rate to fuel mass flow rate must be held approximately around 14.7. Fuel injection into the intake manifold or inlet port is an increasingly common alternative to a carburettor (Heywood, 1998). With port injection, fuel is injected through individual injectors from fuel supply system into each intake port. The engine system can be divided into three parts: air flow system, fuel flow system and torque generation system. In this investigation, the engine operation is simply summarized using a structure shown in Fig 3.1 Air flow through throttle body and into intake manifold enters into engine cylinder, at the same time fuel has been injected into engine cylinder. Spark plum ignite the air/fuel mixture to combustion.

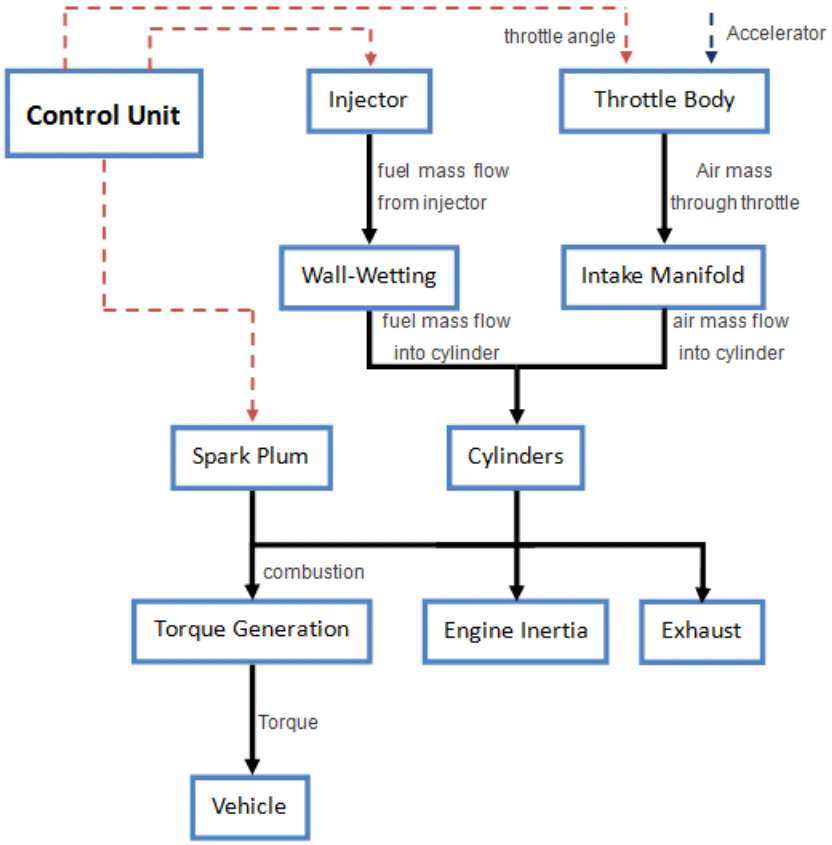

Figure 3.1: Engine Operation Structure

Following previous discussion and Fig 3.1, the engine operation is divided into five major mathematical modules which are: throttle body model, intake manifold dynamic model, fuel delivery model, torque production model and engine rotational dynamics. Each engine operation event and the signal delivery are strictly adhered to real engine operation, so there is a data delay between each event or signal block is introduced. This chapter is organized as follows: Section 3.2 introduces the throttle body model, Section 3.3 discusses about intake manifold dynamic formula, Section 3.4 introduces the fuel delivery model, Section 3.5 is the torque production, Section 3.6 presents the engine rotational dynamics, Section 3.7 discusses about transport delay between engine events and sensor signal, followed by the summary in Section 3.8.

3.2 Throttle Body Model

The function of a throttle body is to restrict and throttle the air flow into the engine to control the torque output. The flow of air through a throttle valve can be considered as a special case of the isentropic flow of compressible fluid (Hendricks & Sorenson, 1991). The throttle body model is based on the one-dimensional isentropic compressible flow

equation for flow across an orifice. The mass air flow rate through the throttle including the discharge coefficient can be written as below (Heywood, 1988; Guzzella & Onder, 2010).

$$\dot{m}_{at} = \begin{cases} C_d A(\theta) \dfrac{\rho_0}{\sqrt{RT_0}} \left(\dfrac{\rho}{\rho_0}\right)^{\frac{1}{k}} \left\{ \dfrac{2k}{k-1} \left[1 - \left(\dfrac{\rho}{\rho_0}\right)^{\frac{k-1}{k}} \right] \right\}^{\frac{1}{2}} & \dfrac{\rho}{\rho_0} > \left(\dfrac{2}{k+1}\right)^{\frac{k}{k-1}} \\ C_d A(\theta) \dfrac{\rho_0}{\sqrt{RT_0}} k^{\frac{1}{2}} \left(\dfrac{2}{k+1}\right)^{\frac{k}{2(k-1)}} & \dfrac{\rho}{\rho_0} \leq \left(\dfrac{2}{k+1}\right)^{\frac{k}{k-1}} \end{cases} \tag{3.1}$$

where:

$\dot{m}_{at}$	Air mass flow rate through throttle valve	[g/sec]
C_d	Discharge coefficient	---
$A(\theta)$	Cross-sectional area of throttle opening	[m^2]
ρ_0	Up-stream stagnation pressure	[kPa]
ρ	Throttle throat pressure	[kPa]
T_0	Up-stream stagnation temperature	[K]
R	Ideal gas constant for air	287×10^{-5} [bar $\cdot \frac{m^3}{kg} \cdot$ K]
k	Ratio of specific heat	---

In the above equation the minimum throttle intake area of $A(\theta)$ corresponding to the export pressure increased value can be ignored (Harrington & Bolt, 1970), and the intake manifold pressure can be approximated by taking the value of the plenum pressure. From the discharge coefficient it can be seen that the throttle is not the real one-dimensional orifice, the discharge coefficient is a nonlinear function of the throttle angle and throttle pressure (Heywood, 1988). The steady-state flow tests show that these two factors are independent of engine operating conditions (Guzzella & Onder, 2010). The cross-sectional area of the throttle body is a nonlinear function of the throat diameter. The throttle rod diameter will affect cross-sectional area of the throttle body when the throttle opening angle is at big position. The cross-sectional area of throttle opening is represented by equation as below (Harrington & Bolt, 1970; Guzzella & Onder, 2010).

$$A(\theta) = -\frac{dD}{2}\left[1-\left(\frac{d}{D}\right)^2\right]^{\frac{1}{2}} + \frac{dD}{2}\left[1-\left(\frac{d}{D}\frac{cos\,\theta_0}{cos(\theta_0+\theta)}\right)^2\right]^{\frac{1}{2}}$$
$$+\frac{D^2}{2}sin^{-1}\left\{\left[1-\left(\frac{d}{D}\right)^2\right]^{\frac{1}{2}}\right\}$$
$$-\frac{D^2}{2}\frac{cos(\theta_0+\theta)}{cos\,\theta_0}sin^{-1}\left\{\left[1-\left(\frac{d}{D}\frac{cos\,\theta_0}{cos(\theta_0+\theta)}\right)^2\right]^{\frac{1}{2}}\right\} \quad (3.2)$$

where:

d	Throttle shaft diameter	[m]
D	Throttle bore diameter	[m]
θ	Throttle open angle	[deg]
θ_0	Angle for minimum leakage area	[deg]

When the throttle opening cannot increase its effective area or ($\theta \geq cos^{-1}\left(\frac{d}{D} - cos\,\theta_0\right) - \theta_0$), the cross-sectional area of throttle opening is represented by equation as below (Harrington & Bolt, 1970).

$$A(\theta) = \frac{D^2}{2}sin^{-1}\left\{\left[1-\left(\frac{d}{D}\right)^2\right]^{\frac{1}{2}}\right\} - \frac{dD}{2}\left[1-\left(\frac{d}{D}\right)^2\right]^{\frac{1}{2}} \quad (3.3)$$

At the small throttle opening, there is an error between the ideal cross-sectional area and the actual area due to machining variation (Carpenter & Ramos, 1985), the minimal leak area of empirical data can be obtained by a large number of experiments, the error correction for this can be written by $cos(0.91\theta_0 - 2.59)$ instead of $cos\,\theta_0$.

Once the upstream stagnation pressure and temperature are determined, the flow through the throttle is a function of the air mass flow rate, the throttle valve and cross-sectional area of throttle opening. Stagnation pressure and stagnation temperature change may significantly alter the flow through the throttle Body. Accordingly, it can be written by three normalized functions as (Yoon, Park & Sunwoo, 2000):

$$\dot{m}_{at} = C_d \cdot \dot{M}A \cdot TC \cdot PRI \quad (3.4)$$

Where the maximum possible air flow through the throttle body (MA) is given by.

$$MA = \frac{\rho_0}{\sqrt{RT_0}} C_{d1}(\theta_{max}) A(\theta_{max}) C_{d2}(0) \left(\frac{2}{k+1}\right)^{\frac{k+1}{2(k-1)}} \tag{3.5}$$

Where TC (the normalized flow as a function of the cross-sectional area) is determined as:

$$TC = \frac{C_{d1}(\theta) A(\theta)}{C_{d1}(\theta_{max}) A(\theta_{max})} \tag{3.6}$$

And, PRI (the normalized flow as a function of pressure ratio) is calculated using

$$PRI = \begin{cases} \frac{C_{d2}\left(\frac{\rho}{\rho_0}\right)}{C_{d2}(0)} \left(\frac{\rho}{\rho_0}\right)^{\frac{1}{k}} \left(\frac{2}{k+1}\right)^{\frac{k}{2(k-1)}} \left\{\frac{2k}{k-1}\left[1 - \left(\frac{\rho}{\rho_0}\right)\right]^{\frac{k-1}{k}}\right\}^{\frac{1}{2}} & \frac{\rho}{\rho_0} > \left(\frac{2}{k+1}\right)^{\frac{k}{k-1}} \\ \frac{C_{d2}\left(\frac{\rho}{\rho_0}\right)}{C_{d2}(0)} & \frac{\rho}{\rho_0} \leq \left(\frac{2}{k+1}\right)^{\frac{k}{k-1}} \end{cases} \tag{3.7}$$

$$C_d = C_{d1} + C_{d2} \tag{3.8}$$

where:

C_{d1}	Coefficient of the throttle angle	---
C_{d2}	Coefficient of the pressure ratio across the throttle.	---
$A(\theta_{max})$	Maximum cross-sectional area of throttle opening	[m^2]

On most fuel injected engines used in modern throttle bodies, there is a small air by-pass of the throttle plate. In this passage there is a valve which controls the cross-sectional area of this passage, and limits the air flow through the bypass. This by-pass and valve is known as the idle air control. Idle speed controls the mass air flow rate through the throttle (Guzzella & Onder, 2010).

$$\dot{m}_{IAC} = \begin{cases} \dot{m_{cal}} \frac{T_0|_{cal}}{T_0} \frac{\rho_0}{\rho_0|_{cal}} \frac{\left(\frac{\rho}{\rho_0}\right)^{\frac{1}{k}} \left\{\frac{2k}{k-1}\left[1 - \left(\frac{\rho}{\rho_0}\right)\right]^{\frac{k-1}{k}}\right\}^{\frac{1}{2}}}{0.667} & \frac{\rho}{\rho_0} > \left(\frac{2}{k+1}\right)^{\frac{k}{k-1}} \\ \dot{m_{cal}} \frac{T_0|_{cal}}{T_0} \frac{\rho_0}{\rho_0|_{cal}} & \frac{\rho}{\rho_0} \leq \left(\frac{2}{k+1}\right)^{\frac{k}{k-1}} \end{cases}$$

(3.9)

where:

m_{IAC}	Idle air mass flow rate into the cylinder	[kg/s]
m_{cal}	Idle air mass flow rate through the throttle	[kg/s]
$T_0\|_{cal}$	Idle air temperature	[K]
$\rho_0\|_{cal}$	Idle air pressure	[bar]

3.3 Intake Manifold Dynamics

In this section a physical insight into the intake manifold fuel dynamics is given through the description of the mean value model. Mean value model is a dynamic model which describes dynamic engine variable (or state) responses as mean rather than instantaneous values on time scales slightly longer than an engine event.

The conservation of air mass in the intake manifold equation is (Hendricks et al., 1996):

$$\dot{m_{at}} = \dot{m_{at}} - \dot{m_{ap}} \tag{3.10}$$

Where

$\dot{m_{at}}$	Air mass flow in intake manifold	[kg/s]
$\dot{m_{ap}}$	Air mass flow into intake port	[kg/s]

The differential form of the air mass in the intake manifold equation is:

$$\dot{m_{at}} = \frac{d}{dt}\left(\frac{P_m V_M}{R T_M}\right) \tag{3.11}$$

Where

P_m	Intake manifold air pressure	[bar]
V_M	Manifold and port passage volume	$[m^3]$
R	Gas constant	$[287 \times 10^{-5}\ \text{bar} \cdot \text{m}^3/\text{kg} \cdot \text{K}]$
T_m	Intake manifold air temperature	[K]

For the derivation of the manifold pressure state equation, the common procedure is to use the conservation of air mass in the intake manifold and differential of the ideal law to derive the equation (Hendricks et al., 1996).

$$\dot{P}_m = \frac{RT_m}{V_m}\left(\dot{m}_{at} - \dot{m}_{ap}\right) + P_m\left(\frac{\dot{T}_m}{T_m}\right) \tag{3.12}$$

Because heat transfer in the intake manifold system is small for nearly all important operational modes due to the relative intake manifold pressure time changes are much larger than the relative intake manifold temperature time changes. Thus the manifold pressure state equation can be approximately written as:

$$\dot{P}_m \approx \frac{RT_m}{V_m}\left(\dot{m}_{at} - \dot{m}_{ap}\right) \tag{3.13}$$

The air mass flow passes the throttle plate can be obtained from throttle model. In general, the port air mass flow is a mainly a function of the crank shaft speed and the intake manifold pressure, this function is an algebraic function because the equilibrium of the air mass flow is within a few millisecond and this time is for the most part much less than the time scale on which the crank shaft speed can change (a few second). The mass airflow out of the intake manifold is represented by a well-known speed density algorithm. In a four stroke and four cylinder engines, this relationship can be written as (Hendricks et al., 1996):

$$\dot{m}_{ap} = \frac{V_D}{120RT_m}\eta_{vol}P_m N \tag{3.14}$$

where:

V_m	Engine volume	$[m^3]$
η_{vol}	Volumetric efficiency	---
N	Engine speed	[RPM]

Apart from constants, the speed density relationship is represented by $\eta_{vol}P_{man}N$ and the value in the parenthesis, $\eta_{vol}P_{man}$ is proportional to the actual air charge pre stroke (Bayraktar & Durgun, 2003). This quantity $\eta_{vol}P_{man}$ can be called as the normalized engine air charge.

$$m_{an} = \eta_{vol}P_m \tag{3.15}$$

where:

m_{an}	Air mass flow charge pre stroke	[kg/s]

In order to use Eq (3.15), it is necessary to obtain an expression for the volumetric efficiency in terms of the crank shaft speed and the manifold pressure. This can be done by integrating the P-V diagram of Spark Ignition engine during the pumping cycle. The expression obtained is (Hendricks et al., 1996):

$$\eta_{vol} P_m = s_m P_m - y_m \tag{3.16}$$

where:

s_m	Physical constant	---
y_m	Physical constant	---

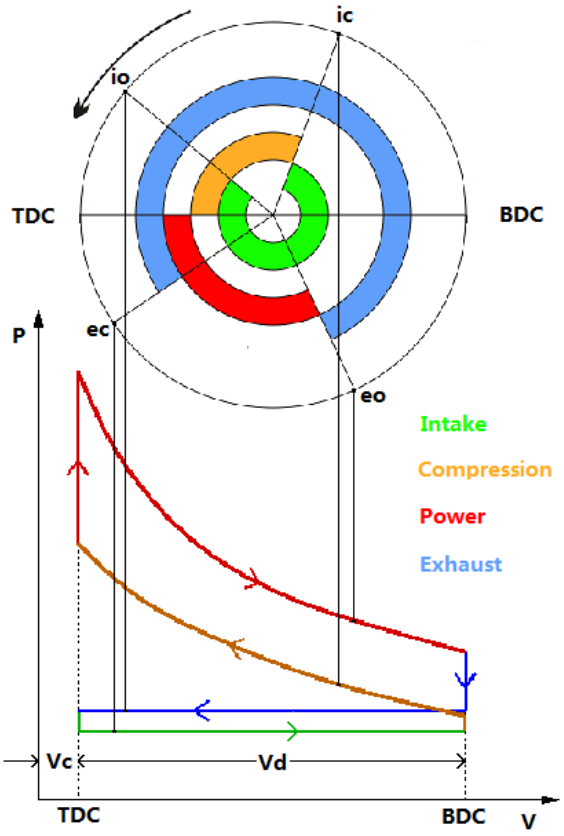

Figure 3.2: Engine Four-stroke cycle P-V Diagram

where:

eo	Exhaust valve open	---
ec	Exhaust valve close	---
io	Intake valve open	---
ic	Intake valve close	---
TDC	Top Dead Center	---
BDC	Bottom Dead Center	---
Vc	Clearance volume	[m^3]
Vd	Displaced cylinder volume	[m^3]

In order to derive a physical expression for a volumetric efficiency, it is more convenient into separate four cycle engine equations. The top of Fig 3.2 is the four-stroke cycle table, under which is the idealized four-stroke Otto cycle p-V diagram. Assume that the engine operation in ideal model, the exhaust pressure is bigger than intake pressure from exhaust valve closes between intake valve open. The intake manifold pressure falls immediately to cylinder when the intake valve open, and will keep the pressure until the intake valve close. In an actual engine cycle the exhaust valve closes after TDC and the intake valve open before TDC, thus there is a valve overlap. In this time the beginning back flow will into the intake manifold and follow to intake stroke, as the crank angle increases at power cycle, fresh air flows into the engine cylinder. So the intake process equation can be shown as (Hendricks et al., 1996).

$$\int_{io}^{ic} [M_{IN-OUT}]\, dt = \int_{io}^{ec} [M_{IN-OUT}]\, dt + \int_{ec}^{is} [M_{IN-OUT}]\, dt + \int_{is}^{ic} [M_{IN-OUT}]\, dt \tag{3.17}$$

where $M_{IN-OUT} = \left(\dot{m} c_p T\right)_{in} - \left(\dot{m} c_p T\right)_{out}$

where

in	Intake operation	---
out	Output operation	---
c_p	Heat capacity at constant pressure	[bar]
T	Temperature	[K]
is	Intake of fresh mixture starts	---
M	Air mass	[Kg]
IN-OUT	From intake to output pressing	---

During overlap the enthalpy flow into the cylinder from the exhaust port is balanced by the enthalpy flow from the cylinder to the intake manifold. The amount of enthalpy that flow into the cylinder from the exhaust port during the overlap period, since we can assume this gas returns prior to the start of induction. Hence, the volumetric efficiency of four-stroke engine in first law of thermodynamics applied to an open system doing only boundary work can be shown as:

$$P_{ic}V_{ic} - P_{io}V_{io} = (\kappa - 1)\left(-\int_{io}^{ic} P dV + \int_{io}^{ec} \left(\dot{m} C_p T\right)_{ov} dt \; + C_p T_i \int_{is}^{ic} \dot{m}_{in} dt + \int_{io}^{ic} \dot{Q} dt \right) \tag{3.18}$$

where:

P	Cylinder pressure	[bar]
V	Cylinder volume	[m^3]
κ	Ratio of the specific heats = 1.4	---
ov	during the overlap period	---
T_i	Intake manifold temperature	[K]
$\dot{m}_{in}$	Intake manifold air mass rate	[Kg/s]
Q	Mass of intake air	[Kg]

According to Eq (3.17) and Appendix 2, s_{man} and y_{man} finally be written as:

$$s_m = \left(\frac{1}{1+\frac{\Delta T}{T_i}}\right)\left(\frac{(\kappa-1)(r-1)}{\kappa(r-1)}t\right)P_m \tag{3.19}$$

$$y_m = \left(\frac{1}{1+\frac{\Delta T}{T_i}}\right)\left(\frac{P_e}{\kappa(r-1)} - \frac{(\kappa-1)}{\kappa}\frac{T_{ov}m_{ov}}{T_i V_d}\right) \tag{3.20}$$

where:

ΔT	Mean temperature rise of the intake air during the intake stroke	[K]
r	Compression ratio	--
P_e	Exhaust manifold pressure	[bar]
T_{ov}	Mean temperature during valve overlap	[K]
m_{ov}	Air mass lost during overlap	[Kg/s]

From Eqs (3.19) and (3.20), it can be found that s_m and y_m are constant value, if some of variables cannot be obtained experimentally, two constant values can be estimated using the mean value model principle.

3.4 Fuel Delivery Model

Fuel injection is a system for admitting fuel into an internal combustion engine. It has become the primary fuel delivery system used in automotive engines. When signalled by the engine control unit the fuel injector opens and sprays the pressurized fuel into the engine. Different injection modes affect the fuel mass into cylinder differently. Gasoline direct injection and port fuel injection are now mainstream injection modes. Gasoline direct injection is latest technology and is emulating the diesel engines injection modes. In some applications, gasoline direct injection enables stratified fuel charge (ultra lean

burn) combustion for improved fuel efficiency, and reduced emission levels at low load. Right now, SI engines mainly use port fuel injected injection engine, where the injector sprays gasoline in the intake tract or cylinder port, flowing into the cylinder afterwards the. There are various injection schemes as: single-point injection, continuous injection, multiport fuel injection and so on. Different injection modes and various injection schemes are described in more detail below.

3.4.1 Injection Dynamics

The duration and times that the injector opens (called the pulse width) is proportional to the amount of fuel delivered. Depending on the injection scheme, the timing of when injector opens is related to either each individual cylinder (for a sequential fuel injection system), or injectors for multiple cylinders that may be signalled to open at the same time (in a batch fire system). Therefore the injection dynamics equation can be written as:

$$m_{fi} = f\ (Injection\ Time, Injection\ Voltage, Pump\ Pressure) \tag{3.21}$$

3.4.2 Port Fuel Injected

"*One of the most important dynamic effects in the fuel path is caused by the Wall-Wetting phenomena*." (Guzzella & Onder, 2010, P53). In the surface of intake port wall and back face of the intake valve some fuel will be absorbed, and the absorbed fuel will enter the cylinder in the next intake stroke. Therefore, the fuel mass injected and the fuel mass into the cylinder can be balanced as follow (Hendricks & Sorenson, 1991):

$$\dot{m}_{ic} = (1 - \kappa_c)\dot{m}_{ii} + \frac{m_{wf}}{\tau} \tag{3.22}$$

$$m_{wf} = \kappa_c \dot{m}_{ii} - \frac{m_{wf}}{\tau}\Big|_{\Delta T} \tag{3.23}$$

where

m_{ic}	the fuel mass flow into the cylinder	[Kg/s]
m_{ii}	the fuel mass flow from injector	[Kg/s]
m_{wf}	The fuel film mass flow	[Kg/s]

κ_c	Coefficients (percentage of fuel from injector and adsorbed fuel)	---
τ	Coefficients (rate of fuel film mass change until next stroke)	---
ΔT	Time delay for each intake stroke	[K]
κ *and* τ	depend on the engine speed, fuel temperature, load and so on	

As provided in Eqs (3.22) & (3.23), $(1-\kappa)\dot{m}_{ii}$ is the mass of fuel evaporates from all droplets, and m_{wf}/τ is the mass of fuel evaporating from the wall film. The two evaporation processes are based on the theory with well-known thermodynamic analogies, the fuel mass flow resulting from the evaporation process is given by (Guzzella & Onder, 2010):

$$\dot{m}_{EV} = h_m \rho_f A_f ln(1+B) \tag{3.24}$$

Where

h_m	Mass transfer coefficient	---
ρ_f	The density of the liquid fuel	[kg/m^3]
A_f	The area of the surface on which the evaporation takes place	[m^3]
B	Spalding number	---

The Spalding number describes the evaporation properties of the liquid. The mass transfer coefficient must be calculated with thermodynamic analogies as $(S_h \cdot D_{AB})/d$. S_h is the Sherwood number, D_{AB} is the diffusivity coefficient and d is droplet diameter. Thus, the equation can be (Guzzella & Onder, 2010):

$$\dot{m}_{EV} = \frac{D_{AB}\rho_f A_f}{d} S_h ln(1+B) \tag{3.25}$$

Droplet evaporation is the difference between the injected mass and the mass flow that evaporates from the droplet while airborne. The volume balance for one single droplet can be calculated as $\frac{d}{dt}V_D = \frac{1}{2}\pi d_D^2 \frac{d}{dt} d_D$. According to the equation of area of circle, and combining Eq (3.25), the mass of evaporated fuel can easily be calculated as (Guzzella & Onder, 2010):

$$(1-\kappa)m_{ii} = \frac{1}{2} D_{AB}\rho_f \pi d_D S_{hD} ln(1+B) \tag{3.26}$$

To calculate the total mass of evaporated fuel due to droplet evaporation for one injection pulse, the differential equation for the evaporation must be integrated over an interval which starts with the beginning of the injection pulse and ends with the closing of the intake valve. Combining Eq (3.26) with one injection pulse, the coefficients of rate of fuel film mass change until next stroke can be defined as (Guzzella & Onder, 2010):

$$\kappa = 1 - \left[\frac{1}{2}\mathrm{D_{AB}}\rho_{\mathrm{f}}\pi\mathrm{d_D}\mathrm{S_{hD}}\ln(1+\mathrm{B})\right] \Big/ \left(\int_{t_{is}}^{t_{IVC}} m_{ii}\right) \tag{3.27}$$

Where

t_{IVC}	Inlet-valve closing timing	[s]
t_{is}	Spark ignition timing	[s]

The change of the mass of fuel on the manifold wall can be expressed as the amount of fuel impinging on the walls minus the amount of fuel evaporating from the walls. There are many approaches that describe the geometry of the wall film evaporation (Yoon, Park & Sunwoo, 2000). One solution is to represent it by a cylindrical ring of fuel around the intake valve with thickness and height as proposed by (Guzzella & Onder, 2010). The height (h_F) is the actual state variable of the wall film, whereas the thickness (d_F) is a parameter which varies slowly depending on the wall temperature, thus the wall film area can be assuming $A_F = \pi d_F h_F$. Combining Eq 3.25 with A_F, the mass change of fuel evaporating from the wall film can then be described as (Guzzella & Onder, 2010):

$$\frac{m_{wf}}{\tau} = \frac{\rho_{fvs} A_F}{d_F} D_{AB} Sh_F ln(1+B) = \rho_{fvs} \pi h_F D_{AB} Sh_F ln(1+B) \tag{3.28}$$

By utilizing the assumption $\rho_f = 2\rho_{fvs}$ (Guzzella & Onder, 2010) in Eq (3.28), the mass of fuel in the wall film is defined as (Guzzella & Onder, 2010):

$$m_{wf} = 2\rho_{fvs}\pi d_F \delta_{th} h_F \tag{3.29}$$

By substituting Eq (3.29) into Eq (3.28) the coefficients of fuel film mass change is found as (Guzzella & Onder, 2010):

$$\frac{1}{\tau} = \frac{D_{AB} Sh_F ln(1+B)}{2 d_F \delta_{th}} \tag{3.30}$$

3.4.3 Gasoline Direct Injection (GDI)

The gasoline is highly pressurized, and injected via a common rail fuel line directly into the combustion chamber of each cylinder. Because of its mechanical structure, the wall wetting effect is not present in gasoline direct injection engines. The mass of fuel from the injector will immediately enter into cylinder by GDI controller. Thus it can be assumed that the mass of fuel from the injector is equal to that into the cylinder.

3.5 Torque Production Model (Yoon, Park & Sunwoo, 2000)

The combustion process in the cylinder is to produce engine torque, and the torque produced is influenced by the mass of air and fuel into the cylinder, spark timing, and combustion efficiency. In the literature review, torque production is assumed to be the dynamic, e.g. torque of the engine is a function of engine speed, air charge, spark timing, and the AFR. Based on this assumption, the predictive torque production model is derived from the steady state engine experiments. The development of the torque production model objective is to achieve the identification of the optimal spark timing (MBT) and a wide range of AFRs at each of the operating conditions.

Actually, the indicated torque generated by the combustion of an in-cylinder mixture, is reduced by engine friction and pumping loss. The brake torque is equal to indicated torque subtract the friction and pumping loss (as Eq (3.31)). The indicated torque will be introduced first here, and then friction and pumping torque are presented.

$$T_{brake} = T_i - T_{f\,\&\,p} \tag{3.31}$$

where:

T_{brake}	Brake torque	[Nm]
T_i	Indicated torque	[Nm]
$T_{f\,\&\,p}$	Friction and pumping torque	[Nm]

3.5.1 Indicated Torque

The best ignition time and ideal air inflow (air fuel ratio = 14.7) can normaly be estimated using the maximum torque under ideal state. However in actual operate conditions, the maximum possible torque will be reduced by two factors. The first one is an AFR influence. Because of the response speed of air/fuel control system and lean combustion system, the actual air fuel ratio cannot be kept on 14.7. Thus the AFR influence function represents the decreased torque when there is not enough fuel to utilize all of the air in the cylinder, or if there is insufficient air to burn all of the fuel. In the extreme case, it represents lean burn limits and decreases in torque at rich mixtures. This is an empirically determined function derived from fuel perturbation data. The second influence is the spark advance timing. The actual spark timing could not all the time stay MBT spark timing because of the engine knock problems. Therefore, the spark advance timing influence function decreases the indicated torque as a function of how far the spark is advanced from the MBT spark timing. To sum up, the indicated torque at an arbitrary engine condition is obtained from Eq (3.32), which is multiplied by the efficiencies of the spark timing and the AFR, both of which reflect the changed operation conditions.

$$T_i = T_{ideal} \cdot I_{\Delta SA} \cdot I_{a/f} \tag{3.32}$$

where:

T_{ideal}	Indicated torque in ideal condition	[Nm]
$I_{\Delta SA}$	Sparking timing influence	---
$I_{a/f}$	Air/fuel ratio influenc	---

If AFR and sparking are fixed, the indicated torque of an engine is a function of engine speed and air charge. Therefore the indicated torque at MBT and the stoichiometric AFR can be represented by (Hendricks & Sorenson, 1991):

$$T_{ideal} = ti_1 + ti_2 n + ti_3 n^2 + (ti_4 + ti_5 n) m_{ac} \tag{3.33}$$

where:

ti_*	Assumed Indicated torque in ideal condition function parameters

3.5.2 Spark Influence

The sparking timing influence can be assumed as a function of the difference of spark timing between the MBT at an arbitrary AFR condition and spark timing at the current operation. The functions are shown below (Hendricks & Sorenson, 1991):

$$I_{\Delta SA} = is_1 + is_2(\Delta SA) + is_3(\Delta SA)^2 \tag{3.34}$$

$$\Delta SA = MBT - SA \tag{3.35}$$

where

ΔSA	Difference of spark timing between the MBT	[s]
MBT	Optimal spark timing	[s]
SA	Spark timing	[s]
is_*	Assumed sparking timing influence function parameters	

MBT map is derived from test data, and is considered as a function of engine speed, mass of air into cylinder and AFR. When the AFR effect is not considered, the MBT at the stoichiometric AFR will be affected by various engine speed and air into cylinder.

$$MBT = m_1 + m_2 n + m_3 n^2 + (m_4 + m_5) m_{ac} \tag{3.36}$$

where:

m_*	Assumed MBT map parameters

After that, the identification of the MBT at various AFR conditions is shown in Eq 3.37. The difference between the MBT at the stoichiometric AFR and the MBT at an arbitrary AFR at various engine operating conditions is denoted by $\mathrm{MBT_{AFR}}$. Because only influence of AFR changes on MBT is considered the function can be assume based on AFR. Based upon research, the MBT at an arbitrary AFR can be represented below (Hendricks & Sorenson, 1991):

$$MBT_{AFR} = MBT + \Delta MBT_{AFR} \tag{3.37}$$

$$\Delta MBT_{AFR} = ma_1 + ma_2 \lambda + ma_3 \lambda^2 \tag{3.38}$$

where:

MBT_{AFR}	MBT consider AFR change	[s]
ΔMBT_{AFR}	MBT influence consider on AFR change	[s]
ma_*	Assumed MBT influence consider on AFR change parameters	

3.5.3 Air/Fuel Influence

The AFR influence is a normalized function that is developed empirically from perturbation of fuel supply rate data. The air/fuel influence function should contain the effect of reduced torque due to partial burns and misfires. Stoichiometry AFR is 14.7, and stoichiometry air/fuel influence can be easily calculate from the air/fuel analysis data. As the Fig 3.3 shows, if the AFR is either too high, or too low, it can cause the engine to stall. But considering engine control system performance and arithmetic logic, the air fuel ratio will be controllable probably between 10 and 20 (lambda between 0.8 and 1.3). The red dashed boxes in Fig 3.3 indicate that air fuel influence dictating the AFR is from 6 until 26. It can be found that black curve is very similar to green dotted curve, which is a quadratic curve. Thus AFR influence function is then assumed like quadratic equation shown below.

$$I_{a/f} = i_1 + i_2\lambda + i_3\lambda^2 \tag{3.39}$$

where:

i_*	Assumed Air/fuel influence function parameters

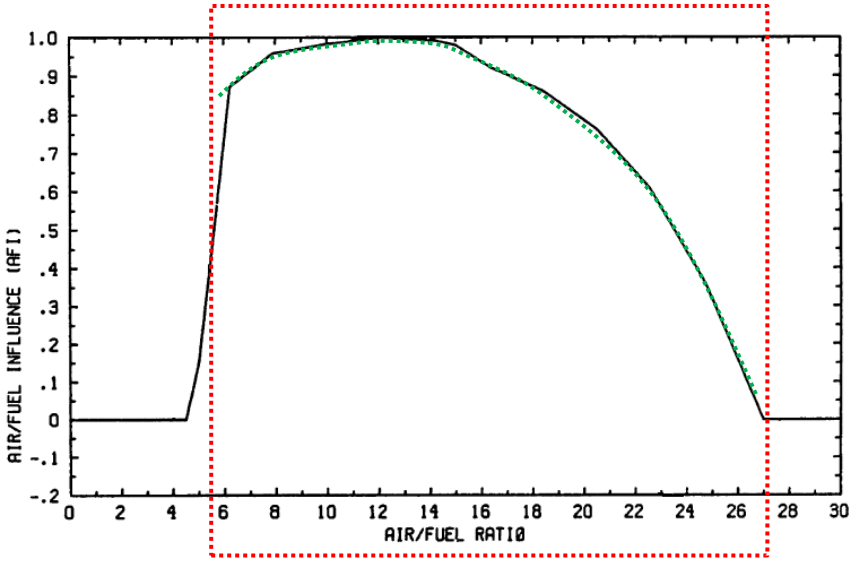

Figure 3.3: Air/fuel Influence on Indicated Torque (Chang, 1988)

3.5.4 Friction and Pumping Torque

For a transient engine speed condition, when the intake air charge density increases, friction and pumping torque will decrease at the same time. At high intake manifold pressure especially at high engine speeds, torque either becomes constant or begins to rise. For a constant engine speed condition, a decrease in pumping torque is expected as intake gas density increases since intake gas density and mass of air and fuel are proportional to intake manifold pressure. An increase in manifold pressure tends to decrease the pumping loop and lower pumping torque. The high speed increase in friction and pumping torque as mass of air per cylinder increases is unexpected. Taken together, results suggest that the friction and pumping loss is a function of the engine speed and intake manifold pressure (Meyer, 2007). Thus the friction and pumping torque can be approximated by a polynomial of engine speed and air charge as shown in below (Hendricks & Sorenson, 1991).

$$T_{f\,\&\,p}(t) = fp_1 + fp_2 n + fp_3 n^2 + (fp_4 + fp_5 n) m_{ac} \tag{3.40}$$

where:

fp_* Assumed friction and pumping torque function parameters

To summarize the torque production model proposed in this study, this model has four inputs (engine speed, air charge, fuel flow rate and spark timing), six subsystem models which are approximated by polynomials, and brake torque as the output. In order to provide the dynamic characteristics of the torque production model, three different transport delays based on different engine events will be introduced, and a detailed introduction will be given in section 3.7.

3.6 Engine Rotational Dynamics

The rotational dynamics of an engine is modelled under the assumption of a lumped parameter system with constant inertia. "*In an actual engine, the effective polar moment of inertia of the crankshaft, connecting rod, piston, and the valve mechanism change cyclically due to the varying geometry of the slider crank mechanism"*（Chang, 1988）. Under normal circumstances the torsional vibration damper is mounted on the crankshaft, damping any torque excited by the front end of the cylinder. The simplicity

goal of the engine model proposed in this study is the prediction of the mean value of each state variable, and the approximations stated previously can be regarded as reasonable assumptions (Yoon, Park & Sunwoo, 2000).

The fundamental law from which most rotational dynamics analyses begin is the second law formulated by Sir Isaac Newton (1642-1727) (Gillespie, 1992). The sum of the torques acting on a body about a given axis is equal to the product of its rotational moment of inertia and the rotational acceleration about that axis (Gillespie, 1992).

$$\sum T_x = I_x \cdot a_x = I_x \cdot \dot{\omega}_x \tag{3.41}$$

where:

T_x	Torques about the x-axis	[N]
I_x	Moment of inertia about the x-axis	[Nms^2]
a_x	Acceleration about the x-axis	[m/s^2]
ω_x	Engine speed	[RPM]

More exact estimation of engine speed requires the consideration of the mechanical system properties. Starting with the engine, the actual torque delivered to the production vehicle acceleration has to be reduced by the inertia of the rotating components which requires accelerating (Gillespie, 1992).

$$T_i(t) = T_{ideal} \cdot I_{\Delta SA} \cdot I_{a/f} \tag{3.42}$$

Thus using Newton's second Law, the state equation for engine speed base by sum of the torque is given by

$$T_{sum}(t) = T_i(t) - T_{f/p}(t) - T_L(t) - I_e \cdot \dot{\omega}_e \ = I_{eff} \cdot \dot{\omega}_e \tag{3.43}$$

Therefore, engine speed unit-conversion to revolutions per minute is

$$\omega_e = \frac{1}{I_{eff}} \cdot \int_{t_0}^{t_i} \sum_{i=1}^{n} T_{sum} dt + w_{e_0} \tag{3.44}$$

where:

ω_e	engine speed	[rev/ min]

T_{sum}	actual torque delivered to vehicle	[N]
T_L	Engine rotating torque	[N]
I_e	Engine rotational inertia	[Nms^2]
I_{eff}	Effective inertia	---

Engine speed base on the engine event is:

$$\omega_e \left[\frac{rev}{min}\right]\left[\frac{min}{60(s)}\right]\left[\frac{2\cdot\pi}{rev}\right] = \frac{1}{I_{eff}}\cdot\int_{t_0}^{t_i}\sum_{i=1}^{n} T_{sum}dt + w_{e_0} \tag{3.45}$$

$$\omega_e = \frac{1}{I_{eff}}\cdot\frac{30}{\pi}\cdot\int_{t_0}^{t_i}\sum_{i=1}^{n} T_{sum}dt + w_{e_0} \tag{3.46}$$

where:

t_i	Event end time	[s]
t_0	Event start time	[s]
w_{e_0}	Event start engine speed	[event/rev]

3.7 Transport Delay between Engine Events and Sensor Signals

In order to provide realistic dynamic characteristics of the torque production model, transport delays are necessary for each engine event. This approach is reasonable for real time control applications because the combustion process of the engine occurs much faster than the transport dynamics of air and fuel and also the use of mean value models. Moreover, the engine control is affected by sensor signal delays, sensor through the induction of a cylinder operating condition, and transport signal to ECU computing control signal delivered to next operation of a cylinder.

3.7.1 Engine Event Delay

The timing diagram (Fig 3.4) is used to show four stroke events occur time on four-stroke Otto cycle engine. The diagram is set on a vertical and horizontal axis. There are 360 degrees around the axis. At the top of the diagram, the piston would be located exactly at TDC (top dead center). Any event that happens before TDC is referred to as BTDC (before top dead center). Any event that happens after top dead center is called

ATDC. In the same way, at the bottom of the graph would illustrate the position of the piston at BDC (bottom dead center). During the complete four-stroke Otto cycle, the crankshaft revolvers two revolutions, inner and outer rings show the two revolutions respectively. Valve overlap is the condition when both the inlet and the exhaust valves are open at the same time during so many degrees of crankshaft rotation.

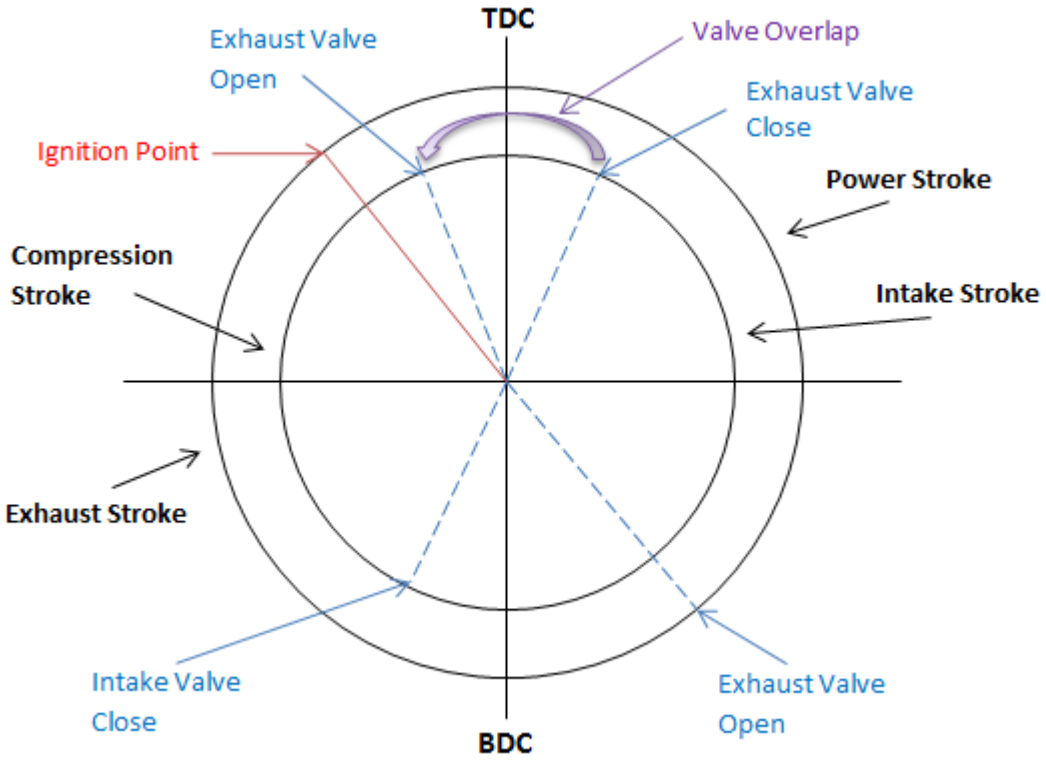

Figure 3.4: Engine Valve Timing Event (Guzzella & Onder, 2010)

The order of engine event operations is: (1) the intake stroke starts when the exhaust valve closes after TDC, (2) the intake valve remains open after BDC. (3) the compression stroke then starts and compresses the air/fuel mixture up to TDC. (4) the ignition varies but in this case, occurs before TDC. (5) the power stroke starts at TDC and continues until before BDC. (6) the exhaust valves start to open and the exhaust stroke ends before BDC, at which time the intake valve starts to open again.

The brake torque described in Eq (3.47), can be obtained by substituting Eq (3.35) into Eq (3.31). The brake torque equation has four factors: MBT indicated torque, sparking timing influence, air/fuel influence, friction and pumping torque function. According to the order of engine event operation and brake torque equation factors, the delay relationship can be presented as a table below:

Table 3.1: Delay Relation		
Delay event	Delay relation	Delay nomenclature
MBT indicated torque	Intake to torque delay	Δt_{MBT}
Sparking timing influence	Injection to torque delay	Δt_{SA}
Air/fuel influence	Spark to torque delay	$\Delta t_{a/f}$
Friction and pumping torque function	Intake to exhaust delay	$\Delta t_{f\,\&\,p}$

The brake torque equation with transport delay can be presented as

$$T_{brake} = T_{ideal}|_{(t-\Delta t_{MBT})} \cdot I_{\Delta SA}|_{(t-\Delta t_{SA})} \cdot I_{a/f}\big|_{(t-\Delta t_{a/f})} - T_{f\,\&\,p}\,\big|_{(t-\Delta t_{f\,\&\,p})} \tag{3.47}$$

In Eq (3.48), the transport delay is based on engine event per stroke. But the dynamic engine model will be based on engine speed, thus the transport time delay can be represented as (Hendricks & Sorenson, 1991):

$$\Delta t_* = \frac{\Delta\varphi_*/360(deg)}{\omega_e/60(s)} = \frac{\Delta\varphi_*}{6\cdot\omega_e} \tag{3.48}$$

3.7.2 Sensor Response Delay

Based on the studies in the previous sections, the air and fuel mixture is through a throttle valve across the intake manifold, and combusted in the cylinder. After exiting the cylinder, the exhaust gases mush reach the oxygen sensor, transport delay of oxygen sensor which must be considered in an air fuel ratio loop model. The oxygen sensor transport can be approximated by: intake delay; combination delay; exhaust delay and system response time, and the function can representation as:

$$t_{oxygen} = \frac{\Delta\varphi_{in}}{6\cdot\omega_e} + \frac{\Delta\varphi_{com}}{6\cdot\omega_e} + \frac{\Delta\varphi_{ex}}{6\cdot\omega_e} + \tau_s \tag{3.49}$$

where:

t_{oxygen}	Oxygen sensor transport delay	[s]
$\Delta\varphi_{in}$	Intake delay	[s]
$\Delta\varphi_{com}$	Combination delay	[s]

$\Delta\varphi_{ex}$	Exhaust delay	[s]
τ_s	System response	[s]

3.8 Summary

This Chapter studies the engine system mathematical modelling problem for the purpose of engine simulation package development. The engine dynamic system model has been divided into 6 categories for detailed investigation, throttle body model, intake manifold dynamics, fuel delivery mechanism, torque production, engine rotational dynamics, transport delay between engine events and sensor signals. Based on thermal and mechanical dynamic principles, a number of differential and algebraic equations have been developed to describe various engine dynamic behaviours. Those equations will be used for the development of simulation package in Chapter 4.

All the equations can be divided into two categories: nonlinear equation from physical principles and functional equation associated with mean value theorem. The reasons use mean value model equations are physical equations not available or equation parameters cannot be measured in a test lab. The simulation package must be able to simulate a wide range of operation conditions with the guaranteed accuracy. Model equations are summarized as following:

1. *Throttle Body Model*: This Model is described by nonlinear equations which are derived from physical principles. All the equation parameter can be measured through the engine specification or experimental tests. There is very little difference in the model for different engine throttle body structure.

2. *Intake Manifold Dynamic Model*: The air charge/discharge effect at intake manifold is the important factor that affects engine AFR output error stability. Intake manifold dynamic model nonlinear equations are derived from its physical principles, the equation parameters are difficult to measure through the engine specification or experimental tests. However, it can be found that two parameter s_m and y_m are almost constant value, and they can be estimated using the mean value method. These two parameters directly influence intake charge/discharge effect; and consequently influence the air/fuel ratio controller development.

3. *Fuel Delivery Model*: The most important AFR dynamic effects in the port injection engine path are caused by the Wall-Wetting phenomena. In the surface of intake port wall and back face of the intake valve some fuel will be absorbed, and the absorbed fuel will enter the cylinder in the next intake stroke. This effect is presented by equations derived from physical principles, and equation parameters can be measured in a test lab. Different engine oil film response affect is difference. The fuel film effects are not considered here, if the test engine uses direct injection technology.

4. *Torque Production Model*: The mass of air and fuel into the cylinder is the main factors determine engine torque output. The AFR and spark timing is the main factors that affects engine torque output. The effects are best described by functional equations determined by the mean value theorem. The equation parameters can be derived from the steady state engine experiments. The development of the torque production model objective is to achieve the identification of the optimal spark timing (MBT) and a wide range of AFRs at each of the operating conditions.

5. *Engine Rotational Dynamic Model and Delay Model*: These two models are described by logic functions and they directly influence on the engine simulation model dynamic response.

Chapter 4: Development of SIMULINK-Based Engine Dynamic Simulation Package

4.1 Introduction

This chapter descrpes the development and verification of the engine simulation package, which will be used in design and optimization of engine control systems. The process of developing SIMULINK-based engine dynamic simulation package is as follows: The first stage is to compile engine simulation model according to engine dynamic equations as well as model parameter data obtained from the engine testing platform. The second stage is to design testing methods and procedures to analyse simulation data and to optimizes simulation settings. The third stage is to insert an engine controller into engine simulation package. The final stage is to verify the package by comparing experimental data with simulation data. The SIMULINK-based engine dynamic simulation package can be summarized into four parts according to the process (Fig 4.1), input subsystem, engine module, control module and output module.

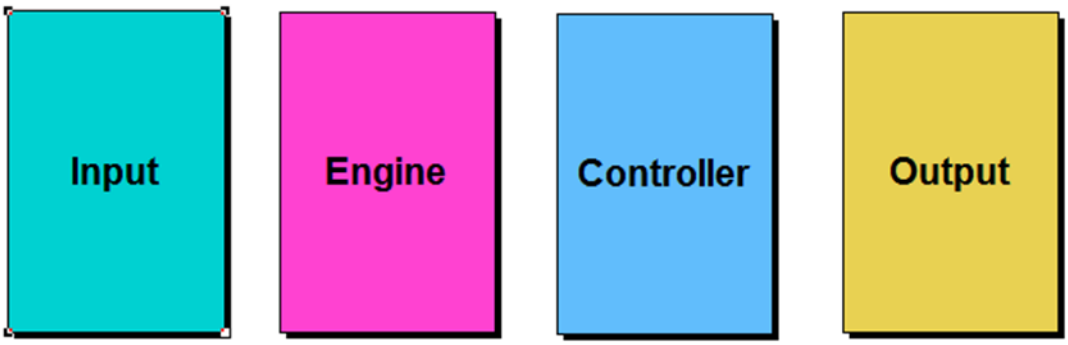

Figure 4.1: SIMULINK-Based Engine Dynamic Simulation Package

This chapter will be divided into five parts according to the compilation steps and the simulation package structure: firstly the SIMULINK implementation of engine model is discussed, secondly the engine testing platform is reviewed, thirdly the design of the input module with association of driving cycles is introduced, Fourthly the engine controller is introduced, and finally engine simulation results are produced and they are compared with experimental data.

4.2 Engine Model SIMULINK Implementation

The simulation of engine dynamic system is based on engine standards and dynamic equations described in Chapter 3. As shown in Fig 4.2 the engine simulation subsystem model has seven parts: throttle body model, intake manifold dynamics model, lambda dynamic model, injection dynamic model, wall-wetting dynamics model, torque production model and engine rotational dynamics model. The modular structure makes it easy to check the model correctness and performance. This simulation model can be easily adapted to simulate different engines due to the modular structure.

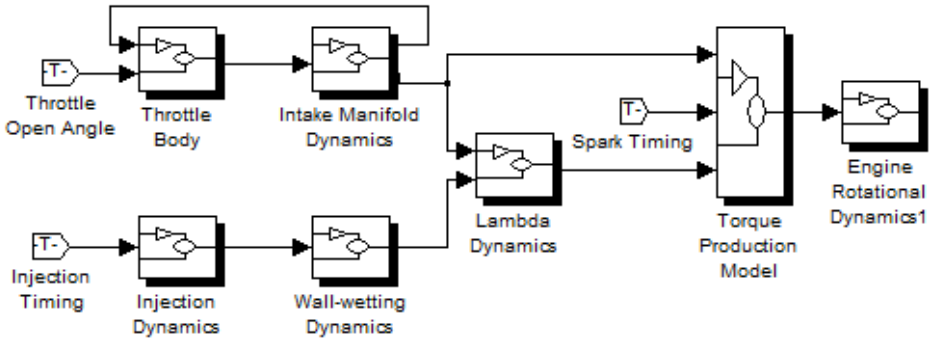

Figure 4.2: Engine Model Subsystem

4.2.1 Throttle Body Model

Based on Eq (3.1) and equations relevant to Eq (3.1), the air throttle flow rate is generated according to the function:

$$Air\ Throttle\ Flow\ Rate = f\ (Throttle\ Open\ Angle, Manifold\ Pressure) \quad (4.1)$$

The structure of throttle model can be described by the Fig 4.3 below. The throttle open angle depends on driving mode which will be presented at input subsystem. The manifold pressure will be introduced later in intake manifold dynamics model.

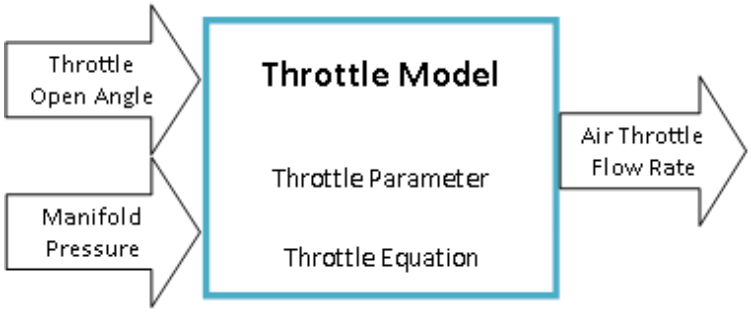

Figure 4.3: The Structure of Throttle Model

The throttle model parameters in Eqs (3.1) to (3.9) are introduced as: discharge coefficient of throttle valve, ambient pressure, ambient temperature, gas constant, maximum throttle area, specific heat ratio, engine displacement volume, volume of intake manifold, throttle bore diameter, throttle shaft diameter.

Fig 4.4 shows the SIMULINK model of throttle body, the model is used to calculate air throttle flow rate according to Eq (3.4). The function subsystem is developed according to Eq (3.6). The SIMULINK saturation block limit throttle opening angle to the upper (90°) and lower (0°) saturation values.

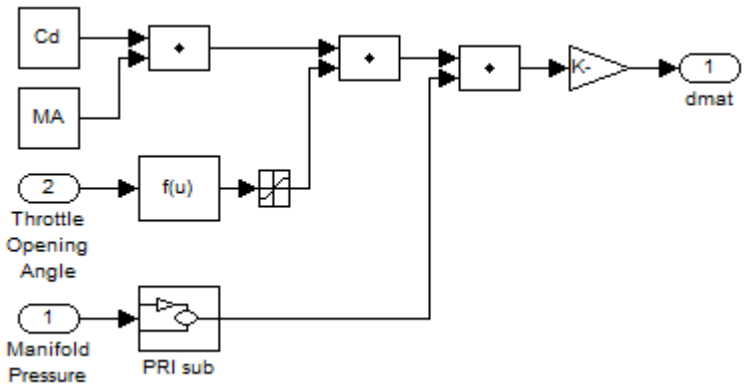

Figure 4.4: Subsystem of Throttle Body Model

The PRI sub model of throttle body in Fig.4.5 is based on Eq (3.7),

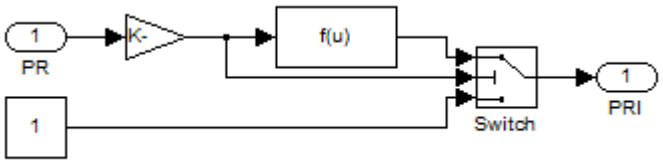

Figure 4.5: Subsystem of PRI Sub Model

4.2.2 Intake Manifold Dynamics Model

When the air from throttle body is delivered to intake manifold, the pipe bend will affect the flow rate and pressure changes on both sides of the intake manifold. Thus the intake manifold dynamics model will only calculate flow rate and pressure at intake manifold end. From Eqs (3.10) to (3.20), it can be figured out that the engine speed is an input factor for intake manifold model. Therefore the structure of intake manifold model can be described as the Fig 4.6 below.

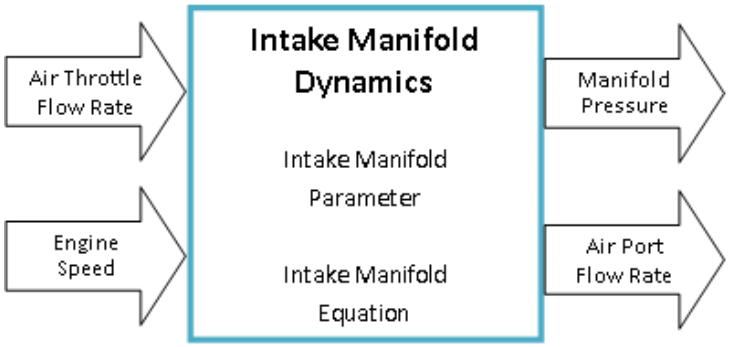

Figure 4.6: The Structure of Intake Manifold Dynamics Model

From Fig 4.2 we can see that the air throttle flow rate can be calculated from throttle body model, and the engine speed can be obtained from engine rotational dynamic model. Therefore we can conclude that intake manifold parameters that can be determined are: mean temperature rise of the intake air during the intake stroke, intake manifold temperature, compression ratio, ratio of the specific heats, exhaust manifold pressure, mean temperature during valve overlap, air mass lost during overlap, gas constant.

The subsystem for intake manifold dynamic block in Fig 4.7 is based on Eqs (3.10) and (3.13). The Fun 1,2,3 & 4 blocks are used to implement Eq (3.19), Eq (3.20), Eq (3.15) and Eq (3.14) respectively.

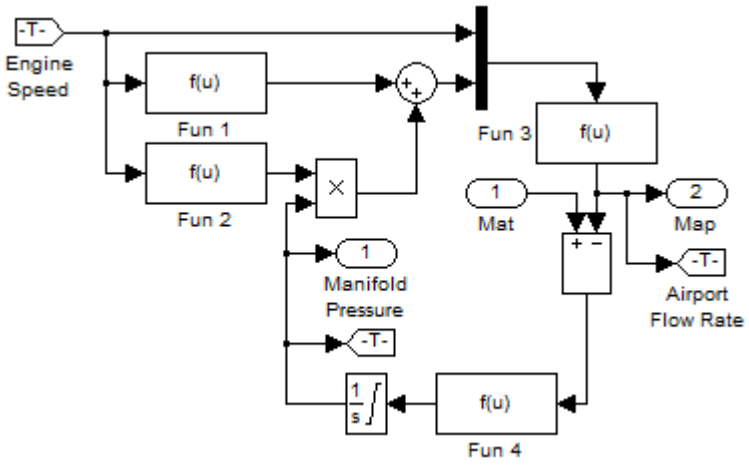

Figure 4.7: Subsystem of Intake Manifold Dynamic Model

4.2.3 Fuel Delivery Model

When the injection system receives pulse signal from the engine control unit it will inject fuel, the fuel then goes through a small nozzle under high pressure, and the injection atomizes the fuel by forcibly pumping into intake port or cylinder. Therefore

fuel delivery model structure can be designed as in Fig 4.8, inputs are the injection time and voltage to the injector and the output is the fuel flow rate into cylinder. Note that wall-wetting dynamic effect is included due to its significance in the fuel delivery mechanism.

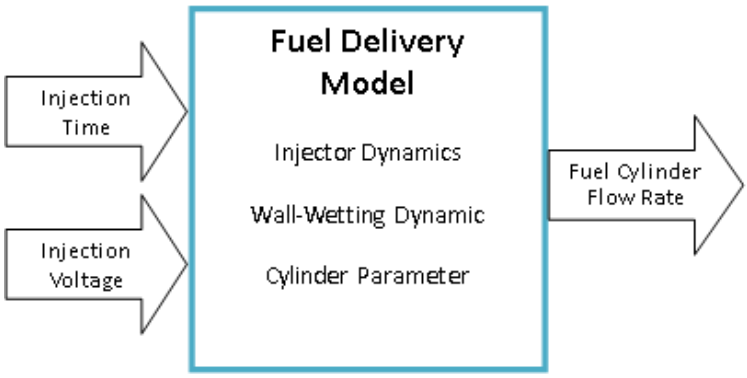

Figure 4.8: The Structure of Fuel Delivery Model

Because of the variety of fuel injection methods and nozzle types, as shown in Fig 4.9, the fuel delivery simulation model has been separated into two parts: injection dynamics and wall-wetting dynamics. Fig 4.10 shows the subsystem of wall-wetting dynamic block based on Eqs (3.22) & (3.23).

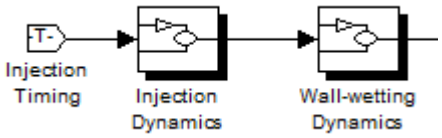

Figure 4.9: Fuel Delivery Simulation Model

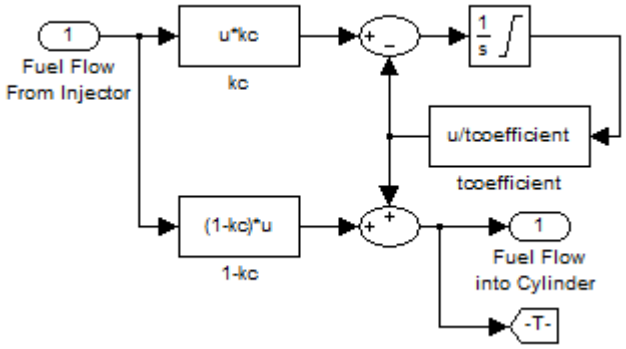

Figure 4.10: Subsystem of Wall-wetting Dynamic

4.2.4 Torque Production Model with Transport Delay

The torque production model is based on a variety of the submodels, as shown in Fig 4.11. It is a steady-state model which does not contain any dynamic elements except for

the process delays associated with the four stroke combustion process. This approach is consistent with the real time control goals, and is justified since the combustion dynamics are much faster than air, fuel, or spark time transport dynamics.

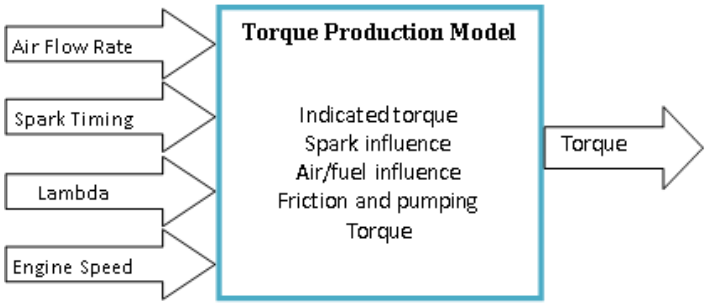

Figure 4.11: The Structure of Torque Production Model

Fig 4.12 shows a subsystem for torque production model (base on Eqs (3.31) & (3.32)). The Fun blocks 1 to 4 are based on Eq (3.33), Eq (3.34), Eq (3.41), and Eq (3.42) respectively. The Func blocks 5, 6 and 7 are all based on Eq (3.49).

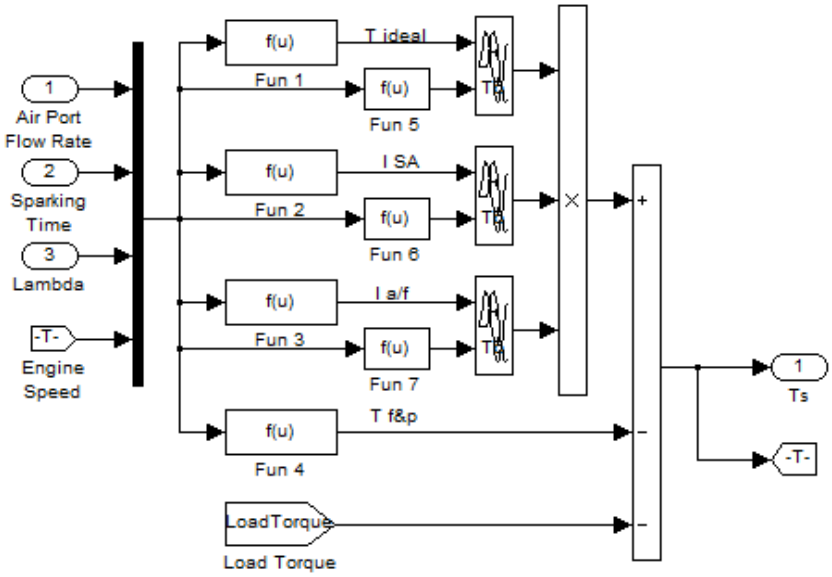

Figure 4.12: The Subsystem of Torque Production Model

4.2.5 Engine Rotational Dynamics

The engine speed as well as the torque needs to be determined from the simulation.. From the analysis of Eq (3.45), we can conclude that the engine speed depends on the torque change and engine effective inertia; thus engine rotational model module structure can be summarized as in Fig 4.13:

The engine speed is calculated by dividing the integrated torque with the effective

engine rotational inertia (ref Eqs (3.43) to (3.48)). Since the engine operating under actual working condition is in fixed range, an integrator limited block is used as shown in Fig 4.14.

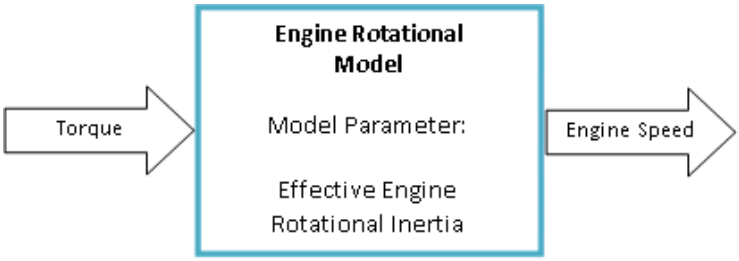

Figure 4.13: The Structure of Engine Rotational Dynamics

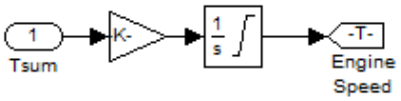

Figure 4.14: The Subsystem of Engine Rotational Dynamics

4.2.6 Lambda Dynamic Model with Transport Delay

Oxygen sensor is an indispensable component in the engine in order to use three-way catalyst converters to reduce the vehicle tail gas emission (Falk & Mooney, 1998). The catalyst reactions occur most efficiently when the engine AFR value slightly above ideal AFR. Lambda sensors are located in the exhaust stream, they do not directly measure the air or the fuel entering the engine. But when information from lambda sensors is coupled with information from other sources, it can be used to indirectly determine the AFR. Thus lambda dynamic simulation is absolutely vital for the determination of AFR and the development of engine control system. It is not easy to achieve the combustion state and exhaust simulation. Therefore the lambda dynamic simulation block can be assumed as the air mass amount into cylinder divided by fuel mass amount into cylinder (Eq (3.51)) In order to realize the accuracy of the simulation, the lambda signal will be delayed a reasonable time before it is fed into the control model. The simulation block structure is illustrated by Fig 4.15.

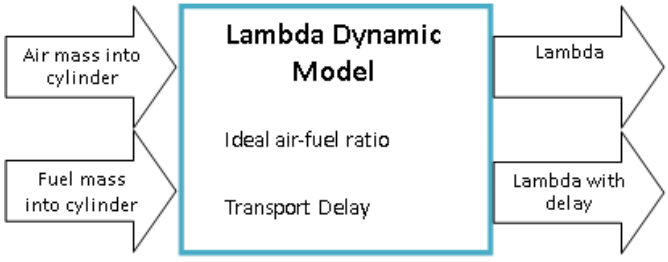

Figure 4.15: The Structure of Lambda Dynamic Model

4.3 Engine Testing Platform

Parameters in models presented in Section 4.2 need to be obtained either theoretically or experimentally. Experimental tests were performed at the power systems research department test facility of one engine research laboratory in China. The tests were conducted on a Mitsubishi Sirius 4G64 engine without any engine and controller modification. The engine was manufactured by Shenyang Aerospace Mitsubishi motors engine manufacturing Co., Ltd. It must be said, though, that the 4G64 engine are using outdated technology. Due to its high reliability, low price and widely available parts, the engine is used widely in China's economic type of car industry: Mitsubishi Pajero, Chery EASTAR, JEEP 2500, Shuanghuan SCEO, Great Wall Haval etc. The platform engine can be modified and optimized by the motors research laboratory. The engine testing platform is designed and installed in accordance with the engine model parameters test requirements. The 4G64 engine's Electronic control unit (ECU) has been replaced by a PC-based engine control system with identical functions.

4.3.1 Engine Information

The engine specifications from Mitsubishi motors engine 4G64 workshop manual is list in Table 4.1. The 4G64 engine is a single overhead camshaft, 4 cylinder 4 valves per cylinder. Cylinder head use iron and cylinder block use aluminium. The 4G64 engine block section is illustrated in Fig 4.16.

Table 4.1: Engine Specification (Mitsubishi, 2001)

Descriptions	Specifications
Cylinder layout	In-line 4
Combustion chamber	Pentroof type
Valvetrain	Single overhead camshaft
Displacement	2.351 L
Bore x stroke	86.5×100（mm*mm）
Compression ratio	9.0:1
Maximum power	99(5000) kw(r/min)
Maximum torque	201(2500) N*m (r/min)
firing order	1-3-4-2
Intake valve open/close	16° BTDC / 53° ABDC
Exhaust valve open/close	50° BBDC / 16° ATDC

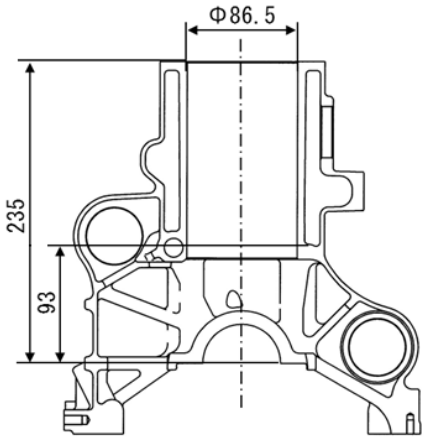

Figure 4.16: Sectional View of the 4G64Engine Block (Mitsubishi, 2001)

Fig 4.17 shows 4G64 performance curves, of which the red line is engine power performance and the green line is engine torque performance. When the engine operates at high speed the performance is mediocre, but the engine can output max torque at 2500 rpm which is 201 Nm, so that 4G64 engine is good performer at low-speed. The maximum power output of 99 kW is low when the engine speed is 5000 rpm.

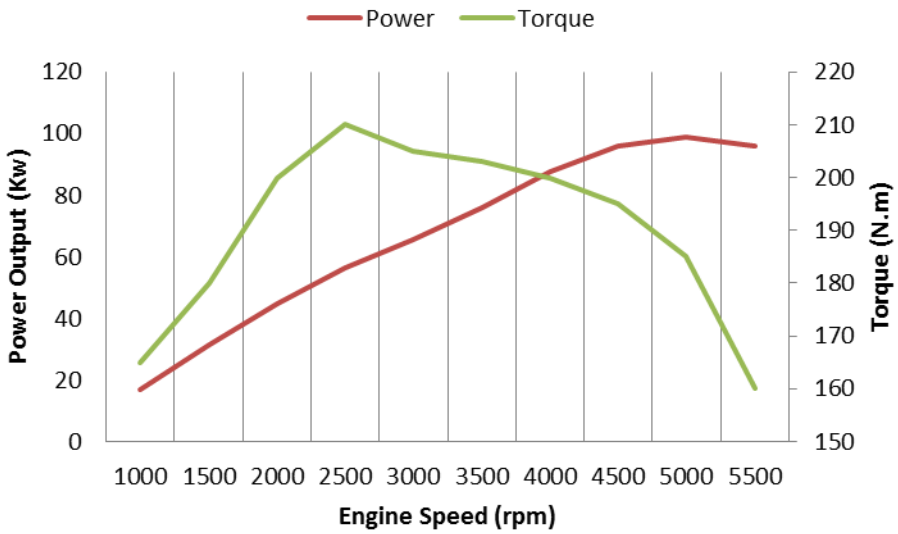

Figure 4.17: 4G64 Engine Performance Curres (Mitsubishi, 2001)

Fig 4.18 shows intake manifold section and related diameter parameters. According to Eqs (3.19) and (3.20), one can calculate all parameters of the intake manifold dynamics model.

The model parameters of throttle body model and intake manifold dynamics can be measured by the engine or obtained from engine workshop manual. But other models parameters will be measured through instrument measurement and test methods. T testing platform and test methods are discussed in the following.

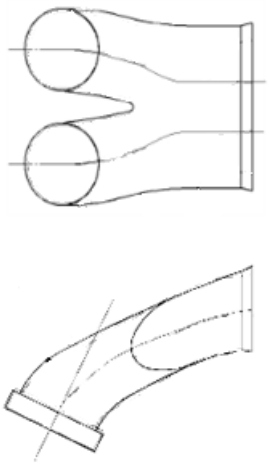

4G64		
Valve Head Diameter	IN	34 mm
	EX	31.5 mm
Throatsection Diameter	IN	28 mm
	EX	25 mm
Valve Diameter	IN	33 mm
	EX	29 mm
Inlet Area		1085.57 mm²

Figure 4.18: Sectional View of the Intake Manifold (Mitsubishi, 2001)

4.3.2 Testing Platform Information

In order to use test data to determine the engine operation and performance, the test results should be verifiable, comparable and reusable. Therefore a common test automation and data platform is required. The main requirements for an engine testing platform are summarised as follows:

1 Provides firm support for the engine and supply systems for engines operation testing.
2 Use a platform engine controller instead of OEM engine control unit.
3 Provide the engine load testing data for variable speed or torque.
4 Have automation systems and/or procedure for data acquisition and test automation

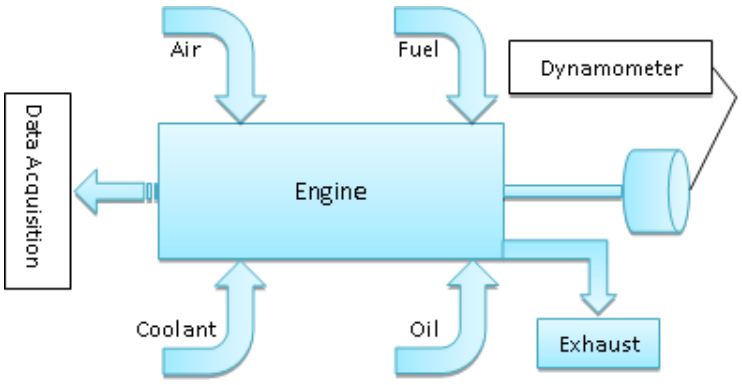

Figure 4.19: Engine Testing Platform Structure

Fig 4.19 shows the testing platform structure which consists of three parts: dynamometer platform, controller and data acquisition. Each part plays an important role for achieving engine certification testing.

4.3.2.1 Dynamometer Platform

Dynamometer platform is very complicated, there are a lot of instruments included in addition to a dynamometer. One of the major functions of dynamometer is to measure engine torque. The secondary function of dynamometer is to determine the torque required to operate the engine to ensure the achievement of engine test procedures and result validations.

A load torque is applied to the engine by a dynamometer, coupled to the engine with a compliant shaft. The engine supply system combined with the dynamometer platform is similar to the system the engine to be worked with in order to minimizing the difference between the testing and real application.. The desired oil and coolant temperature are specified by the operators through a closed loop heating/cooling control circuit.

The throttle angle in the air supply system is adjusted by a stepper motor which is connected to the throttle linkage. The platform can be operated either by the operator via joystick or by the dynamometer automatically. The fuel delivery system uses a constant pressure variable pump so that the pressure is stable. Output flow variables are controlled by a new controller which will be detailed in next section. The input system (as shown on the top of Fig 4.19) for support engine combustion supplies air and fuel into cylinder combustion to generate power.

In order to obtain model parameters of the torque production model discussed in Chapter 3, two test procedures (steady state test and load sweep test) need to be carried out. The steady state test is the test when the engine held at a specified speed for a desired amount of time by the variable brake loading as provided by the power absorber unit. For the sweep test, the engine is tested under a constant load which the engine speed varies in continuous fashion from a specified lower "starting" speed to a specified "end" speed.

4.3.2.2 Controller

The engine's OEM controller controls the spark advance at optimum point and the AFR is always kept close to 14.7. In order to observe air/fuel influence and spark influence at a wide range of settings, we need an adjustable controller in laboratory tests. Therefore

a new controller is designed to fulfil the requirement of experiment. This new PC-based controller controls the spark advance and the fuel pulse width in replacement of the OEM controller. The control system can adjust the AFR and spark advance according to the experimental objectives. The throttle is controlled by the user via a stepper motor connected to the throttle linkage. A potentiometer is used to measure the throttle angle from closed position.

4.3.2.3 Data Acquisition

There are two main ways of gathering data: the dedicated digital data acquisition system (installed in the Dynamometer platform) and PC-based system. It can record engine output torque, engine speed, fuel injection, throttle open angle, air fuel ratio, etc. Spark advance was recorded using a digital to analog converter coupled through an interface module to the computer. Alternatively, an oscilloscope can be attached to any sensors on the engine, to record the signals e.g. intake manifold pressure, intake air temperature, engine temperature, crankshaft angle, throttle air mass flow, etc.

4.4 Input Module Description

In order to facilitate an intuitive engine model testing framework and determine the impact of the control system optimization, the engine dynamic simulation package needs a reasonable input subsystem. The common industrial practice is to test vehicles using the driving cycle s. Therefore the driving cycle testing method is selected as a useful reference for the selection and implementation of engine tests. According to the driving cycle testing method and the engine model performance requirements, the input module requires to have two substantially new blocks: (1) the vehicle dynamic block which can provide the load torque for the engine model, (2) the driving cycle block which provides test reference input (vehicle speed, gear number, etc.). Each block will be examined in turn with details description about their contents.

4.4.1 Vehicle Dynamic Block

Generally speaking, a comprehensive vehicle dynamic system involves a lot of complex dynamic problems, but in special circumstances we can eliminate the need to consider

tire performance, brake performance, vehicle cornering dynamic, road grade load, etc. In this case, the comprehensive vehicle dynamic system can be simplified as a vehicle linear running resistance block, with the transmission speed and torque sub-block. The resistance block considers only the most important factors which are: aerodynamic losses, rolling resistance losses, vehicle acceleration resistance losses, engine and transmission inertia torque losses. The transmission block will be based on gear radio and gear number dynamic calculation for the engine speed and torque load.

4.4.1.1 Resistance Block

Because the air flow over a vehicle is so complex, it is necessary to develop semi-empirical blocks to represent its effect. The aerodynamic drag is characterized by the equation below (Gillespie, 1992):

$$F_a = \rho_a \cdot {V_f}^2 \cdot C_D \cdot \frac{A}{2} \tag{4.1}$$

where ρ_a is air density, V_f is vehicle forward velocity, C_D is aerodynamic drag coefficient and A is frontal area of the vehicle.

The other major vehicle resistance force on level ground is the rolling resistant of the tire. Considering the vehicle as a whole, the total rolling resistance is the sum of the resistance from all the wheels assume as (Gillespie, 1992):

$$F_r = \begin{cases} f_r \cdot W & V_f \geq 0 \\ 0 & V_f < 0 \end{cases} \tag{4.2}$$

where f_r is rolling resistance coefficient and W is weight of the vehicle.

In accordance with the Newton's second law, the vehicle acceleration resistance can be derived as (William & William, 1995):

$$F_x = m \cdot a = m \cdot \dot{V} \tag{4.3}$$

where m is vehicle mass and a is vehicle acceleration.

As can be seen in Fig 4.20-a, this block is based on Eqs (4.1) to (4.3). This block calculates the torque at wheel. Fig 4.20-b represents the subsystem for the rolling resistance block, if input speed is not zero the rolling resistance block will be switched, otherwise it will be convective .

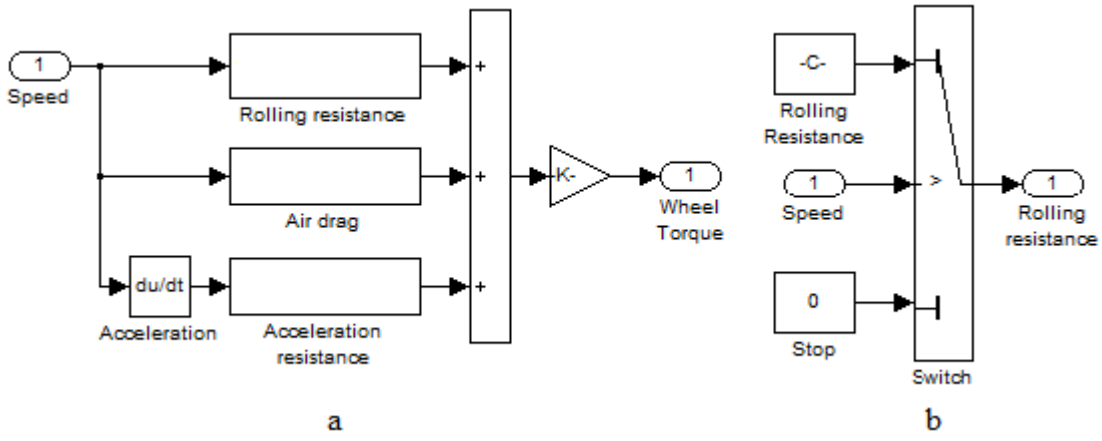

Figure 4.20: The subsystem of Resistance Block

4.4.1.2 Transmission Block

Starting with the engine, the actual torque delivered to the drivetrain has to be reduced by the inertia of the engine rotating components which requires acceleration. Based on the Newton's second law, the torque at clutch can be described as:

$$T_{clutch} = T_{engine} - I_{engine} \cdot \dot{r}_{engine} \tag{4.4}$$

where I_{engine} is engine rotational inertia and r_{engine} is engine rotational speed.

The torque delivered at the output of the transmission is amplified by the gear ratio of the transmission, and it is decreased by inertial losses in the gears and shafts. So the total torque output to the driveshaft transmission can be summarized as:

$$T_d = (T_{clutch} + I_t \cdot \dot{r_e}) \cdot N_t \tag{4.5}$$

where I_t is transmission rotational inertia and N_t is numerical ratio of the transmission.

The working process of the transmission block can be expressed as below: the vehicle speed signal is divided by the radius of the tire and this produces the wheel speed which is then combined with the gear schedule in the transmission block, and finally the

transmission block produces the engine speed. At the same time, the vehicle resistance torque from resistance block and the additional wheel rotational resistance are added to transmission block, the transmission block will then calculate the total resistance torque according Eqs (4.4) and (4.5). Detailed transmission block working process is depicted in Fig 4.21.

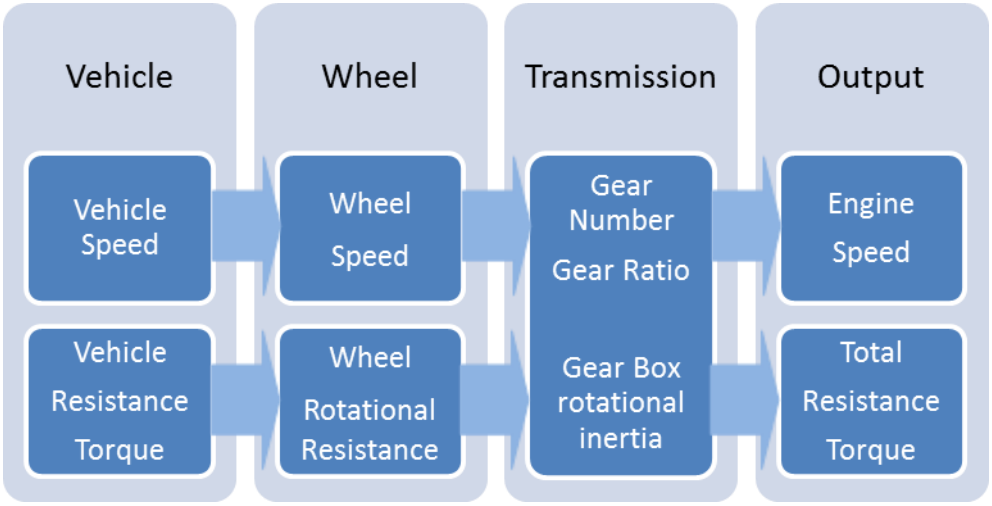

Figure 4.21: Working Process of the Transmission Block

In addition to the engine speed and total resistance torque described above, a few special engine operations must be accounted for: engine idle, fuel cut-off and engine overspeed. Fig. 4.22 shows an overview of the special engine operating cases logic.

(1) If the simulation engine speed goes over the maximum engine speed limits, the simulation package will stop and prompt error message at MATLAB command window, meanwhile record the simulation stops time so as to modify shift changing strategy.

(2) If not, the vehicle moves at a constant velocity or acceleration, engine load input will be based on the vehicle dynamic resistance torque.

(3) If the vehicle speed is diminishing and clutch in unlocked, the engine load will be calculated by the idle torque.

(4) If the clutch in lock but the simulation engine speed less than or equal to the idle engine speed, the system will automatically disconnect clutch and the engine load will be calculated by the idle torque.

(5) If the simulation engine speed is greater than the idle speed, the fuel supply system will be at this moment according to the standard in modern fuel injection control systems, , therefore there is no torque input to the engine model.

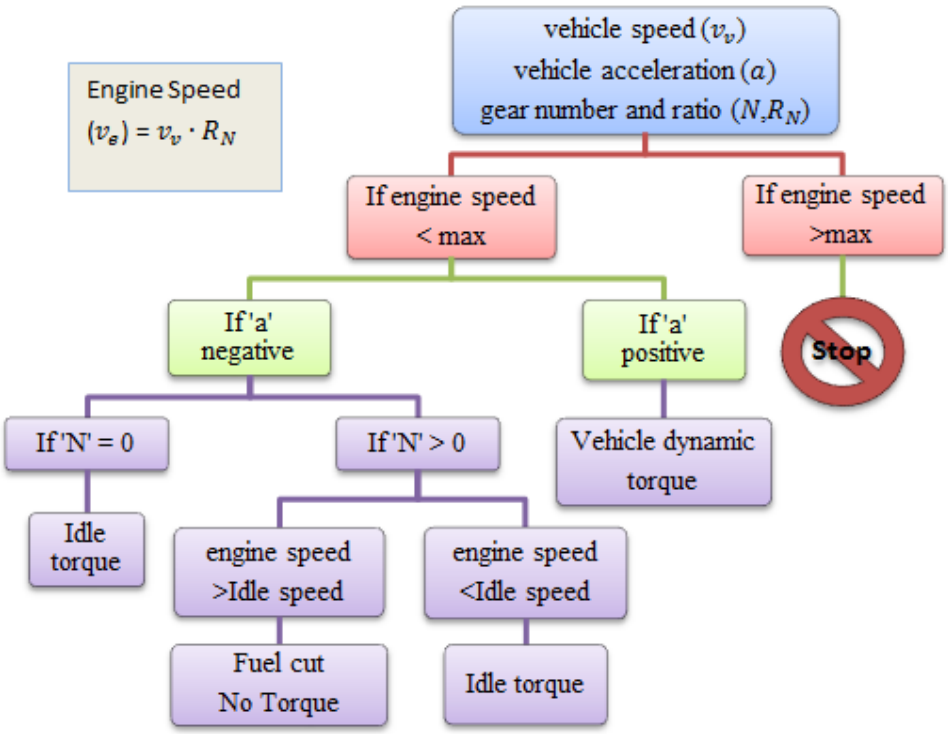

Figure 4.22: An Overview of the Special Engine Operating Cases Logic

The left side of Fig 4.23 represents the subsystem of transmission block in which the wheel speed and wheel torque are directly inputted into the transmission block, the gear number inputs into the multiport switch block which will select the gear ratio to be used into transmission block. The transmission block presented in Fig 4.22 uses MATLAB Function block to programme the logical relationship. On the right side of Fig 4.23 the user interface of transmission block is based on Eqs (4.4) and (4.5)., The parameters of transmission block are: mass of the vehicle, vehicle cross section area, drag coefficient, wheel diameter and gear ratio.

Table 4.2: Vehicle Parameter

Vehicle	Vehicle Mass (kg)	1380	Moment of inertia (kg*m^2)	2444
	Aerodynamic drag coefficient	0.32	Frontal area (m^2)	2
	Air density	1.225	Full Load	
Tire	Tire radius (m)	0.25	Wheel inertia (kg*m^2)	0.01
Transmission	Output shaft Inertia (kg*m^2)	0.1	1st gear ratio and efficiency	3.42 (98%)
	2nd gear ratio and efficiency	2.14 (98%)	3rd gear ratio and efficiency	1.45 (98%)
	4th gear ratio and efficiency	1.03 (98%)	5th gear ratio and efficiency	0.77 (98%)
	Final drive	4.06:1 (98%)		
Engine	Engine and impeller inertia (kg*m^2)	0.1	Idle speed (rad/s)	16*2*pi

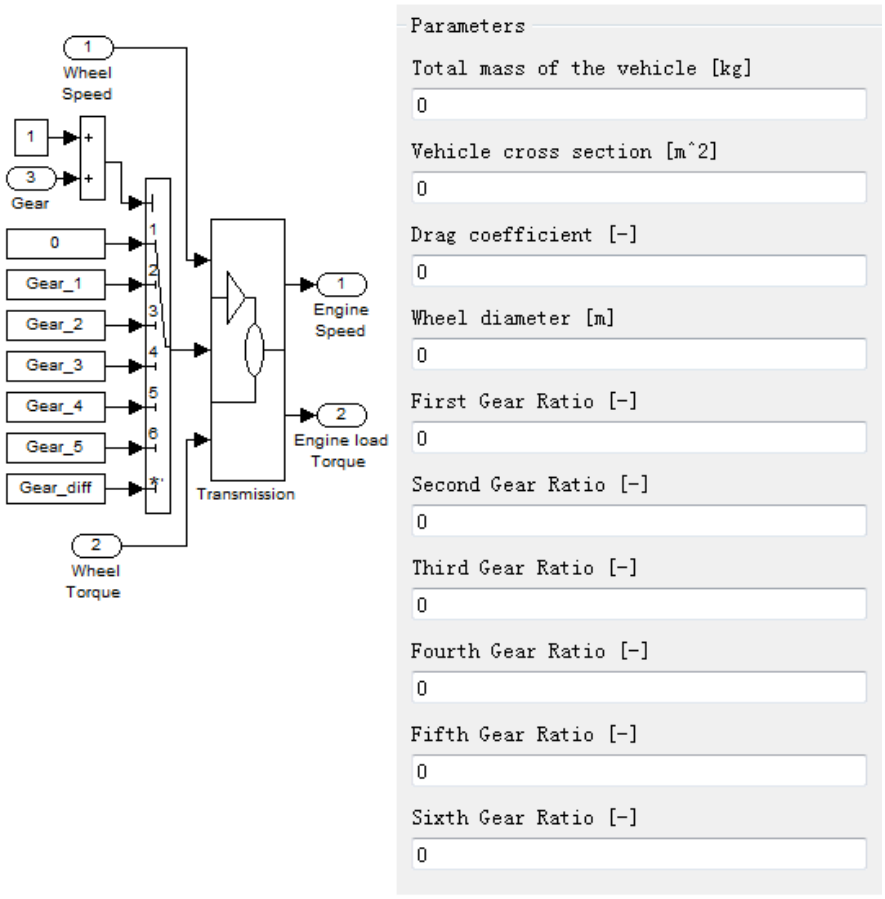

Figure 4.23: Subsystem of Transmission Block

4.4.1.3 Vehicle Dynamic Block Default Parameters

The vehicle parameters are shown in table 4.2. All data are from Ford Granada and Ford MTX-75 gearboxes.

4.4.2 Driving cycle block (Barlow et al., 2009)

A driving cycle is a standardized driving pattern (Freij & Ericsson, 2005), described by means of a velocity-time table. The track that is to be covered is divided in time-steps, mostly seconds. The acceleration during a time step is assumed to be constant. As a result the velocity during a time step is a linear function of time. Because velocity and acceleration are known for each point of time, the required mechanical power as a function of time can be determined by formulas, which will be discussed later. This function integrated over the duration of the driving cycle produces the mechanical energy needed for that driving cycle. In the case of internal combustion engine driven vehicles, the fuel consumption and emissions are directly measured. The same holds true for the fuel conversion system of hybrid electric driven vehicles. The primary

energy can be calculated from the fuel consumption. For electric vehicles or hybrid electric vehicles which make use of an external electric source (such as the public grid), the electric energy withdrawn from that source will be separately accounted for. The electric energy is turned into the required primary energy by dividing it by the efficiency of power generation. The emissions are determined by using emission values handed up by power companies. In all driving systems the efficiency of the driving system is determined by dividing the calculated mechanical energy by the primary energy.

Driving cycles are produced by different countries and organizations to assess the performance of vehicles in various ways. There are total 256 driving cycles presented in '*A reference book of driving cycles for use in the measurement of road vehicle emissions*'. Typically, there are three standards: European driving cycles, United States driving cycles and Japanese driving cycles. In addition, each driving cycles have various test cycles.

Driving Cycles Simulation Block

In the driving cycle simulation block the most frequently used driving cycles are defined, all the driving cycles were summed up in a single graphic, as can be seen in Table 4.3. The corresponding time, speed, and gear vectors of each cycles are already saved in the block initialization commands. Therefore the user can choose to work with the desired driving cycles. When running the simulation model, the driving cycle data chosen by the user will be loaded to the workspace, at that time the model will change SIMULINK simulation time. In the SIMULINK model, vehicle speed and gear number will be determined by using the lookup table block. Vehicle speed vectors and gear number vectors are defined by the table data block, and the time vectors is defined by the block Breakpoints. The vehicle speed and the gear number are used in the vehicle dynamic block to the corresponding engine speed and load torque.

Table 4.3: Driving Cycle Simulation Block

Europe driving cycles	ECE-15	EUDC
	EUDCL	NEDC
	ECE15+EUDC	
United States driving cycles	FTP 72	FTP 75
	NYCC	
Japan driving cycles	10 mode	15 Mode
	10-15 Mode	

There is a possibility to define the user's own cycles in the input module; but this would require the definition of two (automatic gearbox) or three (manual gearbox) vectors of equal length. The gear values would not need to be predefined for automatic transmission whose gear ratio is given by a control unit. The corresponding time, vehicle speed, and gear number vectors can be defined as SimulationTime, VehicleSpeed, GearNumber MATLAB workspace values. The driving cycle simulation block will produce vehicle speeds and gear numbers based on each cycle standard. To simulate the vehicles with the automatic transmission, the user can enable automatic transmission in the driving cycle block.

Example: Urban Driving Cycle

In order to understand driving cycles, an urban driving cycle is used as an example to discuss in details here. Other driving cycles can be found in the Appendix A(?????). The Urban Driving Cycle, also known as ECE 15 cycle, was first introduced in 1970 as part of ECE vehicle regulations; the recent version is defined by ECE R83, R84 and R101. The cycle has been designed to represent typical driving conditions of busy European cities, and is characterized by low engine load, low exhaust gas temperature, and a maximum speed of 50 km/h.

As can be seen in Figs 4.24 and 4.25, when the engine starts, the car pauses for 11 seconds if equipped with a manual gearbox and the gear is in neutral. At 12th second and at the 1st gear slowly accelerates to 15 km/h in 4 s, cruises at constant speed for 8 seconds, brakes to a full stop for 5 second (at 26th second the clutch is disengaged), stops for 21 seconds. At 49th second, the car slowly accelerates to 32 km/h in 12 seconds, cruises for 24 seconds, slowly brakes to a full stop for 11 seconds. Manual gearbox setting is: 50-60 second in 1st gear, 61-87 in the 2nd gear, and then 6 seconds in the 1st gear. At 117 second, the car slowly accelerates to 50 km/h in 26 seconds, cruises for 12 seconds, decelerates to 35 km/h in 8 seconds, cruises for another 13 seconds, brakes to a full stop in 12 seconds, then pauses for 7 seconds. Manual gearbox setting is: 50-60 second in 1st gear, 61-87 in the 2nd gear, 61-87 in the 3rd gear, then downshift 21 seconds in the 2nd gear and 5 seconds in the 1st gear. The cycle ends on 195 second after a theoretical distance of 994.6 meters, total driving time is 150 seconds and average speed is 18.4km/h.

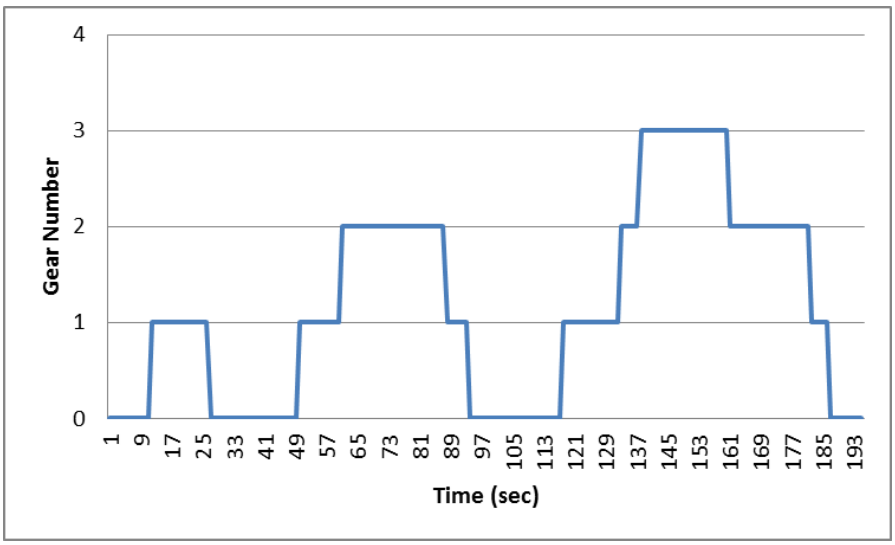

Figure 4.24: Urban Driving Cycle Time-Gear Diagram

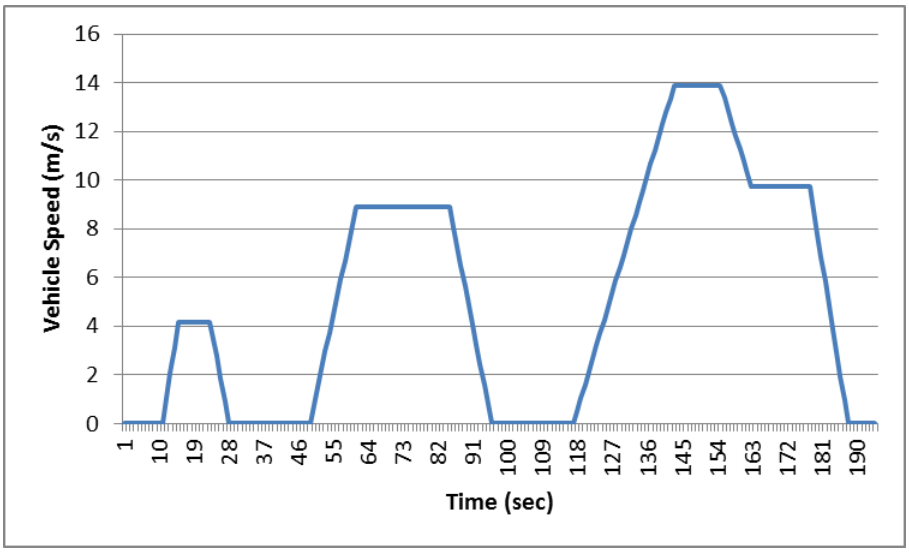

Figure 4.25: Urban Driving Cycle Time-Speed Diagram

4.4.3 Testing Input Block

As discussed in previous two sections, the vehicle dynamic block needs to be combined with a driving cycle block in order to ensure reasonably realistic settings of throttle and engine load which required by the engine model. One advantage of doing so is that it provides a common test and comparison basis. This additional test will decrease test productivity sometimes, e.g. when the fine-tuning controller is involved. However sometimes this is necessary, for example, the engine operation needs to perform at all possible engine speed under different engine loads for training NN controllers (Chapter 6). Therefore, there is one additional testing input block connected to input block to realize diversified testing demands.

The principle procedure of testing input block operation can be summarised as: (1) Choose the test processing option with input graphical user interface. Vehicle dynamic block and driving cycle block are marked with the subsystem enabled, this will allow the user create conditionally executed subsystems that are only executed when the enabling signal is greater than zero. (2) Double-click testing input subsystem block (see screen capture Fig 4.26). (3) Select the corresponding number according to the experiment. Option 1 sets throttle open angle as a constant value. Option 2 allow the user to use the signal builder to draw throttle open angle curves. Option 3 load the customer data from workspace or excel file from lookup table block. Option 4 is a standby option in which the user can use Goto and From block to connect new throttle open block with engine model. The determination of engine load uses the same principle as throttle.

4.5 Control Module and Output Module

4.5.1 Control Module

As discussed in the literature review, the control systems have four parts; AFR control, idle speed control, exhaust gas recirculation control and knock control. The AFR controller will be developed in this research, there is a need for an existing solution for idle speed control, exhaust gas recirculation control and knock control.

The idle speed control system regulates engine idle speed by adjusting the volume of air that is allowed to by-pass the closed throttle valve. The system is necessary to provide the stabilization of the curb idle when the load is applied to the engine and provide cold fast idle on some applications or conditions. But in laboratory testing or simulations it is not necessary to consider some conditions like warm-up, air condition load, electrical load, etc. All the tests are carried out when the engine speed is higher than 1000 rpm, so there is a very simple way to solve the idle speed control problem within the simulation by simply attaching a saturation block at the engine speed output block. The saturation block can limit the input signal to the upper and lower saturation values. This will ensure that the lower simulation engine speed limit is the engine idle speed. The driving cycle test will involve the idle speed control, and the detailed presentation will be given in Chapter 5.

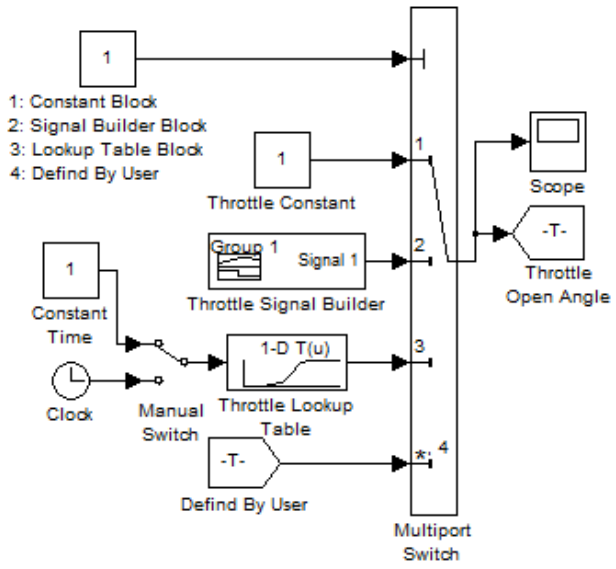

Figure 4.26: Testing Input Block

Exhaust gas recirculation control works by recirculating a portion of an engine's exhaust gas back to the engine cylinders. Most engines now require exhaust gas recirculation to meet emissions standards. Because the influence and significance of exhaust gas recirculation control in this study is not important, it is not involved in the simulation.

Engine knock is very difficult to simulate, engine knock or detonation can be caused by: fuel quality, fuel pump performance, change in altitude, inlet air temperatures, wrong timing values, etc. Therefore when testing the air fuel ratio controller the simulation does not consider the ignition timing influences. Ignition timing will be set as a constant value.

The AFR controller produces a pulse width signal to feed into the fuel injector. The fuel injector will inject the fuel into cylinder according to the AFR control signal and fuel pump pressure. The actual injection quantity depends on the fuel pump and fuel injector nozzle. In order to simplify the simulation system, Air/Fuel-Ratio controller output signal is set as the actual injection fuel quantity instead. The controller will be redesigned based on actual engine control performance requirements.. Different control methods will be discussed in details in Chapters 5 & 6.

4.5.2 Output Module

The output module is divided into two main parts, one is to observe simulation results in

real time during the test, and another is to record the results later uses (e.g. comparison). For the result observations, scope blocks or a display blocks are used to display engine speed and control error as shown in Fig 4.27. Experimental results can be observed directly using the scope block or display block.

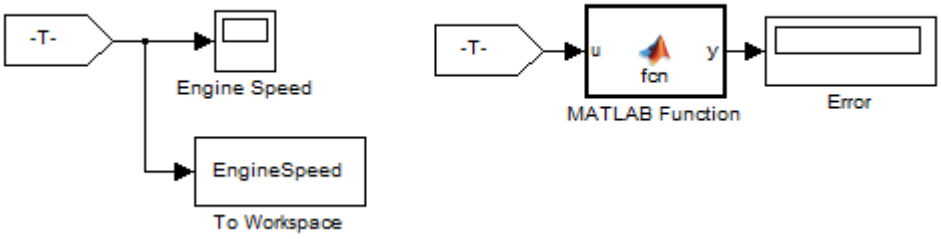

Figure 4.27: An Example of Output Module

4.6 Simulation Package Validation

To validate the developed engine simulation package, steady and transient tests in a wide operating range must be carried out. The algebraic equations have been in this study to produce an approximation of experimental data using the Levenberg-Marquardt method (Zielinski & Allendoerfer, 1997) which is a kind of nonlinear least square estimation technique. The test data and approximation results are depicted in each figure in a comparative manner. The sampling interval for the simulation is selected to be synchronized with the intake event because of the event-based operation characteristics of the engine.

In order to evaluate the accuracy of the simulation package, real test and simulation data from various operating conditions are collected, and a comparative study is done with the predicted values of various variables of the engine simulation using the same input profiles (throttle open angle, fuel flow rate, and sparking timing). All simulations in here use a PID AFR controller which will be introduced in detail in Chapter 5, the simulation controller is designed closely resemble the original engine AFR controller.

The comparison of simulation and experimental results is presented graphically. The percentage error between actual and simulation is defined as by divided the maximum difference by the experiment value.

4.6.1 Model Validation at Steady State Conditions

When the engine is installed in the testing platform in the laboratory, some variations will be occurred in engine intake system, exhaust system and control system. Therefore there will be some discrepancies between engine in real applications and the engine on testing platform. To overcome this problem, all of test data from testing platform for the engine performance curve need to be recalibrated. Platform tests and simulations were carried out at ten different speeds (1000, 1500, 2000, 2500, 3000, 3500, 4000, 4500, 5000, 5500 rpm). The testing input module is used to select different settings: i.e. the throttle open angle is set by constant block with value of 90 degree; the engine load is determined using the actual performance curve moving up or down to adjust until the required engine speed is achieved.

The platform test and simulation results for the 4G64 engine performance are presented at Fig 4.28. The test maximum torque is 210 Nm at 2500 rpm and the simulation maximum torque is 204.9 Nm at 2500 rpm. The test and simulation values are in good agreement. The percentage error between the tested simulated results is 3.91% which is in a reasonable range. That is to say the correctness of simulation result is verified by experiments.

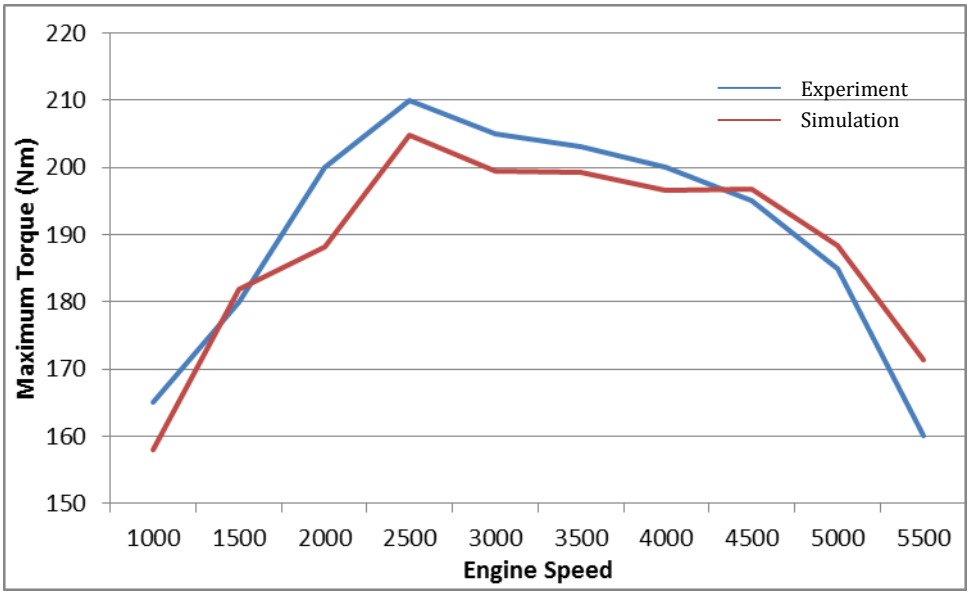

Figure 4.28: Validation on Maximum Torque

In order to further determine the accuracy of the simulation, the mean values of the errors in the simulation predictions and the test data are calculated from 80 operating

conditions of the engine when the throttle open angle range start from 5 to the biggest possible opening (5, 10, 15, 20, 25, 30, 50, 90 degree), and the engine speed range is from 1000 rpm to 5500 rpm (1000, 1500, 2000, 2500, 3000, 3500, 4000, 4500, 5000, 5500 rpm). The results given in Table 4.3 show that a slight error is observed in the operating regions. However, from more steady state conditions test can be seen a relatively large error is observed at low engine speed and low load conditions. Furthermore, the large error is observed at throttle open angle between 30 and 50 degree.

Table 4.4: Model Validation Test Error

Variable	Percentage Error
Engine output torque	4.56%
Intake manifold pressure	3.41%
Mass air flow rate at throttle valve	3.75%

4.6.2 Model Validation at Transient Stages

To validate the behaviour of the engine simulation during transients, the dynamometer is operated at a constant torque and a constant speed, respectively. A set of time responses was recorded for throttle transients. Three variables, the engine speed, the intake manifold pressure and the mass air flow rate are measured directly, and the AFR is measured from the oxygen sensor at the exhaust pipe instead of fuel mass in the film because the fuel film dynamics is not easy to measure. The torque production model is verified through a comparison with the brake torque from the output of the dynamometer controller. The simulation validation is divided into two categories; each category is further divided into 4 groups according to the experiment requirements. The engine speed (or brake torque), AFR, intake manifold pressure and air mass flow rate's comparison between the simulated data and the platform test data have been conducted respectively.

4.6.2.1 Constant Load Torque Tests

For the first test group, the dynamometer is set at a constant torque operation. The experiment will be divided into four groups: (1) small engine torque load with slightly frequent throttle change; (2) big engine torque load with slightly frequent throttle change; (3) small engine torque load with frequent throttle change; and (4) big engine

torque load with frequent throttle change.

Constant Load Torque Test 1

The constant engine load torque is set at 80 Nm. The throttle open angle is shown in Fig 4.29, it starts from a constant pressure of a 13 degrees, and then accelerates to reach a 19 degrees angle at fifteenth second, after 20 seconds the accelerator pedal is released at 13 degrees angle. Figs 4.30, 4.31, 4.32 and 4.33 show engine speed, AFR, intake manifold pressure and air mass flow rate, respectively.

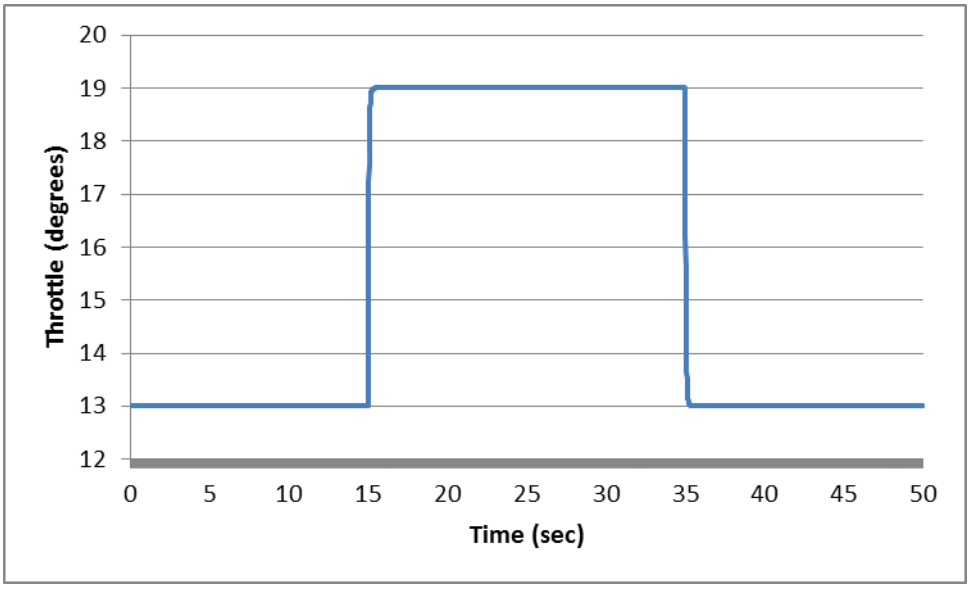

Figure 4.29: Throttle Input Profile for Experiment 1

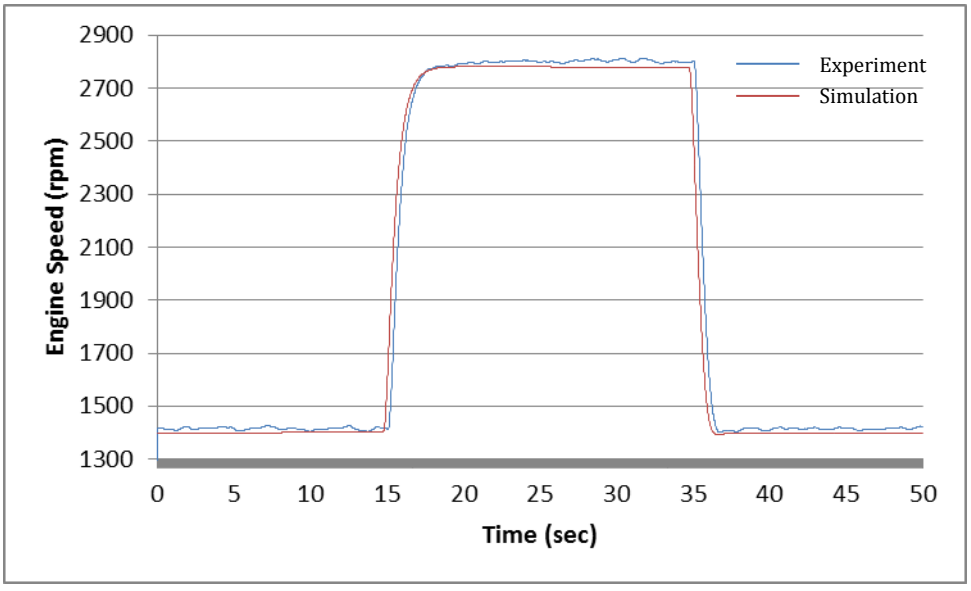

Figure 4.30: Validation on Engine Speed (Fig 4.30 Input Profile)

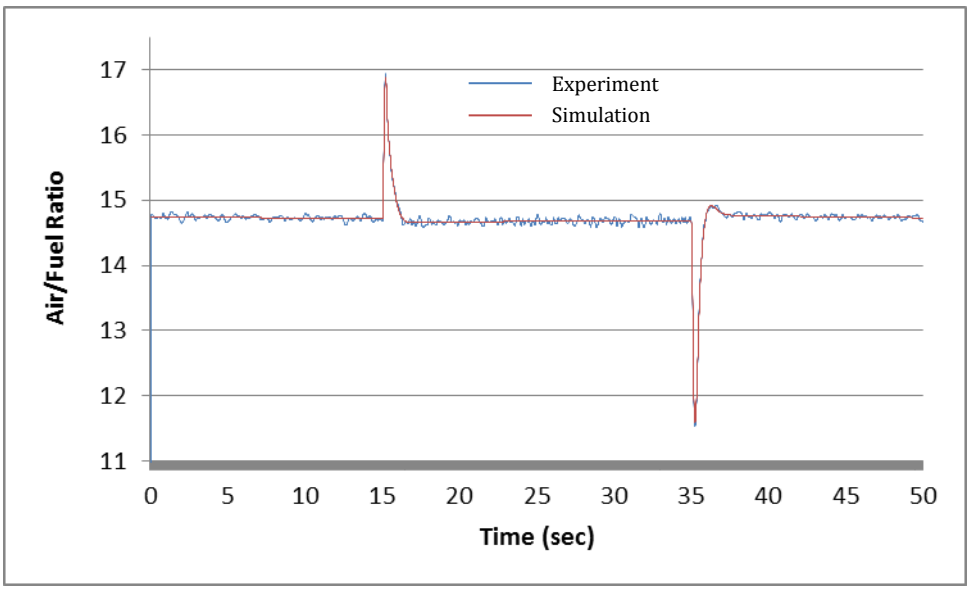

Figure 4.31: Validation on AFR (Fig 4.30 Input Profile)

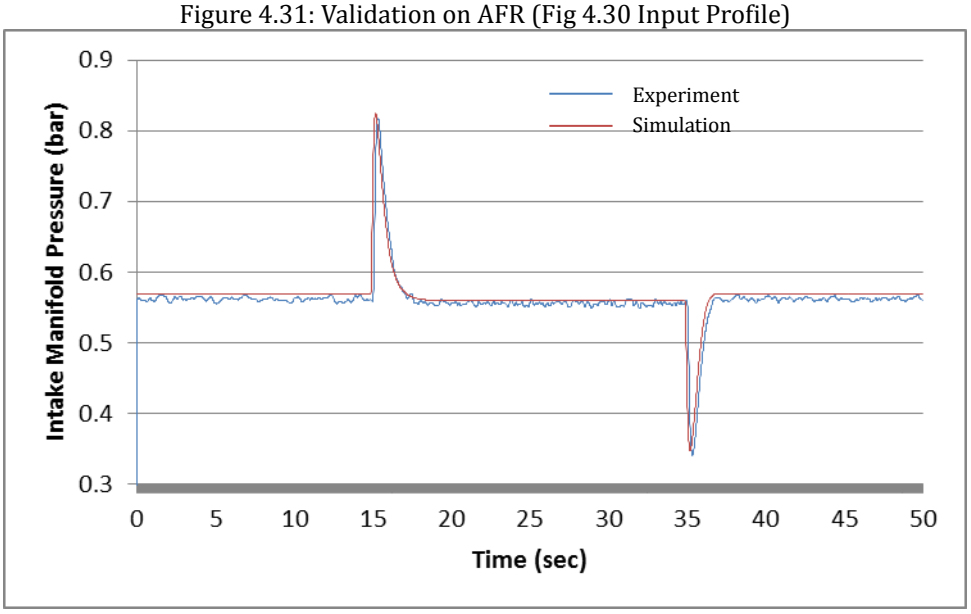

Figure 4.32: Validation on Intake Manifold Pressure (Fig 4.30 Input Profile)

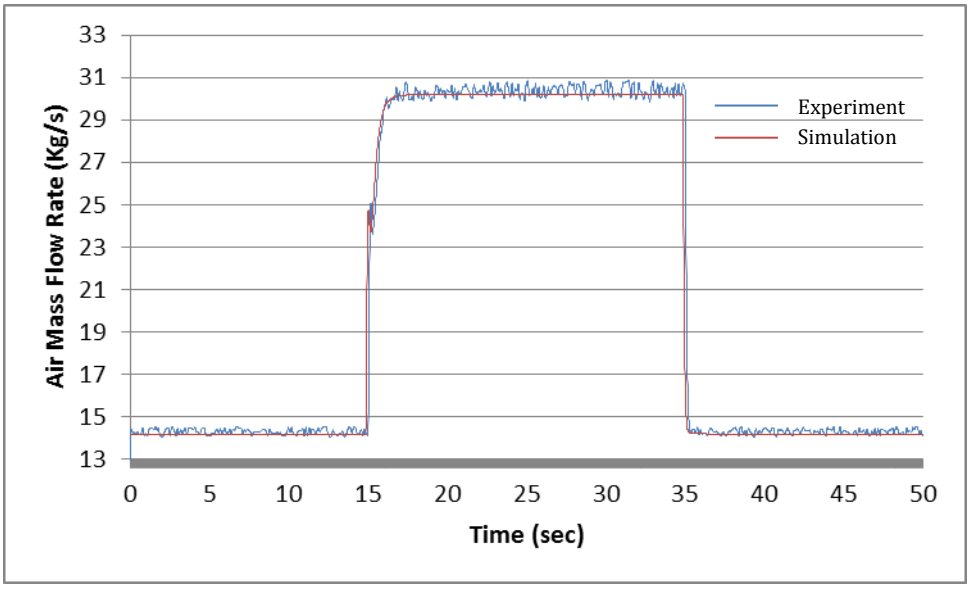

Figure 4.33: Validation on Air Mass Flow Rate (Fig 4.30 Input Profile)

Constant Load Torque Test 2

The constant engine load torque is set at 130 Nm. The throttle open angle is shown in Fig 4.34, it starts from a constant pressure of a 25 degrees angle, and then accelerates to reach a 29 degrees angle at fifteenth second, after 20 seconds the accelerator pedal is released at 25 degrees angle. Figs 4.35, 4.36, 4.37 and 4.38 show engine speed, AFR, intake manifold pressure and air mass flow rate, respectively.

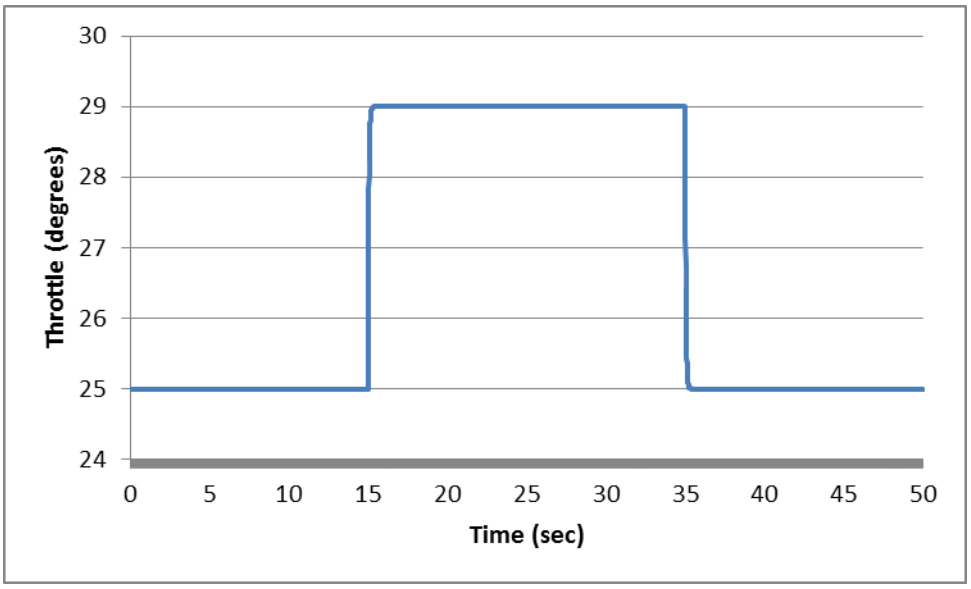

Figure 4.34: Throttle Input Profile for Experiment 2

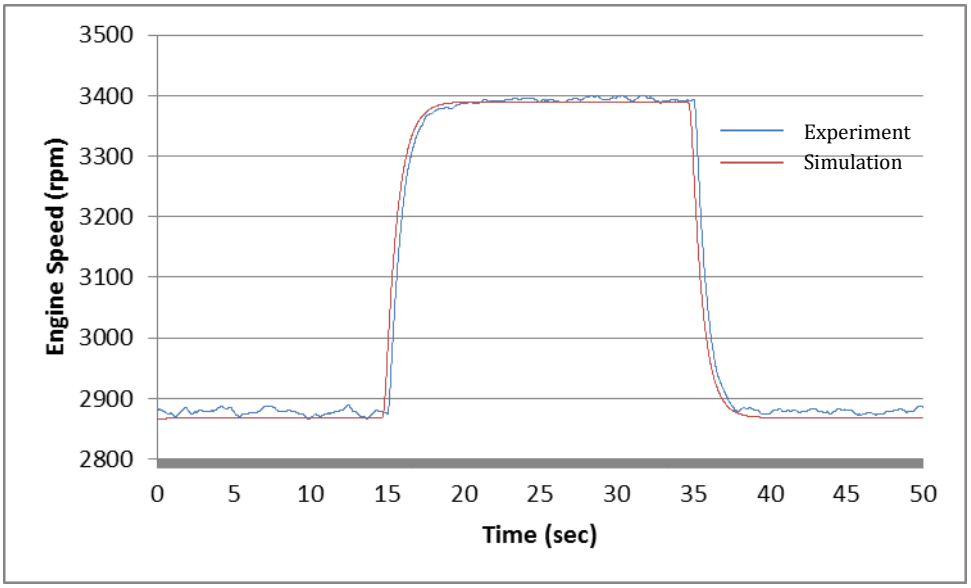

Figure 4.35: Validation on Engine Speed (Fig 4.34 Input Profile)

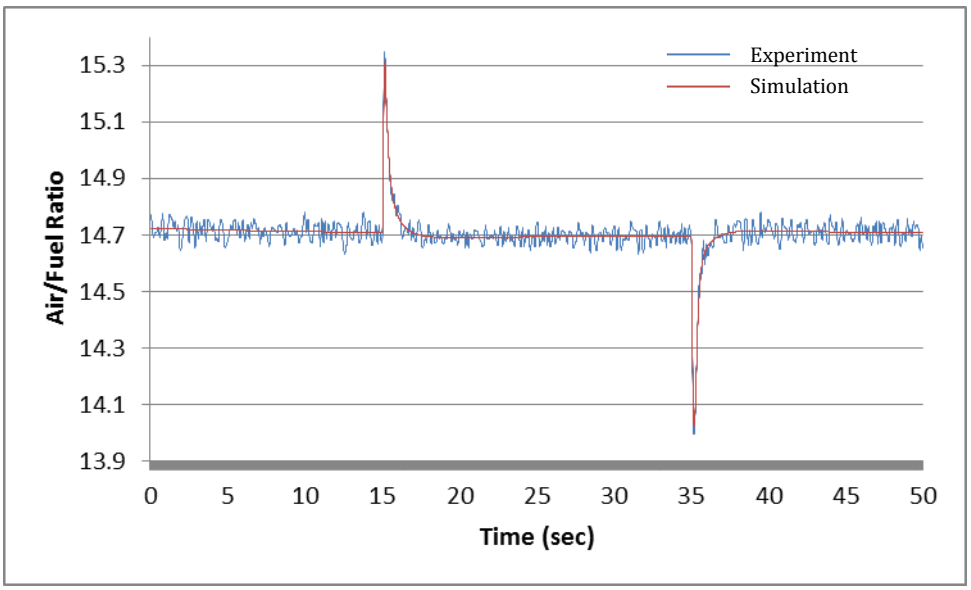

Figure 4.36: Validation on AFR (Fig 4.34 Input Profile)

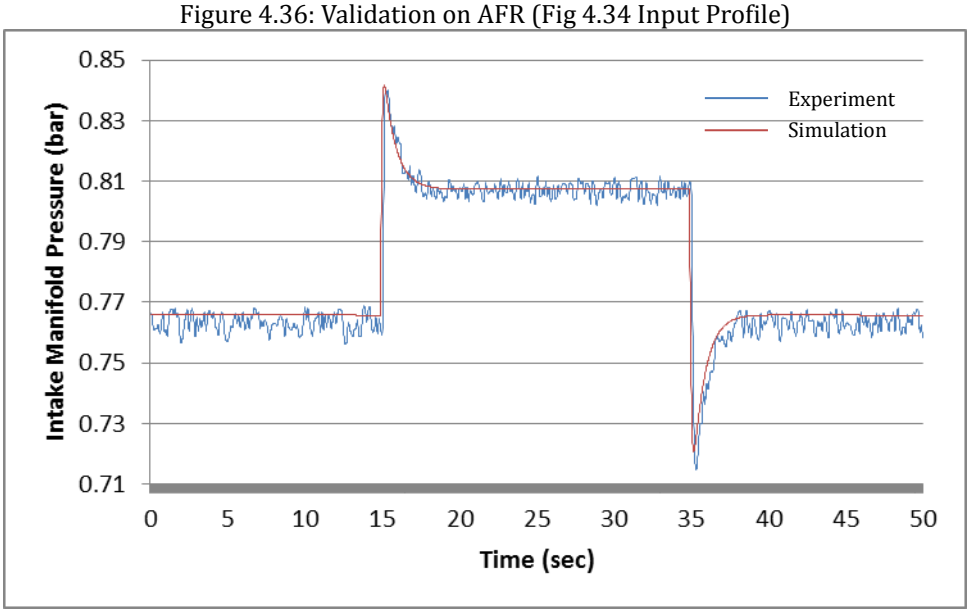

Figure 4.37: Validation on Intake Manifold Pressure (Fig 4.34 Input Profile)

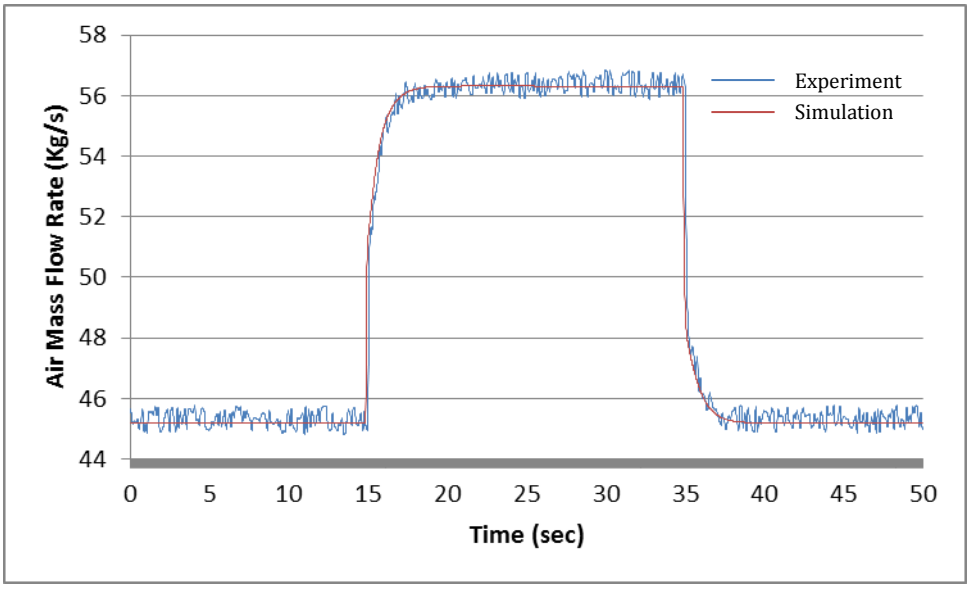

Figure 4.38: Validation on Air Mass Flow Rate (Fig 4.34 Input Profile)

Constant Load Torque Test 3

The constant engine load torque is set at 70 Nm. The throttle open angle is shown in Fig 4.39, it starts from a constant pressure of about 15 degrees angle, and then obtained by randomly pushing and releasing the accelerator pedal, maximum throttle open angle will be about 22 degrees. Figs 4.40, 4.41, 4.42 and 4.43 show engine speed, AFR, intake manifold pressure and air mass flow rate, respectively.

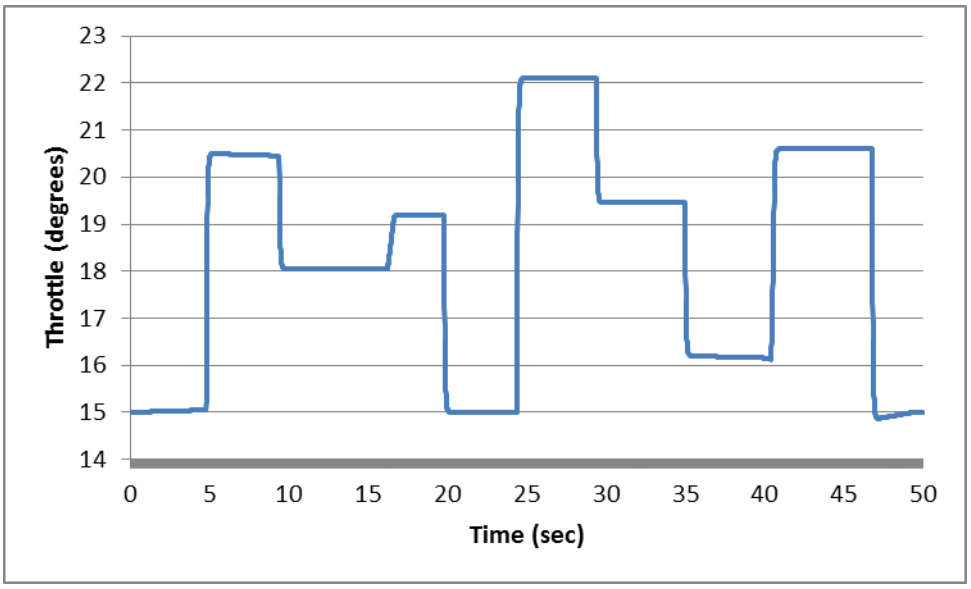

Figure 4.39: Throttle Input Profile for Experiment 3

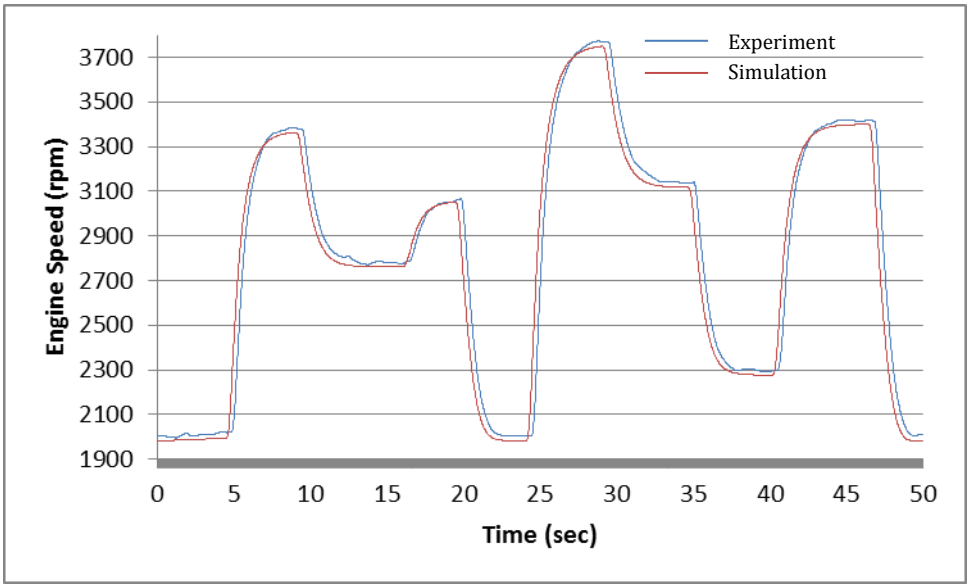

Figure 4.40: Validation on Engine Speed (Fig 4.39 Input Profile)

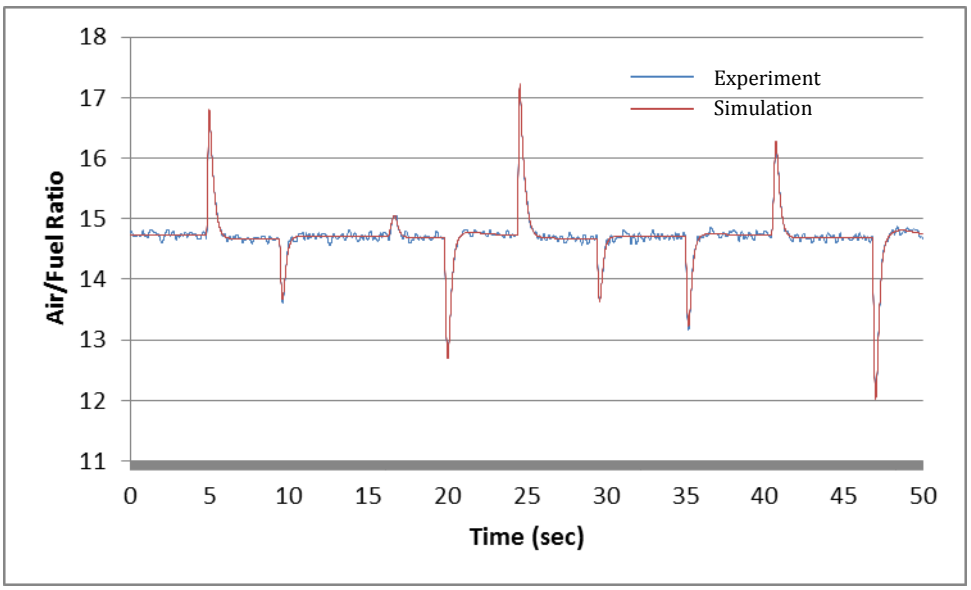

Figure 4.41: Validation on AFR (Fig 4.39 Input Profile)

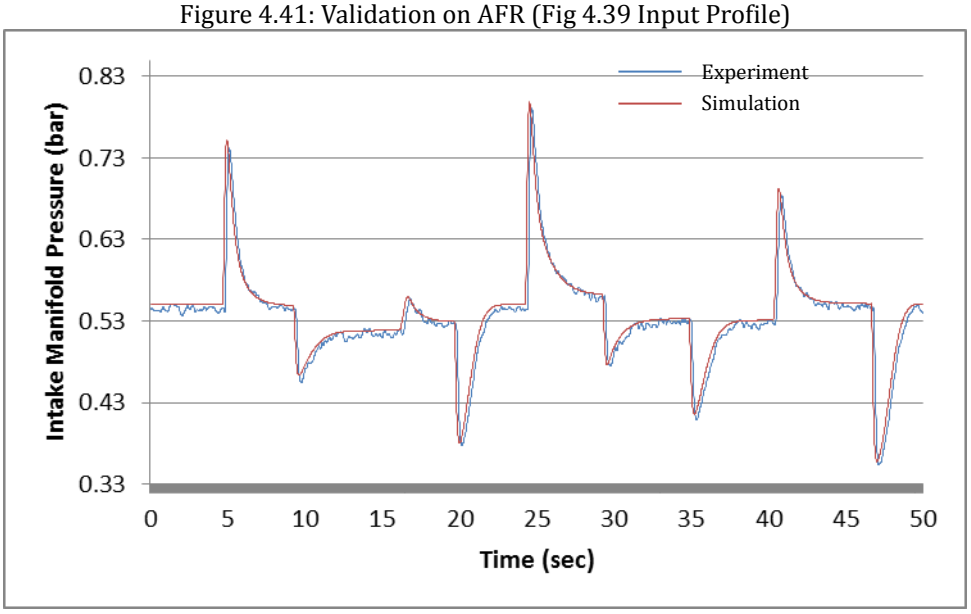

Figure 4.42: Validation on Intake Manifold Pressure (Fig 4.39 Input Profile)

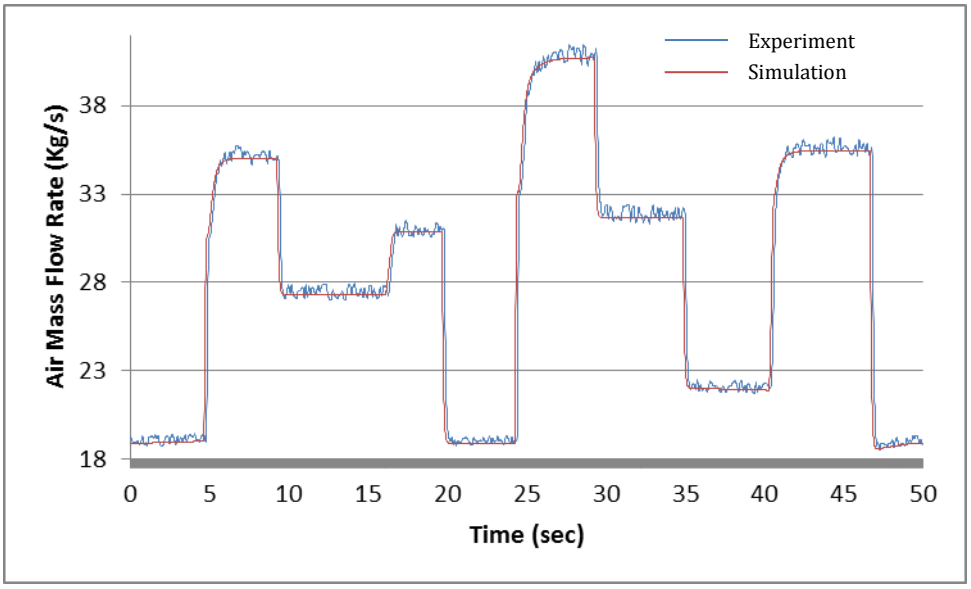

Figure 4.43: Validation on Air Mass Flow Rate (Fig 4.39 Input Profile)

Constant Load Torque Test 4

The constant engine load torque is set at 140 Nm. The throttle open angle is shown in Fig 4.44, it starts from a constant pressure of about 26 degrees angle, and then obtained by randomly pushing and releasing the accelerator pedal, maximum throttle open angle will be about 32 degrees. Figs 4.45, 4.46, 4.47 and 4.48 show engine speed, AFR, intake manifold pressure and air mass flow rate, respectively.

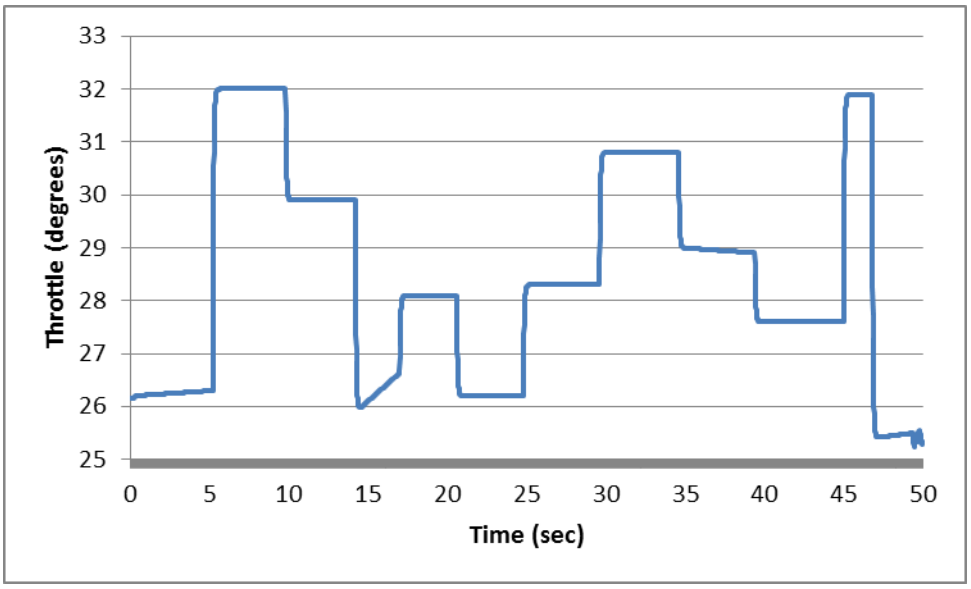

Figure 4.44: Throttle Input Profile for Experiment 4

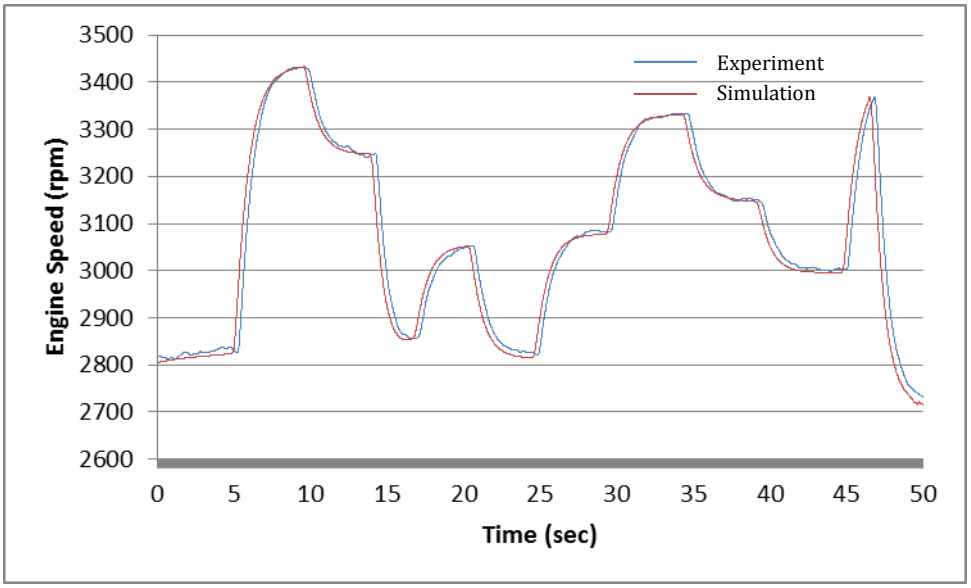

Figure 4.45: Validation on Engine Speed (Fig 4.44 Input Profile)

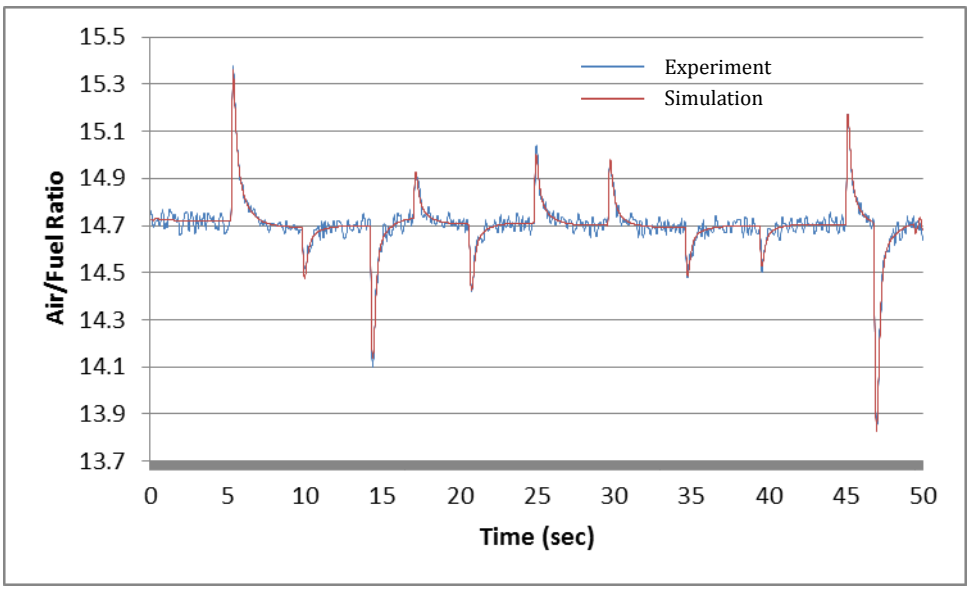

Figure 4.46: Validation on AFR (Fig 4.44 Input Profile)

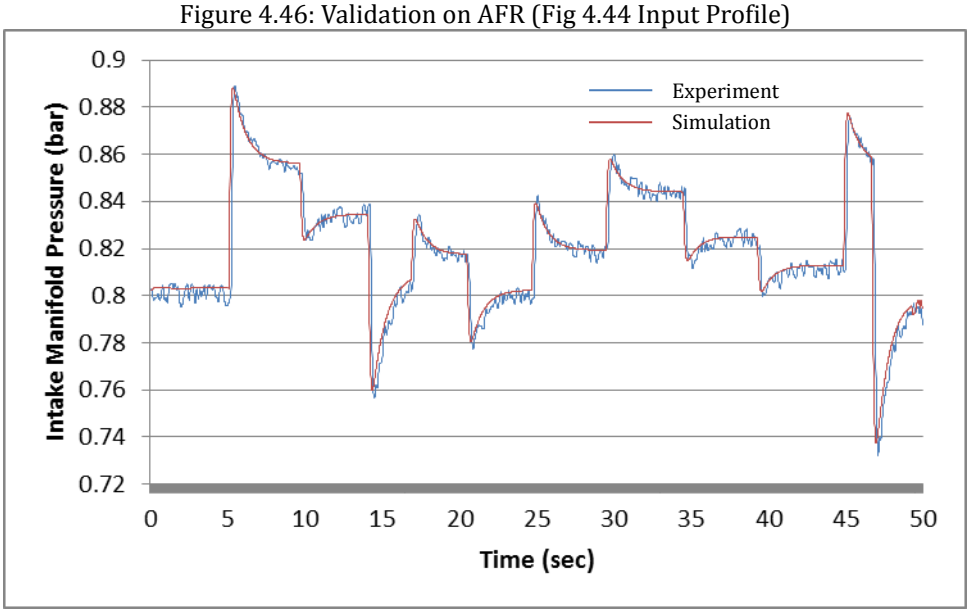

Figure 4.47: Validation on Intake Manifold Pressure (Fig 4.44 Input Profile)

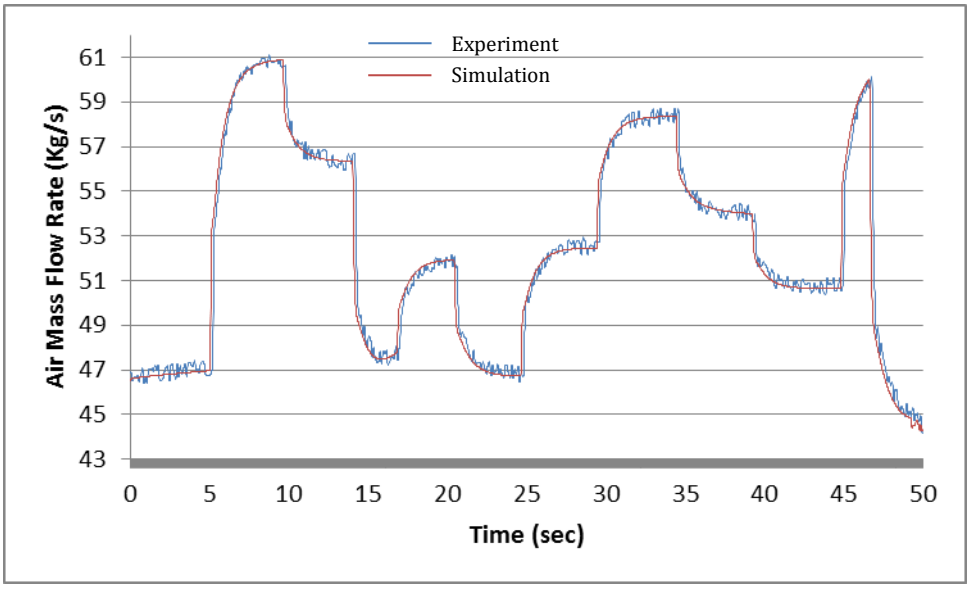

Figure 4.48: Validation on Air Mass Flow Rate (Fig 4.44 Input Profile)

4.6.2.2 Constant Engine Speed

The dynamometer is operated at constant speeds at approximately 1500, 2500, 3000 and 4000 rpm.

Constant Engine Speed 1

The constant engine speed is set at 1500 rpm. The throttle open angle is shown in Fig 4.49, it starts from a constant pressure of about 14 degrees angle, and then accelerates to reach a 15.6 degrees angle at fifteenth second, after 20 seconds the accelerator pedal is released at 14 degrees angle. Figs 4.50, 4.51, 4.52 and 4.53 shown brake load, AFR, intake manifold pressure and air mass flow rate, respectively.

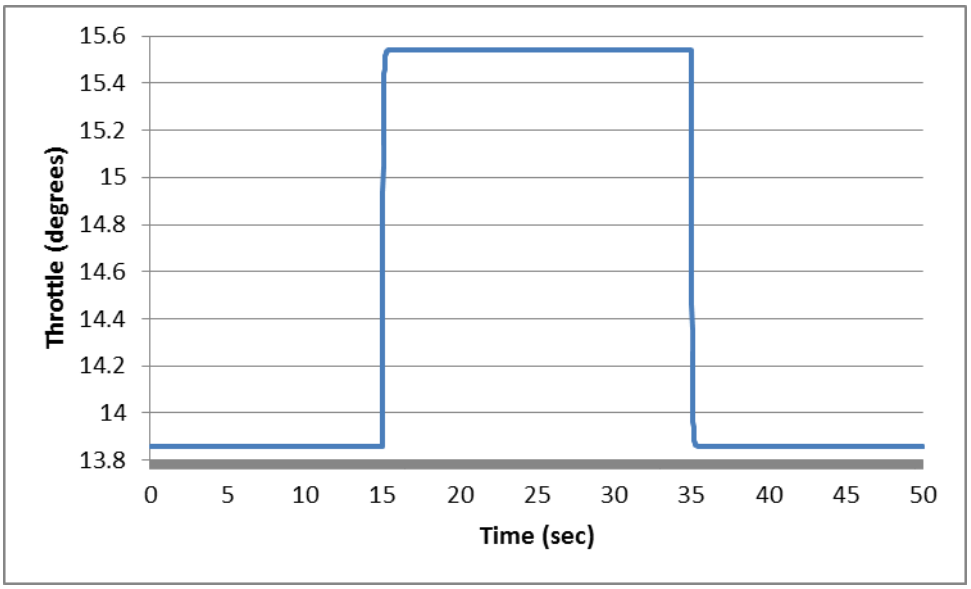

Figure 4.49: Throttle Input Profile for Experiment 5

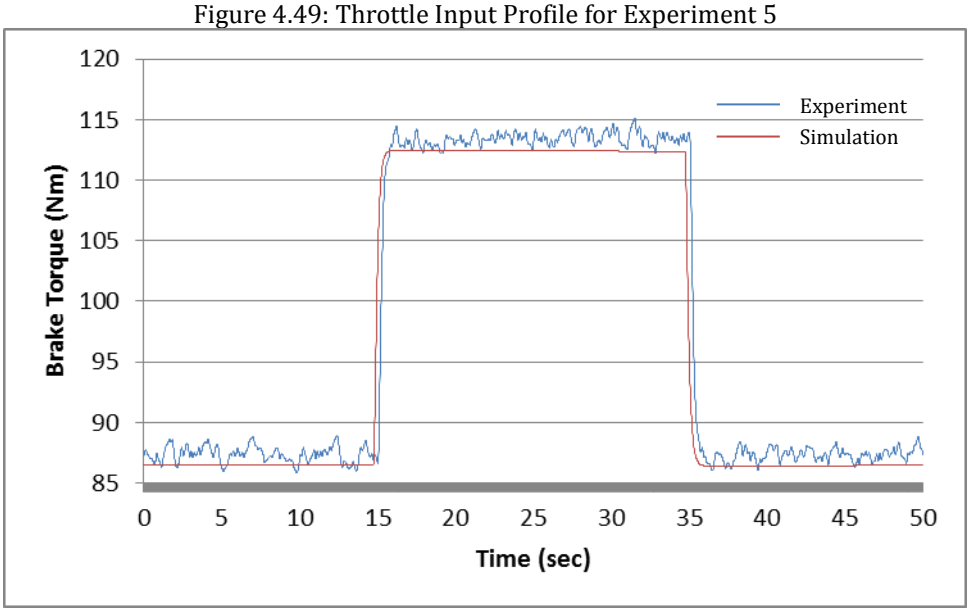

Figure 4.50: Validation on Brake Torque (Fig 4.49 Input Profile)

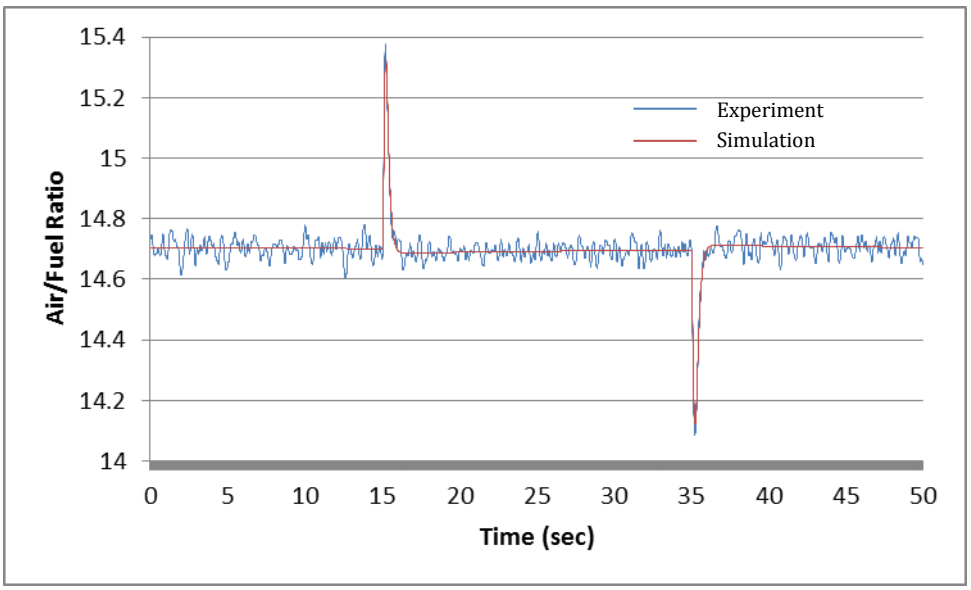

Figure 4.51: Validation on AFR (Fig 4.49 Input Profile)

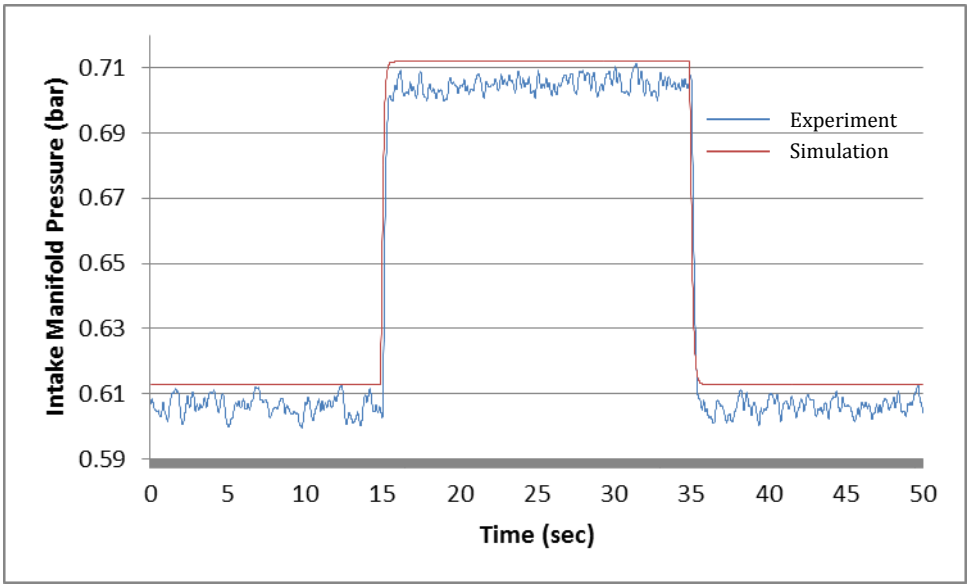

Figure 4.52: Validation on Intake Manifold Pressure (Fig 4.49 Input Profile)

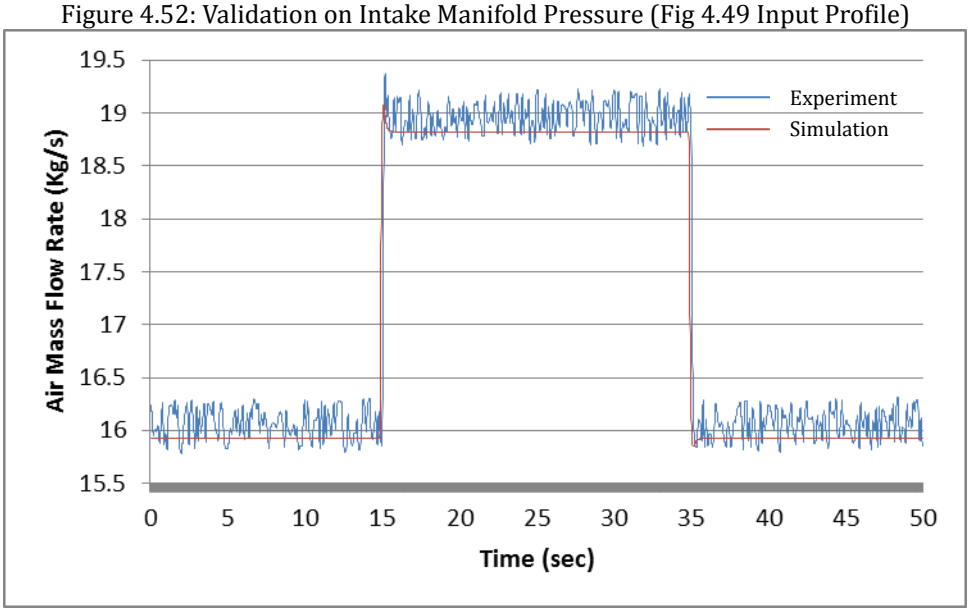

Figure 4.53: Validation on Air Mass Flow Rate (Fig 4.49 Input Profile)

Constant Engine Speed 2

The constant engine speed is set at 2500 rpm. The throttle open angle is shown in Fig 4.54, it starts from a constant pressure of about 15 degrees angle, and then obtained by randomly pushing and releasing the accelerator pedal, maximum throttle open angle will be about 20.5 degrees. Figs 4.55, 4.56, 4.57 and 4.58 show engine speed, AFR, intake manifold pressure and air mass flow rate, respectively.

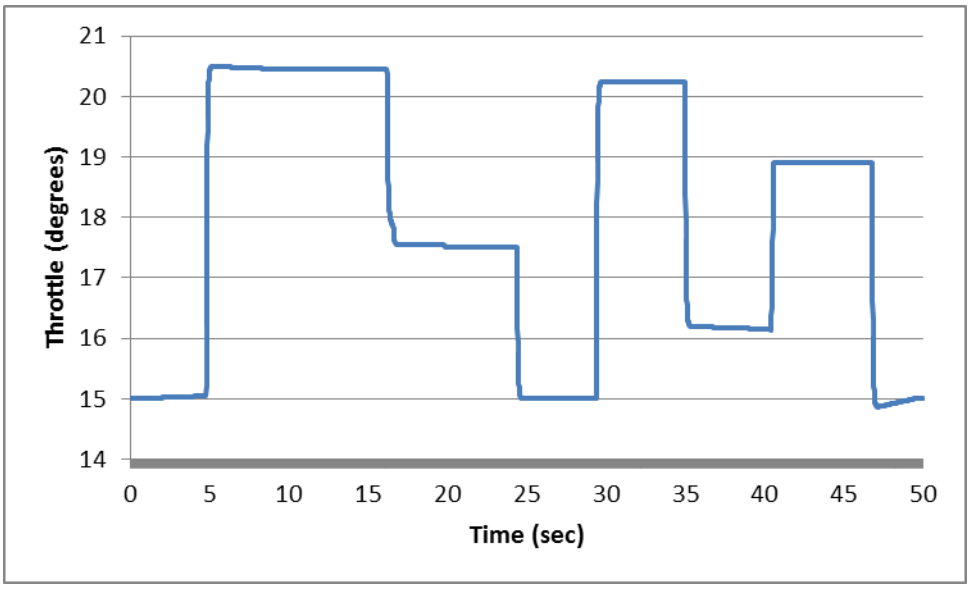

Figure 4.54: Throttle Input Profile for Experiment 6

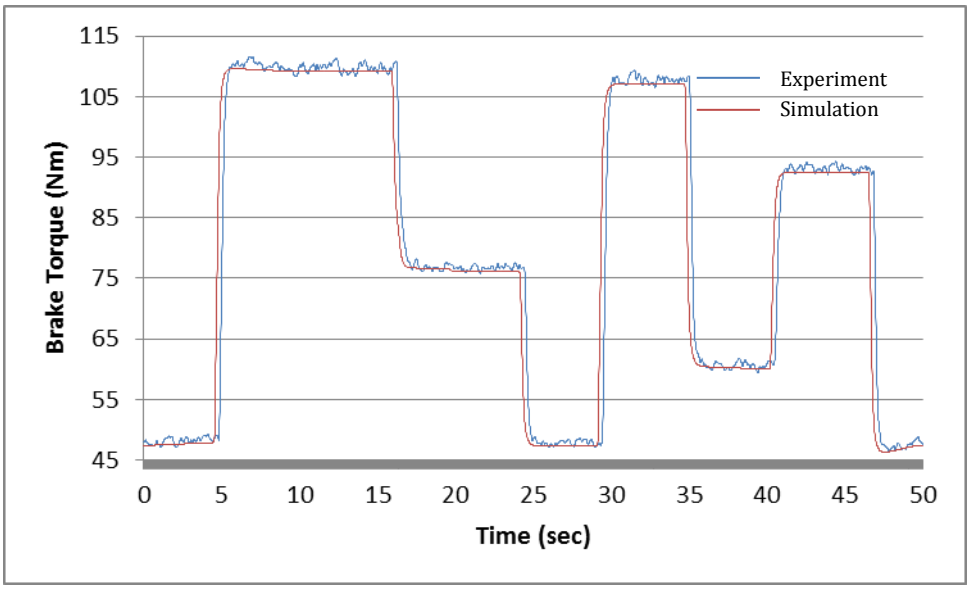

Figure 4.55: Validation on Brake Torque (Fig 4.55 Input Profile)

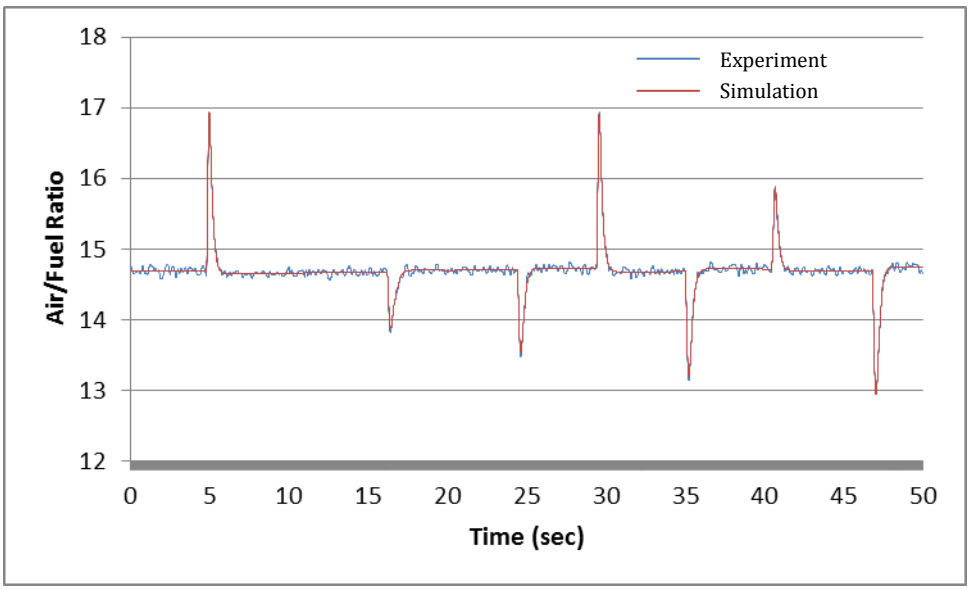

Figure 4.56: Validation on AFR (Fig 4.54 Input Profile)

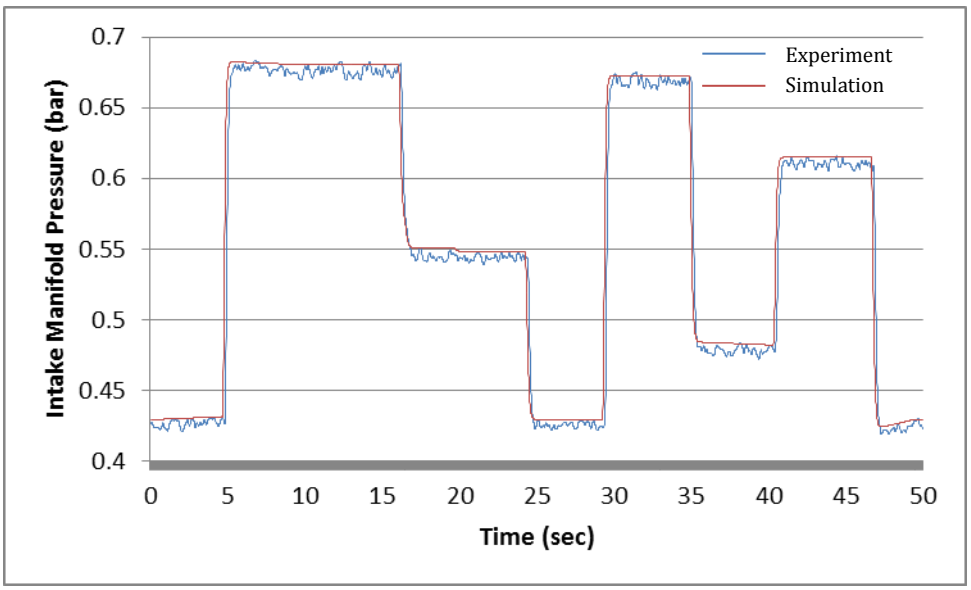

Figure 4.57: Validation on Intake Manifold Pressure (Fig 4.54 Input Profile)

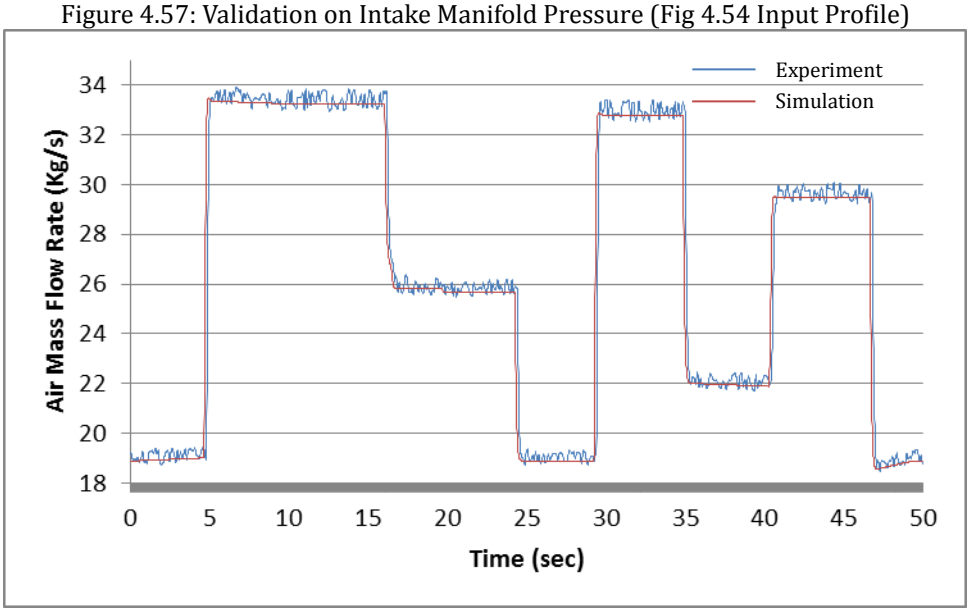

Figure 4.58: Validation on Air Mass Flow Rate (Fig 4.54 Input Profile)

Constant Engine Speed 3

The constant engine speed is set at 3000 rpm. The throttle open angle is shown in Fig 4.59, it starts from a constant pressure of about 21 degrees angle, and then obtained by randomly pushing and releasing the accelerator pedal, maximum throttle open angle will be about 26 degrees. Figs 4.60, 4.61, 4.62 and 4.63 show engine speed, AFR, intake manifold pressure and air mass flow rate, respectively.

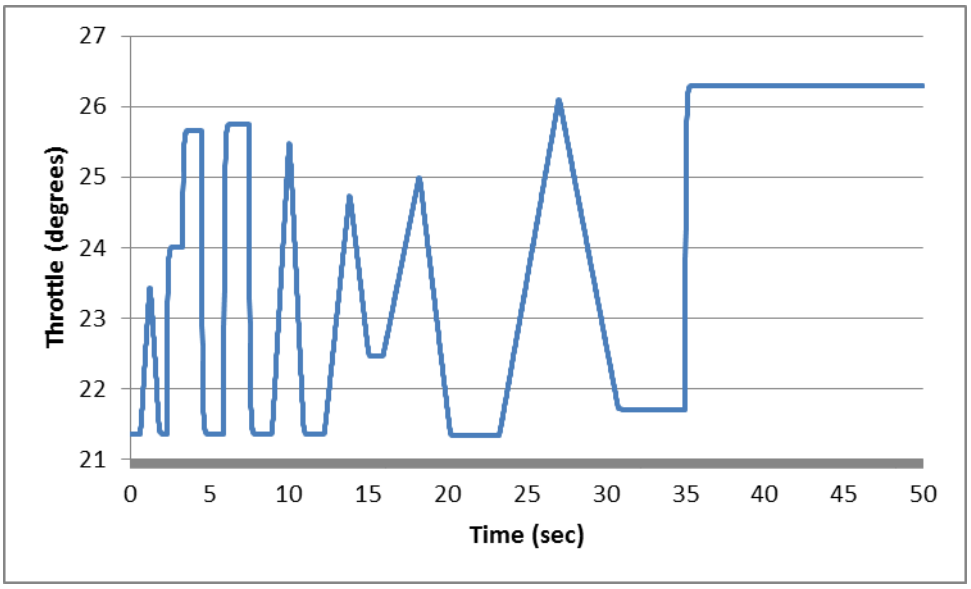

Figure 4.59: Throttle Input Profile for Experiment 7

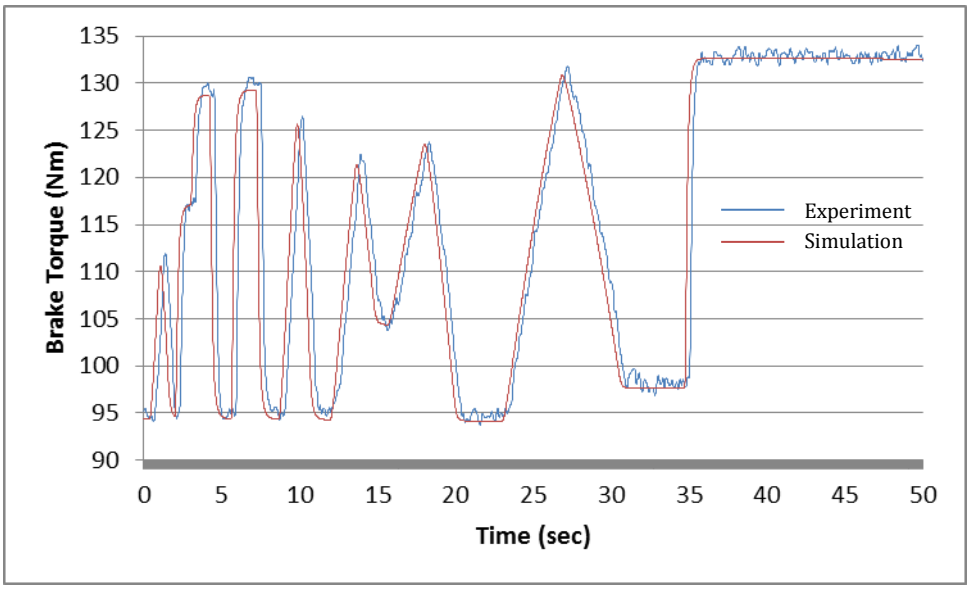

Figure 4.60: Validation on Brake Torque (Fig 4.60 Input Profile)

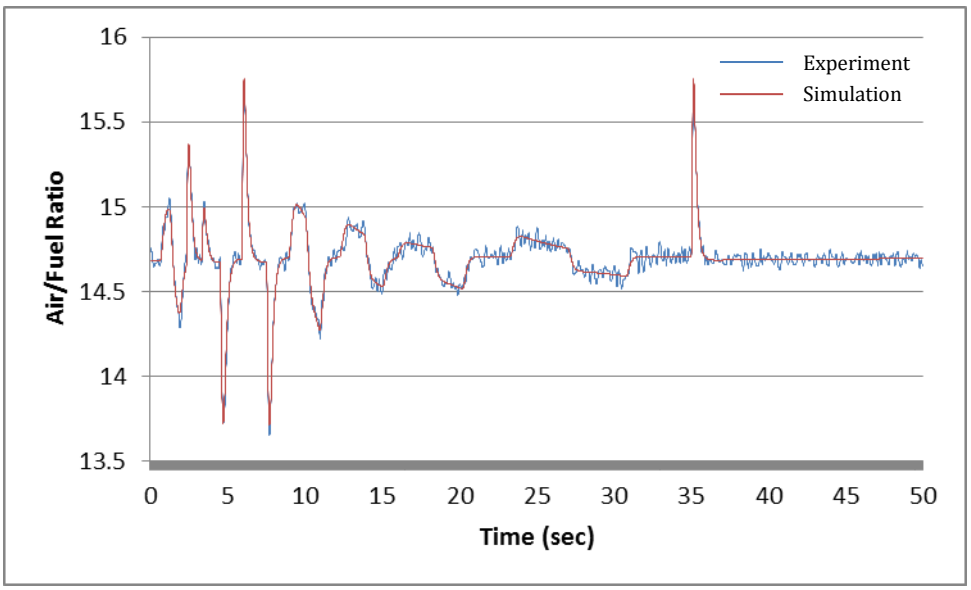

Figure 4.61: Validation on AFR (Fig 4.60 Input Profile)

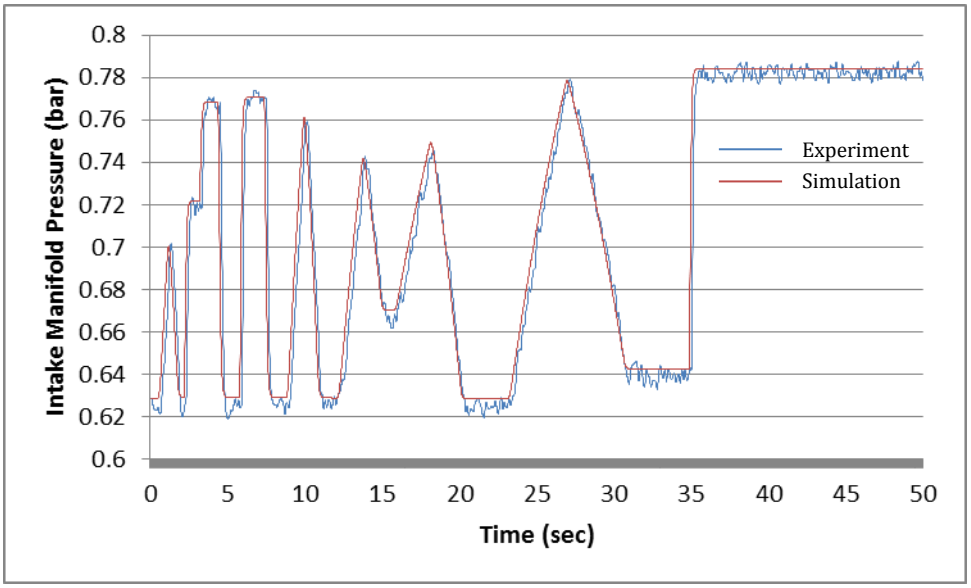

Figure 4.62: Validation on Intake Manifold Pressure (Fig 4.60 Input Profile)

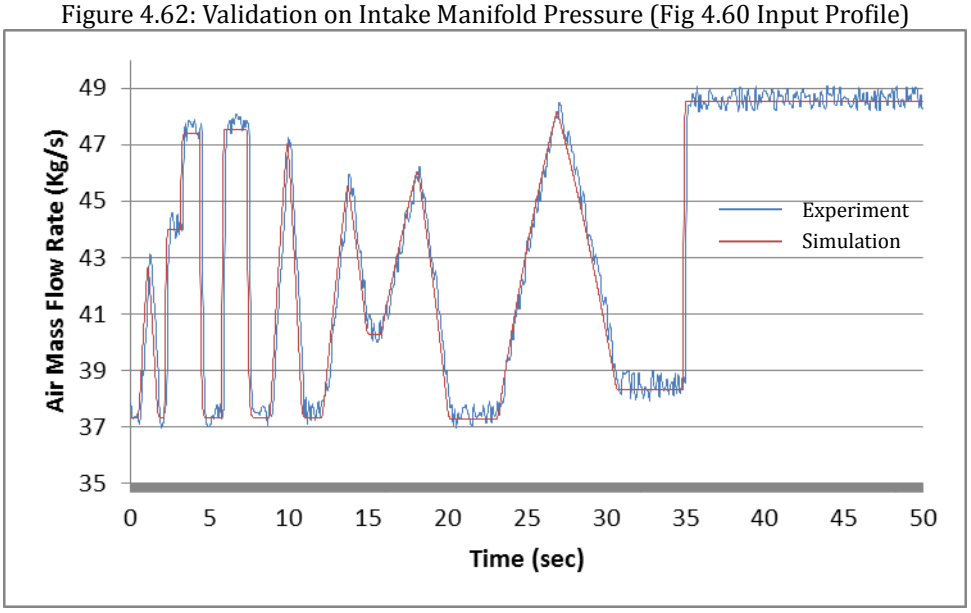

Figure 4.63: Validation on Air Mass Flow Rate (Fig 4.60 Input Profile)

Constant Engine Speed 4

The constant engine speed is set at 4000 rpm. The throttle open angle is shown in Fig 4.64, it starts from a constant pressure of about 26 degrees angle, and then slow accelerates by reaching a 31 degrees angle at around eighteenth second, at 20 seconds release the accelerator pedal at 26 degrees angle, and so on. Figs 4.65, 4.66, 4.67 and 4.68 show brake load, AFR, intake manifold pressure and air mass flow rate, respectively.

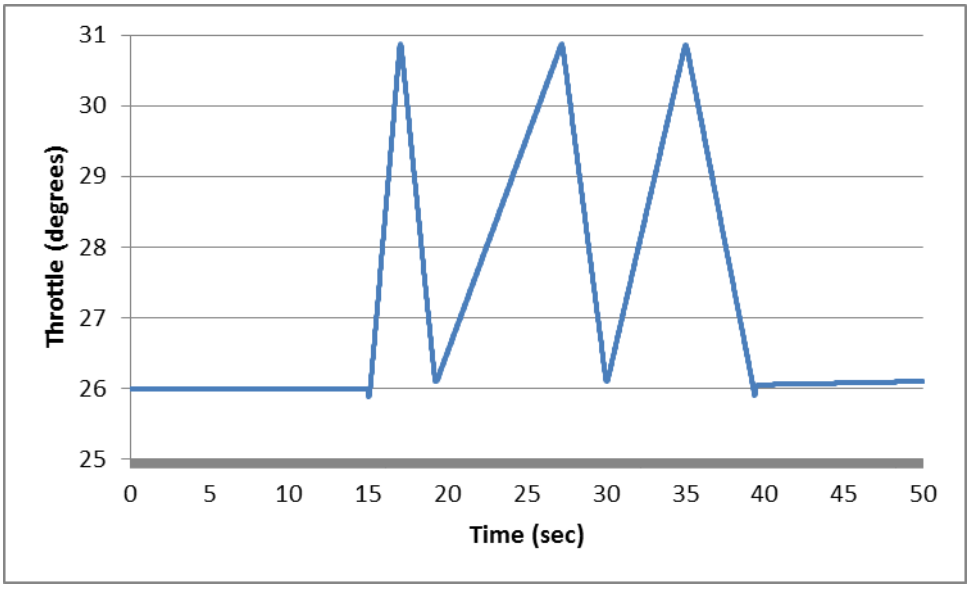

Figure 4.64: Throttle Input Profile for Experiment 8

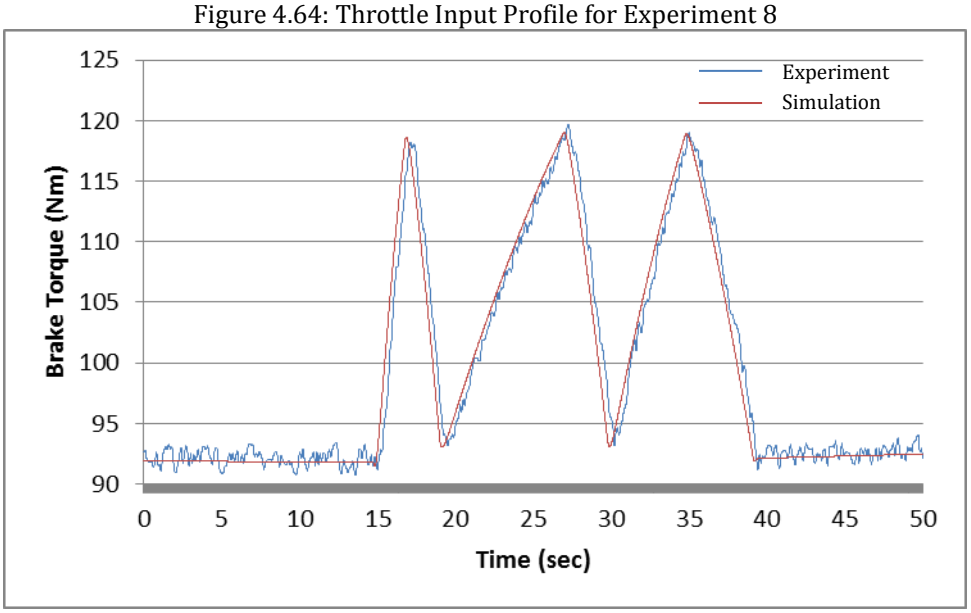

Figure 4.65: Validation on Brake Torque (Fig 4.64 Input Profile)

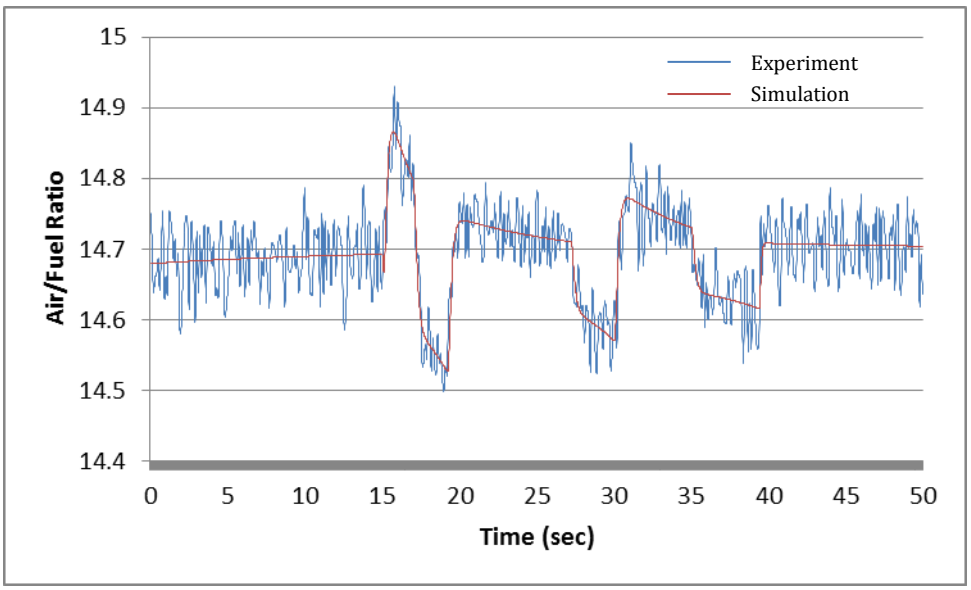

Figure 4.66: Validation on AFR (Fig 4.64 Input Profile)

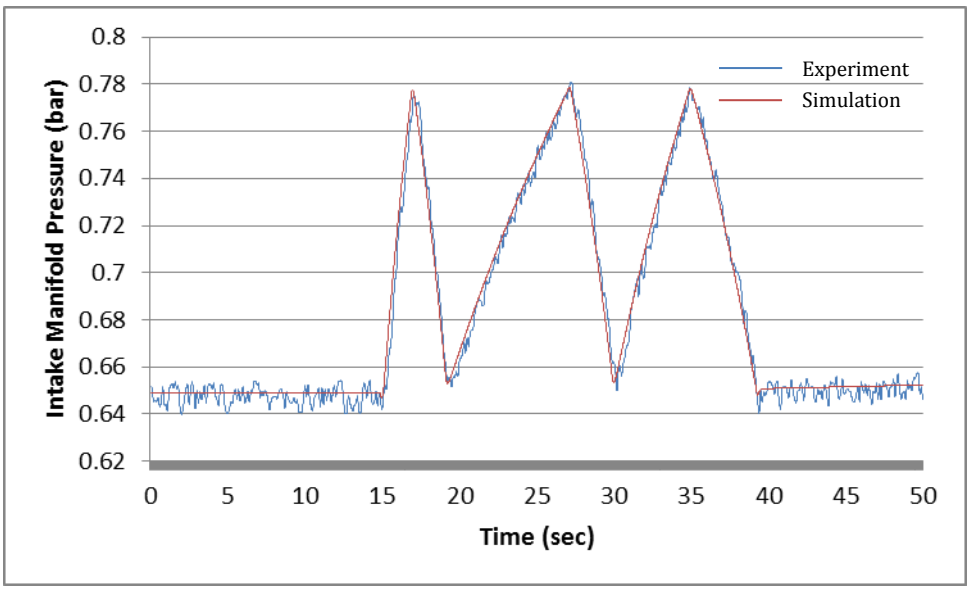

Figure 4.67: Validation on Intake Manifold Pressure (Fig 4.64 Input Profile)

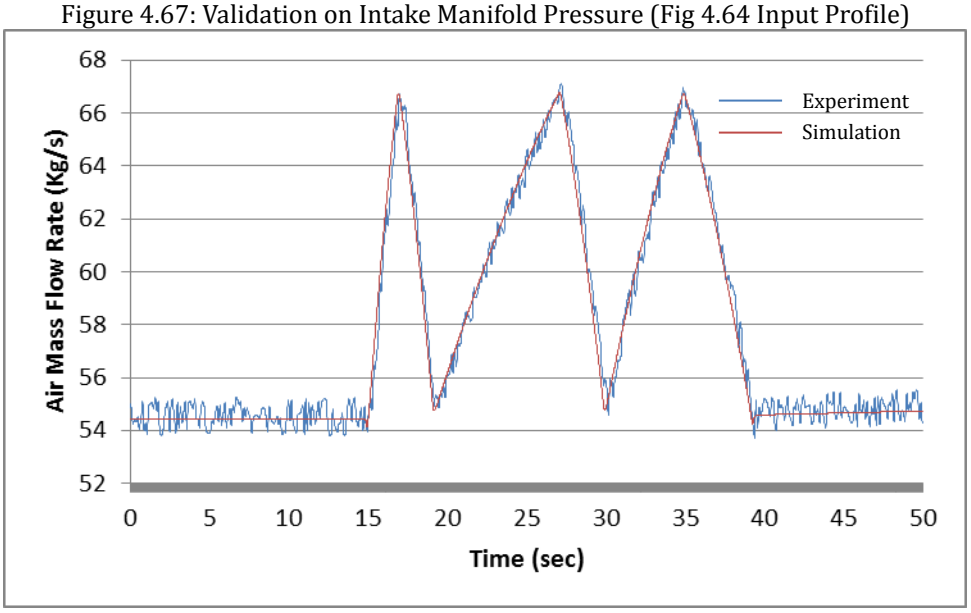

Figure 4.68: Validation on Air Mass Flow Rate (Fig 4.64 Input Profile)

4.6.3 Analysis of Simulation Feasibility

The simulation feasibility experiments are divided into three categories, the first is the steady state test, followed by transient state constant torque test, and finally the transient state constant engine speed test.

Steady state test is aimed at comparing the simulation and real test engine performance in steady state. Therefore it is not required to consider the controller's influence on the system response performance. The following three categories of tests are used to validate simulation accuracy.

(1) Fixed target tests: For example, set a target for engine maximum torque curve, and then the simulation is conducted to achieve this target by adjusting the throttle open angle and load torque. The target and simulation results engine performance are shown in Fig 4.28, it can be seen that two curves are very consistent and the maximum percentage error is less than 6% (Fig 4.28-engine speed at 2000 rpm).

(2) Fixed input tests: For example, use a fixed set of throttle open angle and engine speed or load as a constant variable inputs to simulation a set of intake manifold pressure, fuel mass injected, AFR and engine output torque (or speed). The test results shows in Table 4.5, the steady state average error is 4.64%, the average error is reduced to 2.87% if the engine speed restricted between 1500 and 4500, the large error (6.06%) is observed at throttle open angle between 30 and 50 degree.

(3) Single model linearity tests: For example, set the throttle opening at an angle and change the engine speed and measure the volume change curve from simulation package, and this is then compare with laboratory test data. There are countless similar tests not detailed in the thesis. But the test results of all the variables in the steady state error are less than 5% (Table 4.4).

Transient state tests are designed to verify the engine simulation package for its dynamic transient responses. Through controlling package throttle opening angle and

limiting the load torque (or the engine speed), tests can be done for intake manifold pressure, engine speed or torque AFR response performance, etc

Table 4.5: Steady State Average Error

Average Error (%)		Engine Speed （rpm）									
		1000	1500	2000	2500	3000	3500	4000	4500	5000	5500
Throttle Open Angle （deg）	10	4.81	2.14	1.93	2.03	2.18	2.11	1.95	2.19	5.35	12.07
	20	5.12	2.42	2.65	2.69	2.79	2.65	2.5	2.61	6.83	13.05
	30	5.90	3.79	4.17	4.27	4.38	4.22	3.89	3.84	8.58	15.53
	40	6.54	4.15	4.39	4.69	4.79	4.49	3.95	3.98	9.54	16.78
	50	5.91	3.95	4.03	4.31	4.18	4.27	4.13	4.24	8.91	15.93
	60	5.27	2.79	2.39	2.71	2.75	2.67	2.54	2.47	7.28	14.13
	70	5.09	2.14	1.93	2.09	2.13	2.11	2.13	2.09	6.75	13.57
	80	4.95	1.97	1.84	1.95	1.95	1.96	1.93	1.92	5.56	12.01
	90	4.96	1.9	1.85	1.92	1.98	1.97	1.75	1.81	5.38	11.33

Dynamometers can be equipped with two types of control systems to provide different type of tests. The first is constant force type test where the dynamometer has a braking torque regulator which is configured to provide a set braking force torque load. These tests are done while the prime mover is configured to operate at whatever throttle opening, fuel delivery rate, or any other variable it is desired to test. The second is constant speed tests where the dynamometer has a speed regulator (human or computer), and the Power Absorption Unit is to provide a variable amount of braking torque that is necessary to cause the prime mover to operate at the desired engine test speed. In order to cooperate with the platform tests, the acquired data are divided into constant speed and torque two groups.

There were four constant engine torque tests for different torque, different throttle angle, and different throttle frequent changes. For example, test throttle open angle between 13 and 32 degrees, and the engine speed responds between 1400 and 3800 rpm. Constant engine torque test 1 and 2 show that the simulated data is in line with the test data. From test constant engine torque 3 and 4, it can be seen that the simulation provides a prompt control action. Four test groups of simulation engine speed result is lower than the actual speed, further studies found a higher engine speed was associated with lower error, and for other results accuracy is very high with percentage error of 6%.

There were four constant engine speed tests for different torque, different throttle angle, and different throttle frequent changes. Test throttle open angle between 13.8 and 31 degrees, and the engine torque output responds between 45 and 135 Nm. From constant engine speed test 1, it can be seen that the simulated data is in line with the test data. From constant engine speed test 2, 3 and 4, it can be seen that the simulation provides good agreement with experimental data. The test results indicated that the higher the engine speed, the higher the AFR error. Test intake pressure is higher than the laboratory measurement. The accuracy of air flow rate is very high, but as the engine speed increases the response delay will be larger.

Steady state tests have proved that each of models in engine package have a good accuracy. For transient state tests, results show that the simulation outputs of the brake load or engine speed, the AFR, the intake manifold pressure and the air mass flow rate show good alignment with experimental data. For the brake torque or engine speed, a slight time delay is observed during the transient period between the simulated and the test results. But the delay does not affect the dynamic response and accuracy. Overall, the SIMULINK-based engine dynamic simulation package is in line with the actual engine working conditions, the controller controlled performance achieve the expectations, all variable dynamic responses achieved requirements. There the simulation package can be used for further in many application fields such as controller developments and improvements.

4.7 Summary

This chapter is focusing on introducing the development and verification of the engine simulation package, which can be used in design and optimization of engine control systems. Firstly, the engine simulation models are built according to engine dynamic equations and parameters obtained from the engine testing platform. Secondly, the input subsystem and output model were introduced. Thirdly, the engine controller is introduced. Finally, engine simulation results are presented and they are compared with experimental data.

Engine dynamic simulation package deal with all dynamics related to engine operation, such as air dynamics, fuel dynamics and combustion dynamic. Because of the air and fuel dynamics are dealt with separately, the simulation package has very good

scalability which can be joined by turbocharger dynamics, supercharger dynamics, EGR dynamics and any dynamic behaviour which are related to air or fuel.

In order to simply intuitive engine simulation testing framework and to investigate the impact of control system optimization, the engine dynamic simulation package has incorporated a reasonable vehicle dynamic model and a driving cycle model. This has enabled valid theoretical analysis and industrial standard vehicle testing.

The simulation package has been proved very successful with results very close to experimental results. Comparison between the simulated and the test results at transient conditions with step and sinusoidal throttle inputs applied have been made. The simulation outputs of the brake load (or engine speed), the air/fuel ratio, the intake manifold pressure and the air mass flow rate show in good agreement with experimental data. However, for the brake torque or engine speed, a slight time delay is observed during the transient period between the simulated and the test results. There are slight error (average 4%) observed in the wide operating regions at steady conditions. However, relatively large errors (10%) are observed at low engine speed and low load conditions, and also observed when the throttle open angle between 30 and 50 degrees. However, these does not affect the overall validity of the simulation package.

Chapter 5: PID and Fuzzy Logic AFR Control

5.1 Introductions

The gasoline engine fuel system requires a set of air fuel mixture to provide suitable amount of fuel and air. In order to burn all of the available fuel completely in the engine, a certain quantity of air must be provided. If only exactly enough air amount is supplied to the fuel combustion, the AFR is known as the stoichiometric ratio. Control of AFRs at the constant stoichiometric ratio is not only a key factor on combustion efficiency and engine power performance, but also has essential impact on reduction of pollution emission (Hendricks et al., 1993; Heywood, 1998; Pace & Zho, 2009; Wong, Wong & Vong, 2012).

The goal of this chapter is to develop an AFR control system, where the desired AFR is set as a function of the engine speed. Some other variables can be added to this AFR control system, for example, the throttle valve level can be used as an additional factor ensuring a good AFR regulation even during fast transient conditions. The first part of this chapter presents the engine AFR control system structure. Two additional control methods based on the extension of this control system structure are then proposed. Simulation results are presented to demonstrate their efficiency, and the advantages and disadvantages are analysed and summarized. Finally further improvements on the AFR control system are discussed.

5.2 Engine AFR Control Systems

A good engine AFR control system requires good stability and good accuracy under different working conditions. Normally, the AFR control can be realized by two controllers (see Fig.5.1): the first controller (a feedforward controller) is to determine the “base” fuel mass injection by reading from the lookup table. The second controller (a feedback controller) is used to stabilize the system, to improve dynamic transient responses, and to compensate for any variation from target (ideal) AFR. . Along with the advancements in the exhaust after treatment system technology, studies found that the engine efficiency will be increased by lean burn combustion, and the engine AFR will not need to be kept at 14.7. Therefore, there is a need for the controller to adjust the

desired AFR value. The feedback control is to identify and adjust any error to achieve the desired. Hence the new engine AFR control system consists of two closed-loop and one open-loop controllers, and the control scheme is shown in Fig 5.1. One closed-loop control is for stability and transient response and another is for the target AFR value adjustment.

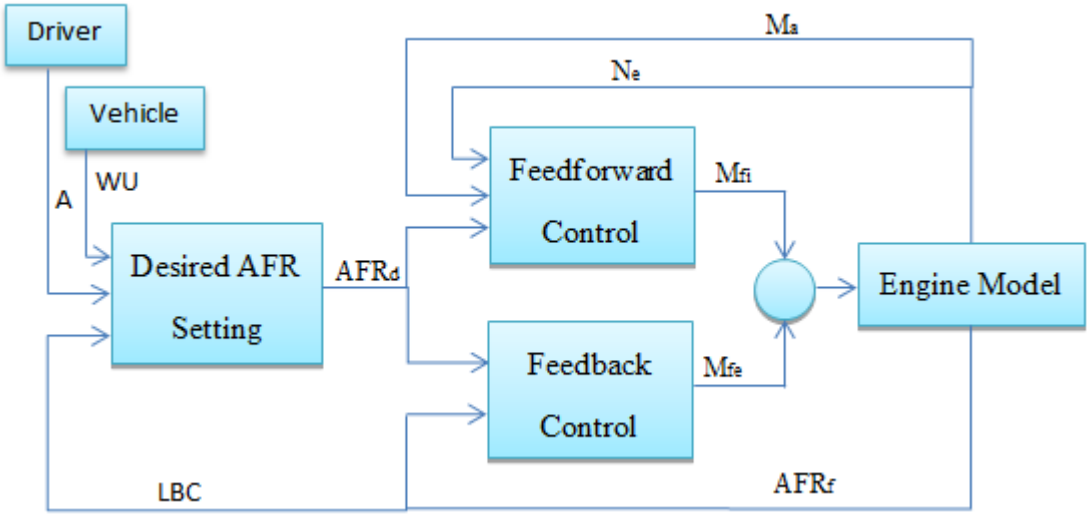

Figure 5.1: Engine AFR Control Scheme

The first control system is a closed-loop controller is used to control the desired AFR setting. The desired AFR setting system has to be adaptable to a vehicle's desired AFR (AFR_d) according to its working conditions, such as warm-up, acceleration and lean-burn combustion. The feedforward control will determine ideal AFR based on reference parameters such as the engine speed (N_e) and air mass into cylinder (M_a) output ideal fuel mass (M_{fi}). When the ideal AFR is determined, the actual AFR should remain within an ideal range. The feedforward control system (as shown in Fig 5.2) is similar to the base fuel injection system.

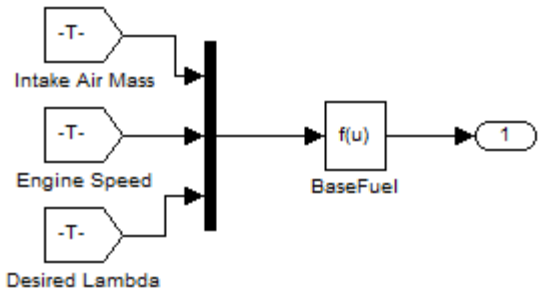

Figure 5.2: SIMULINK Block for Ideal Fuel Control

If a single feedforward open-loop control system is used, AFRs can be inaccurate and

resultant error can degrade engine performance and increase pollution. When only a single closed-loop controller is used, the engine feedback is dependent on its oxygen sensor. The AFR control system can be unstable under certain special conditions, e.g. when the engine exhaust is not fully warmed. The AFR setting feedback closed-loop controller provides the fundamental value of the injected fuel and then calculates the stoichiometric AFR and its differential against feedback from the oxygen sensor. Due to the delay of both oil film and intake air propagation there exists a deviation from the engine's desired AFR, and hence it is necessary to correct such deviation through an error control process. Consequently, the control signal sent to the engine is the sum of both ideal fuel mass and error fuel mass. The error fuel control will be based on desired AFR and correct by AFR feedback (AFR_f) from engine, the output signal is represented by the fuel mass (M_{fe}) correction term. Based on the calculated error an open-loop controller can be used to improve the response and the accuracy of AFR output. The error fuel control will be use PID controller and more detail will be discussing in next section.

5.3 PID Controller Tuning

The PID controller is probably the most widely used controller in industry. Based on classical control theory a PID controller is designed by established tuning methods. Its biggest advantage is that there is no need to understand the controlled object in the control model; instead, the desired output can be achieved as long as parameters of the controller can be adjusted, usually based on experience. The downside is that the controlled output is sensitive to parameters. Due to the fact that PID controllers can be implemented by software programming their parameters are very flexible to change, and thus PID controllers have received a wide range of applications.

The PID control scheme is named after its three correcting terms, whose sum constitutes the manipulated variable (MV). The proportional, integral, and derivative terms are summed to calculate the output of the PID controller. Define u(t) as the controller output, the final form of the PID algorithm is:

$$u(t) = K_p e(t) + K_i \int_0^t e(\tau)\, d\tau + K_d \frac{d}{dt} e(t) \tag{5.1}$$

where

K_p : Proportional gain, a tuning parameter

K_i : Integral gain, a tuning parameter

K_d : Derivative gain, a tuning parameter:

e : Error

t : Time or instantaneous time (the present)

τ : Variable of integration; takes on values from time 0 to the present t.

There are many methods for tuning a PID loop, some of them require insight into the controlled system such as the transfer function model. The system input and output time function can be used to determine the mathematical model which describing the behaviour of the system, this is basically the system identification. The mathematical model was established through system identification with some important parameters estimated that characterize the behaviour of the system. System identification is an important part of the process for tuning PID. The engine system is a nonlinear system, with open loop and closed loop control systems, this makes the mathematical modelling rather different. Therefore, the observed phenomenon can be used to determine a model of a nonlinear system. The identified model using input-output data may not be unique. However in various applications as long as the behaviour of the system input and output is suitable, the lack of a unique model does not affect the nature of this problem.

5.3.1 Use PID Controller Block and PID Tuning Tool

The Lambda PID controller is implemented in Simulation as Fig 5.3. Ideal fuel control is carried by the open loop block, the error fuel control uses PID controller block. PID controller block is a SIMULINK implementation of a continuous or discrete time controller (PID, PI, PD, P, or I). The PID Controller block output is a weighted sum of the input signal, the integral of the input signal, and the derivative of the input signal. The weights are the proportional, integral, and derivative gain parameters. A first-order low pass filters are used for the derivative action tor avoid problems of a “pure” derivative system such as derivative kick.

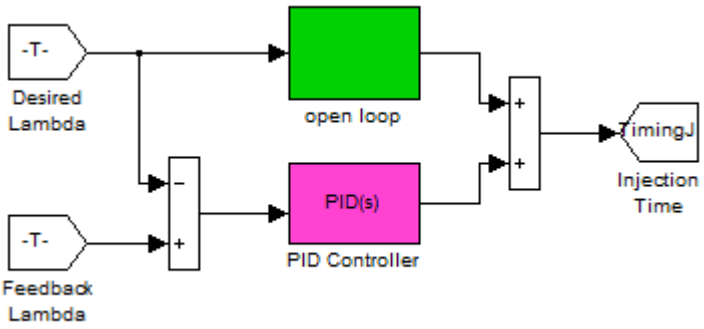

Figure 5.3: Lambda PID Controller Model

5.3.1.1 Introduction to the MATLAB PID Tuning Tool

PID controller gains are tuneable either manually or automatically. Automatic tuning requires SIMULINK control design software PID tuner tool. PID Tuner provides a fast and widely applicable single-loop PID tuning method for the SIMULINK PID Controller blocks. With this method PID parameters can be tuned to achieve a robust design with the desired response time.

A typical design workflow with the PID Tuner involves the following tasks:

(1) Launch the PID Tuner. When launched, the software automatically computes a linear plant model from the SIMULINK model and designs an initial controller. The linear plant model will use Descriptor State-Space Models. In continuous time, a descriptor state-space model shown as Eq 5.2.

$$E\frac{dx}{dy} = Ax + Bu \quad y = Cx + Du \tag{5.2}$$

where: x is the state vector. u is the input vector, and y is the output vector. A, B, C, D, and E are the state-space matrices. The state-space matrices values will be estimated by software automatically.

(2) Tune the controller in the PID Tuner by manually adjusting design criteria in two design modes. The tuner computes PID parameters can robustly stabilize the system.

(3) Export the parameters of the designed controller back to the PID Controller block

and verify controller performance in SIMULINK.

5.3.1.2 Initial PID Design

Open the engine speed control model with PID Controller block as shown in Fig 5.3.Double-click the PID Controller block to launch the PID Tuner with its block dialog. In the main tab, click "Tune". When the PID Tuner launches, the software computes a linearized plant model seen by the controller. The software automatically identifies the plant input and output, and uses the current operating point for the linearization. The plant can have any order and time delays. The PID Tuner computes an initial PID controller to achieve a reasonable trade-off between performance and robustness. By default, step reference tracking performance is displayed in the plot.

Click the Show parameters arrow to view controller parameters P, I and D, and a set of performance and robustness measurements. Fig 5.4 shows the parameters and performance tables. As can be seen that Tuned P and Tuned D are zero, and the Tuned Settling Time is unsatisfactory.

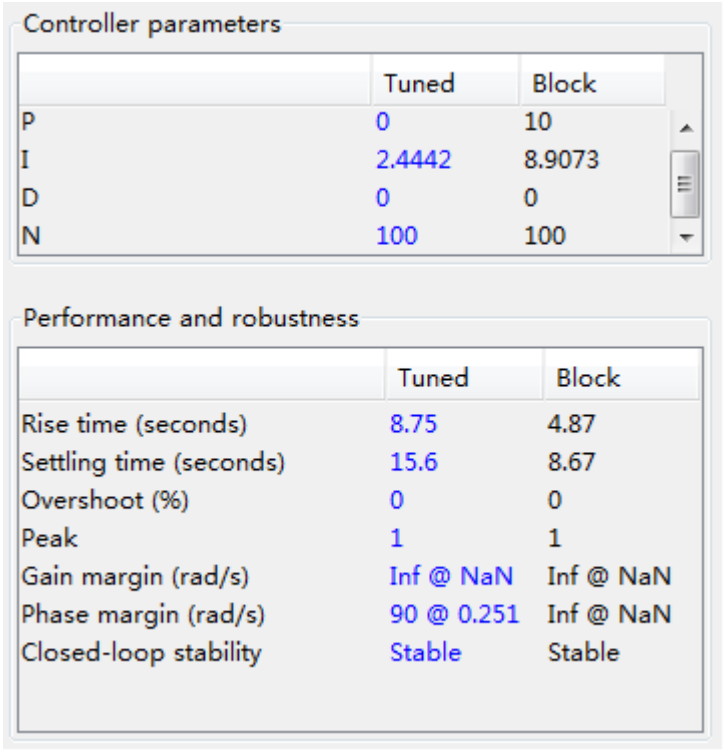

Figure 5.4: The Parameter and Performance Tables

Repeated experiments revealed that the problem is in the plant linearization process.

The delay blocks used in the system causes the system instability after the first two seconds. When this happens, the sampling time calculated is very short and this will lead to an inaccurate estimated linear plant model. Export plant model tab is then used to export the linearized plant into MATLAB workspace which is shown in Fig 5.5. Property a, b, c, d and e are state space model parameters. It can be seen that the model parameters for linearized plant are unreasonable, therefore it is impossible to apply PID Tuner Tool for this experiment.

Property	Value	Min	Max
a	[ ]		
b	[ ]		
c	[ ]		
d	0.1028	0.1028	0.1028
e	[ ]		

Figure 5.5: Linearized Plant Parameter of Transfer Function

On the basis of long term practical experience it is found that many mature classical methods of parameter estimation can obtain satisfactory results. Under the open loop condition the closed-loop control system with feedback will reduce the input and output dynamic characteristics, and this could also trigger the input and output data to be associated which can create identifiability and identification precision bottleneck problems. The system identification for systems under closed-loop condition is not always achievable. This explained why the AFR PID controller tuning based on PID Tuner tool has no success. There are PID design and debug tools available for MATLAB and SIMULINK. A new engine PID controller tuning will be introduced in next section.

5.3.2 PID Tuning Using SIMULINK Design Optimization Toolbox

Through the analysis of the MATLAB and SIMULINK toolbox and engine simulation package, it is found that the design optimization toolbox can be used to realize PID tuning when the design optimization toolbox is in cooperation with simulation.

Design optimization toolbox (Coleman, Branch & Grace, 1999)

SIMULINK Design Optimization provides interactive tools, functions, and SIMULINK

blocks for tuning SIMULINK model parameters using numerical optimization. An interactive tool tune design parameters in a SIMULINK model automatically to meet objectives. Using design optimization techniques, one can optimize controller gains to maximize overall system performance. The software provides Check Step Response Characteristics block that lets users to accomplish optimize model parameters by Graphical User Interface (GUI) or at the command line.

Check Step Response Characteristics Block (Coleman, Branch & Grace, 1999)

This block can be used to check if a signal satisfies step response bounds during simulation. If all bounds are satisfied, the block does nothing; otherwise the block generates a warning message which appears at the MATLAB prompt. The users can then take a number of actions for example, stop the simulation and bring that block into focus. During simulation, the block can also output a logical assertion signal: If all bounds are satisfied, the signal is true and the parameters can be saved to the work space。If a bound is not satisfied, the signal is false and an error message appears in MATLAB command window.

The block can be used in all simulation modes. Step response can be checked to verity if it satisfies all the performance requirements: Step time (seconds), Initial value, Final Value, Rise time (seconds), % Rise, Settling time (seconds), % Settling, % Overshoot and % Undershoot. Fig 5.6 shows an example which sets Check Step Response Characteristics block by default, the segments line represent the step response requirements: amplitude less than or equal to –0.01 up to the rise time of 5 seconds for 1% undershoot; amplitude between 0.9 and 1.2 up to the settling time of 15 seconds; amplitude equal to 1.2 for 20% overshoot up to the settling time of 15 seconds, amplitude between 0.99 and 1.01 beyond the settling time for 2% settling. The user can define their parameters for further tests.

The main function of this block is to test if a controlled signal remains within specified time-domain characteristic bounds. When a system does not violate any bound, you can disable the block by clearing the assertion option. If you modify the system model, you can re-enable assertion to ensure that your changes do not cause the system to violate a bound. If the signal does not satisfy the bounds, block can optimize the model parameters to satisfy the bounds.

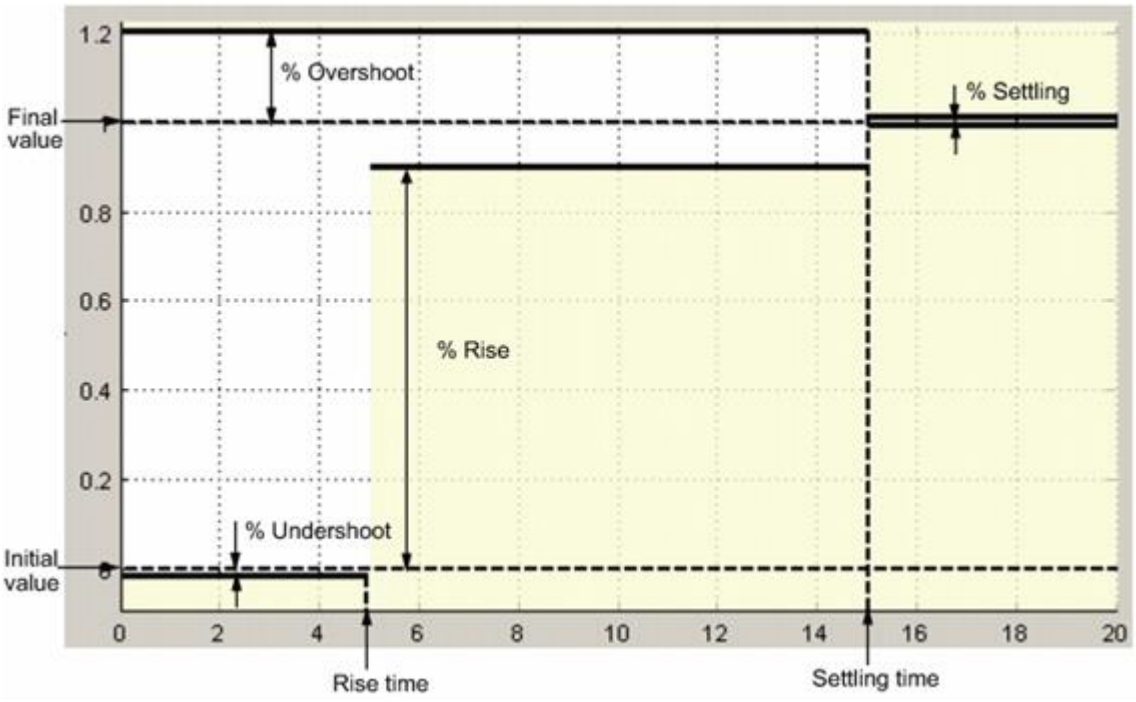

Figure 5.6: Controller Design Optimization Example (Coleman, Branch & Grace, 1999)

5.3.3 Experimentation Process

In order to facilitate tuning and cooperate with the toolbox, PID controller has to be re-designed. The new PID controller is shown in Fig 5.7 which uses Gain, Integrator and Derivative blocks to realize PID control.

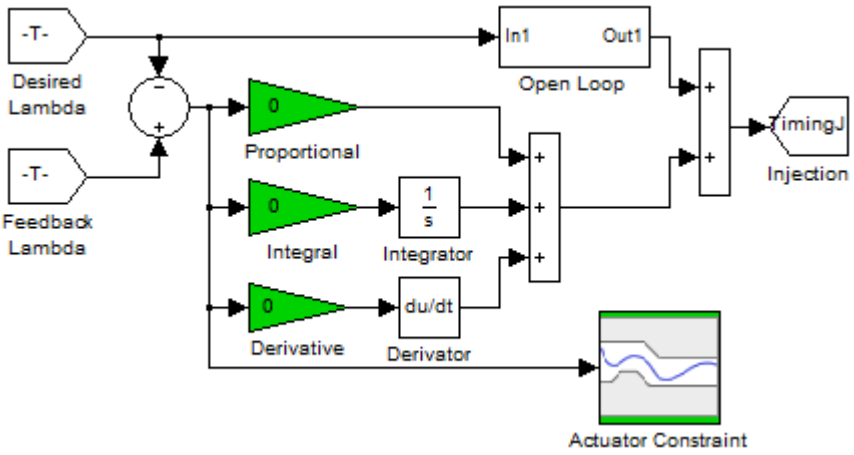

Figure 5.7: SIMULINK based PID Controller

Set PID controller gain block parameters as P，I and D: Double-click Actuator Constraint block, open Block Parameter Dialog, and add three design variables to Design Optimization Workspace. Chick Optimize to start run the simulation. It is noted

that the find operation may take very long time to find a viable solution. This is optimization process is a very inefficient, if one limits some coefficients of design variables the testing time can be reduced. This can be done by changing the maximum and minimum values shown in following table 5.1.

Table 5.1: Maximum and Minimum Values of P, I and D

	Design Variables (3by1)		
	Design Variable(1,1)=	Design Variable(2,1)=	Design Variable(3,1)=
Name	P	I	D
Value	0	0	0
Minimum	0	0	0
Maximum	1000	1000	100
Free	1	1	1
Scale	1	1	1
Info	[1*1 struck]	[1*1 struck]	[1*1 struck]

For engine dynamic simulation model, the change of the throttle open angle and engine load curve can make system unstable. The optimization method discussed above can get system response curve in the scope. As discussed in Section 4.2 the time delay and other modules can lead to system instability in the beginning of engine simulation system. Therefore the input data will give 20 seconds delay to wait system at steady state, the initial throttle open angle is 50 degree and the engine load at 130 Nm. To minimalize transient error response caused by test engine model, the engine throttle open angle and load are changed at the same time, i.e. within 20 seconds, the throttle open angle is reduced from 50 to 15 degree and the engine load decreases from 130 to 60 Nm.

When the input curve is determined, the original engine with numerical PID controller can be used and the test results are shown Fig 5.8. It can be seen that the output error become very small in 19 seconds period and this proves that the system has entered a steady state. Due to the working principle of the engine and the delay of the feedback signal, the input changes make the system response diverges from 20 seconds and the system reaches the maximum error at 20.2 seconds. However, the system returns back to normal at 23.3 seconds with the output error less than or equal to 1%. This can be interpreted as the system error settled with 1% with the settling time of 3.3 seconds. The control overshoot is 0.413.

The target for the engine AFR control is to settle the lambda in the range of 0.99-1.01 within 1.8 seconds. The control maximum error should be as small as possible. Thus the

engine output error settling time is set as 1.8 and the control error should settle within 1% within (1.8+20) seconds. Figs 5.9 and 5.10 below show the limitation block setting for optimal PID tuning.

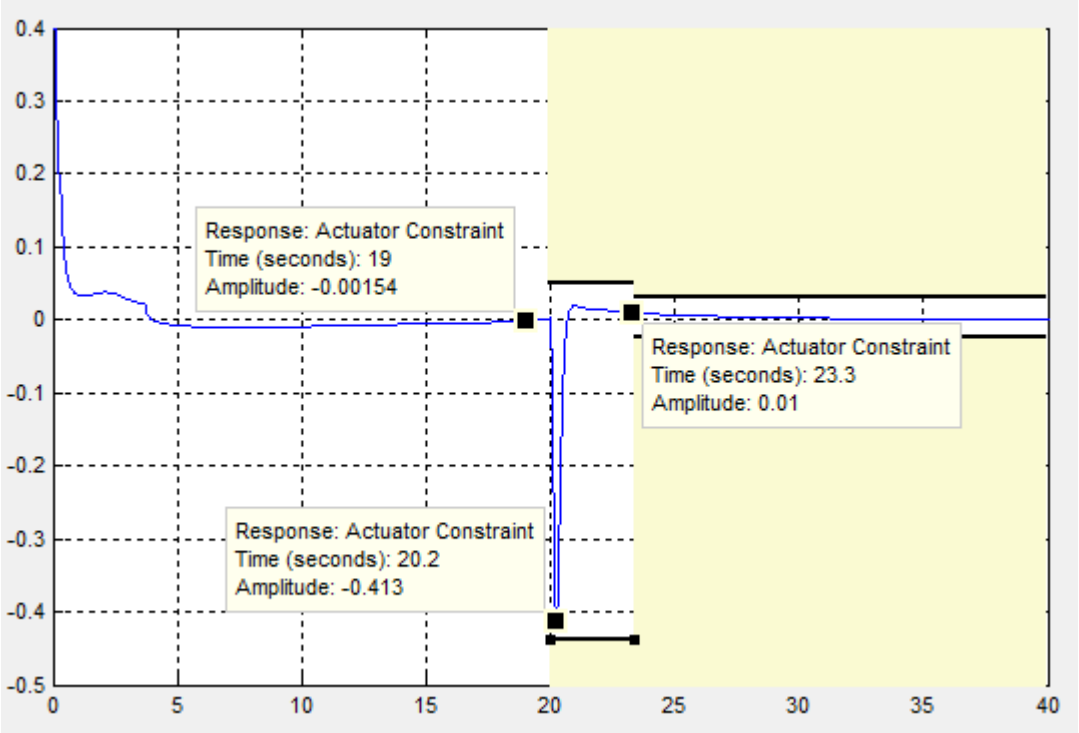

Figure 5.8: Check Step Response Characteristics Block Simulation Result (No Feed Back)

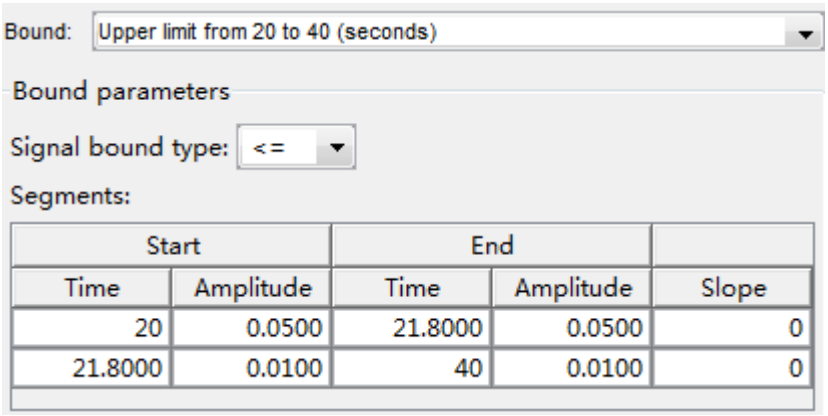

Figure 5.9: GUI of limition Block (Upper)

After all preparations, the simulation is then run to optimize the P, I and D parameters to satisfy the limitation bounds. As the simulation model is complex, the SIMULINK takes a long time to complete. The optimization found P=16.75, I=107.5 and D=1.. From results shown in Fig 5.11, we can see that the preset optimization targets are satisfied. The response settled within 1% range within 21.8 seconds and the maximum output error has been reduced from 0.413 to 0.396.

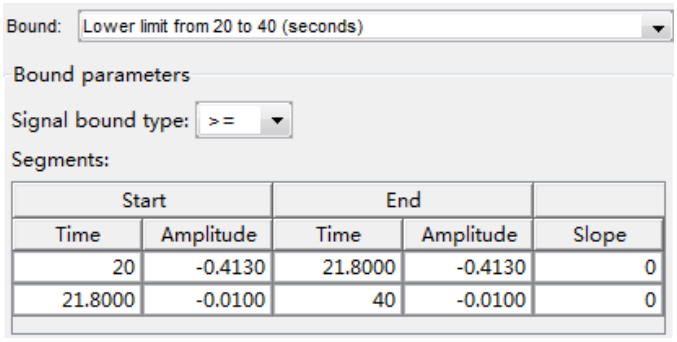

Start		End		
Time	Amplitude	Time	Amplitude	Slope
20	-0.4130	21.8000	-0.4130	0
21.8000	-0.0100	40	-0.0100	0

Figure 5.10: GUI of limition Block (Lower)

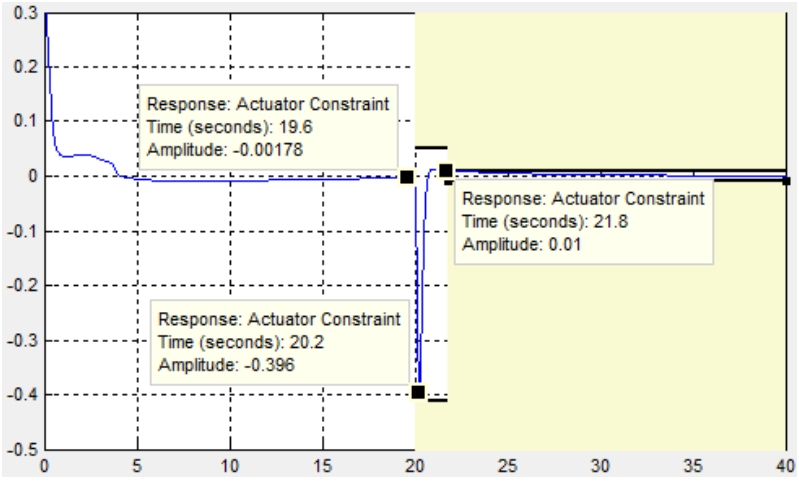

Figure 5.11: Check Step Response Characteristics Block Simulation Result (PID)

The control performance results presented in Fig 5.12 can be further optimized by adjusting P, I and D parameters. By gradually reducing performance target, the maximum transient output error area can be reduced. A better optimized solution found P=35.75, I=156.5 and D=1. From the achieved results shown in Fig 5.15, one can see that the maximum transient output error has been reduced to 0.339.

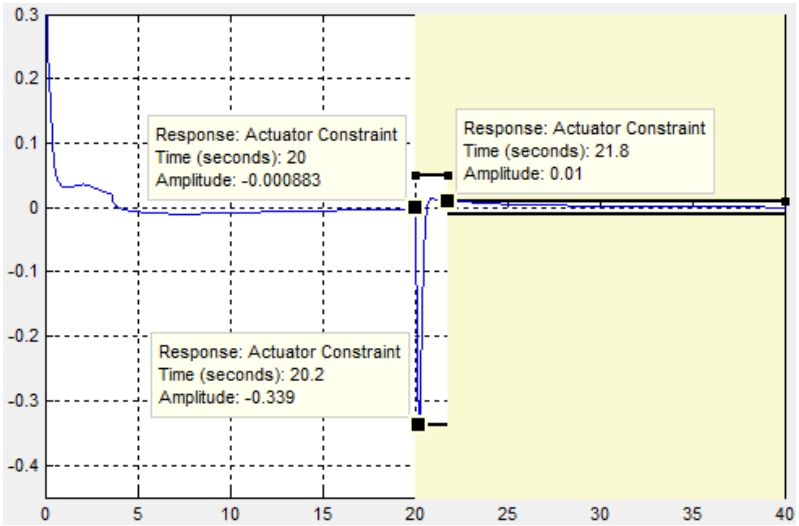

Figure 5.12: Check Step Response Characteristics Block Simulation Result (Optimized PID)

5.3.4 Result and Conclusion

In order to gain more understanding about effects of PID control, more simulation results are presented in here. The test is based on constant load torque at 100Nm. Fig 5.13 shows the throttle open angle during the simulation, Fig 5.14 and Fig 5.15 show the engine speed and controlled AFR. In Fig 5.18 the red line is an ideal AFR.

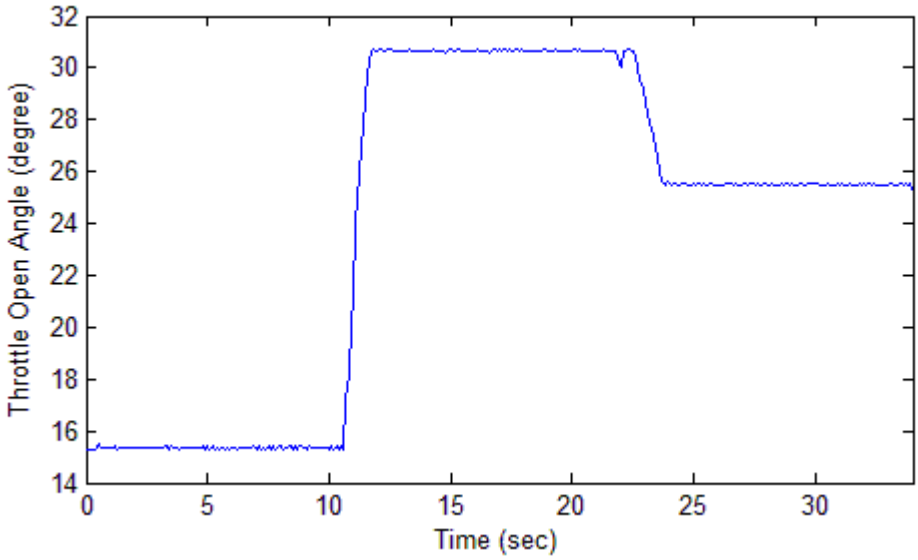

Figure 5.13: Throttle Open Angle During Simulation

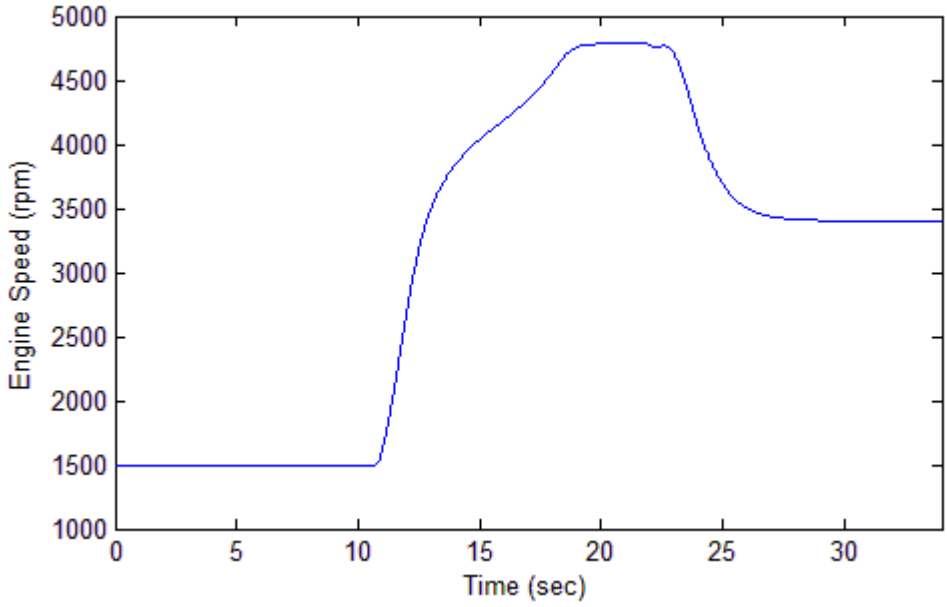

Figure 5.14: Engine Speed From Modelling Results (Fig 5.13 input profile)

From results shown above, one can see the AFR has been effectively controlled by PID controller. However, the output error is too big. Therefore, another type of controller to effectively assist PID controller to achieve better control effect is required. Through the

literature review, fuzzy logic control has been selected for further investigation.

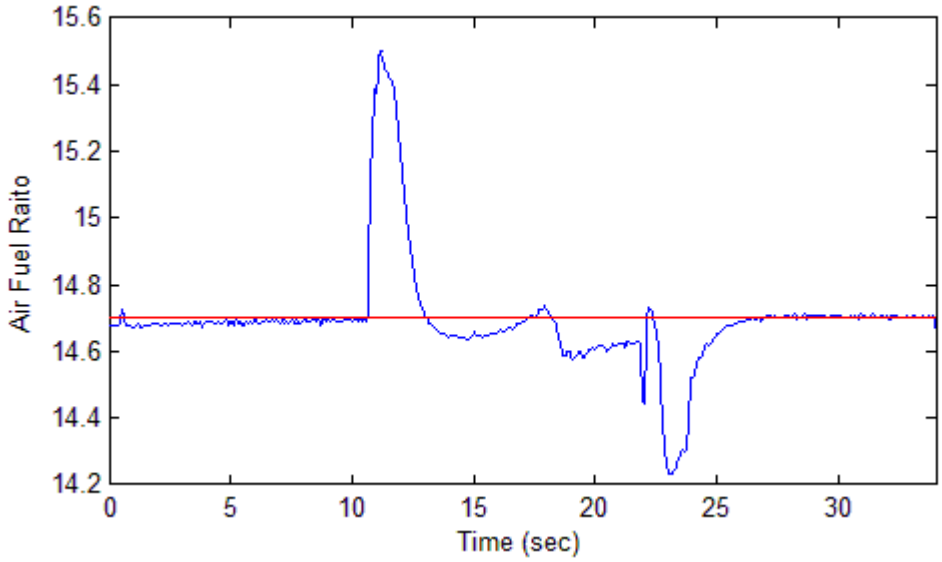

Figure 5.15: AFR Result of the PID Controller (Fig 5.13 input profile)

5.4 Fuzzy Logic Control

The vehicle engine dynamic system is so complex that it inevitably has such characteristics as non-linearity, hysteresis and time-varying. Moreover, some parameters of the system are either unknown or slowly changing; it can also be subject to time delay and random disturbance. All of those make it difficult to have either an accurate mathematical model or if possible the model is very rough. Although the traditional linear controllers, featured with simple structure, good stability/adaptability and high precision, have become the most widely used in control processes; but they are the most effective for linear, time-invariant systems, where satisfactory control outcome can be achieved when appropriate parameters of the PID controller can be determined. However, due to the nature of complex nature of engine system, conventional PID controllers are difficult to set for achieving desired control effect. For the purpose of these applications, fuzzy logic based new control methods have been developed rapidly and been received great attention in the control industry in recent years.

Fuzzy logic control is a digital technology based on fuzzy set theory, fuzzy linguistic variables and fuzzy logic inference. (Zadeh, 1965) founded the fuzzy set theory, and further (Zadeh, 1973) gave the definition and related theorems on fuzzy logic control. (Mamdani, 1974) first suggested a fuzzy controller based on fuzzy control statements,

and successfully applied it to the control system of boilers and steam engines in the laboratory. This pioneering work marks the birth of fuzzy control theory. Fuzzy control is essentially a nonlinear control technique, belonging to intelligence control. The basic idea of fuzzy control is to use computer to implement control experience of human, and majority of experiences are fuzzy rules described by linguistics.

5.4.1 Features of Fuzzy Control (Sivanandam, Sumathi & Deepa, 2010)

- ✧ Fuzzy control is rule-based: It directly uses the linguistic control rules, founded by either experience of site operators or knowledge of experts. Hence, it does not require an accurate mathematical model of the controlled object, making the control mechanism and strategies easy to accept and understand with simple design, ease of application.
- ✧ Qualitative understanding of the industrial process: In practice some objects have dynamic characteristics, which can either be hard to understand or change significantly over time, and hence it is impossible to obtain accurate mathematical models. In these cases, fuzzy control is relatively easy to establish linguistic-based rule control by applying qualitative understanding that have been obtained from the industrial practice.
- ✧ Relative independence of a linguistic control rules: The standard design of a control system is model based, and hence can vary significantly if its starting point and/or performance indicators are different. However, a set of linguistic based system control rules is relatively independent from the model, and controllers that apply fuzzy connections between these control rules the control have better effect than conventional controllers.
- ✧ Fuzzy control algorithms are designed based on heuristic knowledge and linguistic decision rules: The above characteristic contributes to the process and methods for simulating mankind control. It further enhances the adaptability of the control system, ensuring that it has a certain level of intelligence.
- ✧ Fuzzy control system has strong robustness: Strong robustness indicates that the impact of disturbance and parameter variation on the control effect can be dramatically reduced, and hence it is especially suitable for controlling non-linear time-varying and delay systems.

5.4.2 Fuzzy PID Control

Conventional PID controllers are sensitive to variations in the system parameters, fuzzy controllers do not need precise information about the system variables in order to be effective. However, PID controllers are better to control and minimize the steady state error of the system. Hence, a new Fuzzy PID control method which combines conventional PID control with fuzzy control and utilizes the advantages of both PID controller and fuzzy controller is proposed in here. For this new fuzzy PID controller, the fuzzy logic is used to adjust PID parameters based on the deviation between actual and set speeds. The current rate of changes in the deviation can be calculated in a fuzzy inference system by means of fuzzy reasoning, fuzzy inference. The fuzzy inference then output parameters for the PID controller, e.g. the proportional, integral and differential coefficients. Because parameters of the fuzzy controller are adjusted real-time before each action, the optimal control can be achieved.

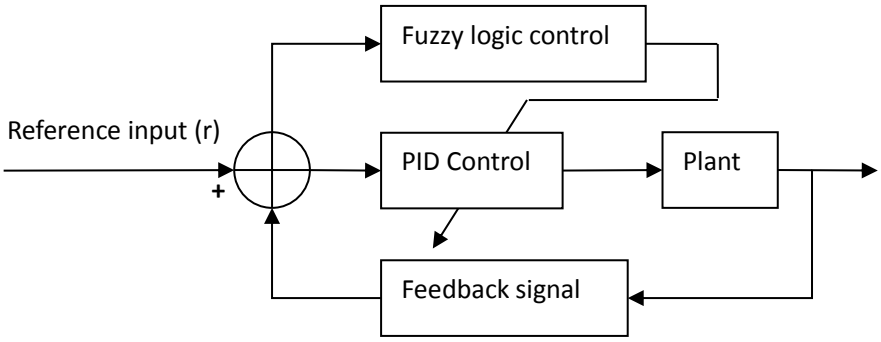

Figure 5.16: Fuzzy PID control

The fuzzy PID controller is the core of a fuzzy control system, which generally uses the system error and the rate of error changes as input. There are 3 basic forms of fuzzy PID controllers (Yesil, Guzelkaya & Eksin, 2003): Fuzzy gain scheduling PID controller is a rule-based scheme for gain scheduling of PID controllers that is remarkably effective in nonlinear systems control (Blanchett, Kember & Dubay, 2000). The performance of a conventionally gain-scheduled PID algorithm significantly improves when a fuzzy inference mechanism is adopted to perform interpolation between local PID control algorithms. More specifically, the resulting hierarchical structure includes a fuzzy controller supervising the PID regulator that is able to cope with imprecise and incomplete knowledge; Direct-action fuzzy PID controller is placed within the feedback control loop and manages the PID actions through fuzzy algorithm. Fuzzy logic

controllers are very effective since the model has nonlinearities. Hybrid fuzzy PID controller can be appeared with various forms, such as the combination of gain-scheduling and direct controller, or combine the PID with fuzzy controller (Paris et al., 2011).

5.4.3 Fuzzy PID Controller Structure

According to the detailed analysis of the performance of fuzzy PID composite controllers can be improved in terms of both the response speed and suppressed overshoot, eliminating the steady state error. The gain-scheduling fuzzy PID controller with the parallel structure is selected for this study. As shown by the SIMULINK configuration diagram of Fig 5.17, the green part is the conventional PID control and the orange part is a fuzzy controller driven by errors. The controller applies a single factor to parameterize the three PID parameters, and when a real time parameter is drifting away the PID controller is used as the basic control for the compensation formula, as such, the output of the process can be automatically adjusted to the given value.

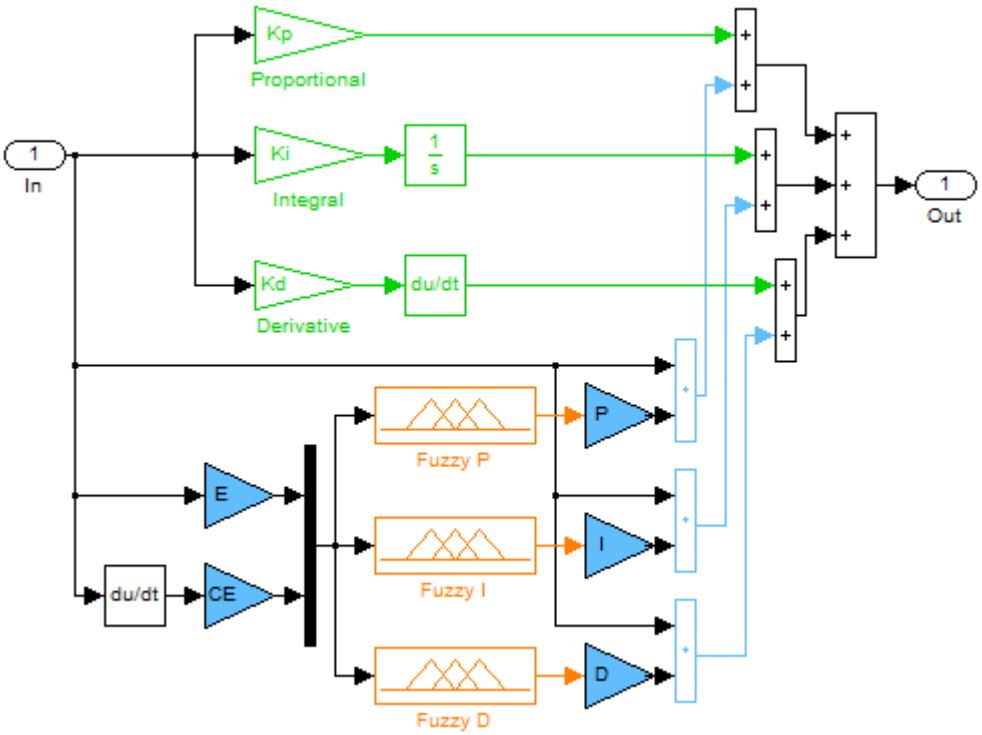

Figure 5.17: Fuzzy PID Controller Structure in SIMULINK

Fuzzy PID control not only has high precision characteristic of PID control, but also has

the flexible and adaptable characteristics of fuzzy control, improving the single PID control and fuzzy control of dynamic and static performance. It has good control effect on the nonlinear and time-varying complex systems (Gao et al., 2011). Gao et al (2011) has studies the AFR control problem of coal-bad gas engine based on fuzzy PID control. The control results show that its performance is very good. The method used in this research for implementing fuzzy PID control AFR in MATLAB and SIMULINK environment is based on some extensions and modifications of Gao et al (2011).

5.5 Fuzzy Controller Design

5.5.1 Fuzzy Controller Design Rules

A language based model - the Mamdani fuzzy model (Mamdani, 1974) is mainly used in fuzzy logic control. Fuzzy model logic is based on a set of fuzzy IF-THEN rules. Both parts of these rules are fuzzy linguistic variables, which have the following general form (Mamdani, 1974):

$$Rules_i: if\ (x_1\ is\ A_1) and \cdots and (x_n\ is\ A_n)\ then\ (y_1\ is\ B_1) and \cdots and (y_n\ is\ B_n) \quad (5.3)$$

where:

$x_1, x_2, \cdots, x_n$	It is the rule antecedent linguistic variables
$y_1, y_2, \cdots, y_n$	Member after the rule linguistic variable to represent the object control amount
$A_1, A_2, \cdots, A_n$ and $B_1, B_2, \cdots, B_n$	Fuzzy linguistic value
Rules_i	Denotes the ith rule.

An important task of PID fuzzy control is to find out the fuzzy relation between the three PID parameters, and error (*e*) (Fig 5.22, E block) and its error change (*ec*) (Fig 5.22, EC block). In practice, both *e* and *ec* are monitored and tested continuously, and based on the established fuzzy control rules these three PID parameters are adjusted on line and real time to meet different combinations of *e* and *ec* values. Generally speaking, different levels of the deviation *e* and the deviation change rate *ec* require various PID controller parameters, e.g. *kp*, *ki*, and *kd*. Therefore, the first part of the linguistic rules describes the error *e* and error change rate *ec* whereas the second part is related to the corresponding adjustments for the PID parameters, i.e. Δkp, Δkd and Δki, with which correct *kp*, *ki* and *kd* parameters for the PID controller based on the fuzzy set can be derived.

5.5.2 Fuzzy Inference System Design

In a control system the actual range of error *e* and the rate of error change rate (*ec*) is called basic universe, denoted as $[-x_e, x_e]$ and $[-x_{ec}, x_{ec}]$. Assume that the set of the error (*e*) or its change rate has the following universe (Sivanandam, Sumathi & Deepa, 2010):

$$x = [|-n|, |-n+1|, \cdots, |0|, \cdots, |n-1|, |n|] \tag{5.4}$$

where *x* is crisp value for the error *e* or error change *ec*, and n is set to either 6 or 7. The universe transformation can be done through the so-called quantisation factors. For example, the quantisation factor for k_e is defined as (Ming, Jun & Hao, 2004):

$$k_e = n/x_e \tag{5.5}$$

For a fuzzy control rule the IF linguistic variables constitute a fuzzy input space, and the THEN linguistic variables form a fuzzy output space. Each linguistic variable has a set of fuzzy language values, which consists of a set of linguistic names. Each linguistic name corresponds to a fuzzy set, values having the same universe. The linguistic names usually have some meanings, for example, N (negative), Z (zero) and P (Positive). The universe can be set to [-1, 1].

The following experiment is carried out to test a discretisation method for continuous variables. These continuous values are accurate and the range is assumed to be within [-3, 3]. This range is further divided into seven levels, with each corresponding an integer. Note that each discretised level has a fuzzy set. This treatment is simple, otherwise, each crisp value would have to be mapped to a fuzzy subset, resulting in infinite fuzzy sets and complicating the fuzzification process. Then, a relationship can be established between the discretised crisp values in the range of [-3, 3] and the fuzzy variables. In fact, once such a relationship is ready, any crisp values within the range can be mapped to the fuzzy variable, denoted as Y. For example, any values around -3 can be viewed as big negative, denoted as the name NB, near -2 referred to as medium negative, or by a linguistic name of NM, NB, NM, NS, ZO, PS, PM, PB (Here, Negative Big, Negative Medium, Negative Small, Zero, Positive Small, Positive Medium, Positive Big are

shorten by the acronyms, respectively.). Input variables error *e* and error change *ec* are all continuous variables, and the approach through which continuous values are first discretised into a finite number of integer values and then fuzzification is very convenient for designing a fuzzy inference system.

A fuzzy subset can be determined by the curve shape of membership functions. The curve can then be discretised to obtain a finite number of points. Each of these points has its own degree of membership, and they constitute a fuzzy set. Theoretical studies reveal that within a number of membership function curves, fuzzy variables having normal distributions are the best for describing human's vague concept of control activities. However, in practice, calculations of fuzzy variables with normal distributions are very complex and slow, and hence a triangular fuzzy variable distribution is more efficient in terms of the computation speed and simplicity. Therefore, many control systems commonly adopt triangular distributions to achieve rapid control effect by relatively simple calculation. However, in order to maintain control smoothness the Z-shaped membership function is used at the beginning whereas the S-shaped membership function is applied at the end. Curves of these discussed membership functions are shown in Figure 5.18.

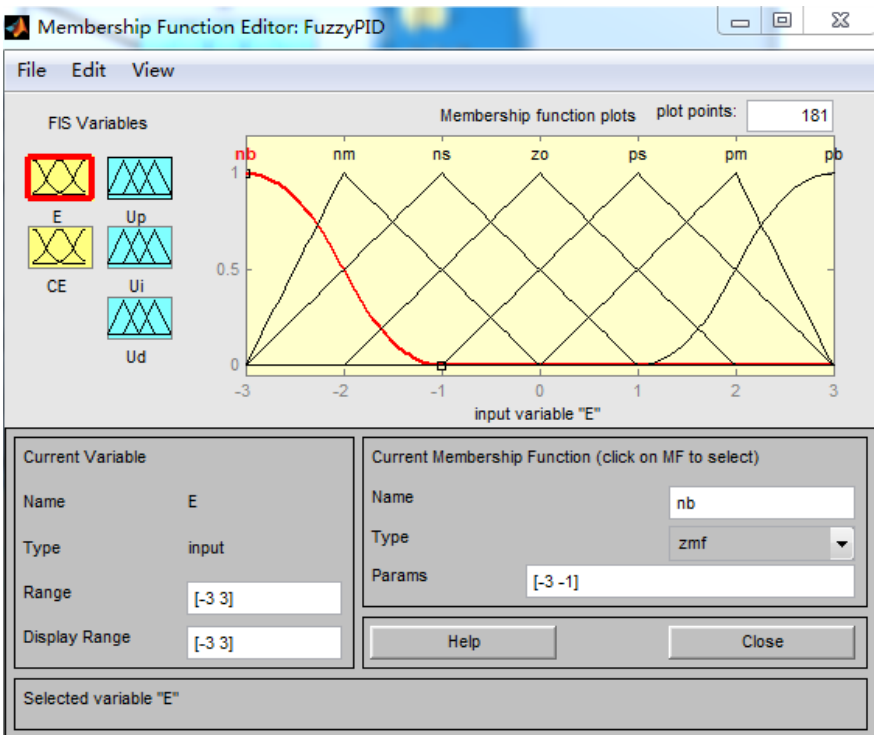

Figure 5.18: GUI for Menbershio Function Editor

Fuzzy control rule table

As discussed previously different deviation *e* and their change speed *ec* have different requirements for PID controller parameters, *kp, ki,* & *kd*. The error curve of a typical second-order system for the unit impulse response are analysed as follows Fig 5.19.

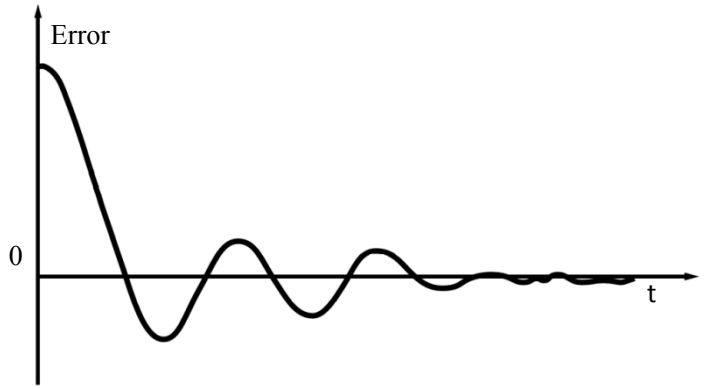

Figure 5.19: Typical Second-Order System Error Curve

It can be seen from the response error curve that:

(1) When error *e* is large and in order to accelerate the response speed of the system larger value of *Kp* should be taken. However, saturation of the differential function caused by large shocks in the deviation *e* at the beginning can lead to the system control exceeding its permitted range and hence should be avoided. For this purpose the value of *Kd* should be set smaller. In the meantime, the value of *Ki* is set to 0 to restrict the integral function. This step is necessary to prevent the system response producing big overshoots, resulting in the problem of integral saturation.

(2) When the size of the deviation *e* is moderate *Kp* should be set small whist the value of *Ki* should be appropriate, which can ensure the system's response to have smaller overshoot. In this case, the value of *Kd* has significant impact on the system, and hence it must be set appropriate to maintain a reasonable response speed given by the system.

(3) When the deviation *e* is smaller closing to the pre-set value the values of *Kp* and *Ki* should be increased so that the system can have good stability feature. Meanwhile, whist avoiding oscillations around the pre-set value the system should be enhanced to vicinity of the settings of the system should have better tolerance to disturbance, and this can be achieved by increasing (decreasing) *Kd* when *ec* is small (big).

The fuzzy control table can be generally obtained in two ways. The first method is to use an off-line algorithm, which is based on fuzzy mathematical synthetic reasoning. By sampling error e and error change speed *ec* the corresponding amount of changes in the parameters can then be calculated. The other one is to form a fuzzy control set from the experience of operators. However, it is obvious that the summarised fuzzy control table by this method is very rough due to the human subjective consciousness, which may not be in line with actual situations. Therefore, it is necessary to run an online control correction process for the fuzzy control table. According to the experience in engineering design, a typical set of fuzzy partition values for both *e* and *ec* have seven fuzzy values, denoting as NB, NM, NS, O, PS, PM, PB. Similarly, the same seven fuzzy values can be set for the output linguistic descriptive parameters, e.g. *Δkp*, *Δkd* and *Δki*. Accordingly, the fuzzy rule table comprises a total of 49 combinations as shown in the following table.

Table 5.2: Fuzzy Rule Table

△kp /△ki /△kd		EC						
		NB	NM	NS	O	PS	PM	PB
E	NB	PB/PB/PB	PB/PB/PB	PB/PB/PB	PB/PB/NB	PS/NS/NB	O/NM/NM	O/NB/NS
	NM	PB/PB/PB	PB/PB/OB	PM/PM/PM	PM/PM/NM	O/NM/O	O/NB/PS	NM/NB/PM
	NS	PB/PB/PB	PM/PM/PM	PM/PS/PM	PS/PS/NS	O/NB/PM	NM/NB/PB	NB/NB/PB
	O	PS/O/O	PS/O/O	O/O/O	O/O/O	O/O/O	NS/O/O	NS/O/O
	PS	NB/NB/PB	NM/NB/PB	O/NB/PM	PS/PS/NS	PM/PS/PM	PM/PM/PM	PB/PB/PB
	PM	NM/NB/PM	O/NB/PS	O/NM/O	PM/PM/NM	PB/PM/PM	PB/PB/PB	PB/PB/PB
	PB	O/NB/NS	O/NM/NM	PS/NS/NB	PB/PB/NB	PB/PB/PB	PB/PB/PB	PB/PB/PB

5.5.3 Controller Test

When fuzzy control is implemented by algorithms using computer simulations the amount of sampled variables must be calculated first to derive the error (*e*) and its change (*ec*). The input variables must be converted from the basic domain to the domain of the corresponding fuzzy sets, through which the input variables are multiplied by the corresponding factor, represented by the quantization factor such as blue triangle *e* and *ec* in Figure 5.22. Quantization and scale factors are derived on the basis of the transformation between the two domains. The quantization factors for the input variables have fuzzy effects whereas the scale factors for output have only proportional effects (Fig 5.2 blue the triangular P, I, and D).

The implementation of a fuzzy controller requires good fuzzy control rules. In addition, it is important to choose a set of both quantization and scale factors for input variables and output variables respectively. This is because the performance of the fuzzy PID controller is determined by the size of these scale factors as well as the relative relationship between different quantization factors.

The size of the quantization factors for *e* and *ec* has big impact on dynamic performance of the control system. If the selected *e* is large, then the system can be overshot, leading to a longer transition process. In theory, a bigger *e* is equivalent to the reduction of the basic domain of the error, increasing its control effect. The enhanced control effect decrease the rise time, but the adjustment can be easily overshot, making the transition process of the system even longer. On the other hand, *ec* is a deterrent of overshoot, that is, a large *ec* can reduce overshoot, but in the meantime slow down the system responses. The size of quantization factors for both *e* and *ec* is suggested to use different weighted degree of the input error and its change, which are interacted mutually.

When the engine running at stable condition, the oxygen sensor's relative changes has small impact on engine AFR, so the feedback closed loop fuzzy controller input variable range and output variable range must be different. The fuzzy control rule table has been considered under steady state working condition, the engine with conventional PID control simulation platform is used to determine the Fuzzy controller input variable ranges. As shown in Fig 5.20, there are two data sets in the simulation. The error (*e*) data and it is derivative (ec) values are stored in the workspace, respectively. When the simulation complete, those data can be used for further analysis.

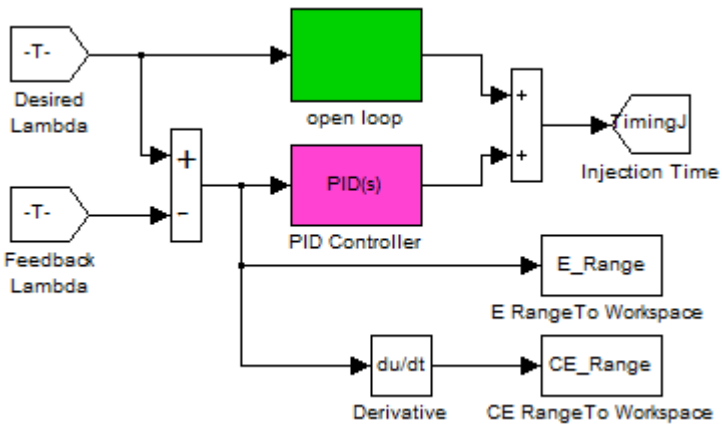

Figure 5.20: Data Collection Model in the simulation

In order to fully test the range of *e* and *ce*, it is decided to connect the vehicle dynamic model on engine simulation package. The range of *E_Range* is found to be between -0.35 and 0.35; *CE_Range* is between -0.3 and 0.3. According to the quantification theory and the theory of discrete integral domain，*e* and *ce* are 8.6 and 10. When quantization factors for *e* and *ec* are determined, scale factors for the PID controller can be looked into. In simulation, they can be tuned by E block and CE block.

5.5.4 Fuzzy PID Control Simulation Results

Fig 5.21 shows the AFR control step response, it can be seen that the Fuzzy PID control optimization targets are satisfied, the response is settled within 0.01 range at 21.4 seconds and also maximum output error is reduced to 0.213 (from 0.339 of optimized conventional PID control).

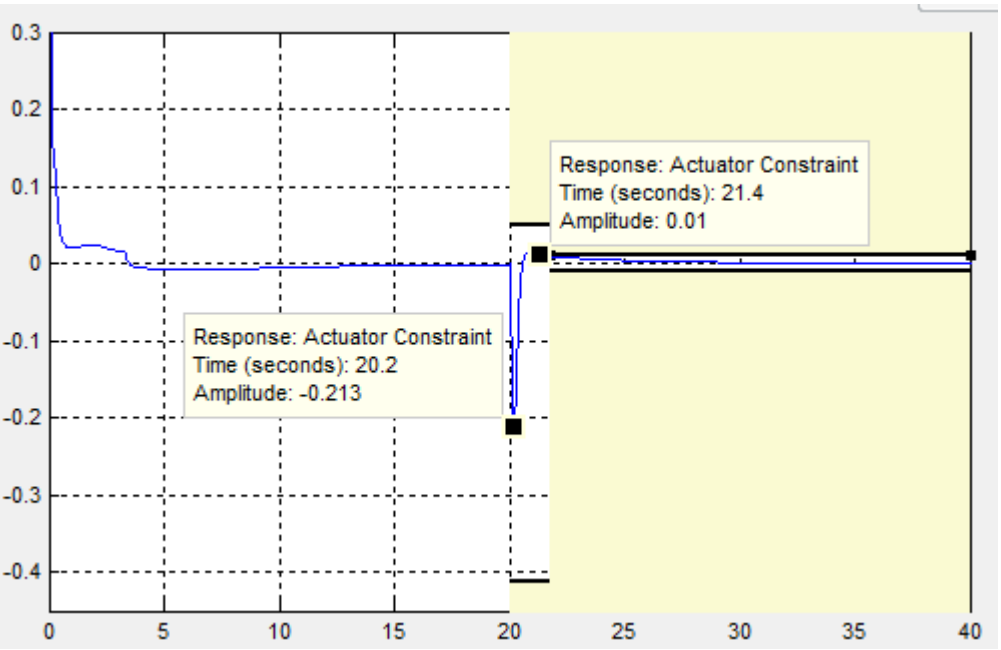

Figure 5.21: Check Step Response Characteristics Block Simulation Result (Fuzzy PID)

In order to gain more understanding about the effects of Fuzzy PID control, PID controller output as well as fuzzy control output curves are collected. When the throttle open angle and engine load changed at 20th second, the system is stabilized in 2 seconds (see Fig 5.22). The output error is negative and this means that too much fuel has been injected. It can be seen that conventional PID control injected more fuel than fuzzy PID control, Moreover, the overshoot and the settling time have both been reduced.

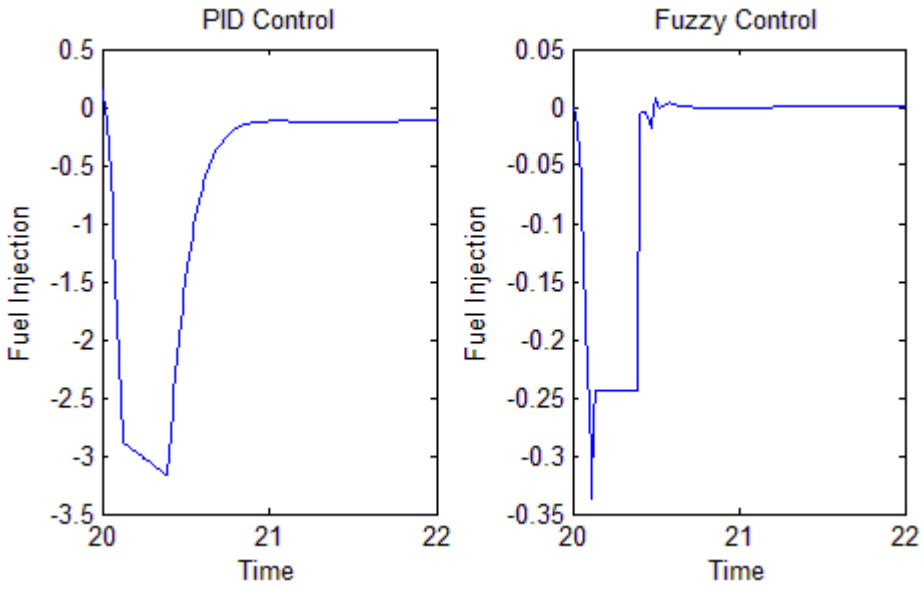

Figure 5.22: Contrast PID and Fuzzy Control Signal

5.6 Analysis and Comparison

The analysis started with the steady state responses comparison, Table 5.3 shows the comparison of each controller performance, the optimized PID controller can achieve engine AFR control requirements, after optimization the response settle within 0.01 at 21.8 seconds and the maximum output error is 0.339. Further improvement for PID control is difficult. Fuzzy PID control has reduced the settling time by 0.4 seconds from PID controller, and the control overshoot is reduced by about 40%.

Table 5.3: Comparison Controllers Performance (steady state)

	Settling time of 1%	Control overshoot
No feedback control	3.3 s	-0.413
PID control	1.8 s	-0.396
Optimized PID control	1.8 s	-0.339
Fuzzy PID Control	1.4 s	-0.213

The controller performance is also tested during transients. In order to provide more detailed contrasting basis reference, the integration of the absolute value of the output error is used for comparison. The sampling period is set as 0.01 seconds, the engine load torque is set at constant operation of 100 Nm, and the throttle open angle is shown in Fig 5.16. The optimized PID controlled AFR and fuzzy PID controlled AFR are shown in Fig 5.23 (the red line is an ideal AFR) and Table 5.4. Maximum up error is occurred at about 11th second, fuzzy PID controller reduced the output error by 28.6%. Maximum down error is occurred at about 23rd second, fuzzy PID controller reduced 32.07% of

output error. Table 5.4 shows the fuzzy PID controller improved the performance about 30%.

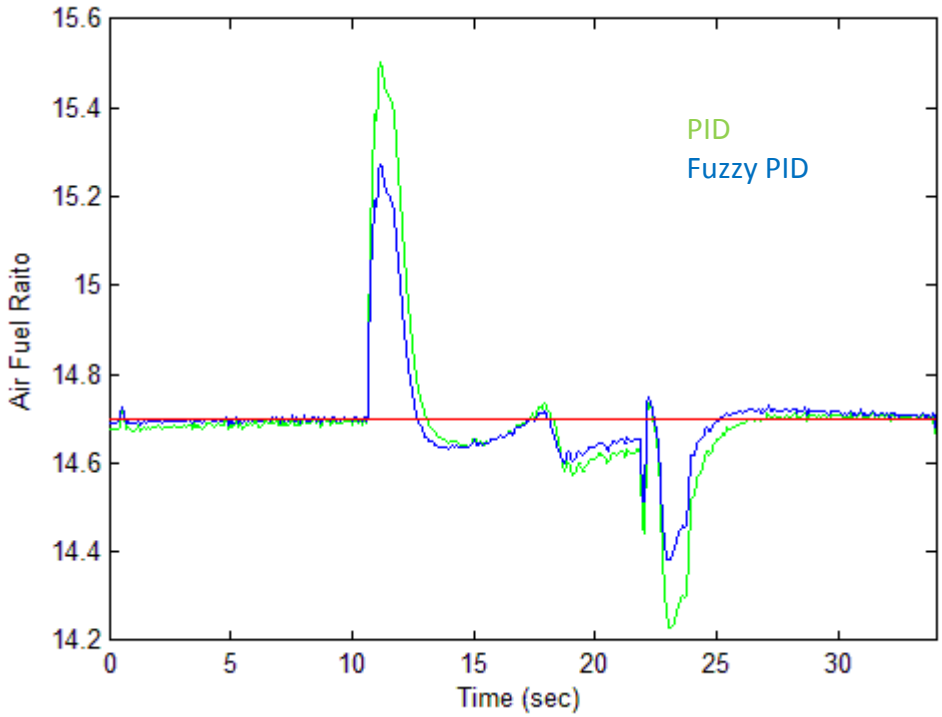

Figure 5.23: AFR Comparison at Constant Torque (Fig 5.13 input profile)

Table 5.4: Comparison Controllers Performance (constant torque)			
	Error Integration	Up Max	Down Max
Optimized PID Control	0.3550	15.5007	14.2295
Fuzzy PID Control	0.2474	15.2717	14.3804
Comparison	30.31%	28.60%	32.07%

The controller performance is also tested during torque transients, for which the engine speed is set at constant value of 2500 rpm and the throttle open angle is shown in Fig 5.16. The optimized PID controlled AFR is compared with fuzzy PID controlled AFR (see Fig 5.24, the red line is an ideal AFR). The performance measures are presented in Table 5.5. It can be seen that the maximum up error occurred at about 11th second, fuzzy PID controller reduced 16.74% of output error. The maximum down error occurred at about 24th second, fuzzy PID controller reduced 23.45% output error. Table 5.5 shows the fuzzy PID controller improved the performance about 14%.

Table 5.5: Comparison Controllers Performance (constant speed)			
	Error Integration	Up Max	Down Max
Optimized PID Control	0.3501	16.1452	14.5588
Fuzzy PID Control	0.3013	15.9033	14.5913
Comparison	13.94%	16.74%	23.45%

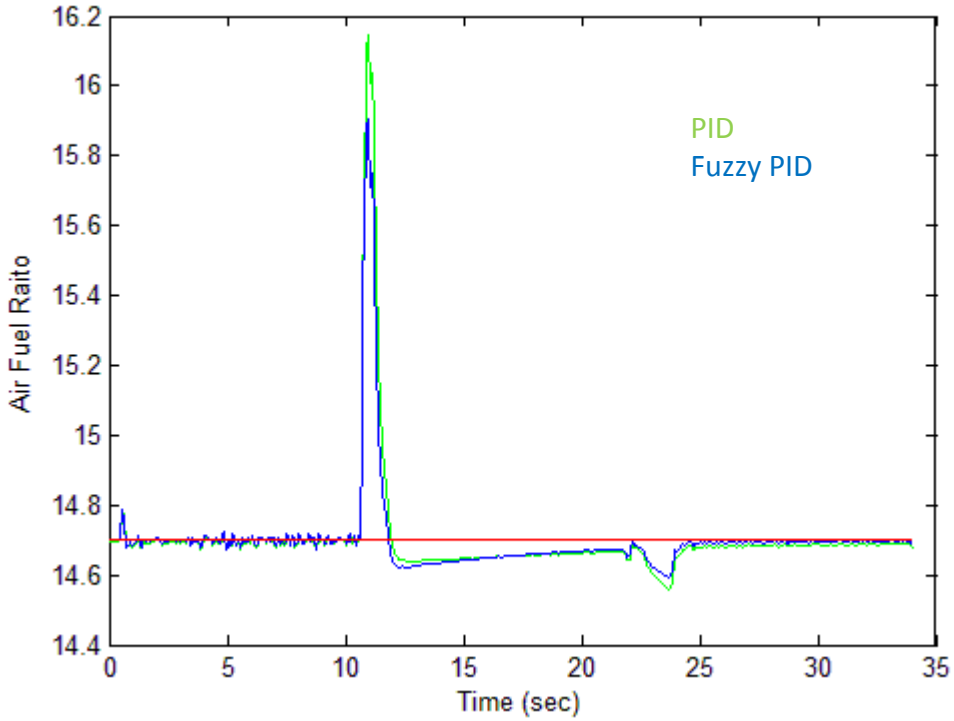

Figure 5.24: AFR Comparison at Constant Speed (Fig 5.13 input profile)

From the analysis and comparison we can find that:

1. Both PID control and fuzzy PID control can obtain good control effect for the AFR of the engine which is in stable operating conditions.
2. With conventional PID control, the AFR has longer response time and bigger oscillations.
3. With fuzzy PID control, the AFR has smaller fluctuations, shorter response time, suggesting ideal control effect.
4. Compared with conventional PID control, fuzzy PID control can achieve better stability of both static and dynamics in the AFR control system, which also exhibits better control and more robustness.

5.7 Summary

This chapter presents the engine AFR control system with PID controller and fuzzy PID controller. For PID controller, the PID tuning tool provided by SIMULINK proved to be successful. The results show that PID controller and optimized PID controller have good control performance. After that a detailed introduction of fuzzy PID control and its relevant information and its operational principle are presented. The fuzzy PID

controller is implemented in the engine simulation package. It is found that fuzzy PID controller can reduce the AFR output error. Both PID control and fuzzy PID control are based on the error analysis, and the benefit of such a control system is that it does not require an in-depth understanding of the causes of deviation of the controlled system. However, such numerical based analysis can result in unpredictable instability no matter how good the controller is. By carrying out a detailed mathematical analysis of a vehicle fuel engine, the bias of AFRs from its desired value is mainly due to dynamic effects, such as the oil film, intake filling and the lagging effect of the oxygen sensor. A simulation module can be used to accurately account for these unstable factors, and hence a predictive system can be established for the AFR control by analysing these three dynamic factors. As such, both static and dynamic characteristics of the AFR control system can become more stable with better control effect and stronger system robustness.

Chapter 6: Neural Network based AFR Control

6.1 Introduction

The theory of artificial neural network (NN) has developed rapidly in recent years and become one of international frontier research fields. It is characterized by many attractive features, such as parallel processing, fault-tolerance, well approximation on almost any nonlinear functions, self-learning, adaptive and associative functionalities. Consequently, the artificial neural network has attracted interest of many researchers, who then have made significant progress in various artificial neural network applications.

Neural network applications is particularly appealing in control fields where highly nonlinear and complex problems (e.g. engine control systems) can be effectively dealt with, such as pattern recognition, controller design, optimization operation and analysis and diagnosis of faults. The control theory by NNs and its applications have sufficiently proved that it can play an essential role in complex control processes. Industries are in great need of advanced control methods, such as NN control, which are both effective and practical. Considering drawbacks of classical control, research on intelligent control is increasingly favoured, for example, robustness and control accuracy of the AFR system has been significantly enhanced by using the NN control theory.

This chapter will focus on the discussion of the NN control for the engine AFR, and it is divided into 5 sections: firstly, the presentation of the principles and structure of the network control, which is followed by the presentation of a new NN control method; thirdly, a NN controller is designed in the MATLAB environment, and this is then followed by the presentation of the controller testing; finally, the results are discussed and conclusions are given.

6.2 Control Applications of Neural Networks

Neural networks can be adopted in many areas due to their capability of good approximation for nonlinear mapping, such as information processing, pattern

recognition, model identification and system control. Huge practices and successful examples are also found in applications of automatic control and pattern recognition. Neural networks demonstrate superb ability of approximation and generalization in control applications. For example, a NN based intelligent control system usually requires two neural networks: one is for system identification and the other is used as a controller. System identification is not only an important area of NN applications in the control system, but also fundamental to the implementation of intelligent control. For this purpose, the next section will be divided into two parts for applications of neural networks in the control area: identification and control.

6.2.1 The Neural Network Identification Technology

System identification is an important area of NN applications in the control system and it is fundamental to intelligent control. The system identification is also critical to adaptive control, and it estimates the mathematical model for an object based on the measurement of its input and output. Therefore, the resultant model can have the same input-output characteristics as those of the object. Because neural networks can approximate any for nonlinear functions and have self-learning capability, they provide a very effective method for system identification, particularly for nonlinear dynamic systems. System identification based on neural networks is essentially adopted to determine an appropriate NN model for approximating the mathematical model for an actual system. Zadeh (1973) gives a definition for system identification: "the determination on the basis of input and output, of a system within a specified class of systems, to which the system under test is equivalent ".

Similar to traditional identification methods, the accuracy of system identification by neural networks is also subject to adjustable parameters, such as the learning step, the number of nodes in both the input layer and the hidden layer of the identification network. The basic design idea is to derive a general and suitable identification network structure, which should have less identification parameters for any repeated and crossover adjustment to achieve the identification accuracy. Through simulation experiments the basic structure for the NN identification model should follow the following principles:

1. The number of nodes for the input layer is based on the dynamic relationship between input and output of the system's equation.
2. For any systems with orders higher than two the number of nodes for the input layer can be determined by a second order plus dead time model.
3. If system identification requires higher accuracy, the number of nodes (neurons) in the hidden layer should be increased.

6.2.2 The Neural Network Control Technology

A neural network has very strong self-learning and powerful mapping ability which can be used widely in controlling complex objects. The features of neural networks, such as large scale parallelism, redundancy, fault tolerance, non-linear essence and the capability of self-organizing, self-learning and self-adaptive has brought control theories renewed vitality. NN control is a control type that does not depend on models and therefore becomes "a new branch of intelligent control". The purpose of NN control is mainly to solve controlling of complex systems that have nonlinear, uncertain and unknown problems. Due to its capacity of nonlinear mapping and self-learning neural networks have received great attention in the field of control engineering, and NN based intelligent control has become a hot research topic, and thus bring about many relevant control structure.

NN direct control (Fig 6.1): NN is used as the error feedback controller of the closed-loop system directly. The NN controller will be trained off-line by the existing control samples. The online learning is achieved by the evaluation function and the learning algorithm is based on mean square error function.

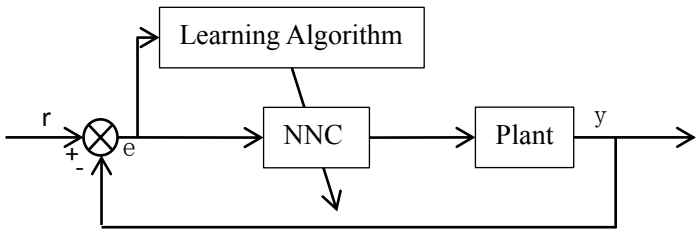

Figure 6.1: Schematic of NN Direct Control Strategy

NN inverse control (Fig 6.2): The basic idea of adaptive inverse control is to apply the

inverse dynamics model of the controlled object's transfer function to the object by an open-loop control. In this situation, the inverse model acts as a series controller. The NN is trained off-line for the inverse dynamics model of the controlled object, and is then used as the feedforward series controller. Due to the lack of stability within the open-loop control the NN also needs continuing to learn online the inverse dynamics model based on the feedback error of the system.

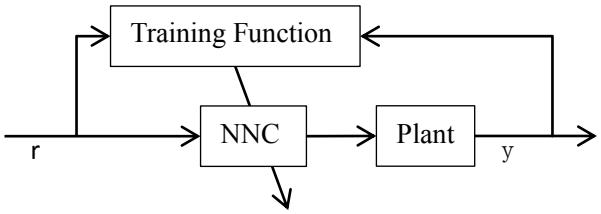

Figure 6.2: Schematic of NN Inverse Control Strategy

NN internal model control (Fig 6.3): Characterized by a control device consisting of the NN controller and plant, the internal model. The internal model loop computes the difference between the outputs of the plant and of the internal model. If the plant is invertible, then the NN controller is simply the inverse of the plant. If the internal model is accurate and there is no disturbance, then perfect control is achieved if the filter is not present. This also implies that if one knows the behaviour of the process exactly, then feedback is not necessary. The primary role of the low-pass filter is to attenuate uncertainties in the feedback, generated by the difference between process and model outputs and serves to moderate excessive control effort.

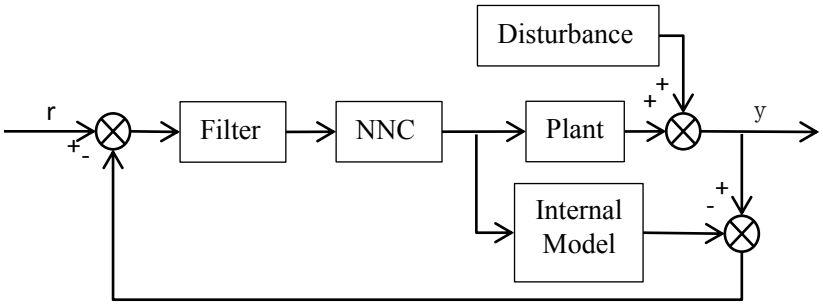

Figure 6.3: Schematic of NN Internal Model Control Strategy

NN direct adaptive control (Fig 6.4): The NN controller learns from inverse dynamics plant, in series with controlled object. The NN will be trained online based on the error function of the controlled plant output and reference model output, so that the error function is minimized.

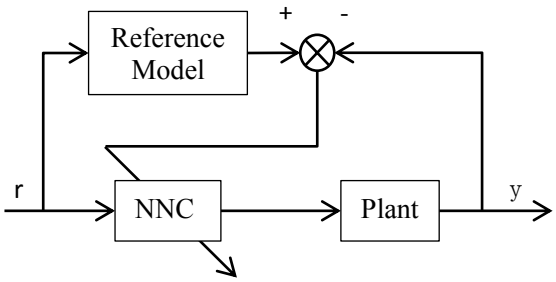

Figure 6.4: Schematic of NN Direct Adaptive Control Strategy

NN indirect adaptive control (Fig 6.5): On the basis of the direct adaptive control, the introduction of a process model is online identification for the NN of controlled object, which can be promptly transmitted to the object model changes to NN controller, so that it can timely effective to train the NN controller.

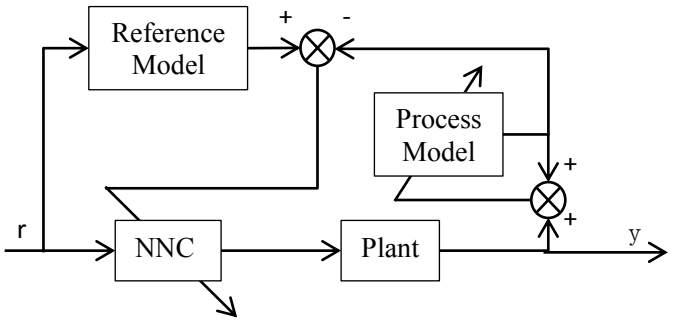

Figure 6.5: Schematic of NN Indirect Adaptive Control Strategy

NN self-tuning control (Fig 6.6): Self-tuning regulator is aimed at automatically adjusting the controller parameters when control system parameter has changed in order to ensure the performance of the system and eliminate the influence of disturbance. The NN is as an estimator to process controller parameters. The controller can be PID controller, sliding mode controller, robust controller, fuzzy controller .etc.

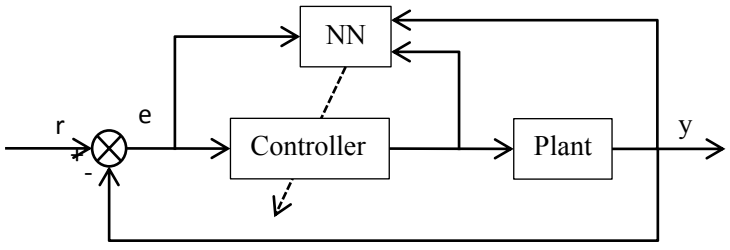

Figure 6.6: Schematic of NN Self-tuning Control Strategy

NN predictive control (Fig6.7): This controller uses a NN model to predict future plant

responses to potential control signals. An optimization algorithm then computes the control signals that optimize future plant performance. The first stage of model predictive control is to train a NN to represent the forward dynamics of the plant. The prediction error between the plant output and the NN output is used as the NN training signal.

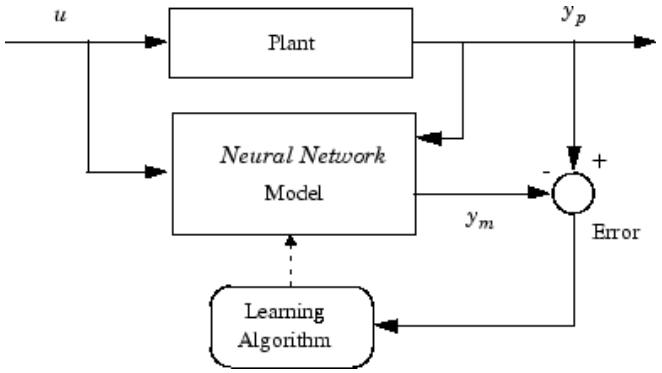

Figure 6.7: NN Predictive Control Training Structure (MathWorks, 2005)

The controller requires a significant amount of online computation, because an optimization algorithm is performed at each sample time to compute the optimal control input. The following Fig 6.8 illustrates the model predictive control process. The controller consists of the NN plant model and the optimization block. The optimization block determines the values of u' that minimize J, and then the optimal u is input to the plant.

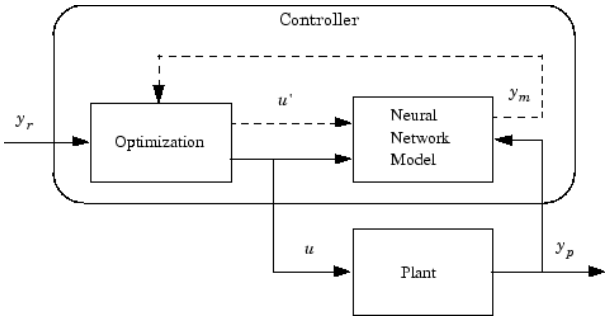

Figure 6.8: NN Predictive Control Strategy (MathWorks, 2005)

NN learning control (Fig 6.9): The NN based adaptive inverse control system combines the NN and the conventional error feedback control. First, the NN is used to learn the inverse dynamics model of the object. Then this trained NN works as a feedforward controller, and together with the error feedback controller to form a composite controller for the object. The output of the feedback controller is used by the system as an evaluation function to adjust the weights of NN. In this case, this adaptive inverse

controller will have stronger adjustment output when the system is less stable. Following the control process the system is more stable, and hence adjustment effect provided by the adaptive inverse controller is weak. This stage requires a conventional controller to eliminate the steady state error generated by the adaptive inverse controller. The controller can be PID controller, sliding mode controller, robust controller, fuzzy controller, etc.

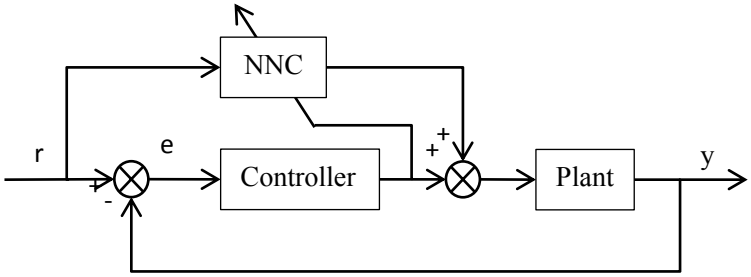

Figure 6.9: NN Learning Control Strategy

As NN learning control and NN self-tuning control have been combined with other controller, there are still many various control methods which combine the NN with the conventional error feedback control (PID controller, sliding mode controller, robust controller, fuzzy controller, etc.).

The roles of NNs in control applications can be summarized into four categories:

- A model for objects in a variety of control structures that require accurate modelling.
- A controller in feedback control systems.
- Act as functions for optimizing calculations in the traditional control system.
- Provide object model, optimization parameter model, reasoning and fault diagnosis together with other intelligent control methods and optimal algorithms.

The success of NN inverse control method is largely determined by the generalization feature of networks. Hence, in practice they should be trained by abundant experience from experts and operators to replace manual operation rather than aiming to solve the inverse dynamic model of the controlled object. The inverse dynamics in actual control systems can produce a small error between the feedback of control output and the actual expected value in their steady states.

It is well known that the features of neural network adaptive control include strong

adaptive ability, robust and fault-tolerant; they however, still have some drawbacks. First, during the initial stage of control the sensitivity of networks is not so accurate due to poor approximation of system output by the identifier. This inaccuracy can easily lead to overshoot and instability of neural networks. Second, as discussed previously two networks have to be set up and trained at the same time. This increases the complexity of the control structure, slowing down the convergence speed of the algorithm and reducing dynamic quality of the control system. Third, the controller uses the system feedback as its input but not the output error, and hence its capacity of resisting disturbance is low.

Although NN learning control is more intelligent than adaptive control method, among others solving the above problems, its convergence speed is also slow due to massive number of parameters. This is refereed in literature as model identifiability and accuracy.

6.3 Neural Network Based Off-Line Tuning Predictive Control

Based on the study of NN based control method structure and features, a new controller (Fig 6.10) scheme is developed for AFR control. Within this scheme, the network training and the controller tuning are based on the ideas from model predictive control. The controller will be designed in two stages controller training and controller tuning.

First stage is to train neural networks for systems under control of original controller (section 5.4), the NN output will be the same as the original controller, and the NN input is referenced in the original controller and principle of intelligent control. The aim of this identification is to realize the NN have the same control performance as the original controller, also have good identifiability during tuning process. Training schematic are shown in Fig 6.15, NN input may refer to all possible variables in control system.

Off-line tuning schematic is presented in Fig 6.11, the controller will use trained NN. Tuning algorithm is based on the analysis of controller error and this is similar to the predictive control technology. Tuning algorithm can be imagined as an error compensation strategy to modify control output. Detailed experimental process will be described in next section.

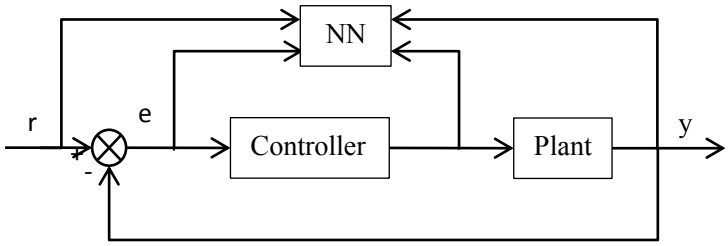

Figure 6.10: NN Training Schematic

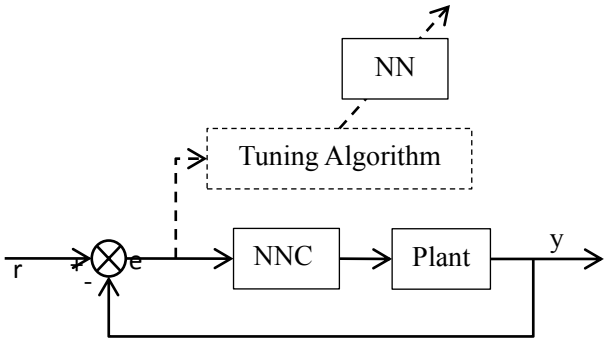

Figure 6.11: NN Controller Tuning Schematic

6.4 Feasibility Analysis of Neural Network Controllers

This section examines the feasibility of engine control applications using NN controllers. The choice of errors criterion is first discussed, and the feasibility of designing different NN controllers based on the conventional control methods is then analysed. After this, the numbers of layers and nodes in these NN controllers are considered in detail and then the input and output are determined.

6.4.1 The Choice of Errors Criterion

Because there are many different ways to calculate the error this section first discusses the chosen error and its reasons. In the NN training process the Mean Square Error (MSE) is chosen, which is reasonable due to the following reasons:

1. The error in the standard BP algorithm is defined as:

$$E_p = \frac{1}{2}\sum_{j=1}^{m}\left(t_j^p - y_j^p\right)^2 \tag{6.1}$$

The weight matrix is updated for each sample. However, each modification does not consider whether the error of all the other sample output can also be reduced after the modification. This leads to an increase in the number of iterations required.

2. The global error based on the accumulative error BP algorithm is defined as:

$$\mathrm{E} = \frac{1}{2}\sum_{p=1}^{p}\sum_{j=1}^{m}\left(t_j^p - y_j^p\right)^2 = \sum_{p=1}^{p} E_p \tag{6.2}$$

This algorithm aims to reduce the global error of the whole training set and not for a particular sample, thus a modification that can reduce the global error does not mean that the error of for one specific sample should be smaller. However, it cannot be used for performance comparison between two networks when their P and m are different. This is because that for the same network, E is larger when P is larger; for the same P value the greater m is the greater E is.

The mean square error (MSE):

$$\mathrm{MSE} = \frac{1}{mp}\sum_{p=1}^{p}\sum_{j=1}^{m}\left(\hat{y}_j - y_j\right)^2 \tag{6.3}$$

where: p - the number of output nodes, m - the number of training samples, t_j - the network output, y_j - actual network output.

The MSE of an estimator is one of many ways to quantify the difference between values implied by an estimator and the true values of the quantity being estimated. MSE measures the average of the squares of the "errors." The error is the amount by which the value implied by the estimator differs from the quantity to be estimated. The difference occurs because of randomness or because the estimator doesn't account for information that could produce a more accurate estimate. Mean square error overcomes the shortcomings of the above two algorithms. Hence, the choice of the mean square error algorithm is reasonable.

6.4.2 Input Analysis of Neural Network Controllers

According to the controller structure (Fig 5.1) presented in Chapter 5 the desired AFR can be viewed as a selector of working conditions, that is, it chooses a reasonable AFR based on working conditions of both the engine and the vehicle, and hence there is no need for further improvement on it. Both the ideal fuel control and the fuel output error are dependent on the difference between the ideal and the actual AFRs. However, the output error produced by the conventional controller introduced in the previous chapter is not good enough, and in order to further reduce both the error and the settling time a new NN controller should be properly designed to replace it, which forms the main purpose of the chapter.

Testing Class

Input to the controller need to be determined by tests, and based on the design idea of NN controllers we should first investigate the input of the original controller. The input of the PID controller consists of engine speed, desired lambda, air-port flow rate and feedback lambda. In addition, the automotive sensor of the throttle angle can be collected as the reference input of the controller. According to both classical NN and traditional AFR control, the controller input can be divided into three groups: traditional, neural and innovative. Each type can further handle the signal delay separately to strengthen controller's controllability. Therefore, input of AFR controllers will be divided into the following classes as shown by Table 6.1 and their feasibility will be tested individually.

Table 6.1: Testing Class

Testing Class	Test Number	Input	Number of Input
Traditional	1	$\lambda_D\ N_e\ m_a$	3
	2	$\lambda_D\ N_e\ m_a\ \lambda_F$	4
	3	$\lambda_D\ N_e\ m_a\ \lambda_F\ \ N_e\|_{\Delta t}\ m_a\|_{\Delta t}$	6
	4	$\lambda_D\ N_e\ m_a\ \lambda_F\ \ N_e\|_{\Delta t}\ m_a\|_{\Delta t}\ \lambda_F\|_{\Delta t}$	7
Neural	5	$\lambda_D\ \lambda_F$	2
	6	$\lambda_D\ \lambda_F\ \lambda_F\|_{\Delta t}$	3
	7	$\lambda_D\ \lambda_F\ \lambda_F\|_{\Delta t}\ \lambda_F\|_{2\Delta t}$	4
	8	$\lambda_D\ \lambda_F\ \lambda_F\|_{\Delta t}\ \lambda_F\|_{2\Delta t}\ \lambda_F\|_{3\Delta t}$	5
Innovative	9	$\lambda_D\ N_e\ m_a\ \lambda_F\ a_T$	5
	10	$\lambda_D\ N_e\ m_a\ \lambda_F\ a_T\ N_e\|_{\Delta t}\ \ m_a\|_{\Delta t}\ \ \lambda_F\|_{\Delta t}\ a_T\|_{\Delta t}$	9

Where: λ_D =Desired lambda, λ_F =Feedback lambda, $\lambda_F|_{\Delta t}$ =Feedback lambda (n-1), $\lambda_F|_{2\Delta t}$=Feedback lambda (n-2), N_e=Engine speed, $N_e|_{\Delta t}$=Engine speed (n-1), m_a=Air-port flow rate, $m_a|_{\Delta t}$=Air-port flow rate (n-1), a_T Throttle angle, $a_T|_{\Delta t}$=Throttle angle (n-1).

The traditional class refers to the design of traditional AFR controllers, which composes four further tests: Test 1 is a controller without feedback; Test 2 is a controller with feedback; Test 3 and 4 are based on the second one but without and with delay of feedback, respectively.

The neural class is a group of controllers based on errors, and it has four tests depending on the number of delays, which ranges between 0 and 3 corresponding to Test 5 to 8.

The innovative class is presented by the existing controller with added input reference signals for throttle angle. Specially, Test 9 is Test 2 with throttle angle whereas Test 10 is Test 4 with both throttle angle and its delay. Detailed test results are shown in the following analysis.

Testing Neural Network Structure

A temporary NN structure is first chosen for test convenience, which is shown by Fig 6.12, a two-layer feed-forward network with sigmoid hidden neurons and linear output neurons, 10 neurons in its hidden layer. The network will be trained with Levenberg-Marquardt back propagation algorithm, unless there is not enough neurons to memory, in which case scaled conjugate gradient back propagation will be used.

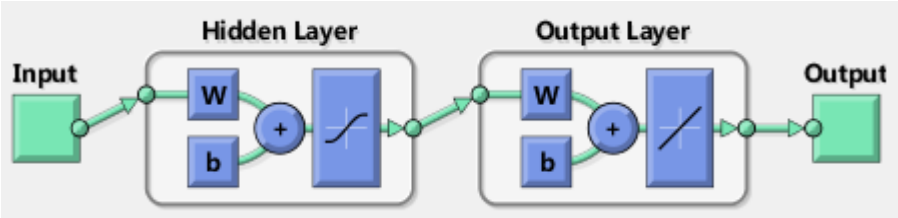

Figure 6.12: Two-Layer Feed-Forward Network Structure

Testing Data Collection

To train the network for neural inverse control, we need to have both system input and output data. In order to quickly test each group of identifiability and controllability we first collect 11 groups of input data and one group of output data from the SIMULINK simulation platform based on the PID control. The following diagram (Fig 6.13) demonstrates the collection of throttle angles using Memory as a function of delay. The simulation's sampling and storage period is 0.01 second and the sampled data are then

stored by the workspace module in MATLAB. This sampling process for throttle angles is the same as other data.

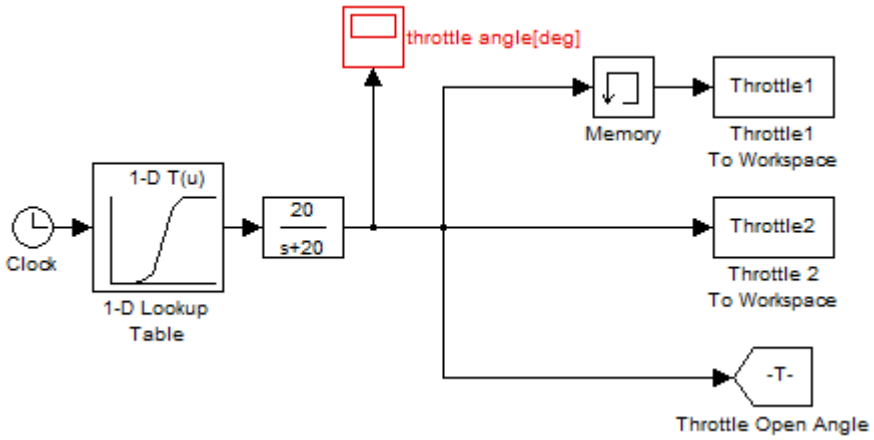

Figure 6.13: Data Collection Model in SIMULINK

Testing Input Data

In order to make the test data more convincing during NN training the sampling process is simulated for 1000 seconds. Hence, each of the variables has 1000001 samples, throttle angle input is set to between 10 and 40 degrees and the engine loading is 100. In particular, throttle angle is sampled every 10 seconds by a random step. Fig 6.14 shows the samples for the first 100 seconds in its generation process.

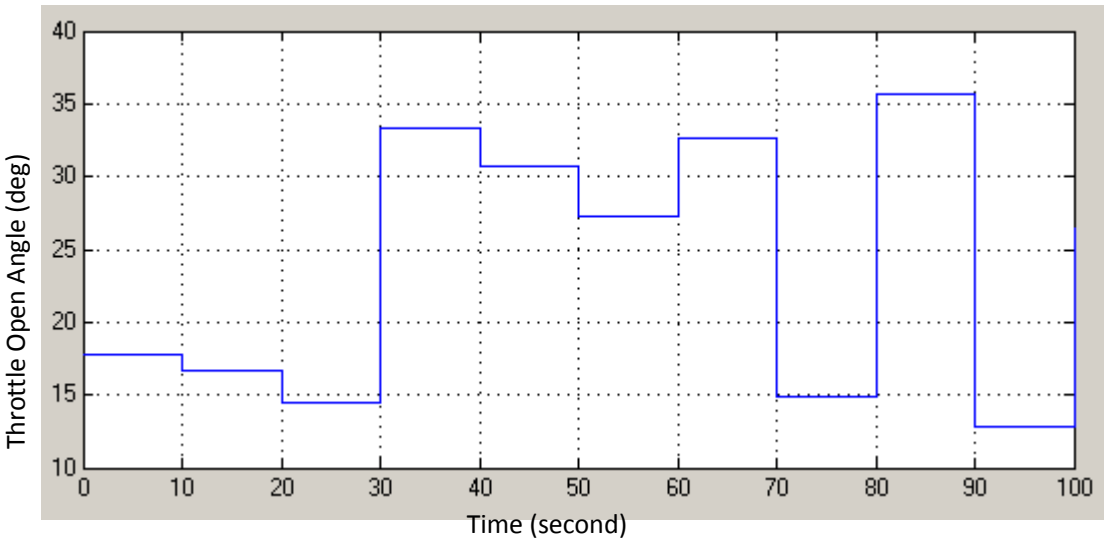

Figure 6.14: The Samples for Random Throttle Open Angle

The range for testing controller's controllability is determined by the range of the training samples, therefore, the test input for the engine loading is unchanged at 100 and

throttle angle has a range from 13 degrees to 36 degrees, randomly increasing every five seconds with a total number of 10 times. Its testing curve is shown below.

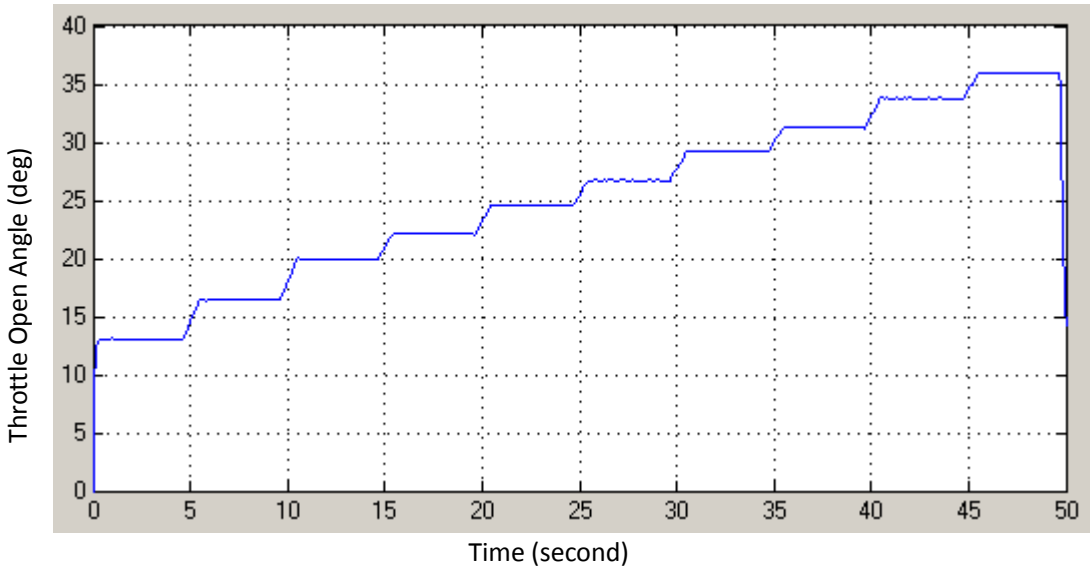

Figure 6.15: Testing Throttle Open Angle

Test results

First, all the collected data will be categorized as different classes in accordance with the Table 6.1 and then trained separately. After training NN are tested against their MSE results. Based on the Table 6.2 the MSE of Test 1, 2, 3, 4, 9 and 10 have very small errors. Although errors of Test 5, 6, 7 and 8 are not as small as the others due to their large training input matrices they are all within a reasonable range. Therefore, controllability of each test group can be represented by these trained NN controllers.

Table 6.2: Controllability Tests MSE Results

Test	1	2	3	4	5	6	7	8	9	10
MES	0.0647	0.0335	0.0219	0.0269	13.5	12.5	10.5	12.5	0.217	0.00265
Controllability	No	No	Yes	Yes	No	No	No	No	No	Yes

During these tests, in order to prevent any simulation with numerical instabilities, which can be triggered by controllers' inability of controlling, a limiter is added to the output of the lambda module. The range is limited to [0.8-1.3] by the limiter. Hence, even if a controller fails the simulation system can still send to the controller a reasonable feedback signal and the simulation process continues until completion. In the meantime the causes of control failure can be diagnosed by the designer. If the controller works

properly after numerous tests the output of the lambda module should remain within the range of [0.8-1.3], and hence the limiter does not affect tests of those normal controllers.

Traditional class analysis: as can be seen from Table 6.2, both Test 1 and 2 fail whereas Test 3 and 4 are successful. The reason can be explained as follows. According to working principles of the engine if it is running at a fixed speed, quantity of fuel injected is the same sometimes for different torque load due to response of oil film. If the delay of both speed and air intake are introduced, torque load and oil film effect can be analysed. Consequently, the engine control can be successful for Test 3 and 4.

Neural class analysis: This group of NN controllers achieves its system control in accordance to the system's output error and its changes. In particular, the analysis of the system error changes can be implemented by entering delayed signal, implying that both the current and the last input information are fed into the controller. Therefore, Test 5, 6, 7 and 8 are designed although none of them is eventually successful. Detailed analysis suggests that the engine AFR control is very complex because of many external interference factors, and hence successful control based on a single, low dimensional error is difficult to achieve. It is possible to obtain this objective by using higher dimensions, for example 10 or more delayed signals, however, the additional amount of calculations may lead to the response time of the controller greater than the required for the engine control.

Innovation class analysis: Test 9 fails whereas Test 10 succeeds. The reason of Test 9's failure is the same as that in Test 2, e.g. they both are caused by too little information. Test 10 is based on Test 4 but with an additional input signal - throttle angle, resulting in better system identification. Further, by looking into the engine Eq (3.2) both the throttle angle and the inlet pressure are important parameters for analysing the quality of actual air in the gas cylinder. When throttle angle is taken into account the effect of the system optimisation at a later stage will be more obvious. Finally, Test 10 will be used as NN controller input.

Fig 6.16 shows a failed example of feedback lambda during feasibility tests. In this example the feedback signal oscillates irregularly within the range between 0.8-1.3. The reason is that the controller cannot maintain reasonable control over the engine by sending the correct control signals. However, due to the existence of the protected

control module the engine can still work properly in the range of [0.8-1.3] for lambda. Consequently the above test results appear. The other failed tests also demonstrate the similar characteristics of the below chart and hence are not discussed in detail anymore.

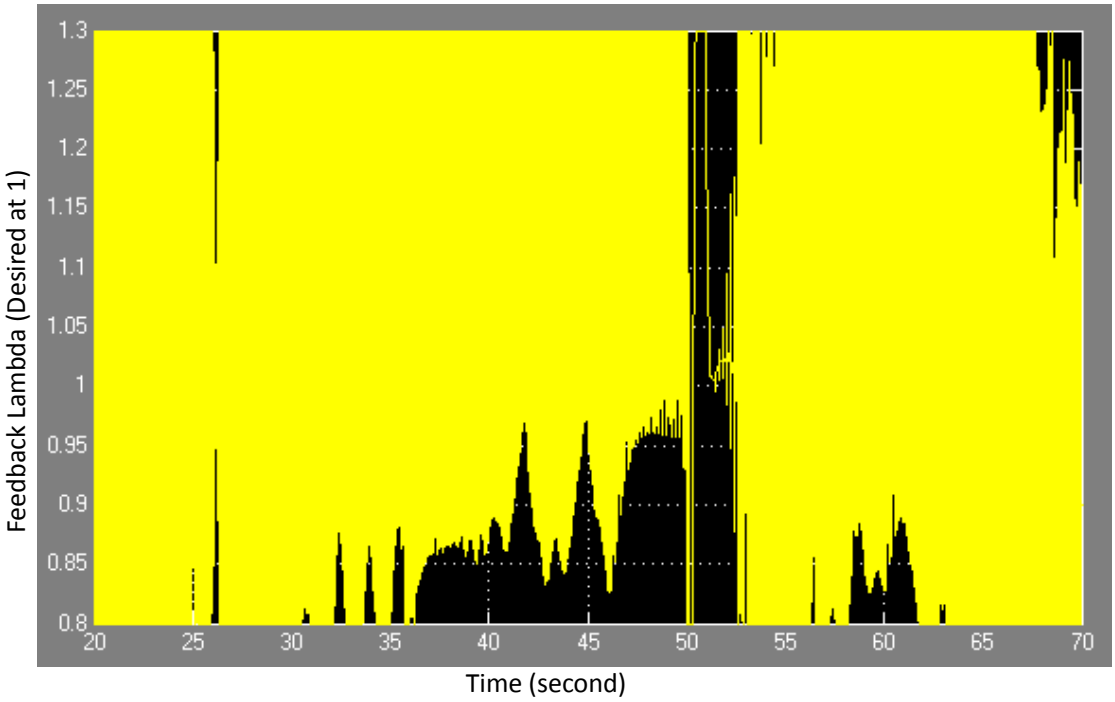

Figure 6.16: Failed Example of Feedback Lambda During Controllability Test

6.4.3 Determination of Layer and Node Number for Neural Network Controllers

The number of hidden nodes is the key for the success of NN control. If the number is too small, the network cannot get enough information to solve problems. If the number is too large, the network not only requires more time for training, but also exhibits the so-called overfitting problem, e.g. the test error increases due to a decrease of the network's generalisation ability. Therefore, it is very important for control performance to choose a reasonable amount of both hidden layers and nodes in each layer. However, the determination of hidden layers and nodes are complex, and a general principle is that the number of nodes in a hidden layer should be small enough provided that the relation between input and output is correctly reflected; as such, the network structure is as simple as possible. Hence, this research adopts a network structure growth method, i.e. the number of nodes is initially set to small, then the network is trained and the training error is tested. The number of nodes, of the network is increased gradually until the training error cannot be significantly reduced further.

Determination of the number of nodes in the hidden layer

In a NN controller the number of neurons in the hidden layer is very important for controllability. If the number is small the network can possibly reach local minima in its training process, resulting in inability of controlling for certain stages; if the number is too big the network will take longer time to train and hence its response speed of the control will be affected. At present, the determination of the number of hidden neurons mainly relies on the experience, which helps determining the initial number. To start the training process, a three-layer BP network with a single hidden layer the number of hidden nodes is chosen according to the following empirical formula:

$$N_{nodes} = \sqrt{n+m} + a \tag{6.4}$$

where: n is the number of input nodes, m is the number of output nodes, a is a constant between 1 and 10. In this research the number of input and output nodes are 9 and 1, respectively, so the calculated N_{nodes} value ranges from 4 to 13. Based on these choices of hidden layer nodes MSE results for each NN controller after training are displayed in the following table.

Table 6.3: Training MSE Results

No:	4	5	6	7	8	9	10	11	12	13
MSE	0.0359	0.0333	0.00647	0.0113	0.00503	0.00244	0.00265	0.0198	0.0208	0.00894

It can be seen that the training error is reduced by increasing the number of hidden nodes, but after the number goes beyond 10 it only fluctuates due to changes in its generalisation ability. Based on all these test results, the number 9 should be chosen as the number of nodes for the best hidden layer. Sometimes the training accuracy and time can be improved by increasing the number of hidden layers whist keeping the total number of hidden layer nodes the same, or just increasing or decreasing its number by as much as merely 1 or 2. The 2 hidden layer structure can be designed and tested, and the structure is shown in Fig 6.17.

In the structure shown in Fig.6.17 the total number of hidden layer nodes is still nine, which can be moved up or down by a maximum of 2. The error test results based on the 1 and 2 Hidden Layer network with different combinations of the hidden layer nodes are shown by Table 6.4. It can be seen that these 2 hidden layer networks do not improve the performance in terms of their training errors. Finally, another test is added with 9+9

neurons, and although there is an increase in its performance but it is not significant; meanwhile, the response speed of the controller is slow. Therefore, we end up with the NN with a 1 Hidden Layer that has 9 neurons.

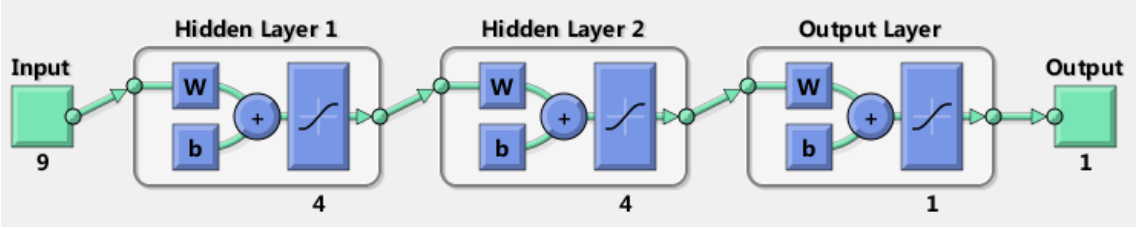

Figure 6.17: 2 Hidden Layer Structure

Table 6.4: Hidden Layer Test	
2 Hidden Layer	Training MSE (200001)
9 neurons	0.00244
4+3 neurons	0.181
4+4 neurons	0.187
5+4 neurons	0.0246
5+5 neurons	0.0131
6+5 neurons	0.0669
9+9 neurons	0.00101

The diagram of the new controller's structure is described in Fig 6.18 where the output of the NN control remains the same as before.

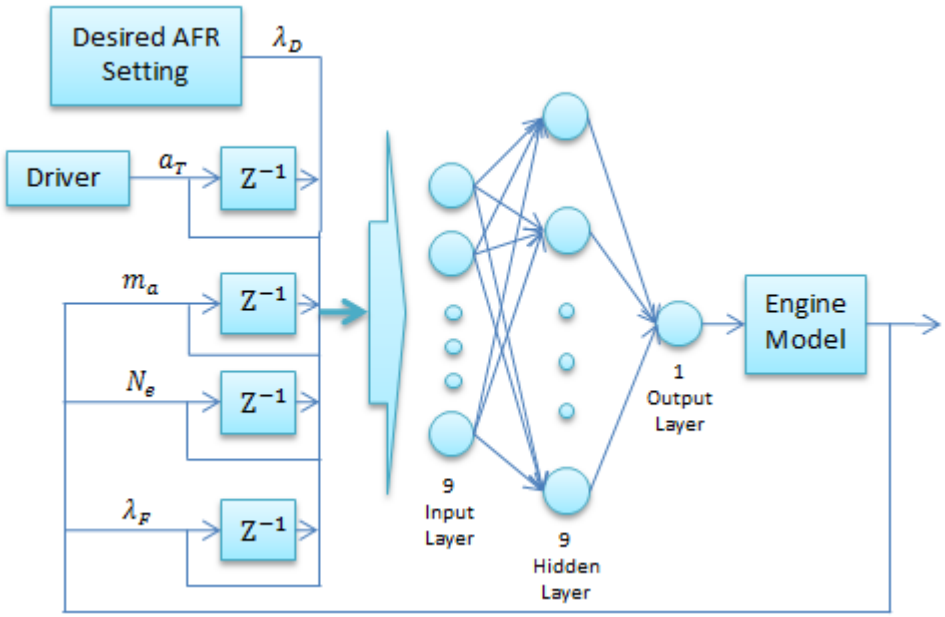

Figure 6.17: The Neural Network Based Control Strategy

6.5 Neural Network Training Process

The training strategy of controllers is the most important for NN controllability, and a logic diagram of its training strategy is shown by Fig 6.19. Firstly, a comprehensive design of a simulation input system is necessary such that the generated data to be used as input for the engine simulation module are based on those of the PID control platform. The simulated data samples are then applied to train NN controllers, and these trained controllers then replace the original controller. The output error is recorded during the first test and by analysing the error the output signal for control is then optimised. Secondly, the optimised output matrix together with the initial input matrix for control is used for training neural controllers again, where the output error of engine simulations is recorded. If the output error is reduced then the logic of the modification deign is proved to be correct, and this process can be repeated until no progress of the output error is found. If the first test output error is not reduced, or even increased then the strategy of controller's optimisation is wrong, in which case the strategy needs to be modified and a new test should be re-run. The design of both a comprehensive input for testing and a correct logic optimisation is the focus of this chapter, and therefore these two parts are discussed in detail in the following section.

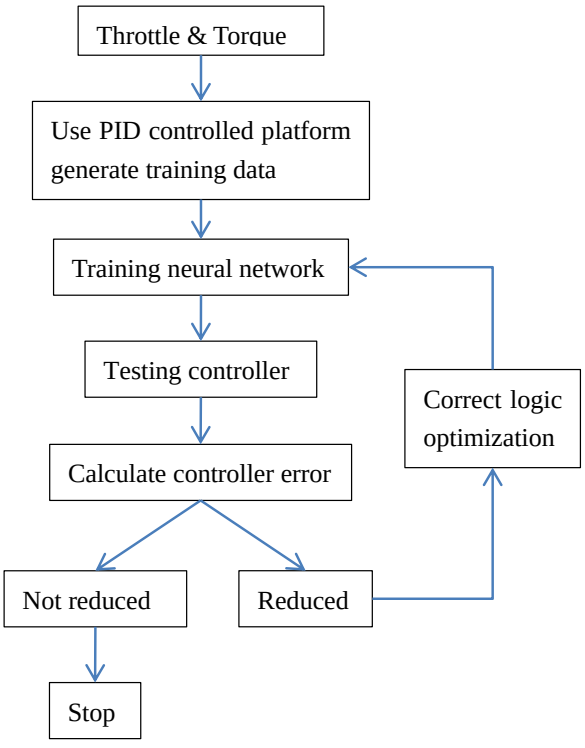

Figure 6.19: Logic Diagram of Training Strategy

6.5.1 Training Input Selection Strategy

Training a perfect NN controller is to ensure that both the input and output data include all possible working conditions. For the training purpose a set of throttle angle data and a set of engine torque load should be generated, both of which are then used for manipulations of the engine simulation module. In addition, 9 data sets required by both the controller and the controller's output data should be stored to achieve full working condition simulations. To determine the throttle angle, the engine idle speed is set at 850 rpm the throttle angle is 8.58 degrees, represent conditions for the steady state of the simulation system at this idle speed. Consequently, the throttle angle is set to the range between 8.58 and maximum angle of 90 degrees.

Once the range of throttle angle is determined, the engine load can then be analysed. Based on the engine's performance, its load is known to be within the range (0-200Nm). As discussed in section 4.4.1, a simulation system that includes the vehicle dynamics model can provide the engine with real-time torque load. However, the model does not necessarily cover all working conditions of the engine due to possible strategy shifts in practice, such as the transmission box. Hence, the engine simulation model torque load input needs to be designed. Consider two randomly generated torque scenarios: one is high torque load when throttle angle is small and this results in engine overloaded and the system error; the other is small torque when throttle angle is large and this leads to high speed of the engine exceeding the maximum safe value at the actual state. Consequently, the module output should be complemented by a protection logic module, with two different algorithms:

(a) The minimum torque protection

The minimum speed of engine is at idle, which is 850 rpm (see Chapter 4), and the maximum torque at this speed is 160 Nm. However, the maximum torque is not suitable for all throttle angles. For example, if 1) the engine load is 160 Nm and the speed is 850 rpm; 2) the throttle angle is relatively small, the actual torque is less than the load torque, and as a result the engine stops running eventually. This situation can be actually avoided by either lowering the speed gear or using biting point of the clutch. In the simulation system these situations are not necessarily taken into consideration, hence a protection module is needed. For example, if the engine is running at 850 rpm then the

protection module starts working by comparing the automatically generated torque load against the maximum torque given by throttle angle. If the generated torque load is larger, the protection module will automatically switch to the corresponding safety value. The maximum output torque with regard to different throttle angle can be obtained through steady state tests of the engine simulation platform, and their results are shown in Fig 6.20 below.

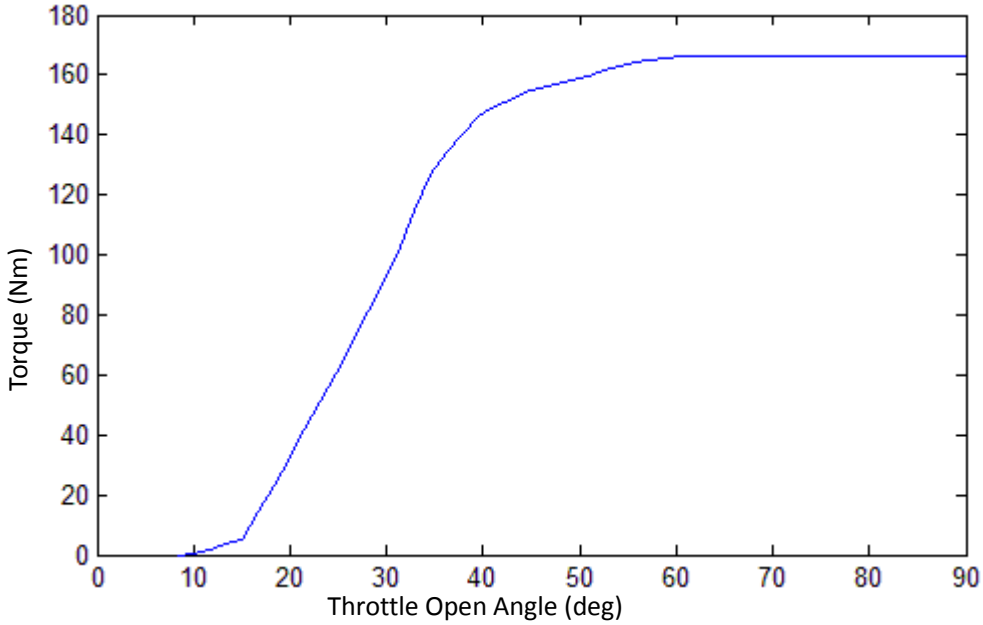

Figure 6.20: Minimum Torque VS Throttle Open Angle

(b) The maximum torque protection

As discussed in Chapter 4, the maximum of precisely simulated speed of the engine simulation platform is 5500 rpm. This is the maximum safe speed of the engine, and simulation results are not accurate for any speed exceeding this number. If the simulated engine speed reaches 5500 rpm, the throttle angle is very large and engine load is small, then the engine speed can be easily increased beyond the safe limit. In order to avoid this situation when torque load is small, a comparison module should be added to the torque module. If the increased engine speed exceeds the maximum safe amount, then the protection system will be connected, providing a reasonable torque load to bring engine speed down to a safe range. This is shown by Fig 6.21 below, where engine torque load is sampled from the engine simulation platform for different throttle angle when the engine speed is set at 5500 rpm.

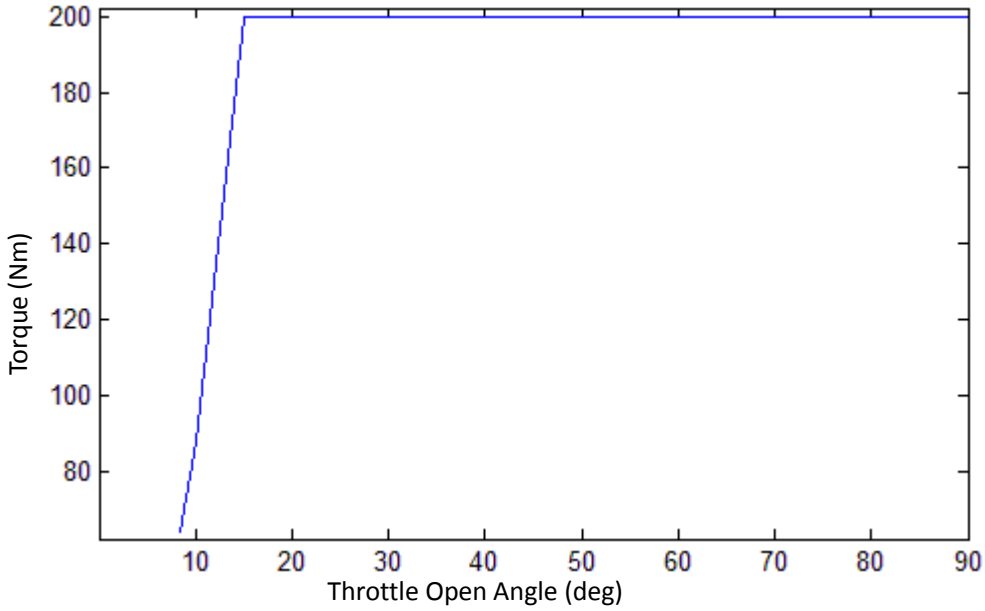

Figure 6.21: Maximum Torque VS Throttle Open Angle

The logic of these two protective modules can be brought together in the following flow chart (Fig 6.22). The torque model randomly generates torque load, and at the same time the throttle module generates a throttle angle. The working process of the engine controlled by the both modules is: if the engine feedback speed is less than or equal to 850 rpm, the Max Torque is activated by the system to produce torque load corresponding to the generated throttle angle. The Max Torque is connected until the engine speed exceeds 850 rpm, at the point the Torque model is switched on again. If the engine speed is greater than or equal to 5500 rpm, the system will switch the load torque signal to the Min Torque model, which has the same basic work principles as that of Max Torque.

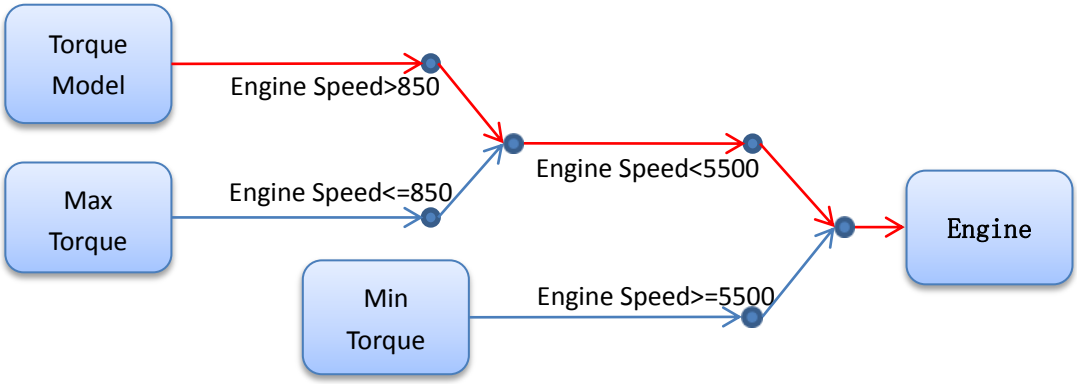

Figure 6.22 Torque Protection Model Flow Chart

SIMULINK compiled by a streamline chart is shown in Fig 6.23. Both Min block and

Max block use lookup table block, and the data are compiled by Fig 6.20 and Fig 6.21. The random throttle and torque data are generated by MATLAB, which also produces a time matrix for them. These established matrices are entered into the corresponding lookup table block, and the Time block is used during simulations to achieve synchronisation.

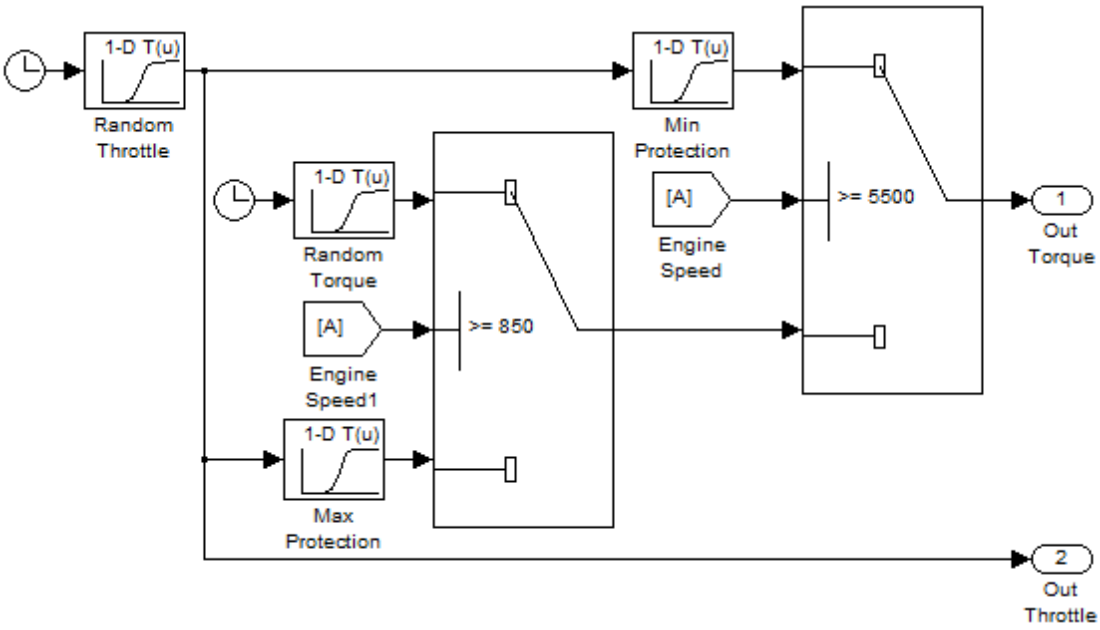

Figure 6.23: Torque Protection Model Flow Chart in SIMULINK

6.5.2 Adjustment Strategy

When testing an engine the output error is the difference between the ideal AFR and the actual one. If the actual controlled AFR is less than the ideal one then the injected fuel of the controller is too much, and vice versa. Due to reasons such as oil film, the inlet and the performance of the controller, the output error can be still large. This section will use predictive control theory to designs a new training logic. That is, if the controlled fuel injection amount is less (more) than it should be increased (decreased) in the previous control loop so as to achieve output error reductions. If there are 90% error from the oil film, 50% of the oil film compensation should be used. For the first test the optimal compensation can reduce 45% of the output error, the second test can reduce 65%, the third test can reduce 80%. Using this logic, repeated training can have good optimization results. Such adjustment strategy is advantageous in that it does not affect the reliability of the engine control as no fuel injection adjustment at the engine's steady states. Another benefit of this strategy is that there is no need to analyse either film

appearance or the engine inlet, both of which are much more complex.

According to the above training strategy we can obtain three sets of data from the simulation: λ_D) ， feedback lambda (λ_F) and the amount of injected fuel (I_t). These control data are already controlled by the PID controller, and they are all n*1 matrices containing ([1 2 3 ⋯ k − 1 k k + 1 ⋯ n − 2 n − 1 n]). The discussed strategy for the adjustment can be expressed as:

$$I_F(k) = \begin{cases} I_t(k) - f(\cdot) & if\ \ \lambda_D(k+1) > \lambda_F(k+1) \\ I_t(k) & if\ \ \lambda_D(k+1) = \lambda_F(k+1) \\ I_t(k) + f(\cdot) & if\ \ \lambda_D(k+1) < \lambda_F(k+1) \end{cases} \tag{6.5}$$

where $I_F$is the modified fuel matrix and $f(\cdot)$ is the adjustment function for the amount of injected fuel.

When the engine is in a steady state, fuel injection amount is based in desired lambda, engine speed and air flow rate. The engine simulation system has the following formula for fuel injection amount:

$$Fuel\ Injection = \frac{m_a}{\lambda_D \times AFRs/N_e} \tag{6.6}$$

According to this injection formula the fuel injection quantity can be adjusted by

$$f(\cdot) = \frac{m_a}{\lambda_D \times \frac{AFRs}{N_e}} \times \frac{|\lambda_F - \lambda_D|}{\lambda_D} \tag{6.7}$$

Therefore, combine both Eq 6.5 and Eq 6.7 we can obtain the final adjustment function given by:

$$I_F(k) = \begin{cases} I_t(k) - \dfrac{m_a(k)|\lambda_F(k) - \lambda_D(k)|}{\frac{\lambda_D(k)^2 AFRs}{N_e(k)}} & if\ \ \lambda_D(k+1) > \lambda_F(k+1) \\ I_t(k) & if\ \ \lambda_D(k+1) = \lambda_F(k+1) \\ I_t(k) + \dfrac{m_a(k)|\lambda_F(k) - \lambda_D(k)|}{\frac{\lambda_D(k)^2 AFRs}{N_e(k)}} & if\ \ \lambda_D(k+1) < \lambda_F(k+1) \end{cases} \tag{6.8}$$

6.5.3 Controller Simulation Validation and Comparison

The testing process will be based on the logic diagram of training strategy shown in Fig 6.19. Firstly, data are collected from the PID controlled engine simulation for the purpose of training NN controllers. The sampling time is 200000 seconds and the sampling frequency is 100 times per second, both throttle angle and torque load change randomly every 10 seconds. At the same time the output error is recorded, which is 312.672 using the output error absolute numerical integration. In order to compare different tests, the throttle angle and the torque load are stored and they are used as an input in the following tests. Secondly, generated NN controllers are applied to control tests, where changes of the engine speed and fuel injection amount are observed and compared against the PID control data. The output error integration is 313.717, and compared to that of PID the difference is only 3/1000, suggesting that the NN training is sufficient. Thirdly, the simulation is used to generate data for 2000 seconds with sampling period of 0.01 to speed up NN training. Both throttle angles and torque load change randomly every 10 seconds. All the data are stored in the workspace and then used by NN controllers when each modification is complete. After the training process is complete, the output error integration for these NN input is 3.148. Fourthly, the design logic is used to modify the data and the NN controllers are trained. This process is repeated twice as shown by Figure 6.19.

According to correct logic optimization process shown in Fig 6.19, the test is repeated until no improvement of the output error is found Table 6.5 shows the test results for seven optimisation tests, and the results for PID and Fuzzy Logic control are listed for comparison purpose. The optimisation strategy demonstrates better control for performance change, where the minimum output error occurred in the sixth test. The dynamic errors of up peak and down peak are decreased by every optimisation strategy and the test 6 provides a very decrease. Therefore, the controllers of test six is chosen as final training result of NN controllers.

Table 6.5 : Optimisation Tests Results

	PID	Fuzzy PID	Test 1	Test 2	Test 3	Test 4	Test 5	Test 6	Test 7
Error Integration	3.148	2.561	3.148	2.815	2.607	2.519	2.495	2.483	2.488
Up Peak	19.4391	16.5118	19.4391	16.5262	15.8319	15.6409	15.5957	15.5743	15.5295
Down Peak	8.3993	11.2633	8.3993	10.7025	11.5329	11.7963	11.8620	11.8939	11.9137

By using the same test method as that for both the PID control and the Fuzzy control we can obtain results shown in Fig 6.24 where transient error is reduced significantly compared to both the PID control (-0. 339) and the Fuzzy (-0.213). Meanwhile, an issue is also found that is the controller's response time is 0.1 seconds longer than that of the Fuzzy control. The reason for this increase is explained later.

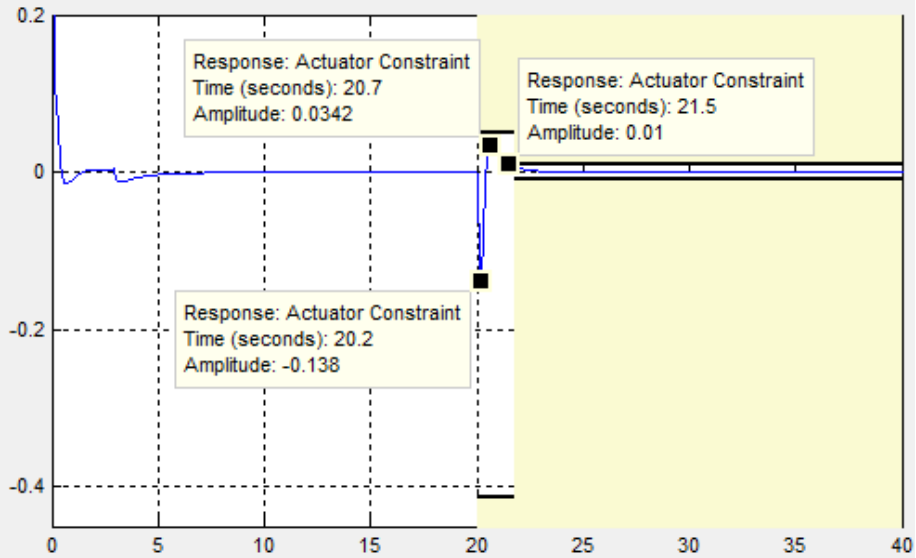

Figure 6.24: Check Step Response Characteristics Block Simulation Result

There is also another issue when comparing the current control result of optimisation to the previous one, which is shown in Fig 6.25. That is, after each optimisation the output error is reduced whereas the control time is slightly longer， this is because the adjustment of fuel injection for the next cycle is based on the error of the previous cycle. Although the adjustment for the last cycle is correct, the oil film effect decreases over time and hence the adjustment is excessive in the next cycle and this cause instability also affects the control time. The transient maximum error is reduced after each optimisation, which greatly offset the effect of increasing control time. Ann example is presented in Fig 6.25 where the blue line represents the control curve after optimisation. Although the control time increased, the error is smaller than another test.

Analysis based on Test 6 and 7 can be derived from Fig 6.25 where the output error for Test 7 is increased. The AFR data stored in MATLAB's workspace reveal that its transient output error actually decreases; such decreased amount is unable to offset the increased amount in the control time. Therefore, the combined analysis suggests that Test 6 represents the best performance for NN controller optimisation discussed in this section.

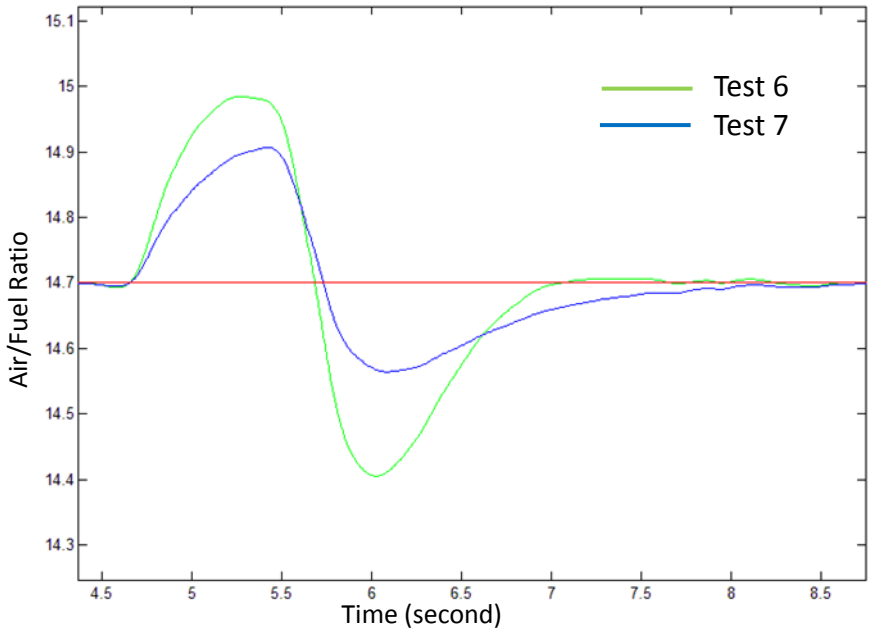

Figure 6.25: AFR Comparation Test 6 with Test 7

6.6 Comprehensive Comparison

In order to present a more comprehensive understanding of the NN controller performance, this section will include PID controller and fuzzy PID controller for comparison. Three types of comparisons will be carried out, the first is the constant load torque test, the second is constant engine speed test, and the third use the driving cycle and vehicle dynamic model to test the pollution reduction efficiency. The tests will use two throttle open angles, the first is a small throttle open angle as shown in Fig 6.26, and the second is a big throttle open angle as shown in Fig 6.27. The small throttle open angle starts from about 11 degrees, and then accelerates to reaches to about 21 degrees at third second, after 3 seconds it is accelerated to 23.5 degrees, finally the throttle is released and pushed 1 more time. The big throttle open angle, start at 16 degrees then reach to 25 degrees, after accelerates to 29 degrees, finally the throttle is released and pushed 1 more time. The third test will use catalytic converters model as a new basis for comparison, the highest efficiency the catalytic converter can achieve is at AFR of 14.664, so that desired AFR will be set at 14.664 for the entire test.

6.6.1 Constant Load Torque Test

In test 1 the constant engine load torque is set at 80 Nm, and the throttle open angle use

small value opening as shown in Fig 6.26, the controlled AFR comparison results are shown in Fig 6.28. After 3 seconds, the system is unstable due to the throttle change, and it can be seen that the NN controlled AFR reduced the maximum error by 50% and 30% from the PID control fuzzy PID control. Between 6 to 11 seconds, the AFR is controlled in the ideal range by the NN control. By releasing the throttle at the eighth second, the system will generate a large output error, however AFR was reduced by 65% and 50% with NN compared with PID control fuzzy PID control respectively.

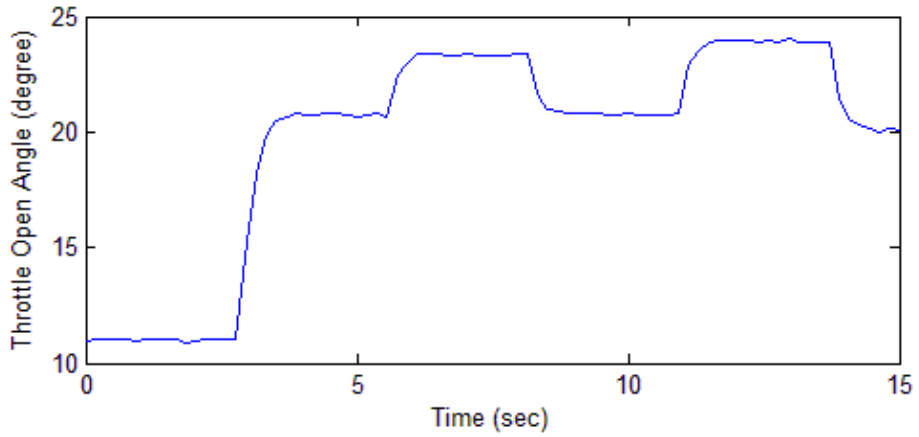

Figure 6.26: Small Value Throttle Open Angle Input Profile

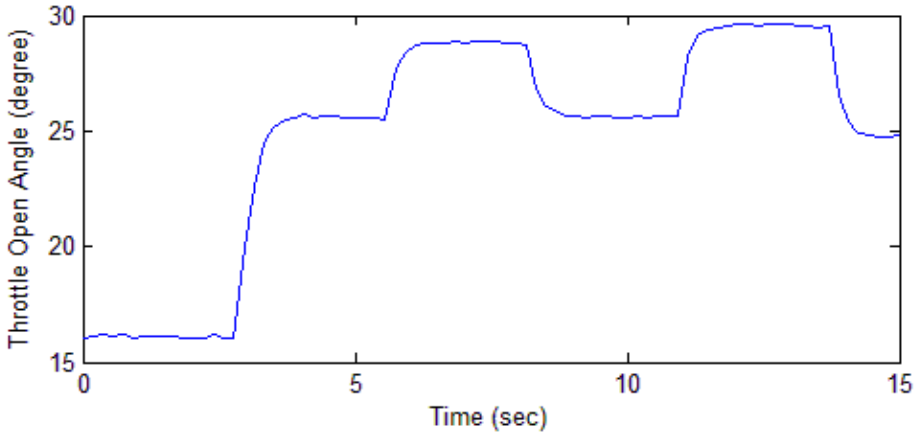

Figure 6.27: Big Value Throttle Open Angle Input Profile

In test 2 the constant engine load torque is set at 150 Nm, and the throttle operation angle uses a large value opening as shown in Fig 6.27, the controlled AFR comparison result are shown in Fig 6.29. There is a small throttle fluctuation at the beginning of 3 seconds. For the low torque tests all three controllers have good control performance, however in high torque test only NN can control the engine AFR in the ideal range, the other two have greater steady-state error. After 3 second, NN controlled AFR reduced

the error by 40% and 25% compared with the PID control and fuzzy PID control. After the eighth seconds, AFR control error was reduced by 60% and 45% by NNC compared with the PID control and fuzzy PID control respectively.

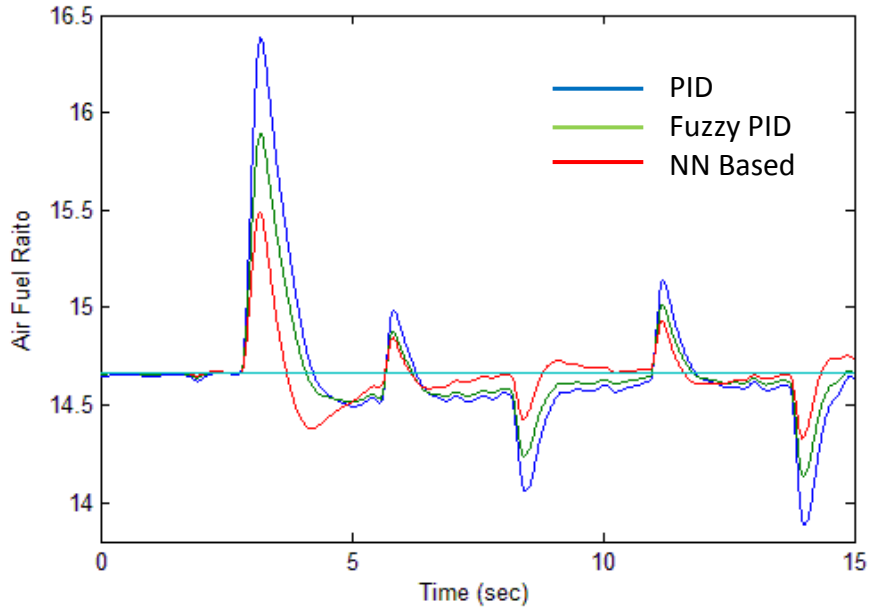

Figure 6.28: AFR Comparison for Test 1

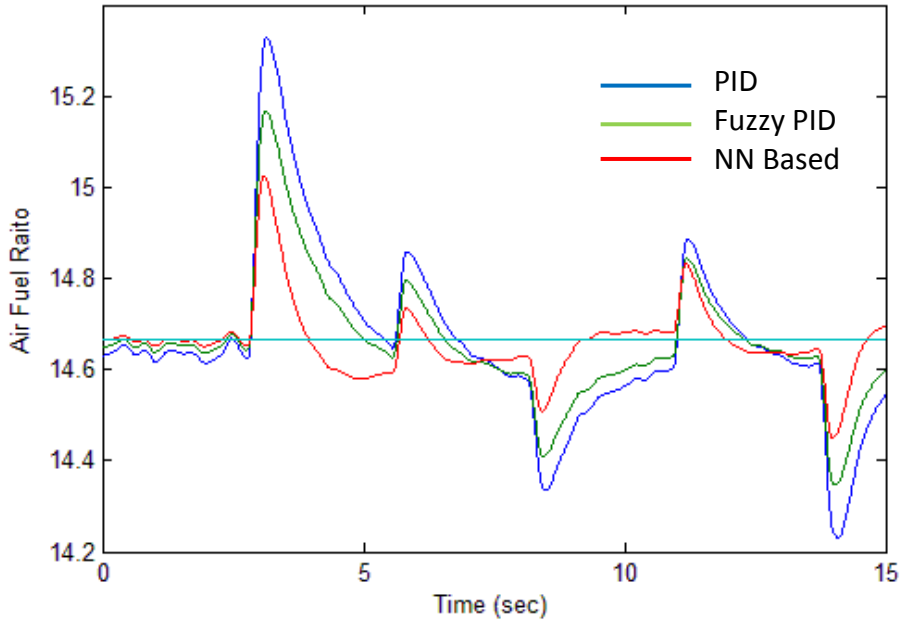

Figure 6.29: AFR Comparison for Test 2

6.6.2 Constant Engine Speed Test

The constant engine speed is set at 2000rpm, and the throttle open angle uses a small value opening as in Fig 6.26, the controlled AFR comparison results are shown in Fig

6.30. After 3 second, the system will be unstable due to the throttle change, and it can be seen that the NN controlled AFR reduced the error by 55% and 35% compared with the PID control and fuzzy PID control. From 6 seconds until the end of the test, the three controllers have controlled the AFR in the small error range, but the NN controlled AFR presents the best control performance. The NN control reduced the AFR control error by 60% and 50% compared with PID control and fuzzy PID control.

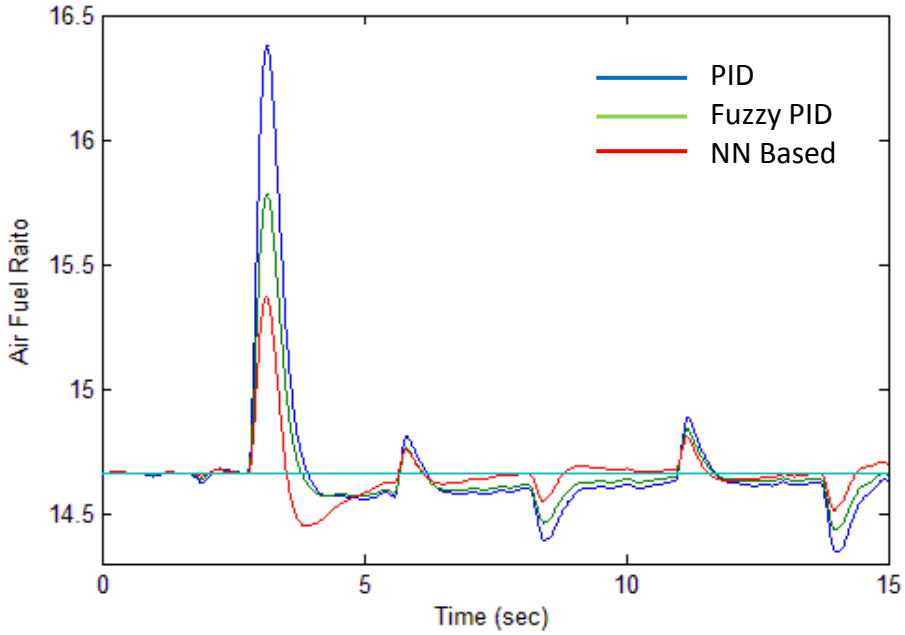

Figure 6.30: AFR Comparison for Test 3

For the another test the constant engine speed is set at 3000rpm, and the throttle operation angle uses a large value opening as shown in Fig 6.27. The controlled AFR comparison result is shown in Fig 6.31. After 3 second, the system will be unstable due to the throttle change, and it can be seen that NN controller reduced the AFR control error by 50% and 30% compared with PID control and fuzzy PID control respectively. From 6 seconds until the end of the test, the NN control reduced the AFR control error by 60% and 50% compared with PID control and fuzzy PID control.

6.6.3 Driving Cycle Test

The aim of driving cycle test is to use different controllers to control the engine under different driving cycle operation to test the efficiency of catalytic converter. Vehicle parameters will be based on Table 4.2 and the different gear shift strategies will be discussed later. The catalytic converter model is detailed in Appendix D. The catalytic

converter model will use the AFR to calculate NO_x, HC and CO catalytic efficiency respectively. Three driving cycle standards introduced in Chapter 2 are used in here; they are European driving cycles, the US driving cycles and Japanese driving cycles. The NEDC, FTP 75 and 10-15 Mode are used in comprehensive tests.

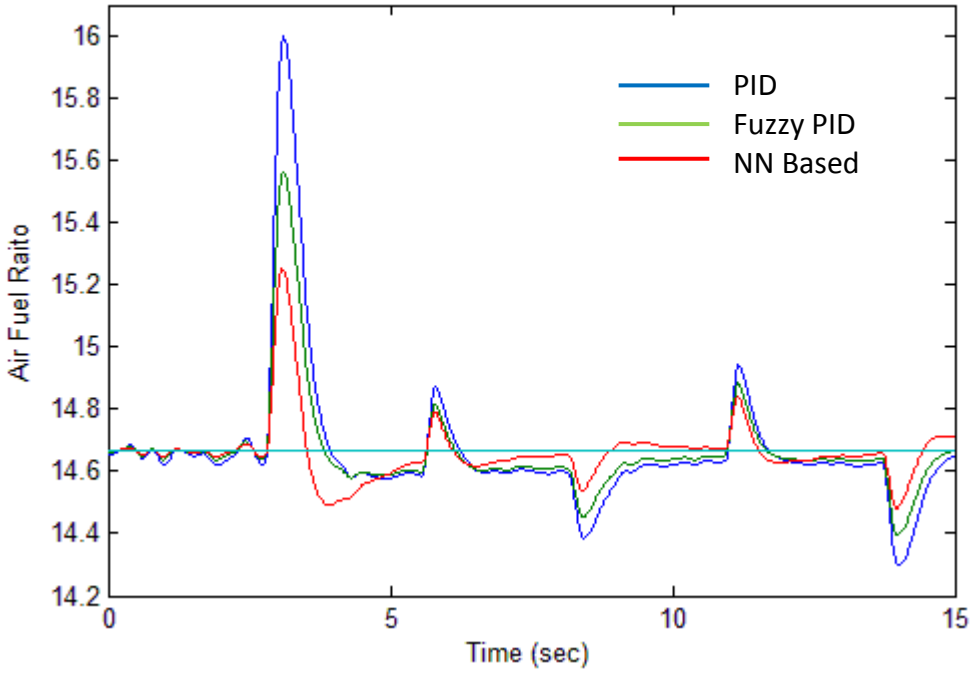

Figure 6.31: AFR Comparison for Test 4

6.6.3.1 European Driving Cycles: NEDC

As can be seen in Table 6.6, the gear shift strategy of NEDC uses first gear when vehicle speed between 0 km/h and 15 km/h, second gear for vehicle speed between 15 km/h and 32 km/h, third gear for vehicle speed between 32 km/h and 50 km/h, fourth gear for vehicle speed between 50 km/h and 70 km/h, fifth gear for vehicle speed between 70 km/h and 120 km/h.

Table 6.6: Gear Shift Strategy of NEDC

Vehicle Speed	0	15	32	50	70	120
Gear Number	1	2	3	4	5	

Table 6.7 shows the catalytic efficiency results: PID controlled catalytic efficiency is about 91% in average, fuzzy PID control and NN control increase the efficiency by 2% and over 5%, respectively. Most noticeably, the NN controlled NO_x catalytic efficiency

is as high as 97%. Moreover, the NN controller has improved AFR standard deviation and output error performance.

Table 6.7: NEDC Driving Cycles Based Catalytic Efficiency			
	PID	Fuzzy PID	NNC
NO_x	91.604 %	94.276	97.157
HC	91.849 %	93.187	94.857
CO	90.244 %	92.414	94.402
Output error integration	2.301	1.26	0.2899
AFR standard deviation	0.035214	0.020234	0.006769

6.6.3.2 US Driving Cycles: FTP-75

As can be seen in Table 6.8, the gear shift strategy of FTP-75 uses first gear when vehicle speed between 0 km/h and 25 km/h, second gear for vehicle speed between 25 km/h and 36 km/h, third gear for vehicle speed between 36 km/h and 64 km/h, fourth gear for vehicle speed between 64 km/h and 72 km/h, fifth gear for vehicle speed between 72 km/h and 90 km/h.

Table 6.8: Gear Shift Strategy of FTP-75						
Vehicle Speed	0	25	36	64	72	90
Gear Number	1	2	3	4	5	

FTP-75 driving cycles based testing results show that the NN controlledNO_x, HC and CO catalytic efficiency were improved by 8%, 5%, and 7.5% compared with the PID control, and 5%, 3%, and 4% compared with the fuzzy PID control.

Table 6.9: FTP-75 Driving Cycles Based Catalytic Efficiency			
	PID	Fuzzy PID	NN
NO_x	87.626	90.846	95.711
HC	89.586	91.499	94.326
CO	86.773	90.226	94.019
Output error integration	5.614	3.223	0.8787
AFR standard deviation	0.059117	0.033915	0.010519

6.6.3.3 Japanese Driving Cycles: 10-15 Mode

As can be seen in Table 6.10, the gear shift strategy of 10-15 Mode, use first gear when vehicle speed between 0 km/h and 20 km/h, second gear for vehicle speed between 20 km/h and 40 km/h, third gear for vehicle speed between 40 km/h and 50 km/h, fourth gear for vehicle speed between 50 km/h and 60 km/h, fifth gear for vehicle speed

between 60 km/h and 70 km/h.

Table 6.10: Gear Shift Strategy of 10-15 Mode						
Vehicle Speed	0	20	40	50	60	70
Gear Number	1	2	3	4	5	

10-15 mode driving cycles based testing results show that the NN controlledNO_x, HC and CO catalytic efficiency were improved by 8.5%, 4%, and 5% compared with PID control, and by 4.5%, 2%, and 2.5% compared with fuzzy PID control.

Table 6.11: 10-15 Mode Driving Cycles Based Catalytic Efficiency			
	PID	Fuzzy PID	NN
NO_x	88.275	92.550	96.930
HC	90.819	92.670	94.824
CO	89.133	92.069	94.416
Output error integration	1.551	0.8438	0.1977
AFR standard deviation	0.038518	0.021777	0.006482

6.6.4 Conclusions

The comprehensive tests prove that NN based off-line tuning predictive control can effectively control the engine AFR. The proposed control method is significantly better than PID and fuzzy control method. At the same time, the tests have proved that an increase of the AFR control performance can also effectively restrict engine harmful emissions send into our atmosphere, being an effective way to help meet the increasing regulations stringent.

6.7 Summary

This chapter first introduces neural network control applications. Based on these existing applications, the new neural network based off-line tuning predictive control structure is proposed and designed. Furthermore, the controller can be further optimized by the adjustment strategy proposed. It has been proved that the NN control can achieve good control for the engine's AFRs in term of the response speed and the AFR error from the target value.

Chapter 7: Conclusions and Future Work

PID, fuzzy PID and neural network based AFR control methods for a conventional Spark-Ignition port fuel injection engine (modeled by means of SIMULINK-based engine dynamic simulation package) have been presented in this Thesis. According to the engine operation structure, a number of engine dynamic equations are collected and organized for engine simulation package which is developed on the MATLAB/SIMULINK computing platform. The system parameters used in the simulation package have been obtained from a Mitsubishi Sirius 4G64 engine testing platform. The operation of the package has been verified using the experimental data. In order to facilitate the controller test and for a better user experience, a modular structure including GUI, input and output modules, has been used for this structure.

Following the simulation, a PID AFR controller is designed according to 4G64 engine control requirements. The PID controller is optimized using MATLAB/SIMULINK optimization toolbox. The principles of fuzzy control and PID control are then combined to develop a gain-scheduling fuzzy PID AFR controller. The simulation results have shown that the fuzzy PID engine AFR controller reached the expected control effect. The neural predictive neural network based AFR control tuned off-line is used to further improve the control performance. The simulation verified the feasibility of the new controller. Finally, more comprehensive understanding of the NN controller performance has been discussed and the results have been compared with PID controller and fuzzy PID controller. The comparison has been divided into three parts, constant load torque test, constant engine speed test and the driving cycle and vehicle dynamic model test.

7.1 Results Summary

7.1.1 Engine Dynamic Simulation Package (Chapter 4)

Engine dynamic simulation package deal with all dynamics related to engine operation, there are air dynamics, fuel dynamics and combustion dynamics. Because of the air and fuel dynamics are dealt with separately, the simulation package has very good

scalability which can be joined by turbocharger dynamics, supercharger dynamics, EGR dynamics and any dynamic behavior which are related to air or fuel.

Air dynamic has two sub-models: throttle and intake manifold models. All parameters in throttle body model can be obtained using experimental procedures. Using idle intake with throttle valve directly operated method, the throttle mass air flow equation effectively express the cross-sectional area of throttle opening and this can improves the simulation accuracy. Intake manifold dynamics model can fully represent the intake manifold charge/discharge effects, and this provides realistic dynamic responses and at the same time produces reasonably good dynamic error control performance.

Fuel dynamics have two submodels: fuel injection and wall-wetting models. The fuel injection dynamics can be modeled according to different injectors with the fuel injection quantity directly used as the model output. In this study, fuel injection and AFR controller output are used as the measure of fuel. The model only needs engine event and engine speed as controlling inputs. Wall-wetting dynamic model is based on double-parameter X-t fuel film equation which is a good description of the dynamic characteristics of fuel film. With this model, the transient AFR control effect can be achieved. When some equation parameters cannot be measured at laboratory, the mean value model is used to implement the simulation model and this is the common practice in many engine simulation studies.

Combustion dynamics have three submodels, in which the torque production has assumed as the dynamic torque of the engine and it is a function of engine speed, air charge, spark timing, and the AFR. Based on this assumption, the predictive torque production model is derived from the steady state engine experiments. The development of the torque production model objective is to use the mean value model method to achieve the identification of the optimal spark timing and wide range of AFR at each of the operating conditions.

In order to simplify the intuitive engine model testing framework and to investigate the impact of control system optimization, the engine dynamic simulation package has incorporated a reasonable vehicle dynamic model and driving cycle model. This has enabled valid theoretical analysis and industrial standard vehicle testing.

The simulation package has been proved very successful with results very close to experimental results. Comparison between the simulated results and the test results at transient conditions with step and sinusoidal throttle inputs applied have been made. The model outputs of the brake load or engine speed, the AFR, the intake manifold pressure and the air mass flow rate show good agreement with experimental data. However, for the brake torque or engine speed, a slight time delay is observed during the transient period between the simulated result and the test result. There are slight error (average 4%) observed in the wide operating regions at steady conditions. However, relatively large errors (10%) are observed at low engine speed and low torque load conditions, and also observed when the throttle open angle is between 30 and 50 degree.

7.1.2 Air/Fuel Ratio controller (Chapter 5 & 6)

Designed AFR controller has been divided into two parts. First part is the desired AFR setting controller which has to be adaptable according to a vehicle's engine working conditions. The second part is ideal AFR controller which is used to control the fuel injection based on ideal AFR setting. This control scheme's advantage are (1) desired AFR setting controller focuses on the best desire AFR analysis; (2) ideal AFR controller can focus on improving the transient control performance. For PID and Fuzzy PID AFR control, the engine is first assumed to operate at stabilization condition and the reference ideal AFR is set based on fuel output. The variation is corrected using PID and Fuzzy PID controller. Neural network based controller directly control the AFR according to the desired AFR.

7.1.3 PID Control and Fuzzy PID Control (Chapter 5)

At the beginning of this research, the PID controller is tuned and optimized using SIMULINK's build in PID tuning tool block. The experimental analysis shows that the PID Tuning Tool is not suitable for nonlinear systems due to delay factors and the linearizing plant process also presents many problems. Through the analysis of the MATLAB and SIMULINK toolbox and engine simulation module, it is found that the design optimization toolbox can be used to realize PID tuning. According to the 4G64 engine control objectives, the control settling time is set as 1.8 seconds. After

optimization, the control error settling time (in the setting percentage of 1%) has been reduced from 3.3 seconds to 1.8 seconds. When the set target settling time is set as a constant value (1.8 seconds), the target control overshoot has been reduced. The final optimization reduces the maximum transient control error from 0.413 to 0.339.

Further optimization is achieved by using fuzzy control theory. The fuzzy controller applies a single factor to parameterize the three PID parameters, and when a real time parameter is drifting away the PID controller is used as the basic control for the compensation formula, as such, the output of the process can be automatically adjusted to the given value. Fuzzy control using seven fuzzy values，however, in order to maintain control smoothness the Z-shaped membership function is used at the beginning whereas the S-shaped membership function is then applied. Fuzzy Rule Table is designed base on typical second-order system error curve and PID AFR control error. Fuzzy PID Control response settled within 0.01 ranges at 1.4 seconds and the maximum control error has been reduced to 0.213. The constant torque test and constant speed test have proved that the Fuzzy PID control can improve over 20% control performance.

7.1.4 Neural Network Based Control (Chapter 6)

The neural network predictive controller is tuned offline. The test performance was evaluated using mean square error as the only performance index. The inputs to the NN controller have been summarized into 10 groups, and three of them can achieve the required performance. In order to have a better training identification performance, an innovative group with throttle angle as additional input to the controller is tested. Controller input variable are: current desired lambda, current feedback lambda, feedback lambda at previous step, current engine speed, engine speed at previous step, current air-port flow rate, air-port flow rate at previous step, current throttle angle, throttle angle at previous step. After a series of testings, the final neural network structure has 1 hidden layer with 9 neurons.

Neural network controller training have ensured that both the input and output data include all possible working conditions. The sampling time is 200000 seconds and the sampling frequency is 100 times per second, both throttle angles and torque load are randomly changed every 10 seconds. The optimization strategy tests demonstrate better

control for performance change with the minimum control error. Maximum transit control error is reduced significantly (0.138) compared to both the PID control (0. 339) and the fuzzy PID (0.213). The constant torque test and constant speed test have proved NN controlled AFR reduced the control error by 50% and 30% compared with the PID control and fuzzy PID control.

Three driving cycle standards have been used in simulation test: European driving cycles- NEDC, US driving cycles- FTP 75 and Japanese driving cycles-10-15 Mode.

In order to estimate the pollution improvement with optimally controlled AFR, the catalytic converter model is used to calculate the NO_x, HC and CO catalytic efficiency. Comprehensive simulation results show that the NN controlled NO_x, HC and CO catalytic efficiency have been improved by 8%, 5%, and 7.5% compared with the PID control, and 5%, 3%, and 4% compared with the fuzzy PID control.

The results show that PID controller and optimized PID controller can realize the engine AFR control. However, both PID control and fuzzy PID control are based on the error analysis without an in-depth understanding of the system internal operation. Such type of numerical based controller design can result in unpredictable instability no matter how good the controller is. The neural network based controller can deal with a wide range of system operating conditions and therefore its stability is inherently better. The comprehensive tests demonstrated that the neural network based off-line tuning predictive control can effectively control the engine AFR so that instability is avoided. The proposed control methods are significantly better in term of AFR control accuracy than PID and fuzzy PID control methods. The tests also revealed that the improved AFR control performance can effectively restrict engine harmful emissions into atmosphere, these reduce emissions are important to satisfy more stringent emission standards.

7.2 Main Contributions of the Thesis

The research presented in this thesis has contributed to the new knowledge and understanding for the engine control problems in the following ways.

Contribution to Engine Simulation

This research has developed an engine simulation package which can simulate a number of engine operating conditions for different driving cycle tests. Use different types of models to achieve best performance. Nonlinear equations from physical principle are firstly used. When physical equations are not available, mean value models are used. Some model blocks are identified from experiment data. The simulation results produced by the package are in agreement with real experiment results. The package has a module structure so that different type of engine can be simulated. The catalytic converter model is included to present controlled AFR ratio. The test input module designed covers a wide range of operation conditions. The package can be used for many engine test scenario, however it is best suited for developing and evaluating different control strategies.

Contribution to PID and Fuzzy PID Control

This research developed a new engine AFR control system debugging method which uses the output error as system response curve. The new AFR controller structure proposed in this research can identify the engine system for different AFR values. This research provided ways of improving PID control performance by automatic adjusting PID parameters through the use of optimization tool available in SIMULINK.

This research developed a new fuzzy PID controller based on the combination of PID and fuzzy control principles. The fuzzy control rule table developed is more suited for port injection engine. The simulation results showed that the AFR control performance (in terms of settling time and target reference flowing error) for the design fuzzy PID control is better than both PID and fuzzy control alone.

Contribution to Neural Network Based AFR Control

This research proposed a new neural network predictive AFR control method which is

based on off line tuning procedure. Firstly, the AFR controller considers throttle open angle change. A wide range of testing using different throttle open angle and engine load settings have been used for tuning neural networks. A new tuning adjustment strategy has successfully reduced control error for both up peak and down peak. The results show that the AFR control performance is significantly better than PID, fuzzy and fuzzy PID control methods. Since the controlled AFR is close to the idea AFR, the catalytic efficiency is improved and the NO_x, *HC* and *CO* mass levels are reduced.

7.3 Recommendation for Future Work

The engine simulation package developed has capability of simulating the engine dynamic behavior for a wide range of operations. The package has been successfully used in developing a number of different AFR controllers in which the NN based controller provides the best control performance. However, there are a number of aspects of this research that can be extended upon.

7.3.1 Improvement on Engine Simulation

In order to make the package more useful in engine control system research and development, the simulation package compatibility for different type of engines and controllers should be improved. The package can be improved in the following ways.

1. The current simulation is based on the ideal temperature state. The introduction of the temperature variables into each model can be considered. For example, the manifold temperature dynamics model as studied by (Wang & Yu, 2007) can be considered. The fuel film model can also be added with temperature factor in mean value model equation.
2. Turbo supercharger and mechanical supercharger dynamics can be attached to the intake manifold model in simulation.
3. The laboratory experiment shows that the exhaust gas recirculation has an influence on torque production and this influence should be integrated into torque production model. Moreover, the re-circulated exhaust gas mass can be attached to the intake manifold model.
4. To use the package to develop the ignition timing controller, the engine knocking

model should be developed and incorporated.

5. Find the way of determining the catalytic converter model outputs (NO_x, HC and CO mass quantity) in order to provide more convincing testing evidence.
6. Modify the fuel system model for engines using alcohol-petrol mixing and other fuels.

7.3.2 Further Research on AFR Control Methods

Further improvement of neural control training strategy or developing hybrid control method to narrowing the control settling time are still desirable. An in-depth study of intake charge/discharge effect and the development of compensation measures in training process could improve the performance further. The model reference and model predictive control methods can be exploited with efficient optimization procedures.

References

Abdi, J., Khalili, A. F., Inanlosaremi, K., Askari, A. (2011) 'Air fuel ratio control in spark injection engines based on neural network and model predictive controller', *Australian Control Conference (AUCC)*, Melbourne, pp.142-147.

Agrawal, A. K., Singh, S. K., Sinha, S., Shukla, M. K. (2004) 'Effect of EGR on the exhaust gas temperature and exhaust opacity in compression ignition engines', *Sadhana,* **29**(3), pp. 275-284.

Ahmed, Q., Bhatti, A. I. (2010) 'Estimating SI engine efficiencies and parameters in second order sliding modes', *IEEE Transactions on Industrial Electronics*, **57**(12), pp.1–9.

Akbiyik, B., Eksin I., Guzelkaya M., Yesil, E. (2005) 'Evaluation of the performance of various fuzzy PID controller structures on benchmark systems', *4rd International Conference on Electrical and Electronics Engineering*, Bursa, Turkey, pp.388-393.

Aken, M. V., Willems, F., Jong, D. D. (2007) 'Appliance of high EGR rates with a short and long route EGR system on a heavy duty diesel engine', *SAE Paper* 2007-01-0906.

Alippi, C., Russis, C.D., Piuri, V. (1998) 'A fine control of the air-to-fuel ratio with recurrent neural networks', *IEEE Proceeding Instrumentation and Measurement Technology Conference*, St. Paul, **2**, pp.924-929.

Alippi, C., Russis, C.D., Piuri, V. (2003) 'A neural-network based control solution to air-fuel ratio control for automotive fuel-injection systems', *IEEE Transactions Systems, Man, and Cybernetics, Part C: Applications and Reviews*, **33**(2), pp. 259-268.

Aquino, C. (1981) 'Transient A/F control characteristics of a 5 liter central fuel injection engine', *SAE Paper* 810494.

Arsie, I., Pianese, C., Rizzo, G., Cio, V. (2003) 'An adaptive estimator of fuel film dynamics in the intake port of a spark ignition engine', *Control Engineering Practice*,

11(3), pp.303-309.

Ault, B. A., Jones, V. K., Powell, J. D., Franklin, G. F. (1994) 'Adaptive air-fuel ratio control of a spark-ignition engine', *SAE Paper* 940373.

AVL Product Description Cruise, (2009), AVL – Advanced Simulation Technologies GmbH,

Balluchi, A., Benvenuti, L., Benedetto, M. D., Cardellino, S., Rossi, C., Sangiovanni-Vincentelli, A. L. (1999) 'Hybrid control of the air-fuel ratio in force transients for multi-point injection engines', *Proceedings of the 38th IEEE Conference on Decision and Control*, Phoenix, **1**(1), pp.316 – 321.

Barry. (1998) Air-fuel ratio and the SRF air-fuel curve. Available at: http://www.mummbrothers.com/SRF_Stuff/Secrets/Driveline/Air_Fuel.htm, [Accessed 9th September 2013].

Baruah, P. C. (1990) 'A Simulation Model for Transient Operation of Spark-Ignition Engines', *SAE Paper* 900682.

Bayraktar, H., Durgun, O. (2003) 'Mathematical modelling of spark-ignition engine cycles', *Energy Sources*, **25**(5), pp.439-455.

Benninger, N. F., Plapp, G. (1991) 'Requirements and performance of engine management systems under transient conditions', *SAE paper* 910083.

Blanchett, T. P., Kember, G. C., Dubay, R. (2000) 'PID gain scheduling using fuzzy logic', *ISA Transactions*, **39**(3), pp.317-325.

Brunt M., Pond C., Biundo J. (1998) 'Gasoline engine knock analysis using cylinder pressure data', *SAE Paper* 980896.

Broomhead, D. S., Lowe, D. (1988), 'Multivariate functional interpolation and adaptive networks', *Complex Systems*, **2**, pp.321-355.

Cairano, S. D., Yanakiev, D., Bemporad, A., Kolmanovsky, I. V., Hrovat, D. (2011) 'Model predictive idle speed control: design, analysis, and experimental evaluation', *IEEE Transactions on Control Systems Technology*, **20**(1), pp.84-97.

Carpenter, M. H., Ramos, J. I. (1985) 'Mathematical modelling of spark-ignition engines', *Applied Mathematical Modelling*, **9**(1), pp.40-52.

Ceviz, M. A., Akin, M. (2010) 'Design of a new SI engine intake manifold with variable length plenum', *Energy Conversion and Management*, **51**(11), pp.2239–2244.

Ceviz, M. A. (2007) 'Intake plenum volume and its influence on the engine performance, cyclic variability and emissions', *Energy Conversion and Management*, **48**(3), pp.961–966.

Chan, K. Y., Ordys, A., Volkov, K., Duran, O. (2013) 'Comparison of engine simulation software for development of control system', *Modelling and Simulation in Engineering Volume 2013*.

Chandra, R., Jha, A., Laxmi, A. V. (2013) 'Performance of diesel engine using exhaust gas recirculation', *International Journal of Advanced Trends in Computer Science and Engineering*, **2(**1), pp.433 – 436.

Chang, R. T. (1988), *A modelling study of the influence of spark-ignition engine design parameters on engine thermal efficiency and performance*. Ph.D. thesis, MIT.

Chang, C. F., Fekete, N. P., Amstutz, A., Powell, J. D. (1995) 'Air/fuel ratio control in spark-ignition engines using estimation theory', *IEEE Transactions on Control Systems Technology,* **3**(1), pp.22-31.

Chang, C. F., Fekete, N. P., Powell, J. D. (1993) 'Engine air-fuel ratio control using an event-based observer', *SAE Paper* 930766.

Chen, G., Ying, H. (1993) 'Stability analysis of nonlinear fuzzy PI control systems', *Third International Conference on Industrial Fuzzy Control and Intelligent Systems*, Houston, pp. 128–133

Choi, S. B., Won, M., Hendrick, J. K. (1994) 'Fuel-injection control of SI engines', *Proceedings of the 33rd IEEE Conference Decision and Control*, Lake Buena Vista, **2**, pp.1609-1614.

Choi, S. B., Hendrick, J. K. (1998) 'An observer-based controller design method for improving air/fuel characteristics of spark ignition engines', *IEEE Transactions on Control Systems Technology*, **6**(3), pp.325–334.

DieselNet. (2013), Emission Standards - Summary of worldwide engine emission standards. Available at: http://www.dieselnet.com/standards/, [Accessed 9th September 2013].

Cook, J. A., Powell, B. K. (1988) 'Modelling of an internal combustion engine for control analysis', *IEEE Control Systems Magazine*, **8**(4), pp.20-26.

Coleman, T., Branch, M. A., Grace, A. (1999) Optimization toolbox for use with MATLAB. The MathWorks, Inc.

Czarnigowski, J. (2010) 'A neural network model-based observer for idle speed control of ignition in SI engine', *Engineering Applications of Artificial Intelligence,* **23**(1), pp.1-7.

Dobner, D.J. (1980) 'A review of ic engine models for development of dynamic engine control', *SAE Paper* 800054.

Ebrahimi, B., Tafreshi, R., Masudi, H., Franchek, M., Mohammadpour, J., Grigoriadis, K., Tafreshi, R. (2012) 'A parameter-varying filtered PID strategy for air-fuel ratio control of spark ignition engines', *Control Engineering Practice*, **20**(8), pp.805-815.

Falk, C. D., Mooney, J. J. (1998) 'Three-way Conversion Catalysts: Effect of Closed-Loop Feed-Back Control and Other Parameters on Catalyst Efficiency', *SAE Paper* 800462.

Ferguson, C. R., Kirkpatrick, A. T. (2001) *International combustion engines: applied thermosciences*. 2nd edn. New York: John Wiley & Sons.

Filippi, R. D., Scattolini, R. (2005) ‘Idle speed control of a F1 racing engine’, *Control Engineering Practice,* **14**(3), pp. 251–257.

Franceschi, E. M., Mucke, R. K., Jones, C. P., Makki, I. (2007) ’An adaptive delay-compensated PID air fuel ratio controller’, *SAE Paper* 2007-01-1342.

Franchek, M. A., Mohrfeld, J., Osburn, A. (2006) ’Transient fueling controller identification for spark ignition engines’, *ASME Journal of Dynamic Systems, Measurement, and Control*, **128**(3), pp.499-509.

Franklin, G. F., Powell, J. D., Naeini, A. E. (2009) *Feedback control of dynamic systems*. 6th edn. United States: Prentice Hall

Freij, K. B., Ericsson, E. (2005) ‘Influence of street characteristics, driver category and car performance on urban driving patterns’, *Transportation Research Part D: Transport and Environment*, **10**(3), pp.213-229.

Foley, J., Fergusson, M. (2003) *Putting the brakes on climate change: A policy report on road transport and climate change*. London: Institute for Public Policy Research

Ganesan, V. (2008) *International combustion engines*. 3rd edn. Singapore: Tata McGraw-Hill.

Gangopadhyay, A., Meckl, P. (1999) ‘Multivariable PI tuning and application to engine idle speed control’, *Proceedings of American Control Conference*, San Diego, **4**, pp. 2678–2682.

Gao, S., Lang, H., Tan, D. R., Shao, J. J. (2011) ‘Study on air-fuel ratio control of coal-bed gas engine based on fuzzy PID control’, *Remote Sensing, Environment and Transportation Engineering*, pp.1624-1627.

Ge, Z.X., Sun, Z.Q. (2007), *Neural network apply with Matlab R2007*, Beijing: Publishing house of electronics industry.

Ghaffari, A. A., Shamekhi, H., Saki, A., Kamrani, E. (2008) ‘Adaptive fuzzy control for

air-fuel ratio of automobile spark ignition engine', *World Academy of Science: Engineering and Technology*, **24**, pp.284-292.

Gillespie, T.D. (1992) *Fundamentals of vehicle dynamics*, Warrendale: SAE International.

Gnanam, G., Habibi, S. R., Burton, R. T., Sulatisky, M. T. (2006) 'Neural network control of air-to-fuel ratio in a bi-fuel engine', *IEEE Transactions on Systems, Man, and Cybernetics, Part C: Applications and Reviews*, **36** (5), pp.656–667.

Grizzle, J. W., Buckland, J., Sun, J. (2001) 'Idle speed control of a direct injection spark ignition stratified charge engine', *International Journal of Robust and Nonlinear Control*, **11**(11), pp.1043-1071.

GT-SUITE. (2009) *Overview - Engine and vehicle simulation platform for concept and system detailed design analysis*, Gamma Technologies, Inc.

Guzzella, L. (1995) 'Models and model-based control of IC-engines a nonlinear approach', *SAE Paper* 950844.

Guzzella, L., Simons, M., Geering, H. P. (1997) 'Feedback linearizing air/fuel-ratio controller', *Control Engineering Practice*, **5**(8), pp.1101-1105.

Guzzella, L., Onder, C. H. (2010) Introduction to modelling and control of internal combustion engine systems. 2nd edn. Berlin: Springer-Verlag.

Ham, Y., Chung, K., Lee, J., Chang, K. (1996) 'Spark ignition engine knock control and threshold value determination', *SAE paper* 960496.

Harrington, D., Bolt, J. (1970) 'Analysis and digital simulation of carburetor metering," *SAE Paper* 700082.

Harrison, M. F. Soto, I. D., Rubio-Unzueta P. L. (2004) 'A linear acoustic model for multi-cylinder IC engine intake manifolds including the effects of the intake throttle', *Journal of Sound and Vibration*, **278**(4–5), pp. 975-1011.

Hashimoto, S., Okuda, H., Okada, Y., Adachi, S., Niwa, S., Kajitani, M. (2006) 'An engine control systems design for low emission vehicles by generalized predictive control based on identified model', *Computer Aided Control System Design, 2006 IEEE International Conference on Control Applications, 2006 IEEE International Symposium on Intelligent Control*, Munich, Germany, pp. 2411 – 2416.

Hendricks, E., Sorenson, S. (1990) 'Mean value modelling of spark ignition engines', *SAE Paper* 900616.

Hendricks, E., Sorenson, S. (1991) 'SI engine controls and mean value engine modelling', *SAE Paper* 910258.

Hendricks, E., Vesterholm, T., Sorenson, S. (1992) 'Nonlinear, closed loop, SI engine control observers', *SAE Paper* 920237.

Hendricks, E., Jensen, M., Kaidantzis, P., Rasmussen, P., Vesterholm, T. (1993) 'Transient A/F ratio errors in conventional SI engine controllers', *SAE Paper* 930856.

Hendricks, E., Chevalier, A., Jensen, M., Sorenson, S., Trumpy D., Asik, J. (1996) 'Modelling of the intake manifold filling dynamics', *SAE Paper* 960037.

Heywood, J. B. (1998) *International combustion engine fundamentals*. New York: McGraw-Hill

Hopfield, J. J. (1982) 'Neural networks and physical systems with emergent collective computational abilities', *Proceedings of the National Academy of Sciences of the United States of America*, **79**(8), pp.2554-2558.

Hopfield, J. J. (1984) 'Neurons with graded response have collective computational properties like those of two-state neurons', *Proceedings of the National Academy of Sciences of the United States of America,* **81**(10), pp.3088-3092.

Hou, Z. H., Wu, Y. H, (2008) 'Predictive control for air fuel ratio based on adaptive expand particle swarm optimization', *Intelligent Control and Automation*, pp.705-709.

Hsieh, F. C., Chen, B. C., Wu, Y. Y. (2007) 'Adaptive idle speed control for spark-ignition engines', *SAE Paper* 2007-01-1197.

Isermann, R., Munchhof, M. (2011) *Identification of dynamic systems: an introduction with applications*, Heidelberg: Springer.

Jansri, A., Sooraksa, P. (2012) 'Enhanced model and fuzzy strategy of air to fuel ratio control for spark ignition engines', *Computers and Mathematics with Applications*, **64**(5), pp.922-933.

Johnson, T. V. (2000) 'Mobile emissions control technologies in review, international conference on 21st century emissions technology', *IMechE Conference Transactions 2002-2*.

Johnson, M. A., Crowe, J., Moradi, M. H. (2006) *PID control: new identification and design methods*. London: Springer.

Jones, V. K., Ault, B. A., Franklin, G. F., Powell, J. D. (1995) 'Identication and air-fuel ratio control of a spark ignition engine', *IEEE Transactions on Control Systems Technology*, **3**(1), pp.14-21.

Kiencke, U., Nielsen, L. (2005) *Automotive control systems for engine, driveline, and vehicle*. 2nd edn. Berlin: Springer-Verlag.

Kim, D., Park, J. (2007) 'Application of adaptive control to the fluctuation of engine speed at idle', *Information Sciences*, **177**(16), pp. 3341–3355.

Kjergaard, L., Nielsen S., Vesterholm T., Hendricks E. (1994) 'Advanced Nonlinear Engine Idle Speed Control Systems', *SAE Paper* 940974.

Kokotovic, P. K., Rhode, D. (1986) 'Sensitivity guided design of an idle speed controller', Ford Motor Company, PK Research, Urbana, U.S.A., Technical Report 1.

Kovalenko, O., Liu, D. R., Javaherian, H. (2004) 'Neural network modelling and

adaptive critic control of automotive fuel-injection systems', *Proceedings of the IEEE International Symposium on Intelligent Control*, pp.368-373.

Kwiatkowski, A., Werner, H., Blath, J. P., Ali, A., Schulalbers, M. (2009) 'Linear parameter varying PID controller design for charge control of a spark-ignited engine', *Control Engineering Practice*, **17**(11), pp.1307–1317.

Li, W. Q., Ma, B. Y. (2010) 'Self-adaptive hybrid electro-magnetic levitation and active balancing system', Publisher: Cornell University. Available at: http://people.ece.cornell.edu/land/courses/ece4760/FinalProjects/s2010/wl336_bm337/ wl336_bm337/ [Accessed 9 September 2013].

Li, X., Yurkovich, S. (2001) 'Sliding mode control of delayed systems with application to engine idle speed control', *IEEE Transactions on Control Systems Technology*, **9**(6), pp.802–810.

Liu, D.R., Javaherian, H., Kovalenko, O., Huang, T. (2008) 'Adaptive critic learning techniques for engine torque and air–fuel ratio control', *IEEE Transactions on Systems, Man, and Cybernetics, Part B: Cybernetics*, **38**(4), pp.988-993.

Lotus Engineering Software user menu, (2011), Lotus Group plc.

Mamdani, E. H. (1974) 'Application of fuzzy algorithms for control of simple dynamic plant', *Institution of Electrical Engineers*, **121**(12), pp1585-1588.

McCartney, K. S. (2003) 'Catalytic converter theory, operation and testing', Bear River Converters. Available at: http://www.bearriverconverters.com/data/CatOpp.pdf. [Accessed 9th September 2013]

Mercorelli, P. (2009) 'Robust feedback linearization using an adaptive PD regulator for a sensorless control of a throttle valve', *Mechatronics*, **19**(8), pp.1334-1345.

Meyer, J. (2007), *Engine modelling of an internal combustion engine*, thesis, The Ohio State University

Meyer, J., Yurkovich, S., Midlam-Mohler, S. (2012) 'Air-to-fuel ratio switching

frequency control for gasoline engines', *IEEE Transactions on Control Systems Technology*, **21**(3), pp.636-648.

Niculescu, S. I., Annaswamy, A. M. (2003) 'An adaptive smith-controller for time-delay systems with relative degree n^*≤2', *Systems and Control Letters*, **49**(5), pp.347-358.

Milliken, W.F., Milliken, D.L. (1995) *Race car vehicle dynamics*, Warrendale: SAE International.

Ming, S., Jun, C. L., Hao, L. (2004) 'Study of fuzzy PID control', *Control Engineering China*, pp.51-55.

Mitsubishi. (2001), *Engine 4G6 workshop manual*, Mitsubishi motors corporation.

Moler, C. (2004), *The origins of MATLAB*. MathWorks.

Moskwa, J.J. (1988) *Automotive engine modelling for real time control*, Ph.D. thesis, M.I.T.

Muller, M., Hendricks, E., Sorenson, S. (1998) 'Mean value modelling of turbocharged spark ignition engines', *SAE Paper* 980784.

Muske, K. R., Jones, C. P. J. (2006) 'A model-based SI engine air fuel ratio controller', *American Control Conference*, Minneapolis.

National Instruments, (2012) 'Subsystems required to control low temperature combustion engines. Available at: http://www.ni.com/white-paper/13516/en/ [Accessed 9 September 2013].

OICA. (2011) *World vehicles in use - All vehicles*. International Organization of Motor Vehicle Manufacturers.

Ohata, A., Ohashi, M., Nasu, M., Inoue, T. (1995) 'Crank-angle domain modelling and control for idle speed', *SAE Paper* 950075.

Onder, C. H., Geering, H. P. (1993) 'Model-based multivariable speed and air-to-fuel

ratio control of an SI engine', *SAE Paper* 930859.

Paris, B., Eynard, J., Grieu, S., Polit, M. (2011) 'Hybrid PID-fuzzy control scheme for managing energy resources in buildings', *Applied Soft Computing*, **11**(8), pp.5068-5080.

Pace, S., Zho, G. G. (2009) 'Air-to-fuel and dual–fuel ratio control of an internal combustion engine', *SAE International Journal of Engines*, **2**(2), pp.245–253.

Powell, J. D., Fekete, N. P., Chang, C. F. (1998) 'Observer-based air-fuel ratio control', *IEEE Transactions on Control Systems Magazine*, **18**(5), pp.72-83.

Piccinini, G. (2004) 'The First computational theory of mind and brain: a close look at mcculloch and pitts's "logical calculus of ideas immanent in nervous activity"', *Synthese*, **141**(2), pp.175-215.

Pieper, J. K., Mehrotra, R. (1999) 'Air/fuel ratio control using sliding mode methods', *American Control Conference*, San Diego, **2**, pp.1027-1031.

Poloni, T., Rohal, I. B., Johansen, T. A. (2007) 'Multiple ARX model-based air-fuel ratio predictive control for SI engines', *Advanced Fuzzy and Neural Control*, **3**(1), pp.72-78

Ricardo software. 2009 *WAVE user's manual. Version 8.0*. Ricardo Inc,.

Rizzoni, G. (2002) 'Estimate of indicated torque from crankshaft speed fluctuations: a model for the dynamics of the IC engine', *IEEE Vehicular Technology*, **38**(3), pp.168-179.

Rumelhart, D. E., Hinton, G. E., Williams, R. J. (1986) 'Learning representations by back-propagating errors', *Nature*, **323**, pp.533 – 536.

Rumelhart, D. E., McClelland, J. L., PDP Research Group. (1986) *Parallel distributed processing: explorations in the microstructure of cognition. Volume 1: foundations*. Cambridge: MIT Press.

Rupp, D., Onder, C., Guzzella, L. (2008) 'Iterative adaptive air/fuel ratio control', *Advances in Automotive Control*, **5**(1), pp.593-600.

Rupp, D. (2009), *Model-based adaptive air/fuel ratio control for an automotive gasoline engine*. Ph.D. thesis, ETH Zurich.

Saraswati, S., Chand, S. (2010) 'An optimization algorithm for neural predictive control of air-fuel ratio in SI engines', *Proceedings of the 2010 International Conference on Modelling, Identification and Control*, Okayama, pp.527-532.

Scattolini, R., Siviero, C., Mazzucco, M., Ricci, S., Poggio, L., Rossi, C. (1997) 'Modelling and identification of an electromechanical internal combustion engine throttle body', *Control Engineering Practice*, **5**(9), pp. 1253-1259.

Sivanandam, S.N., Sumathi, S., Deepa, S. N. (2010) Introduction to fuzzy logic using MATLAB. Heidelberg: Springer.

Souder, J. S., Hedrick, J. K. (2004), 'Adaptive sliding mode control of air-fuel ratio in internal combustion engines', *International Journal of Robust and Nonlinear Control*, **14**(6), pp.525-541.

Sousanis, J. (2011) *World vehicle population tops 1 billion units*. WardsAuto.

Sperling, D., Gordon, D., Schwarzenegger, A. (2009) *Two billion cars: driving toward sustainability*. USA: Oxford University Press.

Stefanopoulou, A. G., Grizzle, J. W., Freudenberg, J. S. (1994), 'Engine air-fuel ratio and torque control using secondary throttles', *IEEE Conference on Decision and Control*, Lake Buena Vista, **3**, pp.2748-2753.

Stefanopoulou, A. (1996) *Modelling and control of advanced technology engines*, Ph.D. thesis, University of Michigan

Stotsky, A. A. (2008), 'Statistical algorithms for engine knock detection', *Institution of Mechanical Engineers, Part D: Journal of Automobile Engineering*, **222**(3), pp.429-

439.
Suh, H. K., Park, S. W., Lee, C. S. (2009) 'Effect of grouped-hole nozzle geometry on the improvement of biodiesel fuel atomization characteristics in a compression ignition engine', *Proceedings of the Institution of Mechanical Engineers, Part D: Journal of Automobile Engineering*, **223**(12), pp.1587-1600.

Takahashi, S., Sekozawa, T. (1995) 'Air-fuel ratio control in gasoline engines based on state estimation and prediction using dynamic models', *IEEE Transactions on Industrial Electronics, Control, and Instrumentation*, **1**, pp.217-222.

Thomas, S., Sharma, R. (2007) 'Model based control of engines', *SAE Paper* 2007-26-025.

Togun, N., Baysec, S., Kara, T. (2012) 'Nonlinear modelling and identification of a spark ignition engine torque', *Mechanical Systems and Signal Processing,* **26**, pp.294-304.

Tomforde, M., Drewelow, W., Schultalbers, M. (2011), 'Air-fuel ratio control with respect to oxygen storage dynamics', I*EEE Transactions on Methods and Models in Automation and Robotics*, pp242-247.

Trefethen, A. E., Menon, V. S., Chang, C. C., Czajkowski, G., Myers, C., Trefethen, L. N. (1996) MultiMATLAB: MATLAB on multiple processors. Computer Science Technical Reports. Publisher: Cornell University. Available at: http://ecommons.library.cornell.edu/handle/1813/7242 [Accessed 9 September 2013].

Turin, R. C., Geering, H. (1995) 'Model-reference adaptive A/F ratio control in an SI engine based on Kalman-Filtering techniques', *American Control Conference*, Seattle, **6**, pp. 4082-4090.

Wagner, J. R., Dawson D. M., Liu, Z. Y. (2003) 'Nonlinear air-to-fuel ratio and engine speed control for hybrid vehicles, *IEEE Transactions on Vehicular Technology*, **52**(1), pp.184-195.

Wang, S. W., Yu, D. L. (2007) 'A new development of internal combustion engine air–

fuel ratio control with second-order sliding mode', *ASME Journal of Dynamic Systems, Measurement, and Control*, **129**(6), pp.757–766.

Wang, S. W., Yu, D. L., Gomm, J. B., Page, G. F., Douglas, S. S. (2006) 'Adaptive neural network model based predictive control for air–fuel ratio of SI engines', *Engineering Applications of Artificial Intelligence*, **19**(2), pp.189–200.

Wang, S. W., Yu, D. L. (2008) 'Adaptive RBF network for parameter estimation and stable air–fuel ratio control', *Neural Networks*, **21**(1), pp.102–112.

Wang, Y., Stefanopoulou, A., Levin, M. (1999) 'Idle speed control: An old problem in a new engine design', *American Control Conference*, San Diego, **2**, pp. 1217–1221.

Wang, Z. L., Wang, S. K., Chen, G.S., Wang, Q. (2008) *MATLAB/SIMULINK and control system simulation*. 2nd edn. Beijing: Publishing House of Electronics Industry.

Weeks, R., Moskwa, J. J. (1995) 'Automotive engine modelling for real-time control using matlab/SIMULINK', *SAE Paper* 950417.

Williams, S.J., Hrovat, D., Davey, C., Maclay, D., Crevel, J.W., Chen, L.F. (1989) 'Idle speed control design using an H-Infinity approach', *American Control Conference*, Pittsburgh, pp.1950–1956.

Won, M., Choi, S. B., Hedrick, J. K. (1998) 'Air-to-fuel ratio control of spark ignition engines using gaussian network sliding control', *IEEE Transactions on Control Systems Technology*, **6**(5), pp.678-687.

Wong, H. C., Wong, P. K., Vong, C. M. (2012) 'Model predictive engine air-ratio control using online sequential relevance vector machine', *Journal of Control Science and Engineering - Special issue on Advanced Control in Micro-/Nanosystems.*

Wu, Y. Y., Chen, B. C., Hsieh, F. C., Ke, C. T. (2009) 'A study of the characteristics of fuel-film dynamics for four-stroke small-scale spark-ignition engines', *SAE paper* 2009-01-0591.

Xue, D., Chen, Y. Q., Atherton, D. P. (2007) *Linear feedback control analysis and*

design with MATLAB. Philadelphia: Society for Industrial and Applied Mathematics

Yesil, E., Guzelkaya M., Eksin I. (2003) 'Fuzzy PID controllers: An overview', *The Third Triennial ETAI International Conference on Applied Automatic Systems,* Skopje, Macedonia, pp.105-112.

Yildiz, Y., Annaswamy, A., Kolmanovsky, I.V., Yanakiev, D. (2010) 'Adaptive posicast controller for time-delay systems with relative degree n^*≤2'', *Automatica*, **26**(2), pp279-289.

Yildiz, Y., Annaswamy, A. M., Yanakiev, D., Kolmanovski, I. (2010) 'Spark ignition engine fuel-to-air ratio control: An adaptive control approach', *Control Engineering Practice*, **18**(12), pp.1369–1378.

Yildiz, Y., Annaswamy, A. M., Yanakiev, D., Kolmanovsky, I. (2011) 'Spark Ignition Engine Idle Speed Control: An Adaptive Control Approach', *IEEE Control Systems Technology*, **19**(5), pp.990-1002.

Yoon, P., Park, S., Sunwoo, M., Ohm, I., Yoon, K. J. (2000) 'Closed-loop control of spark advanced and air–fuel ratio in SI engines using cylinder pressure', *SAE Paper* 2000-01-0933.

Yoon, P., Park, S., Sunwoo, M. (2000) 'A nonlinear dynamic model of SI engines for designing controller', *SAE Paper* 2000-05-0172

Yurkovich, S., Simpson, M. (1997) 'Crank-angle domain modelling and control for idle speed', *SAE Paper* 970027.

Zadeh, L. A. (1965) 'Fuzzy sets', *Information and control,* **8**(3), pp.338-353.

Zadeh, L. A. (1973) 'Outline of a New approach to the analysis of complex systems and decision processes', *IEEE Transactions on Systems, Man and Cybernetics*, **3**(1), pp.28-44.

Zhai, Y. J, Yu, D. W., Guo, H. Y., Yu, D. L. (2010) 'Robust air/fuel ratio control with adaptive DRNN model and AD tuning', *Engineering Applications of Artificial*

Intelligence, **23**(2), pp.283-289.

Zhao, F. Lai, M.C., Harrington, D.L. (1999) 'Automotive spark-ignited direct-injection gasoline engines', *Progress in Energy and Combustion Science*, **25**(5), pp.437-562.

Zhen, X.D., Wang, Y., Xu, S.Q., Zhu, Y.S., Tao, C.J., Xu, T., Song, M.Z. (2012), 'The engine knock analysis – An overview', *Applied Energy*, **92**, pp. 628-636.

Zheng, M., Reader, G.T., Hawley, J.G. (2004) 'Diesel engine exhaust gas recirculation––a review on advanced and novel concepts', *Energy Conversion and Management*, **45**(6), pp.883–900.

Zielinski, T.J., Allendoerfer, R.D. (1997) 'Least squares fitting of non-linear data in the undergraduate laboratory', *Journal of Chemical Education*, **74**(8), pp.1001-1007.

Appendix A: United States Emission Standards

A.1 Tier 1 emission standards

The Tier 1 emission standards are summarized in Table A.1 and Table A.2. Car and light truck emissions were measured over the Federal Test Procedure (FTP 75) and expressed in g/mile. Separate sets of standards are defined for each vehicle category, with more relaxed limits for heavier vehicles

Table A.1: Tier 1 Emission Standards 50,000 miles/5 years

Category	THC	NMHC	CO	NOx† diesel	NOx gasoline	PM‡
Passenger cars	0.41	0.25	3.4	1.0	0.4	0.08
LLDT, LVW <3,750 lbs	-	0.25	3.4	1.0	0.4	0.08
LLDT, LVW >3,750 lbs	-	0.32	4.4	-	0.7	0.08
HLDT, ALVW <5,750 lbs	0.32	-	4.4	-	0.7	-
HLDT, ALVW > 5,750 lbs	0.39	-	5.0	-	1.1	-

Table A.2: Tier 1 Emission Standards 100,000 miles/10 years1

Category	THC	NMHC	CO	NOx† diesel	NOx gasoline	PM‡
Passenger cars	-	0.31	4.2	1.25	0.6	0.10
LLDT, LVW <3,750 lbs	0.80	0.31	4.2	1.25	0.6	0.10
LLDT, LVW >3,750 lbs	0.80	0.40	5.5	0.97	0.97	0.10
HLDT, ALVW <5,750 lbs	0.80	0.46	6.4	0.98	0.98	0.10
HLDT, ALVW > 5,750 lbs	0.80	0.56	7.3	1.53	1.53	0.12

1 - Useful life 120,000 miles/11 years for all HLDT standards and for THC standards for LDT
† - More relaxed NOx limits for diesels applicable to vehicles through 2003 model year
‡ - PM standards applicable to diesel vehicles only

Abbreviations:
LVW - loaded vehicle weight (curb weight + 300 lbs)
ALVW - adjusted LVW (the numerical average of the curb weight and the GVWR)
LLDT - light light-duty truck (below 6,000 lbs GVWR)
HLDT - heavy light-duty truck (above 6,000 lbs GVWR)

A.2 Tier 2 Emission Standards

The Tier 2 emission standards are structured into 8 permanent and 3 temporary certification levels of different stringency, called "certification bins", an average fleet standard for NOx emissions. Vehicle manufacturers have a choice to certify particular vehicles to any of the available bins. The temporary certification bins (bin 9, 10, and an MDPV bin 11) with more relaxed emission limits are available in the phase-in period and expire after the 2008 model year.

The emission standards for all pollutants (certification bins) when tested on the Federal Test Procedure (FTP) are shown in Table A.3 and Table A.4. Where intermediate useful life exhaust emission standards are applicable, such standards are applicable for five years or 50,000 miles, whichever occurs first. The vehicle "full useful life" period for LDVs and light LDTs has been extended to 120,000 miles or ten years whichever occurs first. For heavy LDTs and MDPVs, it is 11 years or 120,000 miles whichever occurs first. Manufacturers may elect to optionally certify to the Tier 2 exhaust emission standards for 150,000 miles to gain NOx credits or to opt out of intermediate life standards. In such cases, useful life is 15 years or 150,000 miles, whichever occurs first. For interim non-Tier 2 LDV/LLDTs, the useful life is 10 years or 100,000 miles, whichever occurs first.

Table A.3: Emission Standards for Intermediate life

Bin#	(5 years / 50,000 mi) , g/mi				
	NMOG*	CO	NOx†	PM	HCHO
Temporary Bins					
11 MDPVc					
10a,b,d,f	0.125 (0.160)	3.4 (4.4)	0.4	-	0.015 (0.018)
9a,b,e,f	0.075 (0.140)	3.4	0.2	-	0.015
Permanent Bins					
8b	0.100 (0.125)	3.4	0.14	-	0.015
7	0.075	3.4	0.11	-	0.015
6	0.075	3.4	0.08	-	0.015
5	0.075	3.4	0.05	-	0.015
4	-	-	-	-	-
3	-	-	-	-	-
2	-	-	-	-	-
1	-	-	-	-	-

Table A.4: Tier 2 Emission Standards for Full useful life					
Bin#	g/mi				
	NMOG*	CO	NOx†	PM	HCHO
Temporary Bins					
11 MDPVc	0.280	7.3	0.9	0.12	0.032
10a,b,d,f	0.156 (0.230)	4.2 (6.4)	0.6	0.08	0.018 (0.027)
9a,b,e,f	0.090 (0.180)	4.2	0.3	0.06	0.018
Permanent Bins					
8b	0.125 (0.156)	4.2	0.20	0.02	0.018
7	0.090	4.2	0.15	0.02	0.018
6	0.090	4.2	0.10	0.01	0.018
5	0.090	4.2	0.07	0.01	0.018
4	0.070	2.1	0.04	0.01	0.011
3	0.055	2.1	0.03	0.01	0.011
2	0.010	2.1	0.02	0.01	0.004
1	0.000	0.0	0.00	0.00	0.000

* for diesel fueled vehicle, NMOG (non-methane organic gases) means NMHC (non-methane hydrocarbons)
† average manufacturer fleet NOx standard is 0.07 g/mi for Tier 2 vehicles

a - Bin deleted at end of 2006 model year (2008 for HLDTs)
b - The higher temporary NMOG, CO and HCHO values apply only to HLDTs and MDPVs and expire after 2008
c - An additional temporary bin restricted to MDPVs, expires after model year 2008
d - Optional temporary NMOG standard of 0.195 g/mi (50,000) and 0.280 g/mi (full useful life) applies for qualifying LDT4s and MDPVs only
e - Optional temporary NMOG standard of 0.100 g/mi (50,000) and 0.130 g/mi (full useful life) applies for qualifying LDT2s only
f - 50,000 mile standard optional for diesels certified to bins 9 or 10

A.3 Tier 3 Emission Standards

The structure of Tier 3 standards is similar to the Tier 2 standards. Manufacturers must certify their vehicles to one of the seven emission bins shown in Table A.5. Vehicles are tested over the FTP-75 test procedure. The standards are applicable to all vehicles, regardless of the fuel type.

Tier 3 standards are to be phased-in starting from 2017, and reaches 30 mg/mi in 2025 (Table A.6). This final Tier 3 fleet average limit is applicable to all vehicle categories—an important change from the Tier 2 regulation that allow more relaxed fleet average emissions from heavier vehicle categories.

Table A.5: Proposed Tier 3 Certification Bin Standards (150,000 miles)				
Bin	NMOG+NOx	PM	CO	HCHO
	mg/mi			
Bin 160	160	3	4200	4
Bin 125	125	3	2100	4
Bin 70	70	3	1700	4
Bin 50	50	3	1700	4
Bin 30	30	3	1000	4
Bin 20	20	3	1000	4
Bin 0	0	0	0	0

Table A.6: Proposed Tier 3 Phase-In of Fleet Average Standards									
Vehicle Category	2017*	2018	2019	2020	2021	2022	2023	2024	2025
LDV, LDT1	86	79	72	65	58	51	44	37	30
LDT2, LDT3, LDT4, MDPV	101	92	83	74	65	56	47	38	30
* Starting from MY2018 for vehicles with GVWR above 6,000 lb									

A.4 Low Emission Vehicle (LEV) Standards

These California emission standards, which applied through model year 2003, were expressed using the following emission categories:

Tier 1
Transitional Low Emission Vehicles (TLEV)
Low Emission Vehicles (LEV)
Ultra Low Emission Vehicles (ULEV)
Super Ultra Low Emission Vehicles (SULEV)
Zero Emission Vehicles (ZEV)

Car manufacturers were required to produce a percentage of vehicles certified to increasingly more stringent emission categories, according to schedules based on vehicle fleet emission averages for each manufacturer. After 2003, Tier 1 and TLEV standards were eliminated as available emission categories.

The same standards for gaseous pollutants applied to diesel and gasoline fueled vehicles. PM standards applied to diesel vehicles only. Emissions were measured over the FTP-75 test and are expressed in g/mile. The additional SFTP procedures were phased-in in California between 2001 and 2005.

Table A.7: LEV Emission Standards for Light-Duty Vehicles, g/mi										
Category	50,000 miles/5 years					100,000 miles/10 years				
	NMOGa	CO	NOx	PM	HCHO	NMOGa	CO	NOx	PM	HCHO
Passenger cars										
Tier 1	0.25	3.4	0.4	0.08	-	0.31	4.2	0.6	-	-
TLEV	0.125	3.4	0.4	-	0.015	0.156	4.2	0.6	0.08	0.018
LEV	0.075	3.4	0.2	-	0.015	0.090	4.2	0.3	0.08	0.018
ULEV	0.040	1.7	0.2	-	0.008	0.055	2.1	0.3	0.04	0.011

A.5 Low Emission Vehicle II (LEV II) Standards

In November 1998, the California ARB adopted LEV II emission standards which were phased-in from 2004 through 2010. Manufacturers may certify vehicles to LEV II emission standards (categories) until model year 2019. Under the LEV II regulation, the light-duty truck and medium-duty vehicle categories of below 8500 lbs gross weight were reclassified and had to meet passenger car requirements, as shown in Table 3. As a result, most pick-up trucks and sport utility vehicles (old MDV4 and MDV5) were required to meet the passenger car emission standards. The reclassification was phased-in by the year 2007.

Table A.8: LEV II Emission Standards for Passenger Cars and LDVs < 8500 lbs (LDT1 & LDT2), g/mi										
Category	50,000 miles/5 years					120,000 miles/11 years				
	NMOG	CO	NOx	PM	HCHO	NMOG	CO	NOx	PM	HCHO
LEV	0.075	3.4	0.05	-	0.015	0.090	4.2	0.07	0.01	0.018
ULEV	0.040	1.7	0.05	-	0.008	0.055	2.1	0.07	0.01	0.011
SULEV	-	-	-	-	-	0.010	1.0	0.02	0.01	0.004

A.6 Low Emission Vehicle III (LEV III) Standards

The LEV III emission standards, adopted in January 2012, are phased-in over the 2015-2025 model years. Manufacturers can certify vehicles to the LEV III standards before model year 2015. Beginning with model year 2020, all vehicles must be certified to LEV III standards. LEV III emission categories and their FTP-75 standards for light- and (chassis-certified) medium-duty vehicles are listed in Table A.9.

Table A.9: LEV III Emission Standards, Durability 150,000 miles

Vehicle Type	Emission Category	NMOG+NOx	CO	HCHO	PM†
		g/mi	g/mi	mg/mi	g/mi
All PCs LDTs ≤ 8500 lbs GVWa All MDPVs	LEV160	0.160	4.2	4	0.01
	ULEV125	0.125	2.1	4	0.01
	ULEV70	0.070	1.7	4	0.01
	ULEV50	0.050	1.7	4	0.01
	SULEV30	0.030	1.0	4	0.01
	SULEV20	0.020	1.0	4	0.01

† - Applicable only to vehicles not included in the phase-in of the final PM standards (Table 7 & Table 8).
a - Loaded vehicle weight (LVW)
b - Adjusted loaded vehicle weight (ALVW)

Abbreviations:
PC - Passenger car
LDT - light-duty truck
MDPV - medium-duty passenger vehicle
MDV - medium-duty vehicle

Appendix B: Engine Volumetric Efficiency Equation (Hendricks et al., 1996)

The volumetric efficiency of four-stroke engine in first law of thermodynamics applied to an open system doing only boundary work can show that:

$$P_{ic}V_{ic} - P_{io}V_{io} = (\kappa - 1)\begin{bmatrix} -\int_{io}^{ic} PdV & (a) \\ +\int_{io}^{ec} \left(\dot{m}C_pT\right)_{ov} dt & (b) \\ +C_pT_i\int_{is}^{ic} \dot{m}_{in}dt & (c) \\ +\int_{io}^{ic} \dot{Q}dt & (d) \end{bmatrix} \quad (B.1)$$

The mass of exhaust that flows into the cylinder from the exhaust system during overlap can be obtained from equation (B.1b).

$$m_{ov} = \int_{io}^{ec} \left(\dot{m}C_pT\right)_{ov} dt \quad (B.2)$$

The mass inducted can be obtained from equation (B.1c).

$$\dot{m}_i = \int_{is}^{ic} \dot{m}_{in}dt \quad (B.3)$$

The mass intake air can be obtained from equation (B.1d).

$$Q = \int_{io}^{ic} \dot{Q}dt \quad (B.4)$$

Eq B.1 then becomes

$$P_{ic}V_{ic} - P_{io}V_{io} = (\kappa - 1)\begin{bmatrix} -\int_{io}^{ic} PdV & (a) \\ +C_p T_{ov} m_{ov} & (b) \\ +C_p T_i m_i & (c) \\ +Q & (d) \end{bmatrix} \qquad (B.5)$$

The equation of volumetric efficiency based on manifold conditions $\eta_{vol} = \frac{m_i}{\rho_i V_d}$, the density $\rho_i = \frac{P_i}{RT_i}$, and the ideal gas with constant specific heats can be shown as $\frac{R}{c_v} = \kappa - 1 \;\; and \;\; \frac{c_p}{c_v} = \kappa \;\Rightarrow\; \frac{R}{c_p}\frac{\kappa}{\kappa-1} = 1.$

The equation (B.5b) can then be reduced to:

$$C_p T_{ov} m_{ov} = \frac{\kappa}{\kappa - 1}\frac{R}{c_p} C_p T_{ov} m_{ov} = \frac{\kappa}{\kappa - 1} T_{ov} m_{ov} \cdot R$$

$$\frac{\kappa}{\kappa - 1} T_{ov} m_{ov} \cdot R = \frac{\kappa}{\kappa - 1} T_{ov} m_{ov} \frac{1}{T_i V_d} \rho_i \frac{1}{\frac{P_i}{RT_i}} V_d$$

$$\therefore \quad C_p T_{ov} m_{ov} = \frac{\kappa}{\kappa - 1}\frac{T_{ov} m_{ov}}{T_i V_d}\frac{RT_i}{P_i}\rho_i V_d$$

The equation (B.5c) can be then reduced to:

$$C_p T_i m_i = C_p T_i \rho_i V_d \eta_{vol} = C_p T_i \frac{P_i}{RT_i} V_d \eta_{vol} = \frac{C_p}{R} P_i V_d \eta_{vol}$$

$$\therefore \quad C_p T_i m_i = \frac{\kappa}{\kappa - 1} P_i V_d \eta_{vol}$$

The equation (B.5d) can be then reduced to:

$$Q = m_i c_p \,\Delta\, T = \rho_i V_d \eta_{vol} c_p \,\Delta\, T = \frac{P_i}{RT_i} V_d \eta_{vol} c_p \,\Delta\, T = \frac{c_p}{RT_i} V_d \eta_{vol} \,\Delta\, TP_i$$

$$\therefore \quad Q = \frac{\kappa}{\kappa - 1} V_d \eta_{vol} \frac{\Delta\, T}{T_i} P_i$$

Thus equation (B.5) simplification as:

$$P_{ic}V_{ic} - P_{io}V_{io} = \begin{bmatrix} -(\kappa - 1)\int_{io}^{ic} PdV & (a) \\ +\kappa \frac{T_{ov}m_{ov}}{T_i V_d}\frac{RT_i}{P_i}\rho_i V_d & (b) \\ +\kappa P_i V_d \eta_{vol} & (c) \\ +\kappa V_d \eta_{vol}\frac{\Delta T}{T_i}P_i & (d) \end{bmatrix} \quad (B.6)$$

Solve for the volumetric efficiency and one finds

$$\eta_{vol} = \left(\frac{1}{1+\frac{\Delta T}{T_i}}\right)\left(\frac{P_{ic}V_{ic} - P_{io}V_{io}}{\kappa P_i V_d} + \frac{(\kappa-1)}{\kappa}\frac{1}{P_i V_d}\int_{io}^{ic} PdV - \frac{T_{ov}m_{ov}}{T_i V_d \rho_i}\right) \quad (B.7)$$

When in small engine speed condition, there should be no pressure drop across the valves at closure, therefore $P_{ic} = P_i$ and$P_{io} = P_e$. Recall that for engine with a short to rod ratio, the cylinder volume can be given by $(V_d + V_c)/V_c = r$ and $V_d/V_c = r$, $V_{ic} = V_d + V_c$ and $V_{io} = V_c$. Here r is the compression ratio.

$$\eta_{vol} = \left(\frac{1}{1+\frac{\Delta T}{T_i}}\right)\left(\frac{(\kappa-1)(r-1)}{\kappa(r-1)}t + \frac{P_e}{\kappa(r-1)P_i} - \frac{(\kappa-1)}{\kappa}\frac{T_{ov}m_{ov}}{T_i V_d \rho_i}\right) \quad (B.8)$$

$$\eta_{vol}P_m = \left(\frac{1}{1+\frac{\Delta T}{T_i}}\right)\left(\frac{(\kappa-1)(r-1)}{\kappa(r-1)}t + \frac{P_e}{\kappa(r-1)P_i} - \frac{(\kappa-1)}{\kappa}\frac{T_{ov}m_{ov}}{T_i V_d \rho_i}\right)P_{man}$$

$$= \left(\frac{1}{1+\frac{\Delta T}{T_i}}\right)\left[\frac{(\kappa-1)(r-1)}{\kappa(r-1)}tP_{man} + \frac{P_e}{\kappa(r-1)} - \frac{(\kappa-1)}{\kappa}\frac{T_{ov}m_{ov}}{T_i V_d}\right]$$

$$= \left(\frac{1}{1+\frac{\Delta T}{T_i}}\right)\left(\frac{(\kappa-1)(r-1)}{\kappa(r-1)}t\right)P_m$$

$$+ \left(\frac{1}{1+\frac{\Delta T}{T_i}}\right)\left(\frac{P_e}{\kappa(r-1)} - \frac{(\kappa-1)}{\kappa}\frac{T_{ov}m_{ov}}{T_i V_d}\right) \quad (B.9)$$

As present the equation (3-17) can be assumed as below:

$$m_{an} = s_{man} P_m - y_m \tag{B.10}$$

Where s_{man} and y_{man} can be summarised and concluded as below:

$$s_m = \left(\frac{1}{1 + \frac{\Delta T}{T_i}}\right)\left(\frac{(\kappa - 1)(r - 1)}{\kappa(r - 1)} t\right) P_m \tag{B.11}$$

$$y_m = \left(\frac{1}{1 + \frac{\Delta T}{T_i}}\right)\left(\frac{P_e}{\kappa(r - 1)} - \frac{(\kappa - 1)}{\kappa} \frac{T_{ov} m_{ov}}{T_i V_d}\right) \tag{B.12}$$

Appendix C: Driving Cycle and Kinematic Parameters (Barlow et al., 2009)

C.1 Economic Commission for Europe Driving Cycle (ECE 15)

This driving cycle represents urban driving. It is characterized by low vehicle speed (max.50 km/h), low engine load and low exhaust gas temperature. Total distance is 994.6 m and total time is 195 s. A graph showing speed as a function of time as well as the values of the parameters is provided in Fig C.1 and Table C.1.

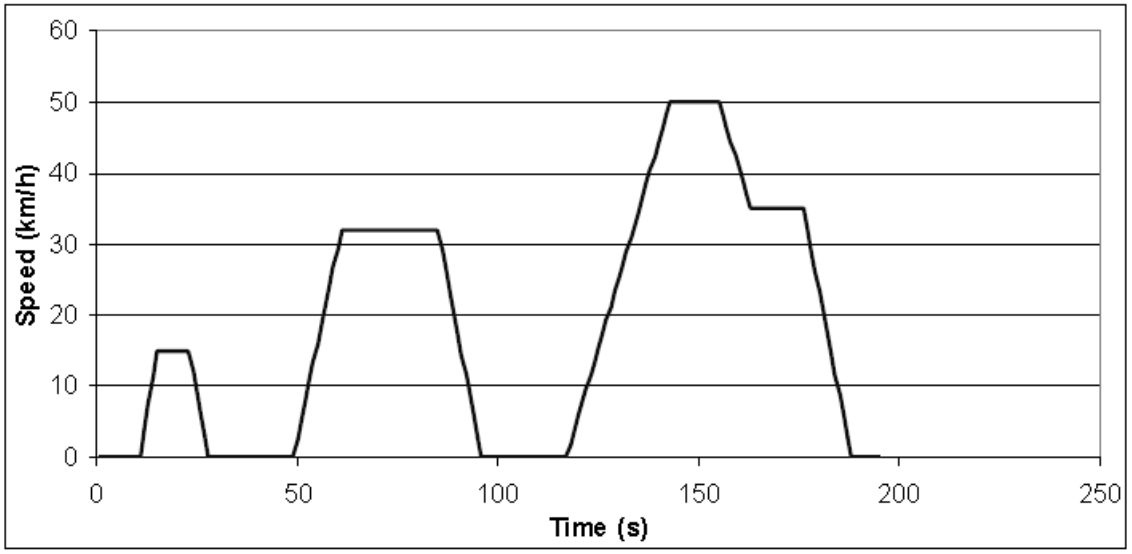

Figure C.18: ECE 15 Driving Cycle Time-Speed Diagram

Table C.1: ECE 15 Driving Cycle Kinematic Parameters			
Total distance	994.6 m	Maximum speed	50.07 Km/h
Total time	195 s	Number of accelerations	3
Driving time	150 s	Number stop	4
Drive time	49 s	% of Driving	76.92%
Time spent braking	40 s	% of braking	20.51%
Standing time	45 s	% of Standing	23.08%
Average speed	18.4 Km/h	Standard deviation of speed	15.58 Km/s

C.2 Extra Urban Driving Cycle [EUDC]

This cycle describes a suburban route. At the end of the cycle the vehicle accelerates to highway-speed. Both speed and acceleration are higher than the ECE 15 but it still is a modal cycle. Total distance is 6955.07 m and total time is 400 s. A graph showing speed as a function of time as well as the values of the parameters is provided in Fig C.2 and Table C.2.

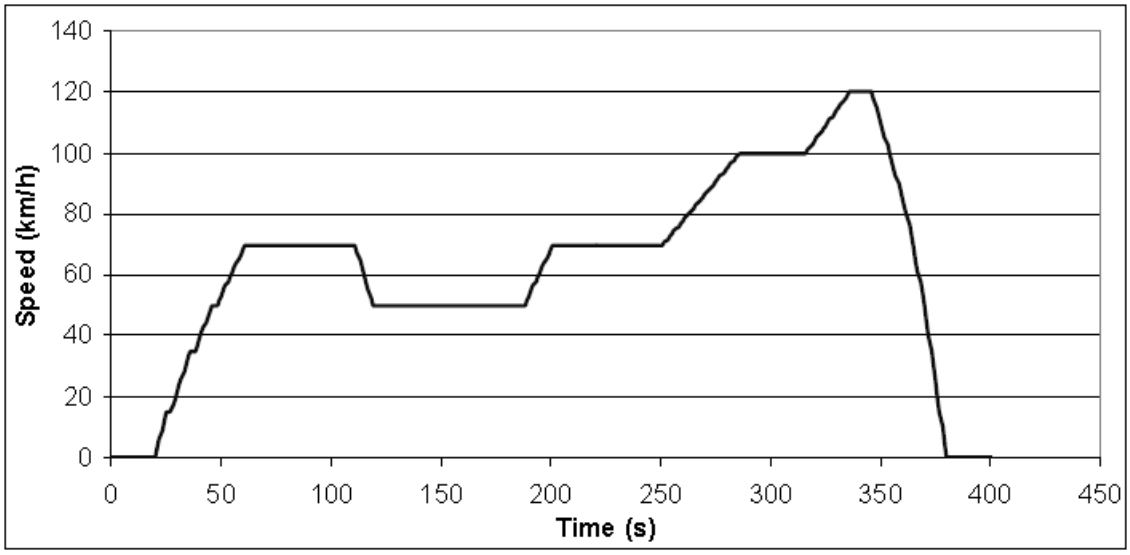

Figure C.19: EUDC Driving Cycle Time-Speed Diagram

Table C.2: EUDC Driving Cycle Kinematic Parameters			
Total distance	6955.07 m	Maximum speed	120.09 Km/h
Total time	400 s	Number of accelerations	4
Driving time	365 s	Number stop	2
Drive time	197 s	% of Driving	91.25 %
Time spent braking	45 s	% of braking	11.25 %
Standing time	35 s	% of Standing	8.75 %
Average speed	62.6 Km/h	Standard deviation of speed	25.88 Km/s

C.3 EUDC for Low Power Vehicles

This cycle is a suburban cycle for low-powered vehicles. It is similar to the EUDC but the maximum speed is 90 km/h. Total distance is 6609.41 and total time is 400 s. A

graph showing speed as a function of time as well as the values of the parameters is provided in Fig C.3 and Table C.3.

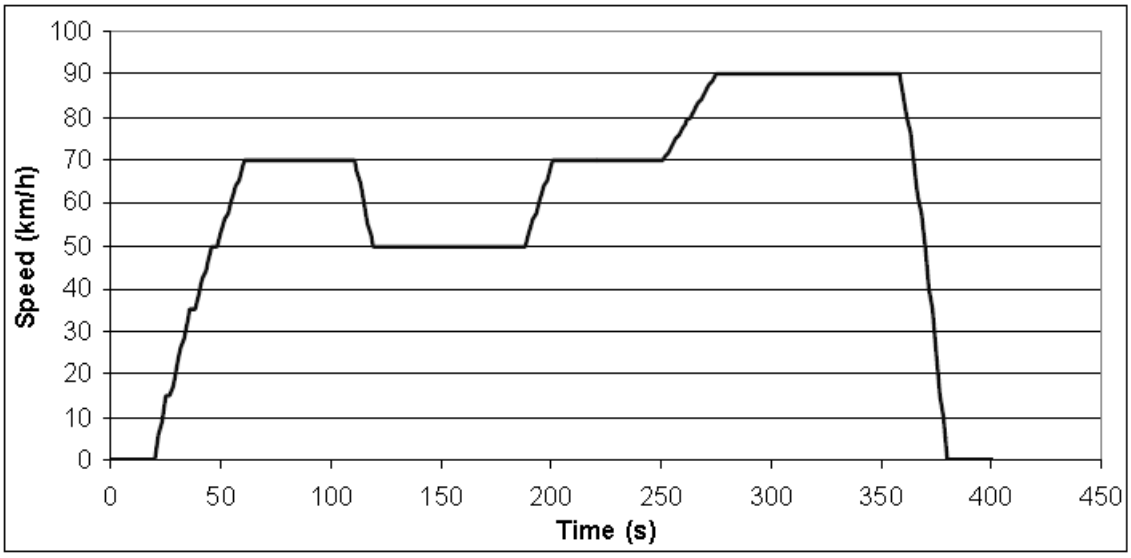

Figure C.3: EUDC for Low Power Vehicles Driving Cycle Time-Speed Diagram

Table C.3: EUDC for Low Power Vehicles Kinematic Parameters			
Total distance	6609.31 m	Maximum speed	90.09 Km/h
Total time	400 s	Number of accelerations	3
Driving time	365s	Number stop	2
Drive time	243 s	% of Driving	91.25%
Time spent braking	33 s	% of braking	8.25%
Standing time	35 s	% of Standing	8.75%
Average speed	59.5 Km/h	Standard deviation of speed	21.08 Km/s

C.4 New European Driving Cycle [NEDC]

This is a combined cycle consisting of four ECE 15 cycles followed by an EUDC or EUDCL cycle. The NEDC is also called the ECE cycle. Total distance is 11016.63 m and total time is 1180 s. A graph showing speed as a function of time as well as the values of the parameters is provided in Fig C.4 and Table C.4.

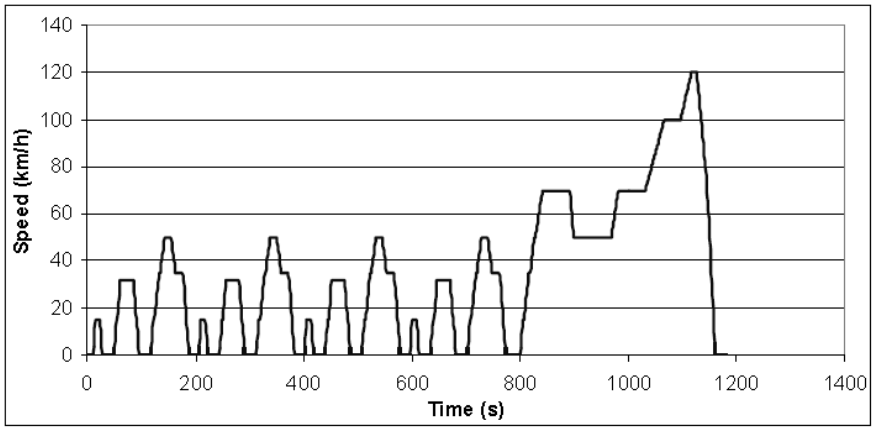

Figure C.20: NEDC Driving Cycle Time-Speed Diagram

Table C.4: NEDC Driving Cycle Kinematic Parameters			
Total distance	11016.63 m	Maximum speed	120.09 Km/h
Total time	1180 s	Number of accelerations	31
Driving time	939 s	Number stop	14
Drive time	458 s	% of Driving	79.58%
Time spent braking	200 s	% of braking	16.95%
Standing time	241s	% of Standing	20.42%
Average speed	33.6 Km/h	Standard deviation of speed	28.91 Km/s

C.5 ECE15+EUDC Driving Cycle

ECE15+EUDC is same as New European Driving Cycle, only have 40 second idle period at start. Total distance is 11016.63 m and total time is 1220 s. A graph showing speed as a function of time as well as the values of the parameters is provided in Fig C.5 and Table C.5.

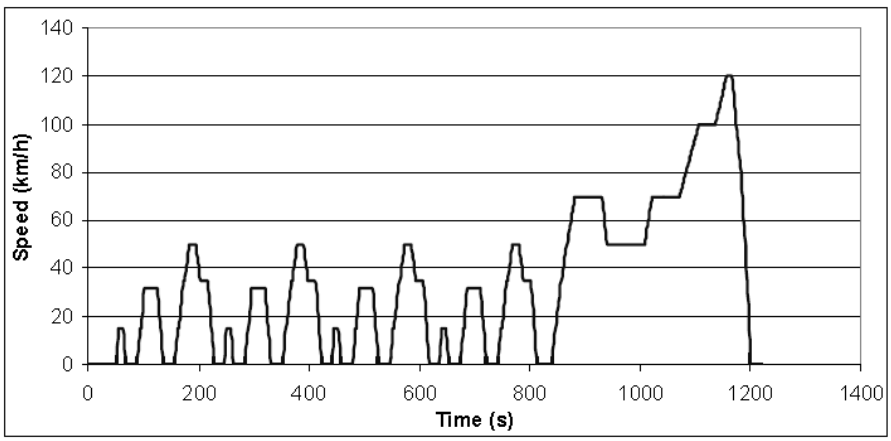

Figure C.5: ECE15+EUDC Driving Cycle Time-Speed Diagram

Table C.5: ECE15+EUDC Driving Cycle Kinematic Parameters			
Total distance	11016.63m	Maximum speed	120.09 Km/h
Total time	1220s	Number of accelerations	16
Driving time	965s	Number stop	14
Drive time	393s	% of Driving	79.10%
Time spent braking	201s	% of braking	16.48%
Standing time	255s	% of Standing	20.90%
Average speed	32.5Km/h	Standard deviation of speed	29.33 Km/s

C.6 Federal Test Procedure 72 [FTP-72]

In the early seventies this cycle has been developed to describe an urban route. The cycle consists of a cold start phase. This phase is followed by a transient phase with many speed peaks which start from rest. The emissions are measured. In the United States weight factors are used for both phases to norm the emissions. The FTP 72 is often called FUDS, UDDS or LA-4. Total distance is 11996.85 m and total time is 1369 s. A graph showing speed as a function of time as well as the values of the parameters is provided in Appendix Fig C.6 and Table C.6.

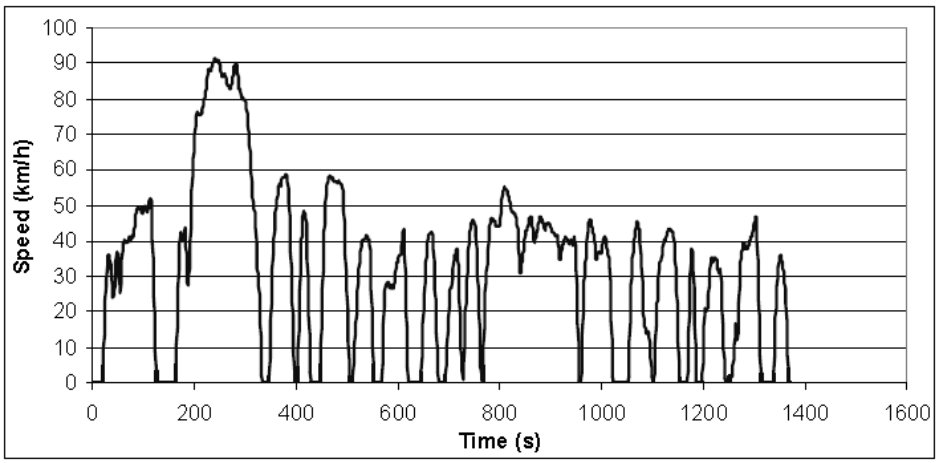

Figure C.6: FTP-72 Driving Cycle Time-Speed Diagram

C.7 Federal Test Procedure 75 [FTP-75]

It is the FTP 72 with an extra third phase. This phase is identical to the first phase of the FTP 72 but is executed with a hot engine. Total distance is 17786.59 m and total time is

1874 s. A graph showing speed as a function of time as well as the values of the parameters is provided in Appendix Fig C.7 and Table C.7.

Table C.6: FTP-72 Driving Cycle Kinematic Parameters			
Total distance	1196.85 m	Maximum speed	91.15 Km/h
Total time	1369 s	Number of accelerations	48
Driving time	1180 s	Number stop	14
Drive time	247 s	% of Driving	86.19%
Time spent braking	271 s	% of braking	19.80%
Standing time	189 s	% of Standing	13.81%
Average speed	31.6 Km/h	Standard deviation of speed	21.46 Km/s

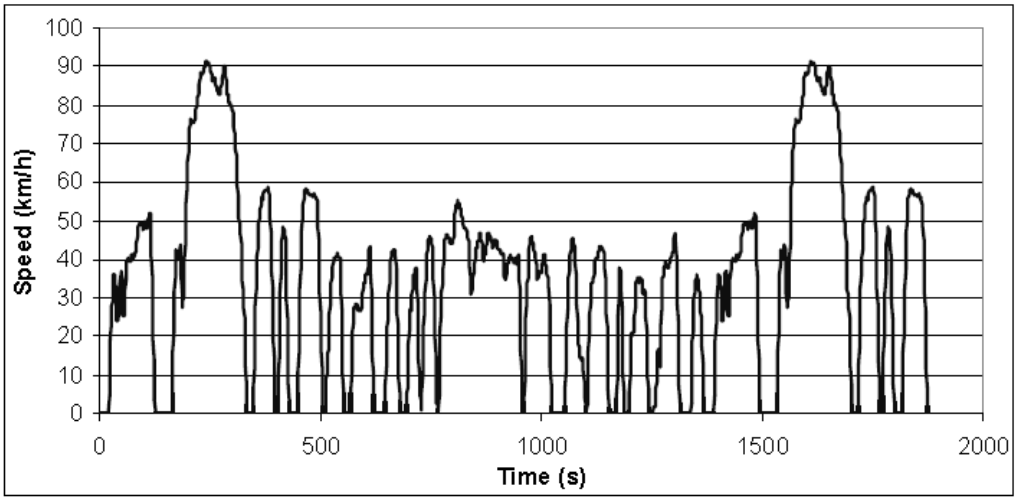

Figure C.7: FTP-75 Driving Cycle Time-Speed Diagram

Table C.7: FTP-75 Driving Cycle Kinematic Parameters			
Total distance	17786.59 m	Maximum speed	91.09 Km/h
Total time	1874 s	Number of accelerations	61
Driving time	1633 s	Number stop	16
Drive time	376 s	% of Driving	87.14%
Time spent braking	383 s	% of braking	20.44%
Standing time	241 s	% of Standing	12.86%
Average speed	34.2 Km/h	Standard deviation of speed	23.51 Km/s

C.8 EPA New York City Cycle [NYCC]

This cycle represents an urban route through New York. A characteristic of this cycle is the low average speed. Total distance is 1902.76 m and total time is 598 s. A graph showing speed as a function of time as well as the values of the parameters is provided in Fig C.8 and Table C.8.

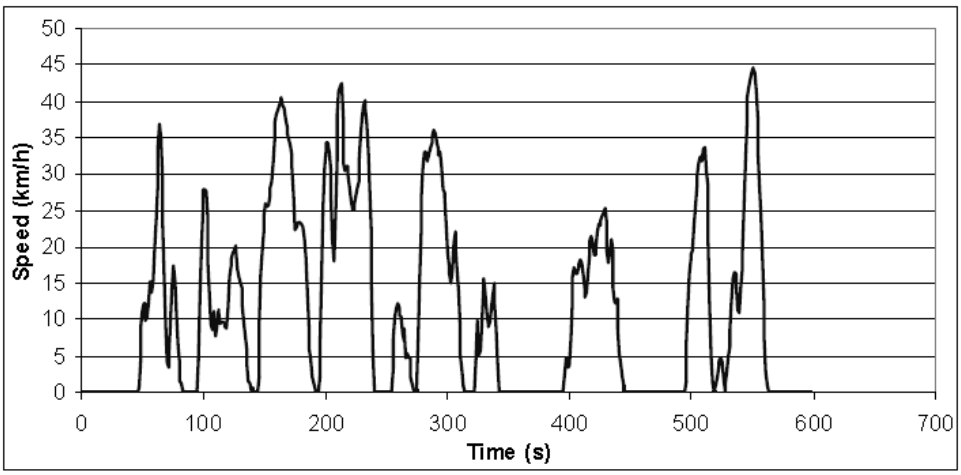

Figure C.8: NYCC Driving Cycle Time-Speed Diagram

Table C.8: NYCC Driving Cycle Kinematic Parameters			
Total distance	1902.76 m	Maximum speed	44.45 Km/h
Total time	598	Number of accelerations	22
Driving time	412 s	Number stop	7
Drive time	61 s	% of Driving	68.90%
Time spent braking	129 s	% of braking	21.57%
Standing time	186 s	% of Standing	31.10%
Average speed	11.5 Km/h	Standard deviation of speed	12.23 Km/s

C.9 10 Mode Driving Cycle

This cycle represents an urban route. Total distance is 663.43 m and total time is 135 s. A graph showing speed as a function of time as well as the values of the parameters is provided in Fig C.9 and Table C.9.

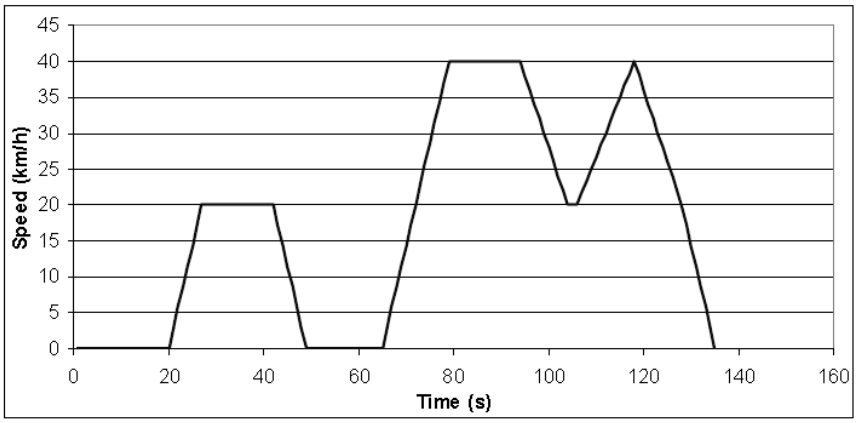

Figure C.9: 10 Mode Driving Cycle Time-Speed Diagram

Table C.9: 10 Mode Driving Cycle Kinematic Parameters			
Total distance	663.43 m	Maximum speed	40.09 Km/h
Total time	135 s	Number of accelerations	3
Driving time	107 s	Number stop	2
Drive time	29 s	% of Driving	79.26%
Time spent braking	34 s	% of braking	25.19%
Standing time	28 s	% of Standing	20.74%
Average speed	17.7 Km/h	Standard deviation of speed	12.75 Km/s

C.10 10-15 Mode Driving Cycle

This is a combination of five cycles. First the 15-Mode, then three times 10-Mode and at last again the 15-Mode. Total distance is 4165.27 m and total time is 660 s. A graph showing speed as a function of time as well as the values of the parameters is provided in Fig C.10 and Table C.10.

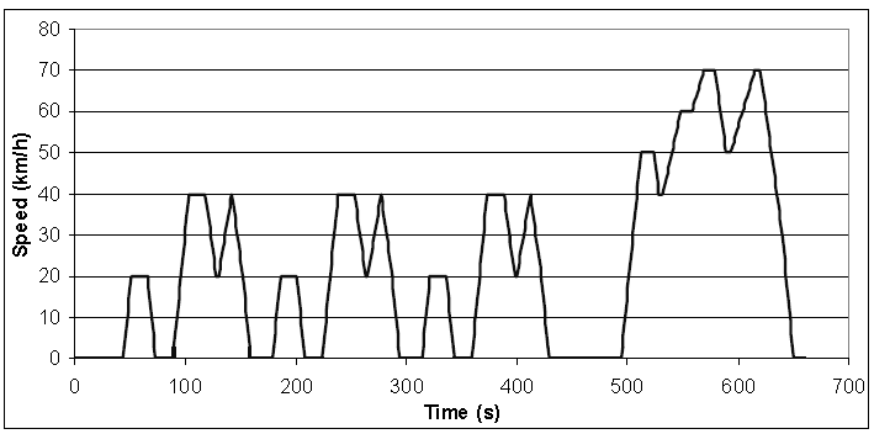

Figure C.10: 10-15 Mode Driving Cycle Time-Speed Diagram

Table C.10: 10-15 Mode Driving Cycle Kinematic Parameters			
Total distance	4165.27 m	Maximum speed	70.09 Km/h
Total time	660 s	Number of accelerations	13
Driving time	488 s	Number stop	8
Drive time	120 s	% of Driving	73.94%
Time spent braking	149 s	% of braking	22.58%
Standing time	172 s	% of Standing	26.06%
Average speed	22.7 Km/h	Standard deviation of speed	19.68 Km/s

Appendix D: Catalytic Converter Model

A catalytic converter is a vehicle emissions control device which converts toxic by-products of combustion in the exhaust of an internal combustion engine to less toxic substances by way of catalysing chemical reactions. The specific reactions vary with the type of catalyst installed. Most present-day vehicles that run on gasoline are fitted with a "three-way" converter, so named because it converts the three main pollutants in automobile exhaust: carbon monoxide, unburned hydrocarbon and oxides of nitrogen.

A three-way catalytic converter has three simultaneous tasks:

1. Reduction of nitrogen oxides to nitrogen and oxygen:

$$\mathrm{NO}_x \rightarrow \mathrm{O}_2 + \mathrm{N}_2$$

2. Oxidation of carbon monoxide to carbon dioxide:

$$\mathrm{CO} + \mathrm{O}_2 \rightarrow \mathrm{CO}_2$$

3. Oxidation of unburnt hydrocarbons (HC) to carbon dioxide and water:

$$\mathrm{CH} + \mathrm{O}_2 \rightarrow \mathrm{CO}_2 + \mathrm{H}_2\mathrm{O}$$

The efficiency of the three-way catalytic converter depends on engine type and the catalytic converter. In order to provide the controller with multi-test analysis, Catalytic converter model calculate the catalytic efficiency of three toxic by-products according to air/fuel ratio. Based on (Stefanopoulou, 1996) engine simulation model, the Catalytic efficiency of three substances can be represented by lookup table block, the data of which are as follows

1. Feedgas Emissions of Oxides of Nitrogen (NOx_x)

Table Data = [91 91 91 91 92 93 96 96.8 97.4 98 98 90 80 70 60 50 40 35 30 20 10 3 0 0]

Breakpoint = [5 14.1 14.2 14.3 14.4 14.5 14.6 14.62 14.64 14.66 14.664 14.674 14.682 14.692 14.701 14.709 14.719 14.726 14.731 14.75 14.774 14.79 14.8 30]

2. Feedgas Emissions of Hydrocarbons (HC)

Table Data = [20 26 42 50 53 60 64.4 70 78 81.6 86 90 96.8 95.5 94.8 94.1 93.85 93.3 93.2 93 93]

Breakpoint = [5 14.1 14.3 14.37 14.4 14.46 14.5 14.542 14.6 14.62 14.64 14.65 14.668 14.7 14.72 14.74 14.76 14.78 14.8 14.83 30]

3. Feedgas Emissions of carbon monoxide (CO)

Table Data = [4 9.5 17 20 30 35 40 50 60 65.6 70 74.1 84 90 93 97.5 98.5 99.1 99.24 99.37 99.49 99.6 99.7]

Breakpoint = [5 14.3 14.4 14.42 14.466 14.5 14.519 14.552 14.583 14.6 14.61 14.62 14.64 14.65 14.66 14.67 14.68 14.7 14.72 14.74 14.76 14.78 30]

According to air/fuel ratio the catalytic converter simulation model outputs catalytic efficiency, the output signal is sampled 100 times per second and recorded to workspace, the following Fig D.1 is catalytic efficiency.

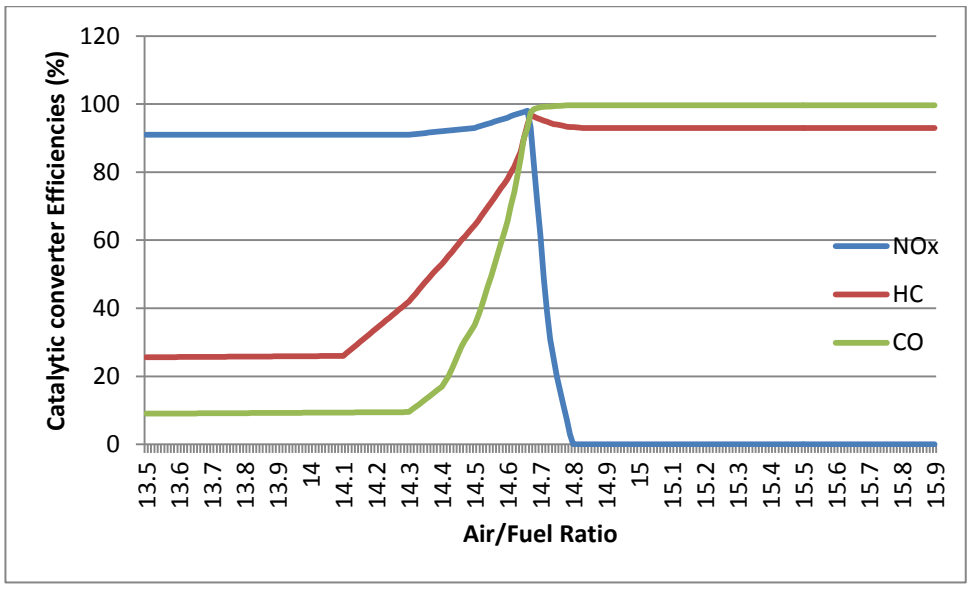

Figure D.1: Typical Three-Way Catalytic Converter Efficiency Curves

Appendix E: Engine Dynamic Simulation Package

E.1 SIMULINK-Based Engine Dynamic Simulation Package

The SIMULINK-based engine dynamic simulation package (Fig E.1) has four main parts: input model, engine model, controller model and output model. The engine model has detailed introduce in Chapter 4, and the controller model has explained in Chapter 5 and Chapter 6. In this appendix, the input model will be mainly introduced.

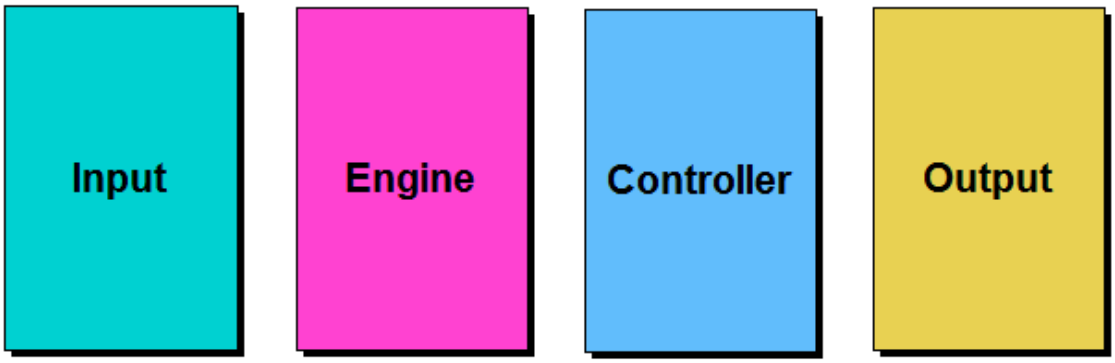

Figure E.1: SIMULINK-Based Engine Dynamic Simulation Package

E.2 Input Model

As shown in Fig E.2 that input model has four parts: throttle angle selection model, engine load selection model, and vehicle dynamic parameter model and transmission parameters. According to the step number operation each model in turn when using the engine dynamic simulation package.

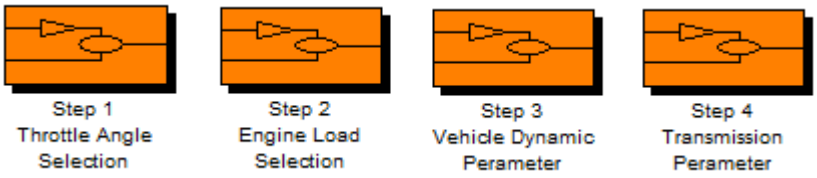

Figure E.2: Input Model

E.2.1 Throttle Angle Selection Model

Fig E.3 shows GUI of the throttle angle selection model, model is used to provide simulation throttle input. The principles of throttle angle selection model operation are: (1) Choose the throttle angle selection option depicted in Table E.1. If choose throttle angle scheme 1 or throttle angle scheme 2, then you can go to next stage. (2) If choose control by driving cycle option, then you can choose a driving cycle which present in Table E.2. (3) If choose custom throttle angle option, then you can enter a constant throttle angle during the simulation. Fig E.4 shows the under mark of throttle angle selection model. Since each throttle option simulation length is different, Fig E.5 shows the initialization commands set simulation stop time.

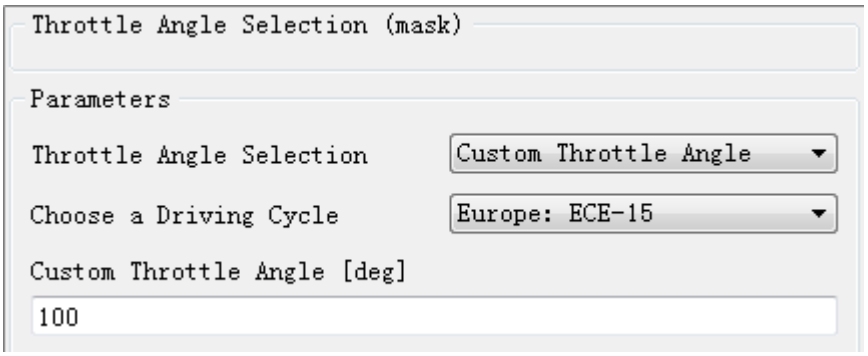

Figure E.3: GUI of Throttle Angle Selection Model

Table E.1: Throttle Angle Selection Pull-down Menu
Throttle angle scheme 1
Throttle angle scheme 2
Control by driving cycle
Custom throttle angle

Table E.2: Choose a Driving Cycle Pull-down Menu
Europe: ECE-15
Europe: EUDC
Europe: EUDCL
Europe: NEDC
Europe: ECE15+EUDC
USA: FTP 72
USA: FTP 75
USA: NYCC
Japan: 10 Mode
Japan: 15 Mode
Japan: 10-15 Mode

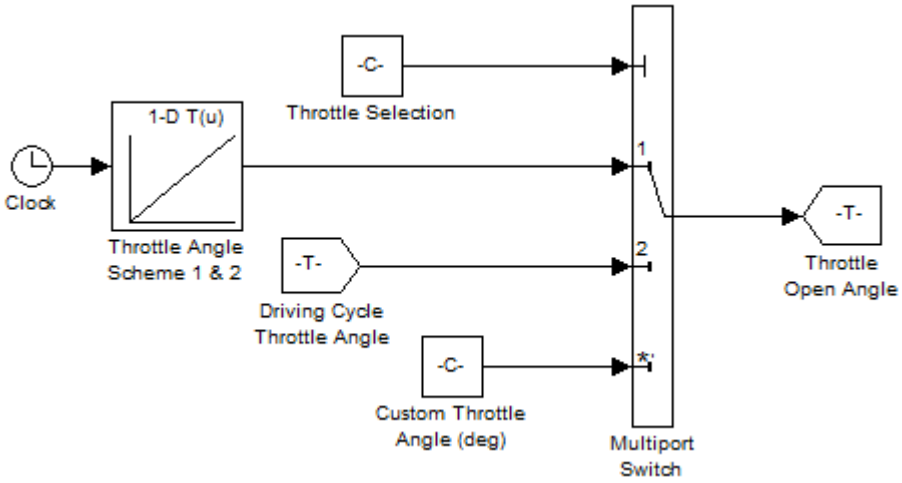

Figure E.4: Under Mark of Throttle Angle Selection Model

```
% Set Simulation Stop Time

stoptime = SimTime;

set_param(char(bdroot(gcb)),'StopTime',num2str(stoptime));
cl_par = struct('stoptime', stoptime);
set_param(gcb, 'UserData', cl_par);
```

Figure E.21: Set Simulation Stop Time

E.2.2 Engine Load Selection Model

Fig E.6 shows GUI of the engine load selection model, model is used to provide simulation load torque and mass input. The principles of throttle angle selection model operation are: (1) Choose the engine torque load option depicted in Table E.3. If choose custom engine load, enter a constant engine load torque during the simulation. (2) If choose from vehicle dynamic option, and need extra mass load on the vehicle, then you can choose custom mass load from vehicle mass load option (Table E.4). The under mark of engine load selection model has introduced in Section 4.4.1.

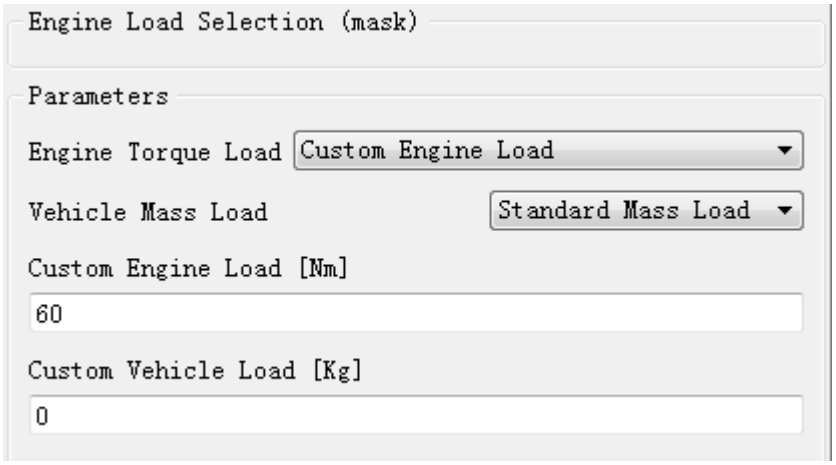

Figure E.5: GUI of Engine Load Selection Model

Table E.3: Engine Torque Load Pull-down Menu
From vehicle dynamic
Custom engine load

Table E.4: Vehicle Mass Load Pull-down Menu
Standard mass load
Custom mass load

E.1.3 Vehicle Dynamic Parameter Model

Fig E.6 shows GUI of the engine load selection model, model is used to determine vehicle dynamic parameter. Fig E.7 shows the under mark of vehicle dynamic parameter model.

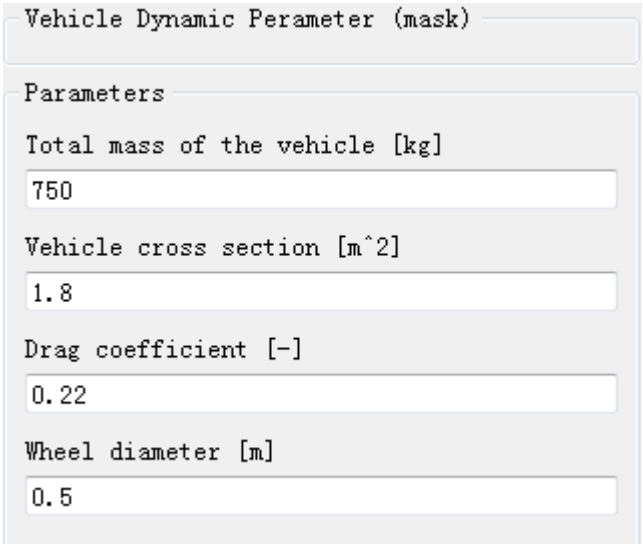

Figure E.6: GUI of the Engine Load Selection Model

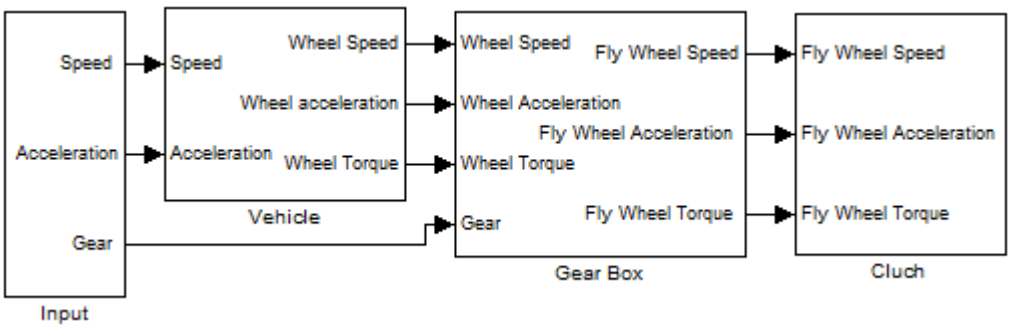

Figure E.7: Under Mark of Vehicle Dynamic Parameter Model

E.1.4 Transmission Parameter Model

Fig E.8 shows GUI of the transmission parameter model, model is used to determine vehicle dynamic parameter. Fig E.9 shows the under mark of transmission parameter model.

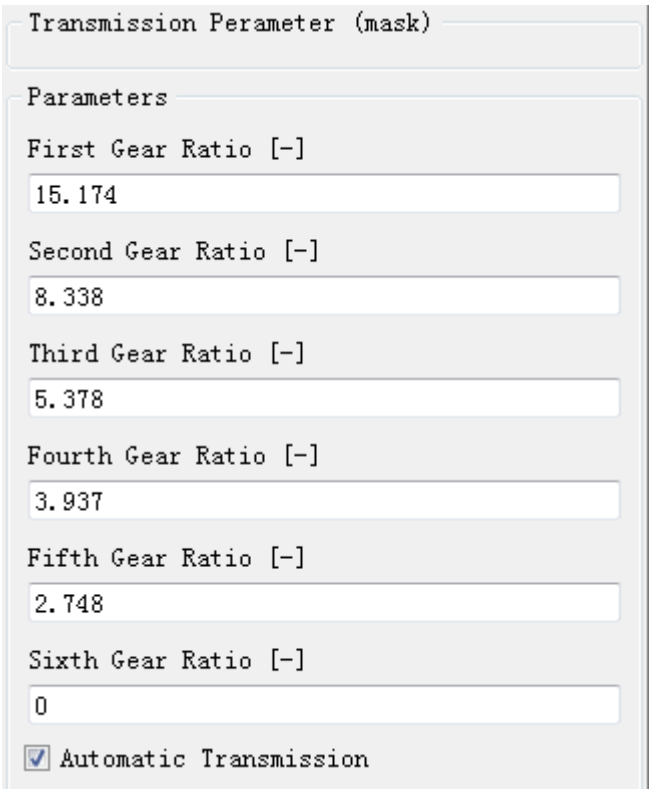

Figure E.8: GUI of the Transmission Parameter Model

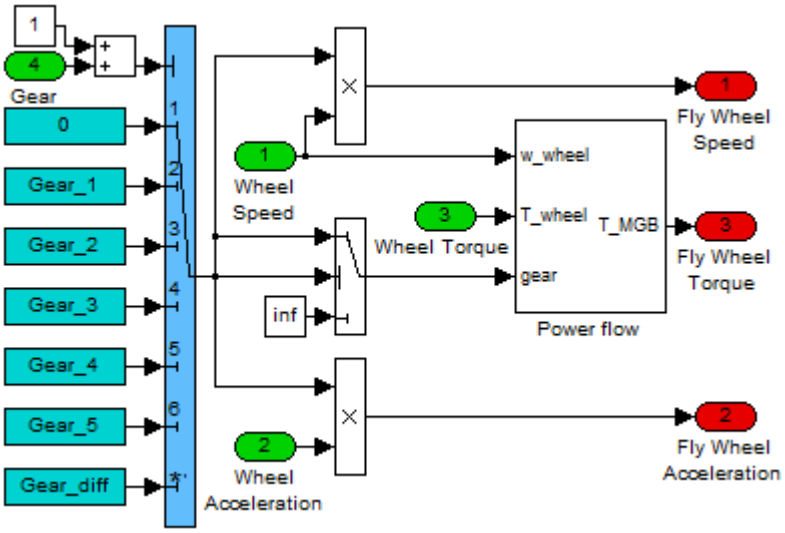

Figure E.8: Under Mark of Transmission Parameter Model

E.2 NN Based AFR Controller

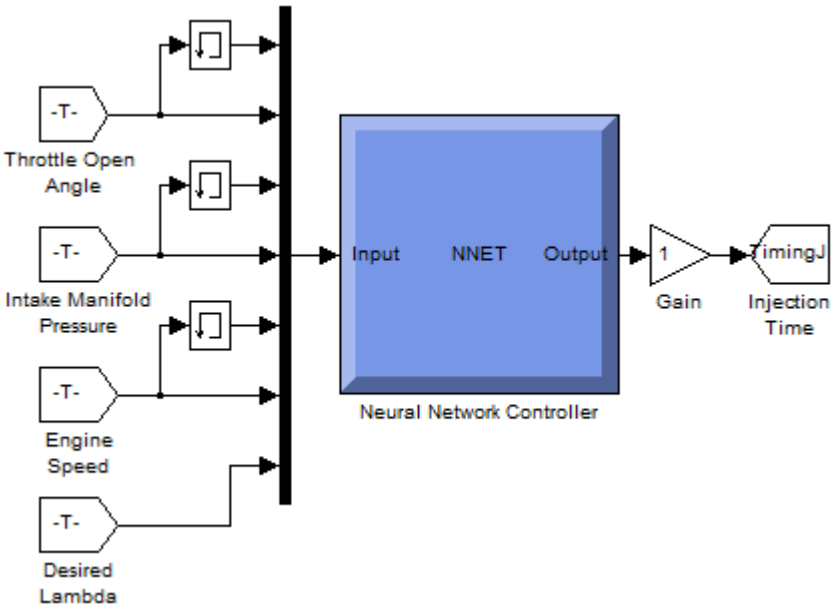

Figure E.10: NN Based AFR Controller

Appendix F: Parameters for Engine Dynamic Simulation Package

The parameters required for engine simulation are listed below in the form of a MATLAB program and this program will be run first for simulations. Most parameters listed here are obtained from real engine laboratory experiments.

```
Cd = 0.7; % throttle valve discharge coefficient of
Pamb = 1.0; % ambient pressure [bar]
Tamb = 273+25; % ambient temperature[oK]
R = 287*10^-5; % gas constant[bar*m^3/kg/oK]
Athmax = 0.001753; % maximum throttle area [m^3]
k = 1.4; % specific heat ratio

MA = Pamb*100000*Athmax/sqrt(R*100000*Tamb);
Vm = 2.351*10^-3; % Engine Displacement Volume [m^3]
Vis = 4.462*10^-3; % Volume of Intake Manifold + Surge tank [m^3]
Tman = Tamb;


% fuel film parameters
tauf = 0.3; % fuel film time constant
kc = 0.6; % fuel film fraction
AFRs =14.68; % stoichiometric air fuel ratio

% torque production model
ti1=-42.65; ti2=14.66; ti3=-0.07; ti4=517.68; ti5=-64.42;
is1=1.00437; is2=-0.00071; is3=0.00022;
m1=30.0; m2=13.95; m3=-3.612; m4=-97.98; m5=25.02;
ma1=-0.10199; ma2=-29.01236; ma3=29.20847;
i1=-0.49075; i2=3.41934; i3=-1.93008;
fp1=19.714; fp2=-3.4751; fp3=2.3947; fp4=72.84; fp5=-26.66;

tideal=590; tSA=74; taf=277; % transport delay

% engine rotational dynamics
Ieff = 0.3; % effective engine rotational inertia [kgm^2]
```